IN VITRO INTERACTIONS OF THE SMALL HEAT SHOCK PROTEIN CHAPERONE HUMAN αB-CRYSTALLIN WITH ITS PHYSIOLOGICAL SUBSTRATES THE LENS γ-CRYSTALLINS

By

Ligia Acosta-Sampson

B.A. Biology
Cornell University, 2004

Submitted to the Department of Biology
In partial fulfillment of the requirement for the degree of

DOCTOR OF PHILOSOPHY

At the
Massachusetts Institute of Technology

August 2010

Signature of Author _____
Department of Biology
August 2010

Certified by_____
Jonathan King
Thesis supervisor

Accepted by_____
Steven P. Bell
Chairman, Department Committee on Graduate Students

IN VITRO INTERACTIONS OF THE SMALL HEAT SHOCK PROTEIN CHAPERONE HUMAN αB-CRYSTALLIN WITH ITS PHYSIOLOGICAL SUBSTRATES THE LENS γ-CRYSTALLINS

By

Ligia Acosta-Sampson

Submitted to the department of Biology at the Massachusetts Institute of Technology on August 31, 2010 in partial fulfillment of the requirements for the degree of Doctor of Philosophy in Biology

ABSTRACT

The passive chaperone α-crystallin, a small heat shock protein, is one of the ubiquitous crystallins in vertebrate lenses, along with the βγ-crystallins. It is composed of two subunits (~ 20 kDa) αA- and αB-crystallin (αA- and αB-Crys), which form a hetero-oligomeric, polydisperse complex of ~ 800 kDa in the lens. Aggregates isolated from mature-onset cataracts, the major cause of sight loss worldwide, contain damaged and misfolded forms of βγ-crystallins, as well as α-crystallins. I have studied the chaperone function of human αB-crystallin interacting with its physiological human γ-crystallin substrates.

Human γD-crystallin (γD-Crys) and γC-crystallin (γC-Crys) are stable and long-lived mammalian γ-crystallins localized in the lens nucleus. Human γS-crystallin (γS-Crys) is abundant in the lens outer cortex. All three γ-crystallins can refold *in vitro* to their native state after unfolding in high concentrations of guanidine hydrochloride (GdnHCl). However, in buffer or very low denaturant concentrations (< 1 M GdnHCl) aggregation of refolding γ-crystallin intermediates competes with productive refolding. Diluting unfolded γC-, γD-, or γS-Crys to low GdnHCl concentrations (at 100 μg/ml, 37ºC) resulted in the protein population partitioning between productive refolding and aggregation pathways. γD-, γC- or γS-Crys protein was allowed to refold and aggregate in the presence of αB-Crys homo-oligomers at different mass-based ratios of γ-Crys to αB-Crys. γD- and γC-Crys aggregation was suppressed to similar levels, whereas γS-Crys aggregation was not suppressed as strongly in assays measuring solution turbidity at 350 nm. SEC chromatograms of the products of suppression reactions showed the presence of a high molecular weight chaperone-substrate complex. This complex was still present 4 days after the suppression reaction was initiated.

Experiments were performed with the αB-Crys chaperone added 2, 6, or 10 s, after dilution of unfolded γD-Crys out of high concentrations of denaturant. The results from these experiments showed that the partially folded, aggregation-prone species that is recognized by αB-Crys chaperone is populated within the first 10 s after refolding and aggregation were initiated. This time period coincided with the refolding of the C-terminal domain of γD-Crys as determined from kinetic refolding experiments *in vitro*.

Human γD-Crys contains four Trp residues with one residue located in each quadrant of the protein. Intrinsic buried Trp fluorescence is quenched in the native state relative to the unfolded state of the protein due to intra-domain partial resonance energy transfer from the highly fluorescent Trp donors (W42 and W130) to the highly quenched acceptor Trps (W68 and W156). The efficient quenching of Trp68 and Trp156 depends on an unusual conformation of

the Trp ring with respect to its backbone amide, as well as the presence of two tightly bound H_2O molecules with oppositely oriented dipoles. Thus, intrinsic Trp fluorescence is a sensitive reporter of the protein conformation.

Using a no-Trp mutant of αB-Crys (W9F/W60F), the conformation of the bound γD-Crys substrate in γD—αB complexes was determined from intrinsic Trp fluorescence emission. The emission spectra for the substrate did not coincide with a native or fully unfolded conformation of the γD-Crys controls. To further characterize the conformation of each domain of γD-Crys in the substrate-chaperone complex, double-Trp γD-Crys mutants, which conserved the Trp pair in the N-terminal (W130F/W156F) or the C-terminal (W42F/W68F) domain, while the counterpart pair was changed to Phe, were used as substrates in aggregation suppression reactions. The fluorescence emission spectra for the double-Trp mutants in complex with Trp-less αB-Crys were similar and they did not coincide with the spectra for their respective native or unfolded double-Trp γD-Crys controls. These results indicated that the bound substrate remained in a partially folded state with neither domain native-like. Triple-Trp γD-mutants that conserved the highly fluorescent Trp residue in the N-terminal or C-terminal domains were also used as substrates in suppression of aggregation reactions with Trp-less αB-Crys chaperone. The fluorescence emission spectra of triple-Trp substrates in the substrate-chaperone complex indicated that these residues were not solvent exposed. These results suggest that Trp neighboring regions could be interacting directly with the αB-Crys chaperone.

To further elucidate the specific region in the γ-crystallins that interacts with αB-Crys in suppression assays, experiments were performed using single-domain constructs of γD-Crys. The isolated N-terminal (γD-Ntd) and C-terminal domains (γD-Ctd) of γD-Crys, expressed in E. coli, can refold to a native state upon dilution out of denaturant to low concentrations of GdnHCl. The C-terminal domain aggregated upon refolding out of high concentrations of denaturant, while the N-terminal did not under the same assay conditions. However, when γD-Ctd and γD-Ntd were unfolded and refolded together, γD-Ctd recruited γD-Ntd into the aggregate. αB-Crys suppressed the aggregation of the γD-Ctd and formed γD-Ctd—αB complexes. Using W9F/W60F αB-Crys, I have determined, through the fluorescence emission of γD-Ctd tryptophans, that the γD-Ctd in the γD-Ctd—αB complexes was partially folded. Inhibition experiments in which the γD-Ntd and γD-Ctd isolated domains were refolded sequentially or simultaneously showed that αB-Crys preferentially recognized γD-Ctd.

These *in vitro* results provide a model for how α-crystallin interacts with aggregation-prone substrates *in vivo* wherein an aggregation-prone region in the C-terminal domain of γD-Crys is exposed in the aggregation-prone species and this region is recognized by αB-Crys. These results also provide support for protein unfolding/protein aggregation models for cataract, with α-crystallin suppressing aggregation of damaged or unfolded proteins through early adulthood, but becoming saturated with advancing age.

Thesis Supervisor: Jonathan King, Professor of Biology.

ACKNOWLEDGEMENTS

It is impossible for me to fully express in words the depth of gratitude that I feel towards all of the people that have made this work possible and who have influenced my life during my tenure at MIT.

I would like to thank my advisor, Professor Jonathan King. I fell in love with the 'protein folding problem' after taking his graduate seminar course. And on the last session of the course, I was inspired by his lecture on the social responsibility of scientists. I have always appreciated his frank and straightforward manner. Jon, thank you for being a mentor, for guiding me through tough times, for caring, for all of the advice, for allowing me to express my scientific theories and ideas without censure. You have kept my interest in becoming an academic alive and I hope someday to emulate your example as a mentor.

Thanks to my committee members: Drs. Bob Sauer, Uttam RajBhandary, and Thomas Schwartz. Thank you for your advice and for the time you have taken to help me transition to the next stage in my academic career. Thank you to Dr. Melissa Kosinki-Collins for taking the time to be part of my thesis committee and to critique my thesis.

Thanks to Drs. Ishara Mills-Henry and Jiejin Chen for welcoming me warmly to the Crystallin Team. Their knowledge, insight and honest critique made many of my initial attempts at establishing working protocols possible. During their tenure in lab, we became close friends and I appreciate their comforting advice and their caring support. Ishara, I could not think of a better person to get lost with while wandering Buenos Aires. Thank you for listening to me and for giving me advice on life and on graduate school. Jiejin, thank you for your advice and for always providing a level-headed counterpoint to my rants. Thank you for comforting me during the most trying moments in my graduate career. I miss the days when I could just turn around and interrupt you with anything that crossed my mind. I will always cherish both of your friendships.

Thanks to the King lab for being such an interesting and supportive place to work. Thanks to all the members of the 'Crystallin Team', past and present. Thanks to Dr. Shannon Thol for taking me under her wing and teaching me the basics of protein purification. Kate Moreau, thank you for always being supportive and caring, and for sharing all of the interesting stories you come across. You have made lab a more enjoyable place to work. Fanrong Kong, I wish you the best of luck with your experiments and I hope that the α-crystallin project flourishes during your tenure in lab. Nathaniel Schafheimer, you have made lab a fun place to be in and your scientific curiosity is a breath of fresh air. I wish you all the best as you go through the next step towards your Ph.D.

I would also like to thank Jeannie Chew for her unwavering optimism and for her warm and candid manner. Jeannie, I enjoyed working with you and becoming friends. You will be a great Doctor someday! I thank Ms. Margaret White for her caring advice, her constant encouragement and for always making sure that I left lab at a reasonable hour every night. Thanks to Dessy Raytcheva for listening and commiserating; I was happy to have someone who understood what I was going through. Thank you to the members of the 'Chaperonin Team' for making the King lab a great place to work: Dr. Kelly Knee, Dan Goulet, and Oksana Sergeeva. Thank you to Drs. Peter Weigele and Yongting Wang for their help and for teaching me some

of the techniques included in this thesis. I would also like to thank Cammie Haase-Pettingell, Cindy Woolley, Althea Hill, and Dr. Takumi Takata.

I thank my loving family. Thanks to my husband, Jason, whose love makes life worth living. His loving support has seen me through the most trying times during my academic career. My tenure in graduate school was bearable because of him. Jason, you make me a better person and enrich my life with your myriad interests. We have grown to love many of the same things and I hope wherever I go you will be by my side. Thank you to my parents and my sisters: Gloria, Mayra and Rosie; as well as their families. Thank you for making me an aunt to my lovely nieces, Gia and Eva. Thanks to Petros, Francine, Tony, Alexandros and Angelos for welcoming me into their family. You have been a real family to me and your love and support have enriched my life.

This thesis is dedicated to my parents: Alvaro Acosta and Rosa Sampson; their loving and nurturing encouragement has fueled my wanderings into academia. They have sacrificed much for the sake of their children, not the least of which was the pursuit of their own intellectual interests. Mom and Dad, thank you for drawing millions of cop cars on demand even though you had spent the day sitting at a drafting table, for helping me make roller coaster models after sleepless nights at your jobs, for reading my first manuscript in its entirety even though you are not biochemists. I know that wherever I go your love will follow me and make me feel at home.

This research was supported by a National Eye Institute grant (EY015834) and a National Institutes of Health grant (GM017980) awarded to Jonathan King.

"And, in this case, science could learn an important lesson from the literati—who love contingency for the same basic reason that scientists tend to regard the theme with suspicion. Because, in contingency lies the power of each person, no matter how apparently insignificant he may seem, to make a difference in an unconstrained world bristling with possibilities, and nudgeable by the smallest of unpredictable inputs into markedly different channels spelling either vast improvement or potential disaster."

Stephen Jay Gould

BIOGRAPHICAL NOTE

Ligia Acosta-Sampson

Education

Ph.D. Expected 2010	Massachusetts Institute of Technology, Department of Biology, Cambridge, MA
B.A. June 2004	Cornell University, Department of Biology, Ithaca, NY Major: Biology, cum Laude Minor: Genetics

Research and Professional Experience

2004 to 2010	Graduate Research Assistant in the laboratory of Professor Jonathan King, Massachusetts Institute of Technology, Department of Biology, Cambridge, MA.
2002 to 2004	Undergraduate Research Assistant in the laboratory of Professor Maureen Hanson, Cornell University, Department of Biology, Ithaca, NY.
1999 to 2000	High School Research Intern at the University of Florida, Tropical Research and Education Center, Miami, FL.

Publications

Acosta-Sampson, L., & King, J. A. 2010. Partially folded aggregation intermediates of human γD-, γC-, and γS-crystallin are recognized and bound by human αB-crystallin chaperone. *J Mol Biol*. 401(1): 143-52

TABLE OF CONTENTS

LIST OF FIGURES

Chapter 1: Introduction

Chapter 2: Partially folded aggregation intermediates of human γD-, γC- and γS-crystallin are recognized and bound by human αB-crystallin chaperone.

C**hapter 3:** Characterization of the small heat shock protein αB-crystallin chaperone binding regions in human γD-crystallin using single domain constructs of γD-Crys

CHAPTER 1:

INTRODUCTION

A. PROTEIN AGGREGATION DISEASES AND THE ROLES OF CHAPERONE PROTEINS

Protein misfolding and aggregation are causative factors of various diseases. Cystic fibrosis and some forms of cancer, for example, are caused respectively by the misfolding and consequent loss of function of the Cystic fibrosis trans-membrane regulator (CFTR) and the tumor suppressor p53 (Chaudhuri and Paul 2006). Protein deposition diseases (e.g. Parkinson's disease, Huntington's disease, Alzheimer's disease, and familial amyloidoses) arise from the aggregation of specific proteins into the well-structured amyloid fibrils found in proteinaceous deposits in afflicted organs (Dobson 2004). In neurodegenerative diseases, amyloid aggregates can accumulate extracellularly, as in the case of prion diseases and Alzheimer's disease, in the cytoplasm of afflicted cells (Parkinson's disease) and aggregates can also accumulate in the nucleus as has been observed for polyglutamine expansion diseases (Aguzzi and O'Connor 2010). Proteolytic cleavage and covalent modifications are found in proteins in the amyloid aggregates (Fujiwara *et al.* 2002). Although congenital forms of these amyloidoses have been reported, the sporadic, age-related onset of these neurodegenerative diseases is the prevalent etiological manifestation (Chiti and Dobson 2006). Amyloid aggregates were considered to be the causative toxic species responsible for the pathology of neurodegenerative diseases, but are now regarded as the product of protective mechanisms aimed at sequestering soluble toxic oligomers (Saudou *et al.* 1998; Arrasate *et al.* 2004; Cohen *et al.* 2006). Such mechanisms represent one of the many protein quality control mechanisms that have evolved to prevent the deleterious effects of protein aggregation in the cell.

In cells, the accumulation of misfolded or aggregation-prone species caused by diverse environmental stresses, such as heat shock, oxidative stress and hypoxia, is countered by the activation of the protein quality control machinery including the heat shock response in the cytosol and the unfolded protein response in the endoplasmic reticulum. The protein quality control machinery consists of different families of protein chaperones that interact with misfolded protein and suppress various stages of protein aggregation. Members from major protein chaperone families were initially identified due to their over-expression following heat shock of salivary glands of *D. melanogaster* (Tissieres *et al.* 1974). These proteins were designated Hsp, or heat shock proteins, and include the major families: Hsp70-Hsp40, Hsp90, Hsp60, Hsp100, and sHsp. These chaperone families interact to form chaperone networks that help fold a number of nascent proteins (Hsp90, Hsp70-Hsp40 and Hsp60 along with the eukaryotic nascent chain-associated complex and prefoldin, and the prokaryotic Trigger factor),

in refolding of misfolded intermediates populated during cellular stress conditions (Hsp90, Hsp70-Hsp40, and Hsp60), and in disaggregation networks that sequester toxic aggregate species into larger aggregate bodies and replenish pools of amino acids (sHsps, Hsp70-Hsp40, in conjunction with protein degradation machineries, Hsp100 and the proteasome in eukaryotes) (Liberek *et al.* 2008; Saibil 2008; Hartl and Hayer-Hartl 2009; Sharma *et al.* 2009). Some of these chaperone families are conserved across the three domains emphasizing their importance for cell viability and survival.

A subset of molecular chaperones interacts with nascent chains cotranslationally to ensure proper folding of their substrates. Folding of the nascent chain, however, begins in the ribosome exit tunnel where secondary structural elements can form (Woolhead *et al.* 2004; Kosolapov and Deutsch 2009). In addition, for some proteins (*E. coli* SufI, *S. cerevisiae* TRP3) the interaction between their Lys and Arg and regions of the exit tunnel or the presence of contiguous rare codons can decrease elongation rates promoting proper folding (Crombie *et al.* 1992; Lu and Deutsch 2008; Zhang *et al.* 2009). Cryoelectron tomography reconstructions showed that ribosomes in *E. coli* polysomes are in a staggered conformation such that the distance between consecutively translated, nascent chains was maximized (Brandt *et al.* 2009). Chaperones also interact with the ribosome to prevent protein misfolding. Trigger factor in prokaryotes binds near the nascent chain exit site forming a cradle that may protect the emerging polypeptide from illicit intermolecular interactions by shielding hydrophobic regions from solvent (Ferbitz *et al.* 2004; Merz *et al.* 2008). Interactions with downstream chaperones, such as Hsp70-Hsp40 system and Hsp60, ensure proper folding into the functional native state of the client protein (Hartl and Hayer-Hartl 2009; Kramer *et al.* 2009). In both prokaryotes and eukaryotes, approximately 10-20% of the proteome interacts with the Hsp70-Hsp40 chaperone system, while 10-15% of the proteome are obligate Hsp60 clients.

A subset of newly translated chains transiently interact with either Hsp70-Hsp40 or prefoldin and are then transferred to the Hsp60 chaperonins (GroEL/S in eubacteria and TriC in metazoans) for proper folding to their native states or for some eukaryotic clients, to Hsp90 (Hartl and Hayer-Hartl 2002). An isoform of Hsp90 is constitutively expressed in eukaryotic cells and, in conjunction with its co-chaperones, keeps bound obligate substrates (such as nuclear steroid receptors, telomerase, protein kinases) in a near-native, folding-competent state pending activation by phosphorylation, partner interactions or ligand binding (Mizuno *et al.* 2007; Sidera *et al.* 2008; Echeverria and Picard 2010; Taipale *et al.* 2010; Zuehlke and Johnson

2010). All of these cotranslational folding mechanisms emphasize the importance of proper folding and of preventing protein aggregation in order to maintain a functional proteome.

Environmental stresses, such as heat shock, affect proteostasis because they can destabilize proteins causing them to transiently unfold and populate aggregation-prone species. Protein quality control systems are primed to summarily suppress protein aggregation and refold misfolded proteins to their functional states. Hsp70-Hsp40 interact with hydrophobic regions that are solvent exposed in misfolded substrates preventing aggregation and, additionally, can deliver refractory substrates to Hsp60 chaperonins if further assistance is necessary (Langer *et al.* 1992; Schroder *et al.* 1993). The Hsp70-Hsp40 system is ATP-dependent and is present in organisms from Eukarya, Archaea and Eubacteria (Hartl and Hayer-Hartl 2002). Isoforms of Hsp70-Hsp40 are present in various cellular compartments where, along with their chaperone function in preventing protein misfolding and aggregation, they are involved in protein translocation across organelle membranes and protein disaggregation processes (Liberek *et al.* 2008; Endo and Yamano 2009). The N-terminal domain of Hsp70 directly binds specific hydrophobic regions of the substrate, sequestering these regions via a latch mechanism and, in this manner, allowing the protein to fold productively and preventing competing intermolecular interactions (Zhu *et al.* 1996). The diverse Hsp40 members recognize substrates and shuttle them to Hsp70 and, along with nucleotide exchange factors, modulate the ATP-regulated cycle of Hsp70 substrate binding and release (Li *et al.* 2009).

Hsp60 chaperonins are ATP-dependent, double-ring assemblies of multiple subunits that contain a central cavity wherein their partially-folded and misfolded substrates are confined for folding (Spiess *et al.* 2004). This family was originally discovered through its requirement for the folding of bacteriophage structural proteins (Georgopoulos and Hohn 1978; Tilly *et al.* 1981). Each subunit is divided into three domains: the equatorial or nucleotide binding domain, the central domain, and the apical domain. In all members of the Hsp60 family, the apical domain is responsible for substrate binding and recognition (Spiess *et al.* 2004; Horwich *et al.* 2007). In disease model systems, induction of Hsp chaperone expression increases cell survival. Overexpression of Hsp70 and Hsp40 reduced cytoplasmic aggregate formation and increased cell survival in a neuronal model of familial amyotrophic lateral sclerosis caused by mutant superoxide dismutase 1 (SOD1) (Takeuchi *et al.* 2002). Further, cell viability was significantly increased compared to controls after H_2O_2- or indomethacin-induced oxidative stress in rat small intestinal epithelial cells overexpressing of Hsp60 (Takada *et al.* 2010).

These studies demonstrated the role of Hsp70-Hsp40 and Hsp60 in preventing stress-induced proteotoxicity.

Chaperone networks responsible for intracellular aggregate clearance also play an important role in cell viability and in preventing cell senescence (Erjavec *et al.* 2007). Hsp70-Hsp40 work in conjunction Hsp100 to disaggregate and refold proteins in intracellular aggregates in plants (Hsp 101), bacteria (ClpB in *E. coli*) and fungi (Hsp104 in yeast) (Glover and Lindquist 1998; Zolkiewski 1999; Zietkiewicz *et al.* 2004). Hsp100 chaperones form oligomeric assemblies and belong to the AAA+ superfamily (ATPase associated with a variety of cellular activities). They contain two ATP-binding (AAA1 and 2) domains essential for quaternary structure and chaperone function. *E. coli* ClpB forms hexameric rings with the AAA domains forming top and bottom rings surrounding a central cavity (~16 Å) (Liberek *et al.* 2008). A full mechanistic description of the disaggregation and reactivation action of the Hsp70-Hsp100 system has not been elucidated, but important details are known. The current model, based on experimental observations, proposes that Hsp70 interacts with aggregates to disentangle misfolded substrates and then shuttles these substrates to Hsp100, where the substrate refolds after being unfolded and translocated through the Hsp100 central channel (Liberek *et al.* 2008). Both chaperones are required for efficient disaggregation and refolding: Hsp70 dissolved aggregates without Hsp100, but the released proteins did not refold productively (Zietkiewicz *et al.* 2006); while dissolution of aggregates was dependent on the presence of Hsp70 (Weibezahn *et al.* 2004). It is not clear whether this bi-chaperone system operates in mammals. However, it has been shown that overexpression of Hsp104 and Hsp27 (a small Heat shock protein chaperone) increased expression of endogenous Hsp70, reduced cell death and affected polyglutamine aggregate morphology and nuclear distribution in neuronal and mouse models of Huntington's disease (Perrin *et al.* 2007).

The small Heat shock proteins (sHsp) are ATP-independent chaperones that have also been implicated in facilitating disaggregation processes. IbpA and IbpB, sHsps in *E. coli*, are involved in inclusion body formation under conditions of prolonged heat shock (Jiao *et al.* 2005a). The disaggregation efficiency of the Hsp70-Hsp100 system increased for IbpA and B-containing aggregates versus aggregates consisting of only substrate (Matuszewska *et al.* 2005).

Intracellular aggregates are also cleared through proteolytic pathways. In prokaryotes, ClpAP, ClpXP, Lon and HslUV proteases are involved in misfolded protein and aggregate degradation. In eukaryotes, protein aggregates are degraded via the ubiquitin-proteasome system and chaperone-mediated autophagy (Liberek *et al.* 2008). Kaganovich *et al.*

investigated aggregate formation of a number of substrates that either misfolded or were amyloidogenic in yeast and mammalian cells (Kaganovich *et al.* 2008). Their experiments led to the identification of two distinct aggregate compartments: a juxtanuclear quality control compartment (JUNQ) and a perivacuolar compartment of insoluble protein deposits (IPOD) (Kaganovich *et al.* 2008). The formation of both compartments after stress conditions was dependent on microtubule integrity. The juxtanuclear compartment seemed to be composed of soluble misfolded proteins and proteasomes, which co-localized with this compartment once formed. The perivacuolar compartment, or IPOD, formed after prolonged periods of stress following the initial formation of the juxtanuclear compartment or when amyloidogenic substrates were expressed. Further, proteasomes did not co-localize with the insoluble protein deposit, pointing to the chaperone-mediated autophagy pathway as responsible for degrading these inclusions (Kaganovich *et al.* 2008). This study offered a new paradigm for aggregate proteolysis and clearance systems.

1. The small Heat shock protein chaperone family

The small Heat shock proteins are a family of ATP-independent protein chaperones that are present in organisms from all three domains. Members have been found in different subcellular compartments (Jakob *et al.* 1993; Lee *et al.* 1995; Narberhaus 2002). Given their wide-spread distribution, sHsps are involved in various cellular processes depending on the organism or cell type. However, most members have cytoprotective properties during thermal and oxidative stress (Narberhaus 2002; Nakamoto and Vígh 2007). The sHsps are not essential for cell viability in some organisms; temperature-sensitive phenotypes for null sHsps mutants in *E. coli* and *Neurospora crassa* were only observed when combined with knockouts for other non-essential chaperones or under starvation conditions, respectively (Narberhaus 2002). In humans, however, αA- and αB-Crys seem to play a more important role since missense mutations in either gene lead to autosomal-dominant congenital diseases. Mutations in αA- and αB-Crys were associated with autosomal-dominant juvenile-onset cataracts (Litt *et al.* 1998; Liu *et al.* 2006), while some missense mutations in αB-Crys were associated with desmin-related myopathy and dilated cardiomyopathy (Vicart *et al.* 1998; Pilotto *et al.* 2006).

Members of the sHsp family range in molecular mass from 12 to 43 kDa and assemble into large, dynamic homo- and hetero-oligomeric complexes *in vivo* of up to 800 kDa in size (Narberhaus 2002). The dynamic nature of these oligomeric complexes has been studied extensively in the case of α-Crys. Bova *et al.* showed subunit exchange between donor- and acceptor-fluorophore labeled human αA-Crys complexes via FRET. The rate of subunit exchange was strongly dependent on temperature, increasing at higher temperatures (Bova *et al.* 1997). Hydrophobic and polar interactions were involved in this process since the rate of subunit exchange decreased in solvents with low and high ionic strength; exchange rates were independent of pH and calcium concentration (Bova *et al.* 1997). Mammalian sHsps—Hsp27/Hsp25, αA- and αB-Crys—were also capable of exchanging subunits to form mixed oligomers (Bova *et al.* 2000). However, studies on plant sHsps showed a more conservative tendency for subunit exchange that was restricted to member of the same sHsp subclass (class I or II) (Helm *et al.* 1997).

Despite their highly dynamic nature, sHsp oligomers can be monodiperse or polydisperse. X-ray crystal structures for wheat (*Triticum aestivum*) Hsp16.9 and *Methanococus jannaschi* Hsp16.5 (MjHsp16.5) showed that the oligomers assembled into discrete dodecamer and 24-mer complexes, respectively (Fig. 1-1) (Kim *et al.* 1998; van

Montfort *et al.* 2001). Polydisperse complexes have been observed for human Hsp27, human αA- and αB-Crys and *E. coli* IbpA and B (Narberhaus 2002; Aquilina *et al.* 2003). There is no single ubiquitous quaternary structure for the ensemble of sHsp members and their oligomeric sizes range from monomers (*C. elegans* Hsp12.6) to multimers of up to 32 subunits (human α-Crys). Nonetheless, dimers are believed to be the building unit for larger oligomers based on known high-resolution structures from divergent sHsps (Kim *et al.* 1998; van Montfort *et al.* 2001; Narberhaus 2002). Bimodal binding orientations of the palindromic motif in the C-terminal extension of the α-crystallins to the β4/β8 edge of the α-crystallin domain of a dimeric partner have been proposed as a mechanism to increase polydispersity (Laganowsky *et al.* 2010). Shi *et al.* engineered *de novo* polydisperse oligomers from monodisperse MjHsp16.5 via the introduction of a sequence from human Hsp27 (Shi *et al.* 2006). This unique 14-residue peptide from human Hsp27 was inserted near the N-terminus of MjHsp16.5 and the insertion resulted in an increase in the oligomer size and a polydisperse distribution of oligomers. These experimental observations led the authors to conclude that the N-terminal domain (N-td) is responsible for polydispersity. Electron paramagnetic resonance spectra from bimane-labeled mutants showed that these polydisperse assemblies retained the dimeric building block observed in the crystal structure for WT MjHsp16.5. The high rates of sequence divergence in the N-terminal and C-terminal regions flanking the α-crystallin domain might have contributed to the quaternary structure variability observed for sHsps.

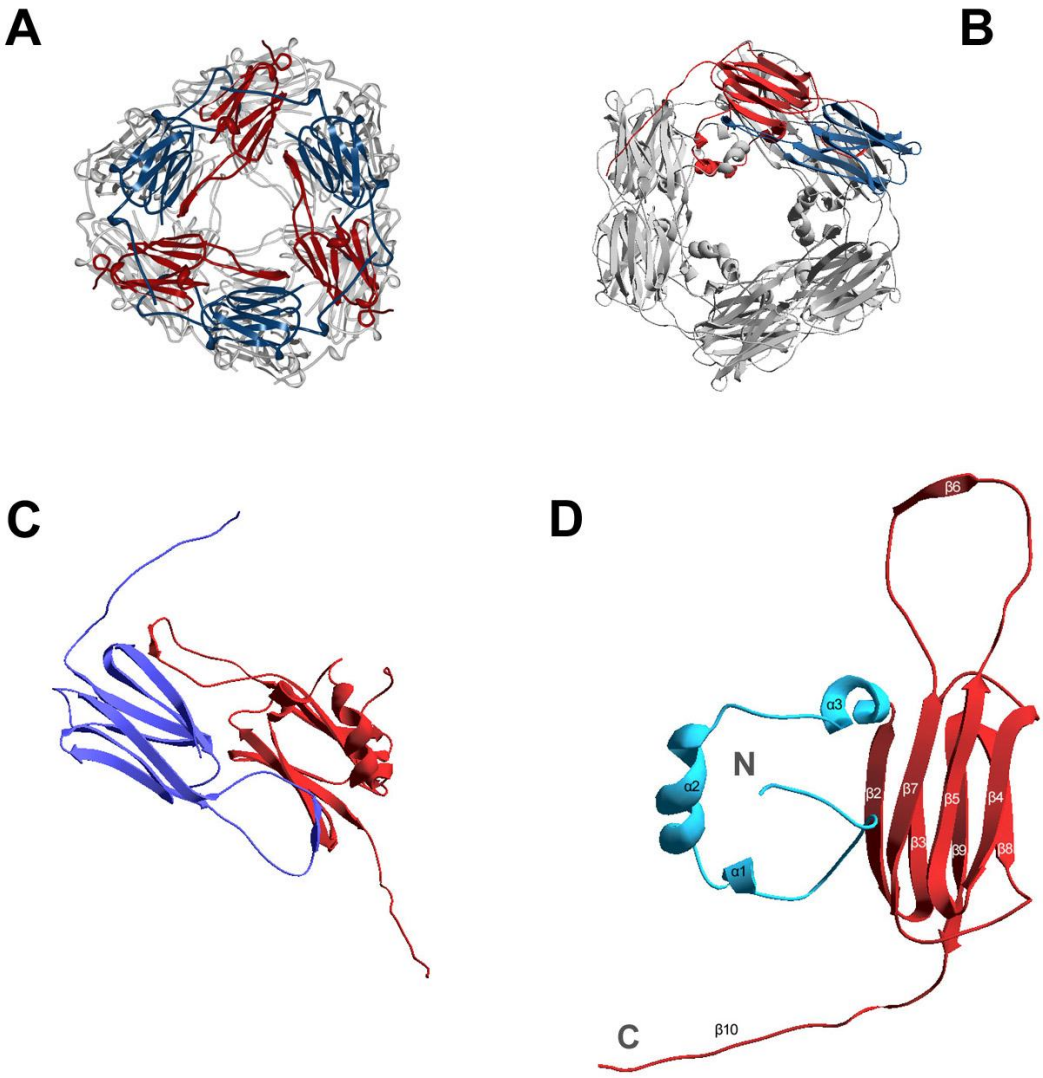

Figure 1-1: High-resolution structures of MjHsp16.5 and *T. aestivum* Hsp16.9.
A) Oligomeric structure of the 24-mer MjHsp16.5. Dimers are highlighted showing one partner in red and the other in blue. The β-sandwich organization of the α-crystallin domain is clearly visible. β6-strand swap between dimeric partners is also visible in this structure. The C-terminal extensions for the blue monomers reach across and interact with the α-crystallin domain of a neighboring dimer on the same plane, while the C-terminal extensions from the red monomers reach down and interact with another monomer (Kim *et al.* 1998).

B) Structure of the dodecameric wheat Hsp16.9. The dodecamer consists of two hexameric disks composed of three dimers. A dimer is highlighted showing one partner in red and the other in blue. The subunit in red has a resolved N-td while the subunit in blue does not. The resolved α-helical N-td interacts with an N-td from a monomer in the opposite disk. The C-terminal extensions of monomers with ordered N-tds (red) interact with the neighboring dimer in the same disk. The C-terminal extensions of monomers with disordered N-tds (blue) interact with the directly opposite dimers in the separate disk. The inter-subunit contacts between the differently-oriented C-terminal extensions are similar. The IXI/V motif in the C-terminal extension

(residues 147-149) interacts with a hydrophobic groove between strands β4 and β8 in the partner α-crystallin domain.

C) Ribbon diagrams of the dimer pair from wheat Hsp16.9. Notice the β6-strand swap between the partners' α-crystallin domains. Also, the different orientations of the C-terminal extensions for each partner are shown.

D) Structure of the ordered monomer from wheat Hsp16.9. The N-td (residues 1-42) is α-helical (shown in light blue). The anti-parallel β-sandwich organization of the α-crystallin domain is shown. The dimerization loop is between strands β5 and β7, with strand β6 interacting with the edge of a β-sheet of the α-crystallin domain of the dimeric partner. Secondary structure elements are designated in the diagram.

All sHsps conserve the ~90 amino acid "α-crystallin domain" that has an immunoglobulin-like, anti-parallel β-sandwich fold (van Montfort *et al.* 2001; Narberhaus 2002). All sHsp high-resolution structures elucidated to date showed that the α-crystallin domain β-sandwiches consist of strands β2-β9 (Fig. 1-1D) and the edges of the β-sandwich form hydrophobic grooves between β2/β7 and β4/β8 strands (Bagneris *et al.* 2009a). X-ray crystal structures for MjHsp16.5 and wheat Hsp16.9 showed that swapping of a single β-strand from one α-crystallin domain to complete the edge of one of the β-sheets from the partner α-crystallin domain mediated dimeric interactions (Fig. 1-1A and B) (Kim *et al.* 1998; van Montfort *et al.* 2001). Truncated αB-Crys mutants containing only the α-crystallin domain formed dimers in solution (Feil *et al.* 2001; Bagneris *et al.* 2009a). These results supported the role of the α-crystallin domain in dimer formation.

The α-crystallin domain is flanked by variable N-terminal and C-terminal regions that are highly divergent in amino acid sequence and size across all members (Fig. 1-2). The α-crystallin domain is involved in dimeric subunit-subunit interactions and chaperone activity, while the more hydrophobic N-td is involved in oligomerization and chaperone function and the polar C-terminal extension is involved in complex solubility and chaperone function (Narberhaus 2002; Reddy *et al.* 2006).

As mentioned previously, the sequence and length of the N-td vary greatly between the sHsps (Fig. 1-2) (Narberhaus 2002). The N-td has been implicated in the regulation of oligomerization and as a binding site for some aggregation-prone substrates in chaperoning interactions. Half of the N-tds of wheat Hsp16.9 were fully resolved in the crystal structure and interacted with monomers in opposite disks, while the remaining N-tds were not structured (Fig. 1-1B and C) (van Montfort *et al.* 2001). Truncated αA-Crys missing the first 20 residues formed oligomers of similar size as WT (between 24-32 subunits), while deleting the first 56 residues resulted in the formation of tetramers (Bova *et al.* 2000). The most striking examples that highlight the role of the N-td in both oligomerization and chaperone activity are the developmentally regulated sHsps from *C. elegans.* These sHsps (Hsp12.2, 12.3, and 12.6) consist of the α-crystallin domain and lack C-terminal extensions and, for Hsp 12.2 and 12.3, the N-tds as well; the α-crystallin domain of Hsp12.6 is flanked by a short N-terminal region of 25 residues (Kokke *et al.* 1998). Hsp12.6 forms monomers, while Hsp 12.2 and 12.3 form tetramers; all sHsps lack chaperone function *in vitro* (Kokke *et al.* 1998). The N-tds from wheat Hsp16.9 show different secondary structures and binding sites within the oligomers (Fig. 1-1B)

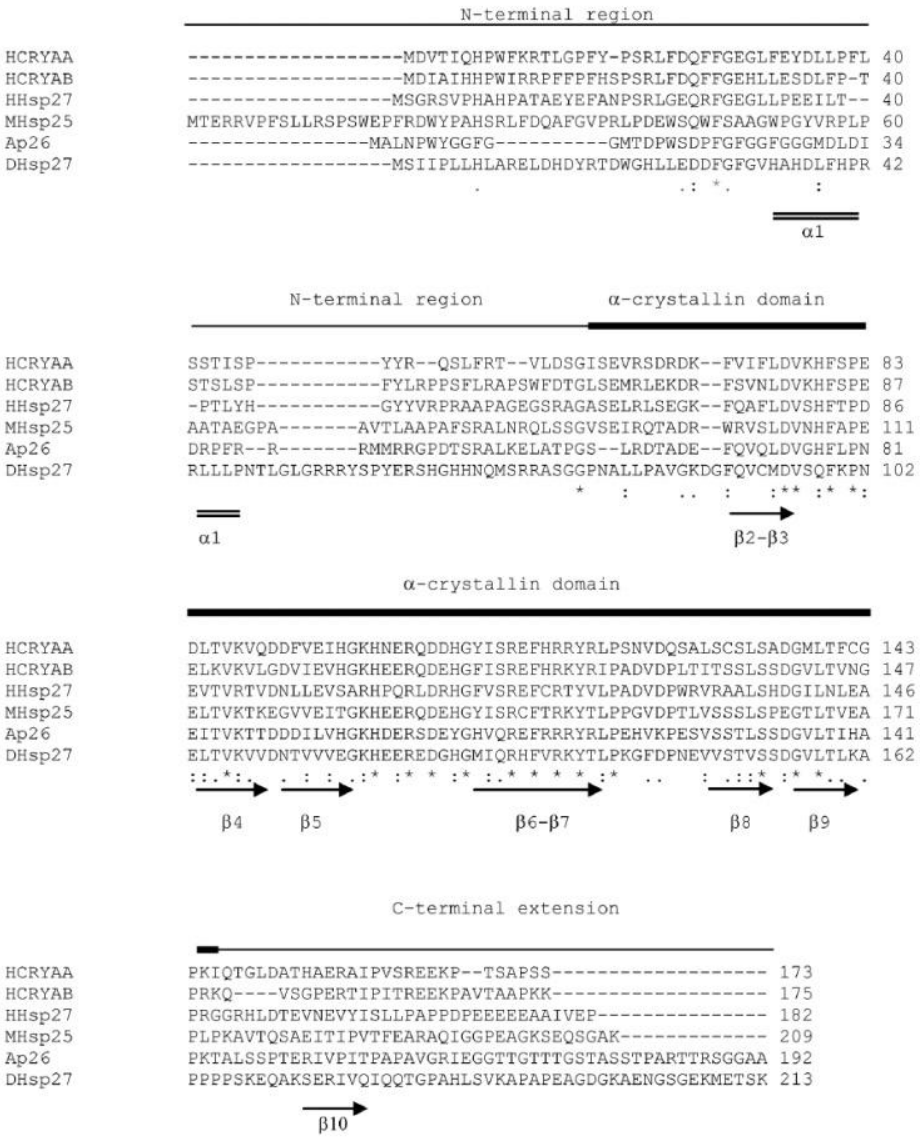

Figure 1-2: Sequence alignment for human αA- and αB-Crys, human Hsp27, murine Hsp25, *Artemia franciscana* p26, and *Drosophila melanogaster* Hsp27.
Sequences were aligned by CLUSTAL W (1.82). Alignments show the conserved α-crystallin domain sequence, along with the N-td and C-terminal extension. Conserved sencondary-structure elements are shown underneath the sequence alignment. Dashes indicate no residue; asterisks indicate conserved residues; colons indicate conserved substitutions; and periods indicate semi-conserved substitutions. Numbers on the right indicate residue number in the sequence. Reprinted with permission from (Sun and MacRae 2005).

The flexible C-terminal extension also varies in length and sequence across sHsps; however, it is polar in nature and contains the well conserved IXI/V sequence motif (Fig. 1-2) (Sun and MacRae 2005). The C-terminal extension is also involved in oligomer solubility. Addition of a Trp residue in the C-terminus of bovine αA-Crys decreased complex solubility, while the addition of charged and polar residues did not have any effect (Smulders *et al.* 1996). Further, the polar nature of the C-terminal extension is thought to contribute to the solubility of substrate-sHsp complexes, which are more hydrophobic than their free parent sHsps (Carver *et al.* 1995; Smulders *et al.* 1996). The IXI/V motif in the C-terminal extension is located near the α-crystallin domain. Close inspection of the crystal structures for wheat Hsp16.9 and MjHsp16.5 revealed that this region is part of a β-strand that binds to a hydrophobic groove between β4 and β8 strands in the α-crystallin domain of neighboring subunits (Kim *et al.* 1998; van Montfort *et al.* 2001; Pasta *et al.* 2004). Similar interactions were observed in the X-ray crystal structures for N-terminal truncated bovine αA- and human αB-Crys (Laganowsky *et al.* 2010). The IXI/V motif, therefore, seems to play a role in oligomer formation and may contribute to the diversity in quaternary structures observed for the sHsp family.

The role of the C-terminal extension in oligomerization of sHsp complexes varies in a sHsp-specific manner. In the case of mammalian αA-Crys, short truncations (< 10 residues) do not significantly affect the secondary or quaternary structure and the chaperone activity (Bova *et al.* 2000; Thampi and Abraham 2003). A truncation of the last 17 residues of human αA-Crys resulted in an increase in oligomer size and markedly decreased chaperone activity (Andley *et al.* 1996). A truncated version of mouse Hsp25 lacking its entire C-terminal extension conserved its quaternary structure and showed biased chaperone activity towards some substrates but not others (Lindner *et al.* 2000). In general, the C-terminal extension is involved in complex solubility, chaperone function and plays a significant role in oligomerization in monodisperse sHsps.

The chaperone activity of sHsps consists of passively binding and sequestering of aggregation-prone substrates, thus preventing protein aggregation (Haslbeck *et al.* 2005). These chaperones are ATP-independent and interact with a variety of substrates (Jakob *et al.* 1993; Nakamoto and Vígh 2007). sHsps seem to specifically recognize aggregation-prone species and do not interact with substrates in fully unfolded, stable molten globule or native states (Carver *et al.* 1995; Treweek *et al.* 2000). A common feature of the chaperone function of the sHsps is the dependence of chaperoning activity with temperature: chaperone activity increases with increasing temperatures (Raman *et al.* 1995; Haslbeck *et al.* 1999b; Narberhaus 2002; Jiao

et al. 2005b). The tertiary and quaternary structural elements involved in chaperone activity have been studied extensively in a variety of monodisperse and polydisperse sHsp chaperones. Given the dynamic nature of the oligomers and the existence of dimeric and oligomeric species in equilibrium in solution, one of the most researched questions has been whether the oligomer is the active chaperone state of the sHsps or whether dissociation of these oligomers into dimers is necessary for chaperone function. Studies have shown that both mechanisms are involved in chaperone activity in a sHsp-specific manner (Nakamoto and Vígh 2007).

Hsp26 from yeast (*Saccharomyces cerevisiae*) and human α-Crys are representative examples where the oligomer state is the active chaperone. Studies have shown temperature-dependent solvent exposure of hydrophobic inter-subunit regions in the oligomer without changes in the quaternary structure. The chaperone function of yeast Hsp26 is heat-modulated (Haslbeck *et al.* 1999b). Initial studies on yeast Hsp26 found that the activation of chaperone-function coincided with the reversible dissociation of the 24-mer complex into dimers (Haslbeck *et al.* 1999b). However, later studies showed that dissociation of the oligomer was not a requirement for chaperone function since disulfide-linked complexes of Hsp26 variants suppressed aggregation to the same levels as the WT oligomers (Franzmann *et al.* 2005). Structural changes resulting in the activation of high-affinity states competent for substrate binding involved rearrangements within intact oligomers (Franzmann *et al.* 2005). Augusteyn carried out a similar experiment with bovine α-Crys (Augusteyn 2004). He cross-linked bovine α-Crys with gluteraldehyde and isolated intra-molecularly cross-linked oligomer species that had the same dimensions as his native controls. The cross-linked oligomers suppressed the thermally-induced aggregation of β_L-Crys more efficiently than the native oligomers. His results showed that in the case of α-Crys dissociation was not required for chaperone function. These studies support the model wherein the oligomer is the active unit in chaperone function, and dissociation into dimers or subunit exchange are not required for chaperone function.

Representative examples of requisite dissociation of the oligomer for chaperone function can also be found in the sHsp chaperone literature. Wheat Hsp16.9 is found as a dodecamer in solution at 25 ºC (van Montfort *et al.* 2001; Wintrode *et al.* 2003). Increasing the temperature to 42 ºC resulted in the dissociation of the oligomers into dimers and a concurrent increase in chaperone function (van Montfort *et al.* 2001). Human Hsp27 is another example of requisite dissociation for substrate binding (Shashidharamurthy *et al.* 2005). Mammalian Hsp25/Hsp27 is phosphorylated *in vivo* by MAPKAP kinase 2/3 (Rogalla *et al.* 1999). Shashidharamurthy *et al.* showed that phosphorylation-mimics of Hsp27 (Ser→Asp

substitutions) resulted in dissociation of the oligomer into smaller multimers and enhancement of chaperone function (Shashidharamurthy *et al.* 2005). The authors proposed a thermodynamic model for the chaperone interactions between sHsps and substrates that is comprised by three coupled equilibria: the folding equilibrium for the substrate, the equilibrium between the inactive and active states of the sHsp chaperone, and the formation of the substrate-chaperone complex equilibrium. Further, the authors suggested that the ΔG_{UNF} for the substrate, the dissociation constant between inactive and active states of the Hsp27, and the binding constant for the active state of the sHsp contribute to the apparent dissociation constants calculated from their substrate binding isotherms. This thermodynamic model fits in with the observed ubiquitous temperature-dependence of the chaperone function of sHsps.

Basha *et al.* investigated the active chaperone species for class I and class II sHsp chaperones from *Arabiodopsis thaliana*, pea (*Pisum sativum*), and wheat (Basha *et al.* 2010). Class I and II sHsp are cytosolic sHsp groups in plants that share ~30% sequence similarity when present in the same species. Both classes are upregulated during heat shock stress in plants and are co-localized to heat shock granules that form in plant cell cytoplasms after heat stress (Kirschner *et al.* 2000). Class I chaperones form dodecamers, prominent examples are wheat Hsp16.9 and pea Hsp18.1, and they dissociate into chaperone-active dimers at higher temperature (van Montfort *et al.* 2001; Basha *et al.* 2006; Jaya *et al.* 2009). Basha *et al.* showed that class II sHsps also form dodecamers, but the oligomer is the active chaperone state. They noted that temperature-dependent structural changes, such as the solvent exposure of buried hydrophobic regions, were correlated with the chaperone activity of class II sHsps (Basha *et al.* 2010). Both classes of sHsps were able to suppress protein aggregation in similar *in vitro* assays demonstrating that both mechanisms effectively protect against protein aggregation.

An equally challenging problem has been to determine the location of the chaperone binding site or sites in the sHsp. A review of the literature revealed that all three domains—the N-td, the α-crystallin domain, and the C-terminal extension—interact with substrates during chaperoning interactions in substrate- and sHsp-specific manner. Jaya *et al.* incorporated a photo-activatible cross-linker at 32 individual sites along the entire sequence in the pea Hsp18.1 (Jaya *et al.* 2009). They used these modified Hsp18.1 dodecamers in suppression of aggregation assays with firefly luciferase and malate dehydrogenase as substrates. Both substrates interacted significantly with regions in the N-td of Hsp18.1, the β7-strand in the α-crystallin domain and the C-terminal extension. However, the relative abundance of cross-linked chaperone and substrate regions in all three domains varied between substrates, *i.e.*

substrates bound different sites on the chaperone. Ghosh *et al.*, using peptide pin arrays of human αB-Crys, identified seven regions spanning the whole sequence of the chaperone that interacted with physiological and non-physiological substrates (Ghosh *et al.* 2005). Both studies show that chaperone binding sites span the length of the sHsps regardless of the nature of the chaperone active species.

The N-td has been shown to be important for chaperone function in a variety of sHsps. Partial or full deletion of the N-td reduces chaperone activity in *E. coli* IbpB (Jiao *et al.* 2005b), yeast Hsp26 (Haslbeck *et al.* 2004), human αA-Crys (Kundu *et al.* 2007), and *Mycobacterium tuberculosis* Hsp16.3 (Fu *et al.* 2005). Hydrophobic regions in the N-td have been implicated in chaperone function. Mutating residues in the phenylalanine-rich (residues 22-28) region in the N-td of human αB-Crys reduced chaperone activity (Plater *et al.* 1996). Further, chaperone binding sites in the N-td and α-crystallin domains of bovine αA- and αB-Crys have been shown to also bind the hydrophobic fluorescent probe , bis-ANS [1,1'-bi(4-anilino)naphthalenesulfonic acid], which supported the role of hydrophobic regions in the chaperoning function of sHsps (Sharma *et al.* 1998). However, regions in the polar C-terminal domain also bind substrates. Alanine substitutions of glutamate residues in the C-terminal extension of mouse Hsp25 did not affect the structural characteristics of the mutants when compared to WT as measured by far-UV CD, intrinsic Trp fluorescence and size-exclusion chromatography (SEC). The mutants displayed reduced chaperone activity and thermostability compared to WT Hsp25 (Morris *et al.* 2008).

The nature of the sHsp-substrate complexes has also been studied in great detail. As stated previously, sHsps recognize specific aggregation-prone species of a variety of proteins (Carver *et al.* 1995; Ehrnsperger *et al.* 1997), bind these species, and form large sHsp-substrate complexes regardless of the quaternary structure of the chaperone active species (dimer or oligomer) (Chang *et al.* 1996; Haslbeck *et al.* 1999b; Stromer *et al.* 2003). These chaperone-substrate complexes were stable hours after formation (Ehrnsperger *et al.* 1997). Experiments coupling hydrogen/deuterium (H/D) exchange and mass spectrometry to label chaperone-substrate complexes showed that pea Hsp18.1 and wheat Hsp16.9 form dynamic complexes with two different substrates (firefly luciferace and malate dehydrogenase) (Cheng *et al.* 2008). The authors did not observe differential H/D exchange at the peptide level between free chaperone and the sHsp in the chaperone-substrate complexes leading them to conclude that the binding interactions between substrate and chaperone in the complex were highly dynamic. Further, the results indicated that substrate bound to either Hsp16.9 or Hsp18.1 had the same

conformation. These results indicate that different sHsps share the same substrate recognition mechanism (Cheng *et al.* 2008).

Unlike other chaperone families, such as the Hsp60 or Hsp70 families, the sHsps do not actively refold their substrates (Lee *et al.* 1995; Ehrnsperger *et al.* 1997). sHsps have also been shown to serve as a reservoir for folding-competent substrates for other refolding chaperones, such as Hsp70 (Ehrnsperger *et al.* 1997). For example, the *E. coli* sHsps, IbpA and B, were initially isolated as ubiquitous components of cell inclusion bodies, and were shown to jointly enhance the ability of the disaggregation chaperone system, Hsp100-Hsp70, to disaggregate protein aggregate *in vitro* and *in vivo* (Veinger *et al.* 1998; Matuszewska *et al.* 2005). These studies have established the role of the sHsp chaperones in the cell as a first-line defense against protein aggregation from heat shock or other environmental stresses. sHsps efficiently capture aggregation-prone species and form stable complexes wherein the substrates are ready for reactivation (Veinger *et al.* 1998). They are an integral part of the disaggregation systems important for clearing proteotoxic aggregate species and recycling amino acids for protein synthesis (Liberek *et al.* 2008). sHsps moonlight as regulators and chaperones of cytoskeletal proteins' stability and quaternary structure. Mammalian Hsp25/Hsp27, and αB-Crys interact with and stabilize cytoskeletal networks after stress (e.g. ischemia, hypoxia, oxidative stress, heat, etc.) (Djabali *et al.* 1997; Huot *et al.* 1997; Preville *et al.* 1998).

B. HUMAN EYE LENS PROTEINS AND CATARACT

Cataract disease is an age-related protein deposition disease of the crystallin proteins in the lens; its incidence increases sharply after the age of 50 (Bloemendal *et al.* 2004). Insoluble protein inclusions accumulate with age with a concurrent decrease in the concentration of soluble crystallin protein (Heys *et al.* 2007). The lens is a highly specialized tissue, whose cellular architecture and molecular composition have been under strong evolutionary pressure to maintain its transparent and refractive properties. As a result, mature lens fiber cells located along the visual axis lack most of the protein turnover and the protein quality control machinery described above, except for very high concentrations of the sHsp α-Crys. α-Crys is the only chaperone system in the mature lens fiber cells, where it retards aggregate formation during most of the adult life of the individual (Bloemendal *et al.* 2004; Lovicu and Robinson 2004).

1. The vertebrate lens

The vertebrate lens is a fine-tuning device for focusing images on the retina (Fig. 1-3A). The lens is part of a multi-component system—including the cornea, the ciliary body and the zonular fibers—that is responsible for the refractive and focusing power of the eye (Lovicu and Robinson 2004). The lens is a biconvex, colorless, and avascular tissue surrounded by a collagenous capsule. It is divided into three different regions: the anterior epithelial layer, the lens cortex and the lens nucleus (Fig. 1-3B). The anterior epithelial monolayer is composed of undifferentiated, cuboidal epithelial cells that are the precursors of the elongated fiber cells. Most of the lens cell mass is in the lens nuclear and cortical regions (Oyster 1999). The lens nucleus is the oldest, central region of the lens, while the cortical region surrounds the lens nucleus. Both regions are composed of elongated fiber cells that have lost their membrane-bound organelles, protein turnover capability, and contain high concentrations (250-400 mg/ml) of the ubiquitous crystallin proteins—α-, β-, and γ-crystallins (Bassnett 2002). The periphery of the lens cortex, however, contains cells that are undergoing maturation and still retain their organelles (Fig 1-3C).

The cellular and molecular architecture of the lens allow it to carry out its two functions: to remain transparent to visible light for transmission to the retina and to contribute to the refractive power of the eye (Oyster 1999). In the subsequent sections, I describe both cellular and molecular characteristics of the lens that contribute to its functions.

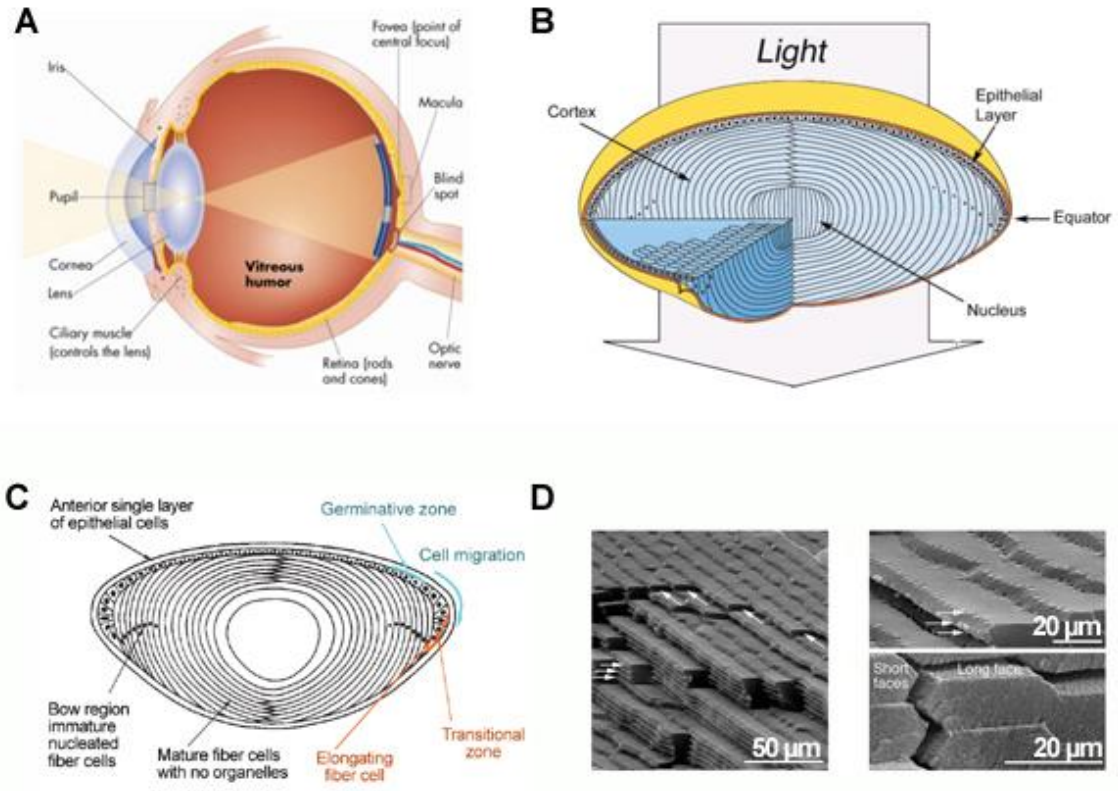

Figure 1-3: Schematic diagrams of the human eye and lens.
A) The lens is located in the anterior region of the lens behind the iris/pupil diaphragm. B) Diagram of the lens showing the anterior cuboidal monolayer of epithelial cells and the nuclear and cortical lens regions that comprise the majority of the lens cell mass. The primary and secondary fiber cells are located in the lens nucleus and cortex respectively (Modified from National Eye Institute, "Vision Problems in the US", 2001).

C) Schematic diagram of the lens highlighting the germinative and transitional zones in the epithelial layer and fiber cells at different maturation stages. Reprinted with permission from (Augusteyn 2008)

D) Scanning electron microscopy micrographs of fiber cells in the cortical region of the lens. The hexagonal shape of the fiber cells maximizes packing between cell layers and reduces intercellular gaps, thus reducing light scattering. Reprinted with permission from (Song *et al.* 2009).

2. Lens morphogenesis and growth.

The lens vesicle forms as an invagination of the ectodermal lens placode tissue (Fig. 1-4A). The anterior cells of the lens vesicle face the presumptive corneal tissue and aqueous humor, while the posterior cells face the optic cup (presumptive retina). The asymmetric exposure to differentiation signals triggers the elongation and differentiation of the posterior epithelial cells into primary fiber cells (Fig. 1-4B). These cells elongate and fill the lens vesicle lumen. During this process, they lose their major organelles and synthesize the crystallin proteins. At this stage the primary fiber cells compose the embryonic lens nucleus, while the anterior cells divide to cover the anterior half of the lens vesicle to become the epithelial layer of the lens, assuming a cuboidal shape (Fig 1-4B). This arrangement between these two specialized cell populations is maintained for life (Fig. 1-4C and D) (Oyster 1999; Lovicu and Robinson 2004).

The lens continues to grow by subsequent addition of secondary fiber cells on top of the embryonic nucleus; this process continues throughout life, although at different rates depending on the age of the individual (Augusteyn 2008). The anterior epithelial cells divide at the germinative zone pushing the cells at the periphery into the transitional zone of the anterior epithelia located at the lens equator (Fig. 1-3C). Epithelial cells in the transitional zone begin to elongate and differentiate to become the long ribbon-like secondary fiber cells of the lens cortex (Figures 1-4C and 1-3C). Like their nuclear counterparts, differentiation of secondary fiber cells consists of elongation and increased synthesis of the highly soluble crystallin proteins (Fig. 1-4D). Maturation results in the loss of membranous organelles and ribosomes (Kuwabara 1975). Mature fiber cells are thus incapable of further division and of protein turnover (Oyster 1999; Lovicu and Robinson 2004).

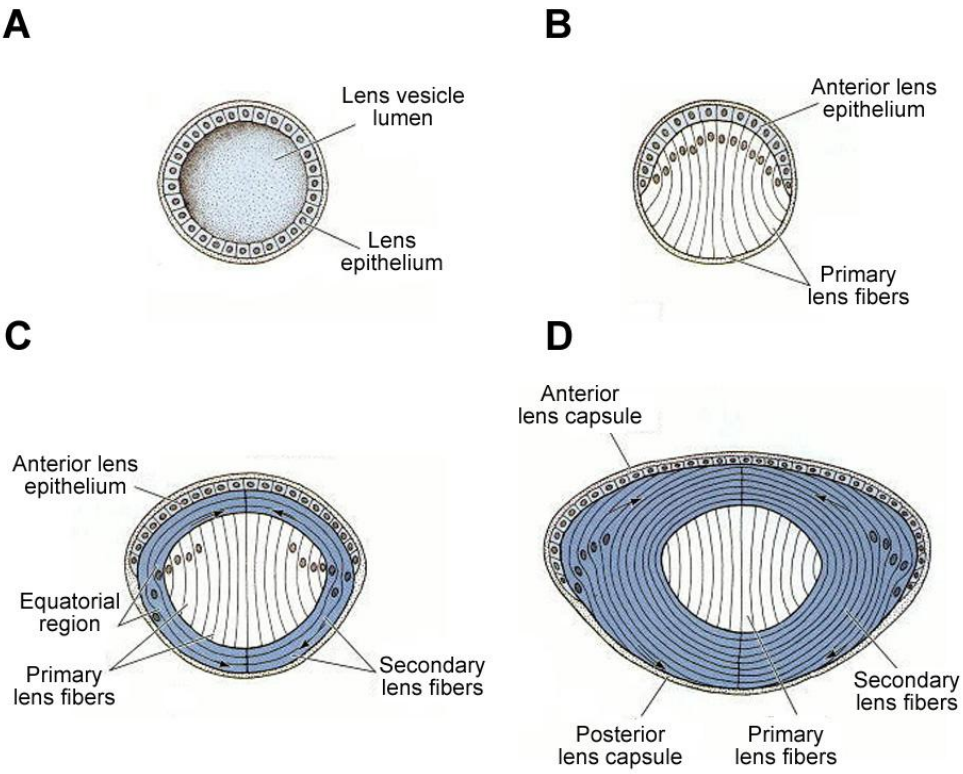

Figure 1-4: Embryonic lens morphogenesis.
A) The lens vesicle has a lumen surrounded by ectodermal epithelial cells. B) Differentiation signals from the optic cup trigger the elongation and differentiation of the posterior epithelial cells of the lens vesicle. Posterior cells elongate to fill the lens vesicle lumen. These elongated cells become the primary fiber cells, degrade their organelles and nuclei and overexpress the lens crystallins. The primary fiber cells constitute the nuclear region of the embryonic lens. The cells facing the presumptive corneal tissue divide to cover the anterior portion of the embryonic lens and become the anterior epithelial monolayer of the lens. C) The lens nucleus grows by the addition of secondary fiber cells, which originate from the elongation and differentiation of epithelial cells in the equatorial transitional region of the lens. D) The lens cortex expands by continuous addition of secondary cells to the periphery. Modified from (Gilbert 2006)

3. Lens transparency

Lens transparency is achieved through a combination of several morphological and molecular processes that occur in the lens cortical and nuclear regions. Transparency in the lens depends on reducing the local variation in refractive index to prevent light scatter along the visual axis of the lens. In the cortical regions of the lens, the regular array of the hexagonal organelle-free lens fiber cells reduces intercellular spaces and thus minimizes light-scatter (Fig. 1-3D). This cell arrangement compensates for the differences in refractive index between the cytoplasm and the cell membrane (Michael *et al.* 2003)

Light transparency in the lens nuclear region is also achieved through the programmed degradation of membrane-bound organelles during fiber cell differentiation, which have a higher refractive index than the cell cytoplasm (Michael *et al.* 2003). Cell membranes in the nuclear region have a lower refractive index than fiber cell membranes at the periphery of the lens cortex (Michael *et al.* 2003; Tholozan and Quinlan 2007). The fiber cells in the nuclear region also have high concentrations of the crystallin proteins, which in turn increase the refractive index of the fiber cell cytoplasm to levels similar to their surrounding cell membranes (protein content accounts for 37% of the wet weight of the lens nucleus) (Van Heyningen 1972; Michael *et al.* 2003; Bassnett 2009). The high concentrations (250-400 mg/ml) of the crystallin proteins result in a glass-like uniform density of the lens cytoplasm caused by the short range order of the crystallin proteins that reduces light scattering (Delaye and Tardieu 1983). Short range order could be established by a combination of repulsive Coulombic interactions and weak heterologous and homologous attractive interactions between crystallin proteins in their native states (Koenig *et al.* 1990; Stevens *et al.* 1995; Ponce and Takemoto 2005; Stradner *et al.* 2007; Takemoto and Sorensen 2008). At these high concentrations, protein crystallization is avoided by the inherent polydispersity of the mixture of different crystallin proteins (α-, β-, and γ-crystallins).

Given the pivotal role these crystallins play in lens transparency and how their short range order contributes to the refractive power and transparency of the lens, it is important that they remain stably folded for the lens to carry out its function. Disruptions to the uniform cytoplasmic density (e.g. large changes in refractive indices due to either phase separation or the population of large protein aggregates) in the lens fiber cells or disruptions in the packing of the fiber cells (e.g. intercellular gaps) would cause light scatter along the visual axis decreasing lens transparency (Ponce *et al.* 2006; Takemoto and Sorensen 2008). Destabilization and

irreversible aggregation of the crystallin proteins has been linked to lens opacification and the development of cataract disease (Sharma and Santhoshkumar 2009).

C. THE UBIQUITOUS CRYSTALLINS OF THE VERTEBRATE LENS

The ubiquitous crystallins, α-, β, and γ-crystallins, constitute approximately 90% of the protein content in mature fiber cells (Oyster 1999). They are present in all vertebrate lenses although their relative distributions vary between species (Bloemendal *et al.* 2004). They are members of two distinct protein families: α-crystallin belongs to the sHsp family of protein chaperones; β- and γ-crystallin belong to the βγ-crystallin superfamily (Ingolia and Craig 1982; Breitman *et al.* 1984; Wistow and Piatigorsky 1988; de Jong *et al.* 1993). Their expression is regulated by lens-specific transcription factors that control the spatiotermporal expression of these proteins during lens morphogenesis and growth (Cvekl and Duncan 2007).

1. The βγ-crystallins

The β- and γ-crystallins are structural proteins in the lens since their packing in fiber cells contributes to the short range order, which is important for lens transparency in the nuclear region (Delaye and Tardieu 1983; Stradner *et al.* 2007). The βγ-crystallins are mostly confined to the lens, but expression has also been detected in the nuclear layer of the murine retina for both groups, and in the inner segments of retinal photoreceptors for the β-crystallins in mice (Xi *et al.* 2003a). Their tertiary structure consists of four intercalated Greek key motifs organized into two domains (Fig. 1-5A). The γ-crystallins are monomeric; while the β-crystallins are oligomeric (i.e. they are isolated from the lens as dimers, tetramers, hexamers, and octamers) (Zigler *et al.* 1980). Another structural feature that differs between β- and γ-crystallins is the presence of N-terminal and C-terminal extensions (basic β-crystallins only) in the β-crystallins (Jaenicke and Slingsby 2001).

The two-domain, four-Greek key organization in this family is thought to be due to tandem gene duplication and fusion events of a single Greek key motif that occurred prior to vertebrate divergence (Lubsen *et al.* 1988). Higher sequence similarity between motifs 1 and 3 and between motifs 2 and 4 supports this view (D'Alessio 2002). A single Greek key motif ancestor has not been identified, but the gene architecture of the β- and γ-crystallin genes also supports this gene duplication model (Jaenicke and Slingsby 2001). In the β-Crys genes (*Cryb*

in humans), each Greek key motif is encoded by individual exons, while in most of the γ-Crys genes (*Cryg* in humans) each single domain (2 Greek key motifs) is encoded by a single exon. The evolutionary intermediates between these two divergent groups are the γN- and γS-Crys, which have hybrid gene structures from the β- and γ-Crys groups (Wistow *et al.* 2005).

The two intercalated Greek key motifs form 2 extended β-sheets that interact to form a β-sandwich or immunoglobulin-like fold at the single domain level (Slingsby and Clout 1999; Bloemendal *et al.* 2004). In this conformation, each Greek key motif has 4 β-strands (strands a-d); the third strand from each motif is swapped with the paired partner (8 β-strands total per domain) (Fig. 1-5B). The βγ-crystallins are also characterized by the presence of a highly evolutionarily conserved β-hairpin that packs over the β-sheet and contributes to the stability of the domain (Slingsby and Clout 1999). A Tyr corner is conserved within each domain in some of the βγ-crystallins and has the conserved sequence LXPGXY. In the βγ-crystallins, it consists of a Tyr residue between strands c and d in Motifs 2 and 4. The hydroxyl group on this Tyr makes H-bonds to a backbone amide and carbonyl groups at the n - 4 residue preceding this Tyr (n = Tyr) (Hemmingsen *et al.* 1994). Bagby *et al.* have proposed the conserved Tyr corner as the folding nucleus of the Greek key β-sandwich domain found in members of the βγ-crystallin family (Bagby *et al.* 1998).

These structural signatures of the domain organization of the βγ-crystallins, along with the complex topology of their tertiary structure, are thought to contribute to the observed high intrinsic stability of the native state of the crystallin proteins (Jaenicke and Slingsby 2001; MacDonald *et al.* 2005). Additional stabilization of the β- and γ-crystallins is provided by interdomain interface interactions; γ-crystallins form an intra-molecular interface, while β-crystallins have an inter-molecular interface. In all cases, the interface consists of a hydrophobic cluster flanked by polar pairs of residues from the N-terminal (N-td) and C-terminal (C-td) domains (Jaenicke and Slingsby 2001). The paired domain architecture of the β- and γ-Crys may be an evolved feature that increased the conformational stability of these proteins facilitating their recruitment as the structural proteins in the cytoplasm of the fiber lens cells (D'Alessio 2002).

The β-Crys monomers range in molecular mass from 22-28 kDa. They can be divided into two sub-groups based roughly on their pIs: acidic (βA1/βA3-, and βA4-Crys in humans) and more basic (βB1-, βB2-, and βB3-Crys in humans) (Lampi *et al.* 1997). Their expression is fiber cell-specific although they are expressed at different developmental stages (Bloemendal *et al.* 2004). In humans, dimeric βB2-Crys is the most abundant β-Crys and it is found in the

cortex and nuclear lens regions. Human βB1- and βB3-Crys are expressed *in utero* and are confined to the lens nuclear region (Lampi *et al.* 1998; Cvekl and Duncan 2007).

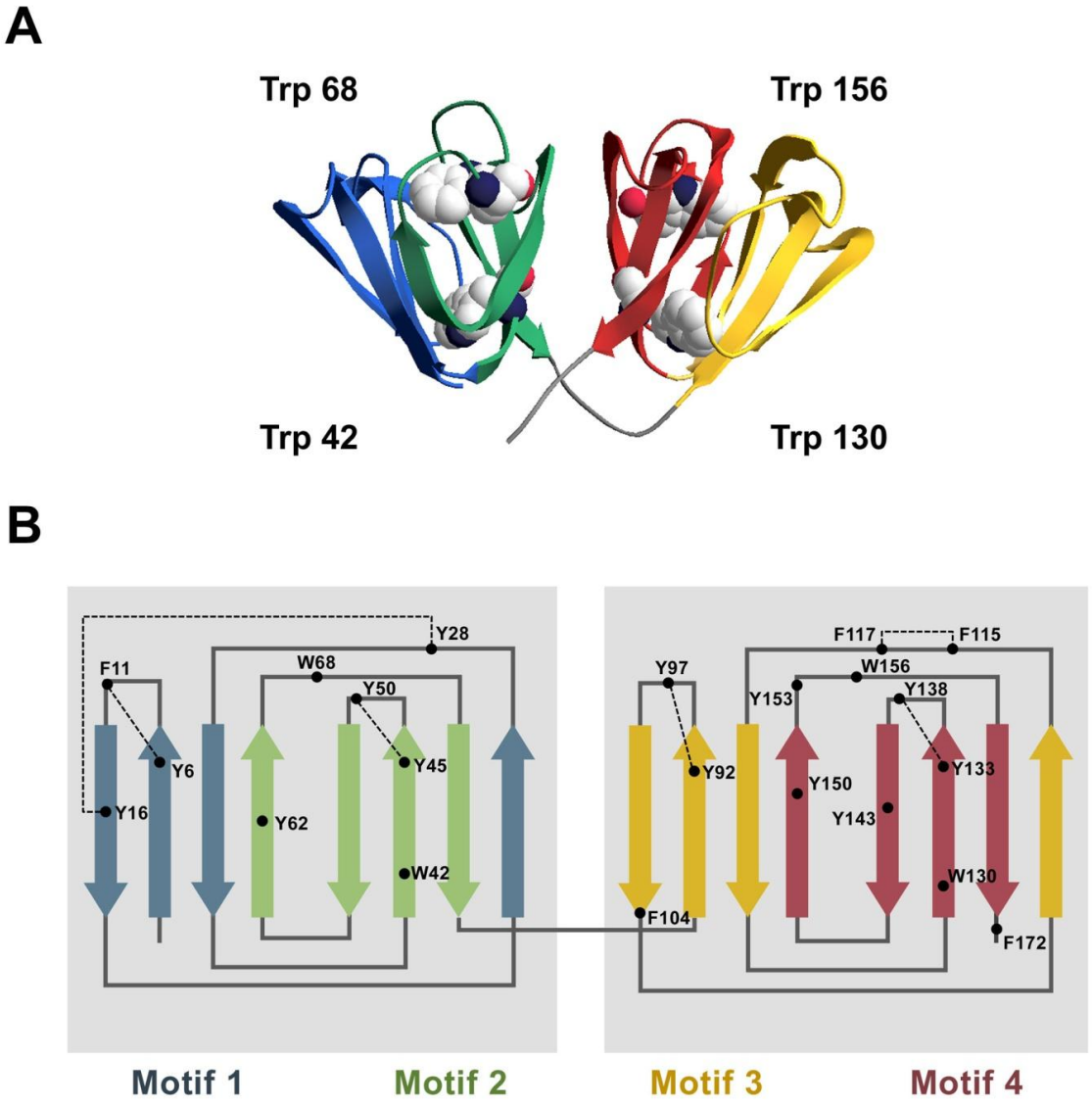

Figure 1-5: Crystal structure and topological diagram of human γD-Crys**.**
A) Crystal structure of human γD-Crys color-coded to show the position of all four Greek key motifs. The four highly-conserved Trp residues are shown [Protein Data Bank (PDB) ID: 1HK0]. B) Topology diagram showing the β-strands for each Greek key motif. The positions of the aromatic residues in human γD-Crys are shown. Dashed lines show putative aromatic pair interactions.

In humans, there are two groups of γ-crystallins: the mammalian-specific γA-γF group and γS-Crys. They are monomers that have an approximate molecular mass of 20 kDa. The most abundantly expressed γ-crystallins in human lenses are γD-, γS- and γC-Crys, which are 7%, 9%, and 11% of the crystallin proteins in young human lenses (Lampi *et al.* 1997; Robinson *et al.* 2006). γA- and γB-Crys are expressed at very low levels in human lenses, while γE- and γF-Crys are pseudogenes in humans (Meakin *et al.* 1985; Siezen *et al.* 1987; Robinson *et al.* 2006). γD- and γC-Crys are expressed early in lens development and are, therefore, most abundant in the nuclear region of the lens; γS-Crys is abundant in the lens cortical region in human lenses (Siezen *et al.* 1987).

a. Fluorescence properties of the buried tryptophans in γ-crystallins

The quenching of tryptophan fluorescence after UV absorption is anomalous in the βγ-crystallins. Trp fluorescence is quenched in the native-state versus the unfolded state of the protein, a characteristic of all γ-Crys proteins studied (Wenk *et al.* 2000; Kosinski-Collins *et al.* 2004; Chen *et al.* 2009). Chen *et al.* have shown for human γD-Crys that rapid electron transfer from the excited Trp indole ring to its amide backbone results in the efficient quenching of the weakly fluorescing, strongly quenched Trp68 and Trp156 residues in each domain (Chen *et al.* 2006). Charged residues and bound water molecules in electrostatically-favorable locations in the vicinity of these strongly quenched Trps facilitate charge transfer. The intra-domain mechanism of quenching of Trp fluorescence in the native state is due to partial resonance energy transfer from the strongly fluorescing tryptophans (Trp42 and Trp130) to their weakly fluorescing counterparts (Trp68 and Trp156). Chen *et al.* later showed that a similar quenching mechanism was at play in murine γS-Crys since the conformations of all four Trp residues were similar to the conformations of Trps in human γD-Crys (Chen *et al.* 2009). This Trp quenching mechanism is very sensitive to the Trp ring conformation, the packing arrangement of nearby residues and the presence and orientation of buried water molecules proximal to the Trp ring (Vivian and Callis 2001; Chen *et al.* 2009). As a result, Trp fluorescence is a very sensitive indicator of the conformations of the γ-crystallins.

b. γD-crystallin

Human γD-Crys is the second most abundant γ-Crys member in the embryonic nucleus of the lens (Robinson *et al.* 2006). It is a 173 amino acid protein with a molecular mass of

approximately 20 kDa (Bloemendal *et al.* 2004). It is 71% identical in primary sequence to human γC-Crys (Wang *et al.* 2009). The elucidation of a high-resolution X-ray crystal structure of human γD-Crys (Basak *et al.* 2003) allowed extensive studies on the sequence and structural factors that confer high thermodynamic and kinetic stability to this protein (Fig. 1-5).

Human γD-Crys has served as the model for studying the aforementioned Trp fluorescence quenching mechanism present in the native state of β- and γ-Crys with known high-resolution structures (Chen *et al.* 2006; Chen *et al.* 2009). Other studies have utilized this protein to study the determinants of the high conformational stability of the γ-crystallins (Kosinski-Collins and King 2003; Kosinski-Collins *et al.* 2004; Flaugh *et al.* 2005b; Flaugh *et al.* 2005a; Mills *et al.* 2007). The unfolding pathway for this protein has also been modeled using molecular dynamics simulations (Das *et al.* 2010).

Human γD-Crys populated a stable, partially folded intermediate during equilibrium unfolding/refolding experiments at pH 7.0 and 37 ºC (Kosinski-Collins and King 2003). Equilibrium unfolding/refolding experiments with human γD-Crys triple-Trp mutants containing a single Trp residue (the remaining three Trps were mutated to Phe) showed that this intermediate had the N-td unfolded and the C-td folded (Kosinski-Collins *et al.* 2004). Studies on the isolated domains of γD-Crys further supported this conformational model. Both domains folded to native-like conformations *in vivo* (in *E. coli* cells) and *in vitro* after dilution out of high concentrations of denaturant (Mills *et al.* 2007). The isolated single N-terminal domain (γD-Ntd) was less stable than the isolated C-terminal domain (γD-Ctd) in equilibrium unfolding/refolding experiments (the C_M values were 1.7 M and 2.8 M GdnHCl, respectively) (Mills *et al.* 2007). Differential stability has also been reported for bovine γB-Crys and human γS-Crys isolated domains (Mayr *et al.* 1997; Mills *et al.* 2007). Interface interactions thus contribute to the conformational stability of γD-Crys (Flaugh *et al.* 2005b; Flaugh *et al.* 2005a). Comparison between the free energies of unfolding for the full-length γD-Crys and its isolated domains revealed that the interactions in the interface contributed a ΔG_{H2O} of approximately 4.2 kcal*mol^{-1} to the stability of full-length γD-Crys protein (Mills *et al.* 2007).

The interface of γD-Crys consists of a highly-conserved hydrophobic cluster (Met43, Phe56, Ile81, Val132, Leu145 and Val170) and two pairs of flanking polar residues (Gln54/Gln143 and Arg79/Met147) (Basak *et al.* 2003). Substituting residues in the hydrophobic cluster and the flanking polar pairs resulted in kinetic and thermodynamic destabilization of the N-td only (Flaugh *et al.* 2005b; Flaugh *et al.* 2005a). These results indicated that the interface of the C-td served as a nucleation center for the folding of the N-td

in full-length γD-Crys. Hysteresis between the unfolding and refolding transitions in equilibrium experiments was observed when γD-Crys was incubated for 6 h at 37 ºC. Increasing the incubation time to 24 h eliminated the hysteresis between the unfolding and refolding transitions (Flaugh *et al.* 2005a). Further investigation revealed that the transition most affected was the transition that corresponded to the unfolding of the N-td (Mills-Henry 2007). These results indicated the presence of a high kinetic barrier to unfolding of the N-td of γD-Crys (Flaugh *et al.* 2005a; Mills-Henry 2007). These results lent support to the view that interface interactions is γD-Crys contribute to both thermodynamic and kinetic stability of the protein (Mills-Henry 2007).

Detailed kinetic unfolding studies for γD-Crys were carried out by Mills-Henry (Mills-Henry 2007). Experiments showed that the kinetic unfolding transitions for γD-Crys unfolded in 5.5 M GdnHCl at 18 ºC were best fit to a three-state model. Chevron plot analysis of the unfolding rates at different GdnHCl concentrations indicated that the first transition, which to corresponded the unfolding of the N-td, had an extrapolated half-life in H_2O of 19 years at 18 ºC (Mills-Henry 2007). The second transition, which corresponded to the unfolding of the C-td, had an extrapolated half-life of 129 days. Such high kinetic stability against unfolding would allow γD-Crys to remain folded in the lens for most of the young-adult lifespan of the individual, barring the accumulation of destabilizing covalent damages.

Molecular dynamics simulations of the unfolding of γD-Crys in 8 M Urea at high temperature (425 K) using all-atom explicit solvent models have shown that interface interactions increase the stability of the N-td in the context of the full length protein (Das *et al.* 2010). In these simulations, the N-td unfolded first forming a partially folded intermediate with the N-td unfolded and the C-td folded. Comparison of the unfolding trajectories of the isolated C-td and the C-td in the full-length protein indicated that the β-hairpin formed by strands a and b in Motif 4 was the folding nucleus of the protein (Das *et al.* 2010). A non-native salt-bridge between Glu135 and Asp142 within this region promoted the formation of the putative folding nucleus by stabilizing the structure of the a-b β-hairpin in Motif 4 (Das *et al.* 2010).

While fully unfolded γD-Crys can refold back to its native state at pH 7.0 and 37 ºC in 1 M GdnHCl, equilibrium unfolding/refolding experiments showed that refolding the protein to lower final GdnHCl concentrations resulted in competitive protein aggregation (Kosinski-Collins and King 2003). Atomic-force microscopy (AFM) images showed that human γD-Crys partitions into a population of productively folded native species and off-pathway macromolecular aggregates (Fig. 1-6). Partially folded aggregation-prone species populated

during dilution out of high concentrations of denaturant into buffer formed fibril-like aggregates 5 min after dilution. These fibril-like species associated into large, amorphous aggregates that scattered light (Fig 1-6D-F). No further polymerization of the fibrils and fiber bundling were observed 2 h after dilution. Despite their fibrillar scaffold (Fig. 1-6C-F), these aggregates did not bind the amyloid-specific dyes, Congo Red or thioflavinT (Kosinski-Collins and King 2003). A similar competitive aggregation pathway was observed in equilibrium unfolding/refolding experiments with human γC-Crys (personal communication, Dr. Yongting Wang), but not in experiments with human γS-Crys (Mills *et al.* 2007).

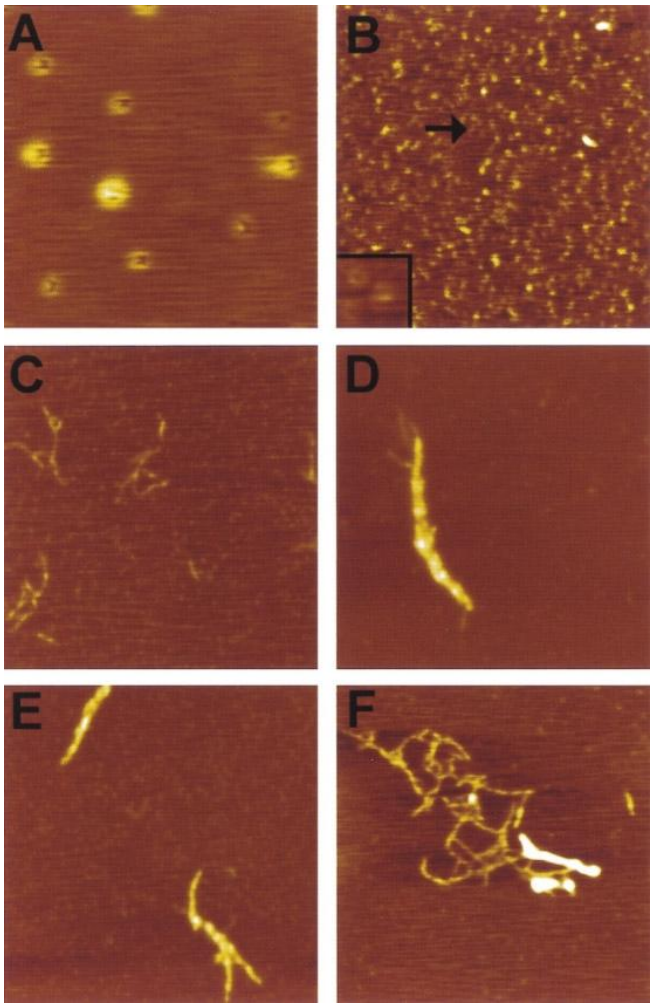

Figure 1-6: Atomic-force microscopy images of human γD-Crys aggregate.
AFM images of human γD-Crys aggregate species recorded at different times after dilution out of high concentrations of denaturant. A) Native γD-Crys; (B) 1 min, (C) 5 min, (D) 24 min, (E) 1h, and (F) 2 h after dilution out of high concentrations of denaturant into low concentrations of buffer. White areas represent high surfaces (5 nm); black areas represent low surfaces (0 nm). Inset in (B) shows refolded γD-Crys. Scanning area for (A) was 300 nm x 300 nm. For B-F, the scanning area is 1 μm x 1 μm. Reprinted with permission from (Kosinski-Collins and King 2003)

c. γS-crystallin

Unlike other γ-crystallins, γS-Crys contains a 5 residue N-terminal extension. γS-Crys is ubiquitous in vertebrate lenses, though its distribution in the lens and abundance relative to other crystallin proteins changes in a species-specific manner (Bloemendal *et al.* 2004). It is initially expressed post-partum and continues to be expressed throughout the life of the individual. Therefore, it is the most abundant γ-Crys protein in adult human lenses (Siezen *et al.* 1987). There is no high-resolution structure for human γS-Crys to date; the only structures available are the X-ray crystal structure of isolated human γS-Crys C-td and the NMR solution structure for murine γS-Crystallin (Fig. 1-7) (Purkiss *et al.* 2002; Wu *et al.* 2005). The amino acid sequences of the N-td and C-td of human γS-Crys are 30% identical and 47% similar (Mills *et al.* 2007).

The quenching mechanism present in the native state of γS-Crys was utilized by Wenk *et al.* to study the structural properties of bovine and human γS-Crys and their isolated N-terminal and C-terminal domains via Trp fluorescence (Wenk *et al.* 2000). Equilibrium unfolding/refolding experiments using GdnHCl as the denaturant at pH 7.0 and 20 ºC showed a highly-cooperative two-state transition for human full-length γS-Crys and its isolated domains. The authors suggested that the two-state transition might be due to comparable, though not equal, stabilities of the N-td and C-td of the γS-Crys at all pH values investigated. However, chevron plots for human γS-Crys and its isolated domains showed rollover (non-linearity) at low denaturant concentrations indicating the presence of kinetic intermediates (Wenk *et al.* 2000).

Mills *et al.* also showed that the N-terminal (γS-Ntd) and C-terminal (γS-Ctd) isolated domains of human γS-Crys were native-like and refolded *in vitro* upon dilution out of high concentrations of GdnHCl (Mills *et al.* 2007). Equilibrium unfolding/refolding experiments showed that the isolated γS-Ntd domain was less stable than the isolated γS-Ctd domain (C_M values equaled 1.7 M GdnHCl and 2.3 M GdnHCl, respectively). These results indicated that interface interactions contributed to the overall stability of the protein though not to the extent observed for bovine γB-Crys and human γD-Crys (Mayr *et al.* 1997; Flaugh *et al.* 2005a; Flaugh *et al.* 2005b). The interface of human γS-Crys is similar to that of γD-Crys except for a substitution of the highly-conserved Phe to Ile at position 56 in γD-Crys on the N-terminal side of the inter-domain interface (Mills *et al.* 2007). Flaugh *et al.* showed that a Phe→Ala

substitution at position 56 destabilized the N-td of human γD-Crys highlighting the importance of the buried hydrophobic cluster packing at the inter-domain interface (Flaugh *et al.* 2005a).

Human γS-Crys is less stable than human γD-Crys. It has lower C_M values and melting temperature than human γD-Crys under similar experimental conditions *in vitro* (Mills *et al.* 2007). Close inspection of the primary and tertiary structures of human γD- and γS-Crys and murine γS-Crys did not reveal any obvious differences that would explain the different stabilities of the human proteins (Mills *et al.* 2007). The most interesting difference is the potential lack of the conserved Tyr corner in the N-td of human γS-Crys since it is absent in the NMR solution structure of the murine γS-Crys N-td, which is highly homologous to its human homolog. Also, the crystal structure of the human C-terminal γS-Crys domain showed an irregular conformation of the Tyr residue in the Tyr corner. Both changes to the Tyr corners in each domain could contribute to the lower stability observed for human γS-Crys (Purkiss *et al.* 2002; Wu *et al.* 2005; Mills *et al.* 2007).

Mills-Henry showed that the kinetic stability (i.e. a high barrier to unfolding) of human γS-Crys was also lower than the kinetic stability of human γD-Crys (Mills-Henry 2007). Comparison between the unfolding rates of the isolated domains of γS-Crys with the full-length protein suggested that interface interactions may account for the increased kinetic stability of the full-length protein.

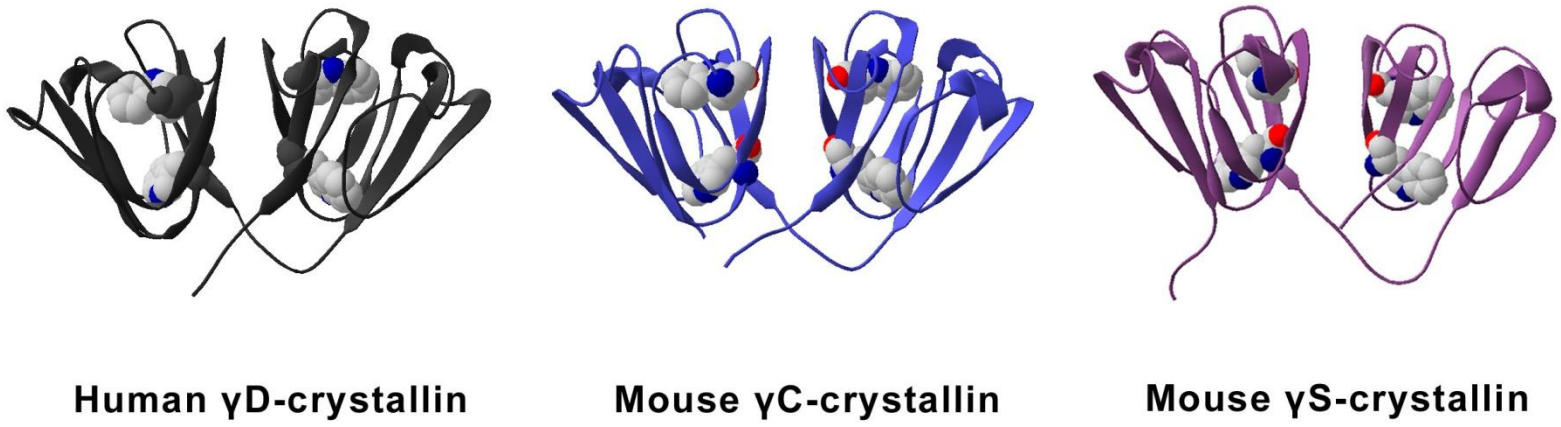

Figure 1-7: High-resolution structures for human γD-Crys, murine γC-Crys and γS-Crys
PDB IDs: 1HK0, 2V2U, and 1ZWM, respectively (Basak *et al.* 2003; Wu *et al.* 2005; Purkiss *et al.* 2007).

d. γC-crystallin

γC-Crys (173 amino acids) is the most abundant γ-Crys in the embryonic nuclear region of the lens (Robinson *et al.* 2006). As mentioned previously, it is expressed during embryonic development in the primary lens fiber cells. There is no high-resolution structure for human γC-Crys, but Purkiss *et al.* solved the solution NMR structure for the mouse homolog (Fig. 1-7) (Purkiss *et al.* 2007). The four highly-conserved Trp residues were present and human and mouse γC-Crys conserved the native-state buried Trp quenching mechanism described in Section C-1a in this chapter (Wang *et al.* 2009).

Unlike other γ-crystallins, human γC-Crys does not have high solubility (Purkiss *et al.* 2007). The lower solubility observed for human γC-Crys is due a substitution of the highly-conserved surface residue Arg79 to Cys. This substitution disrupts an inter-motif ion pair Asp21-Arg79 present in other members of the γ-Crys family. Purkiss *et al.* estimated that this Arg→Cys substitution decreased the magnitude of the dipole moment of the whole protein possibly affecting native-state solution interactions and decreasing solubility at high protein concentrations (Purkiss *et al.* 2007). Despite the comparatively lower solubility, human γC-Crys had higher conformational stability than its highly-soluble murine homolog (Purkiss *et al.* 2007).

Fu and Liang studied the thermodynamic stability of human γC-Crys (Fu and Liang 2002). Equilibrium unfolding experiments using Trp fluorescence to probe the conformational status of the protein showed that γC-Crys unfolds via a three-state mechanism (Fu and Liang 2002). A stable intermediate is also populated during equilibrium unfolding/refolding experiments of bovine γB-Crys [at pH 2.0, (Mayr *et al.* 1997)] and human γD-Crys [pH 7.0, (Kosinski-Collins and King 2003)], but not during similar experiments for human γS-Crys [at pH 7.0, (Wenk *et al.* 2000; Mills *et al.* 2007)]. For both proteins, this stable intermediate had a similar conformation with one domain folded and the other domain unfolded (Mayr *et al.* 1997; Kosinski-Collins *et al.* 2004).

2. α-crystallin

α-Crys is a member of the ATP-independent small Heat shock protein (sHsp) family of molecular chaperones (Ingolia and Craig 1982; de Jong *et al.* 1993). α-Crys constitutes 40% of the protein content in human lens fiber cells (Bloemendal *et al.* 2004). It serves as a structural protein and a protein chaperone in the lens. Lenticular α-Crys is a polydisperse hetero-oligomer composed of two subunits: αA- and αB-Crys (Bloemendal *et al.* 2004). These subunits share 60% sequence similarity and are encoded by two separate genes: *Cryaa* and *Cryab* (Bloemendal and de Jong 1991). The ratio of αA to αB changes with age, and in adult human lenses the ratio of αA to αB is 3:2 (Ma *et al.* 1998).

αA- and αB-Crys are expressed in all cell-types in vertebrate lenses, although expression is up-regulated during fiber cell differentiation (Bloemendal *et al.* 2004). αA-Crys expression is mostly lens-specific, with low expression levels observed in the retina in mice. αB-Crys is expressed in many mammalian tissues aside from the lens including the heart, brain, skeletal muscles, and liver (Graw 2009). Rat and human αB-Crys expression is under the control of a heat shock element in its promoter region which interacts with HSF4, the lens-specific heat shock transcription factor (Somasundaram and Bhat 2004).

Although both subunits are part of the α-Crys complex, mouse knock-out models of each protein have different phenotypes, which reflect in part their respective tissue-specific expression patterns. The αA-Crys null mice had smaller lenses than their WT littermates and developed cataracts at a younger age that consisted of insoluble inclusions that contained αB-Crys and small amounts of γ-crystallins (Brady *et al.* 1997b). The αB-Crys knock-out mouse had a shorter lifespan due to the development of myopathies, but their lenses were morphologically similar to their WT littermates and did not develop cataracts (Brady *et al.* 2001). Lenses from double-knockout mice showed aberrant fiber cell elongation and differentiation accompanied by the failure to regulate nuclei degradation in fiber cells in the lens cortex (Boyle *et al.* 2003). These studies on double-knockout mouse lenses indicated that α-Crys might also have a role in the regulation of lens fiber cell differentiation. The different phenotypes in the single and double gene-knockout mice are correlated to the involvement of αA-Crys and αB-Crys in other cellular processes. In this respect, αA- and αB-Crys are similar to other sHsp proteins.

a. α-crystallin structure

As stated previously, α-Crys isolated from the lens is a hetero-oligomer of αA- and αB-subunits (173 and 175 amino acids long, respectively) and has an average molecular mass of 800 kDa (Reddy *et al.* 2006). In humans, the ratio of these subunits changes with age with fetal lenses (32 weeks) having a 2αA:1αB ratio and lenses from 45-55 year-olds having a 3αA:2αB ratio in the water soluble fraction of whole lenses (Ma *et al.* 1998). Analysis of far-UV CD spectra showed that the secondary structure of bovine α-Crys consisted of 14% α-helix, 35% β-sheet, and the rest of the protein was designated as turns or random-coil (Farnsworth *et al.* 1997). The subunits have the basic sHsp tripartite primary sequence organization, with residues 63-144 and 68-148 encompassing the α-Crys domains αA- and αB-Crys respectively (Reddy *et al.* 2006).

The quest for a high-resolution X-ray crystal structure of αA- and αB-Crys monomers was, until recently, hindered by the inherent polydispersity of these oligomers. High-resolution X-ray crystal structures for N- and C-terminal truncated variants of human αB-Crys (Bagneris *et al.* 2009a; Laganowsky *et al.* 2010) and bovine αA-Crys (Laganowsky *et al.* 2010) were recently elucidated. Bagneris *et al.* elucidated the structure of the isolated α-crystallin domains from rat Hsp20 (residues 65-162) and human αB-Crys (residues 67-157) (Bagneris *et al.* 2009a). The isolated α-crystallin domains for both proteins formed dimers in the crystal lattice (Fig. 1-8A). Laganowsky *et al.* crystallized variants with truncations in the N-terminal and C-terminal ends of bovine αA-Crys (residues 59-163) and human αB-Crys (residues 68-162) (Laganowsky *et al.* 2010). Although this αB-Crys construct, like the truncated variant from Bagneris *et al.,* was missing the N-td, it included a significant portion of the C-terminal extension. This structure provided insight into the binding interactions of the C-terminal extension. Mass spectrometry analysis showed that truncated variants exhibited concentration-dependent oligomer assembly, with most of the oligomeric species consisting of dimers, tetramers, and hexamers. Larger oligomeric assemblies were also observed, but they were relatively less abundant. Laganowsky *et al.* proposed that the preferential population of smaller oligomers allowed crystallization of both proteins (Laganowsky *et al.* 2010).

The α-crystallin domain from monomers from each protein had similar secondary and tertiary structures to each other and to the α-crystallin domains from MjHsp16.5 and wheat Hsp16.9 (Fig. 1-8A). The domains were organized into Ig-like, anti-parallel β-sandwich fold composed of one three-stranded β-sheet and one four-stranded β-sheet (Bagneris *et al.* 2009a; Laganowsky *et al.* 2010). However, interactions contributing to dimerization in αA- and αB-Crys were different from those observed in the structures of non-metazoan sHsps. αA- and αB-Crys did not have a long enough β6-strand loop to swap

between dimeric partners, as is observed in MjHsp16.5 and wheat Hsp16.9 (*vide supra*). Instead, the β2/β7 edges from each partner were adjoining and formed a shared, inter-molecular hydrophobic groove at the dimer interface (Fig. 1-8A). Further, the three-stranded β-sheets from each partners interacted at the dimer interface to form a continuous inter-molecular anti-parallel β-sheet that formed the base for this shared groove (Bagneris *et al.* 2009a; Laganowsky *et al.* 2010). Both studies found a shift in the register of the residues from the β-strands at the inter-molecular interface in the shared β-sheet between αA- and αB-Crys dimers (Fig. 1-8B). The subunits in the αB-Crys dimer were closer together (smaller solvent accessible area) than the dimers for rat Hsp20 or bovine αA-Crys. Laganowsky *et al.* proposed that the ability to shift register could serve as a flexible 'ratchet-based mechanism' that could respond to solvent conditions and interact with different substrates.

The truncated αA- and αB-Crys variants constructed by Laganowsky *et al.* conserved some of the C-terminal extension (Laganowsky *et al.* 2010). These truncated C-terminal extensions in αA- and αB-Crys made different inter-subunit interactions. The differences in the directionality, and as a result in binding partners, were due to the flexibility of the hinge region between the α-crystallin domain and the C-terminal extension, and to the palindromic interacting region. The authors found, through sequence analysis of α-crystallins from other species, a conserved motif—E/D-R-X-I-P-V/I-X-R-E/D-E/D-K—that contained the palindromic sequence. These palindromic sequences, which include the IXI/V motif, interacted with the β2/β8 hydrophobic groove of the neighboring α-crystallin domain and made the same number of hydrogen bonds in both proteins, thus having no change in enthalpy between binding modes while gaining conformational entropy (Fig 1-8C and D). The authors propose that these two characteristics—the palindromic IXI/V motif-containing sequence and the flexible hinge region—contribute to the polydispersity of the α-crystallins since a similar palindromic motif is not present in the monodisperse MjHsp16.5 and wheat Hsp16.9.

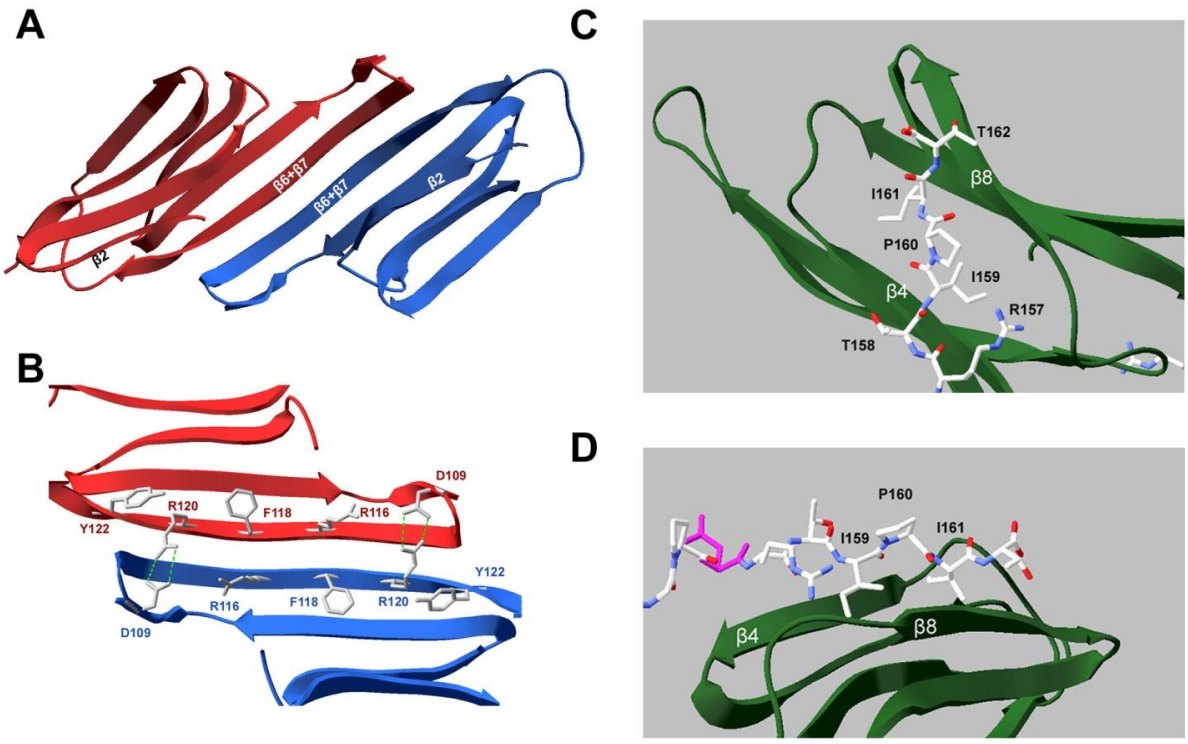

Figure 1-8: High resolution crystal structure for truncated human αB-Crys (PDB ID: 2WJ7 and 3L1G).
A) Ribbon diagram of the α-crystallin domain dimer of human αB-Crys (residues 67-157) from Bagneris *et al.* (PDB ID: 2WJ7). Individual subunits are shown in red and blue. The dimer interface is formed by interactions between the β6+β7 strand from each α-crystallin domain. β-strand edge interactions between both subunits form an extended inter-molecular β-sheet that is the base for a shared groove between the β2/β7 edges of each α-crystallin domain (Bagneris *et al.* 2009a).

B) Ribbon diagram showing residues present at the interface of the human αB-Crys α-crystallin domains (PDB ID: 2WJ7). Residues highlighted are D109, R116, F118, R120, and Y122. H-bonds between D109 from one partner and R120 from the other partner are shown in green. R120G mutations in human αB-Crys are associated with autosomal dominant cataract disease and desmin-related myopathies.

C) Stick diagram of the palindromic motif residues 157-162 (RTIPIT) in the C-terminal extension of the α-crystallin domain human αB-Crys interacting with the β4/β8 edge of the α-crystallin domain β-sandwich. The structure used is that from Laganowsky *et al.* (Laganowsky *et al.* 2010). PDB ID: 3L1G. D) Side view of the same diagram.

The inherent polydispersity of αA- and αB-Crys has also hindered lower resolution structural studies of their quaternary structures. Theoretical models that integrated experimental observations were published over the last 25-years to aid educated predictions of the quaternary structure of α-Crys and guide structural studies (Tardieu *et al.* 1986; Augusteyn and Koretz 1987). α-Crys isolated from human lenses shows a broader distribution of oligomer sizes (average size is 32 subunits) than recombinant human αA- and αB-Crys (Sun *et al.* 1997; Aquilina *et al.* 2003). Recently, relatively homogeneous samples of human αB-Crys (24 subunits) have facilitated three-dimensional reconstructions from negatively stained TEM images. Peschek *et al.* published this 3-D model at 20 Å resolution that resembled the quaternary structure for the 24-mer MjHsp16.5 (Fig. 1-9) (Peschek *et al.* 2009). The reconstruction showed a hollow oligomer with an outer diameter of 13.5 nm (Fig. 1-9A). It consisted of a protein shell, 2.5-4 nm thick, surrounding an inner cavity with a diameter of 8.5 nm (Fig. 1-9B). Similar to MjHsp16.5, several openings (of up to 3.5 nm in diameter) were visible in the protein shell.

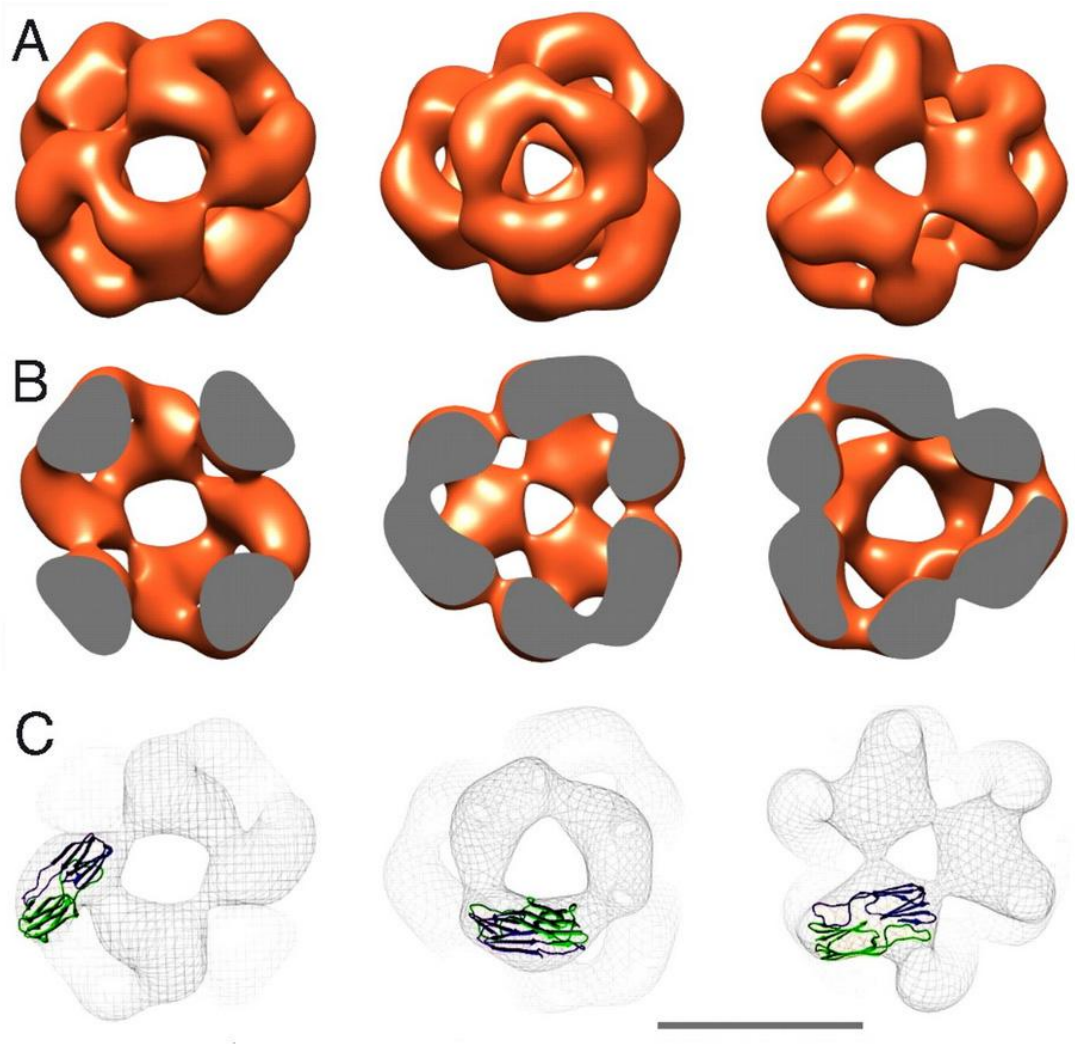

Figure 1-9: Human αB-Crys 3D reconstruction.
A) Surface representation of the 3D reconstruction model viewed, from left to right, from the 2-fold axis and the two 3-fold unequal axes. The authors noted that the density threshold applied was chosen to correspond to the molecular mass for a human αB-Crys oligomer consisting of 24 subunits. B) Cross-section representation highlighting the dimensions of the inner cavity. Orientations are the same as in (A). C) Mesh representation of the 3D reconstruction of human αB-Crys with the ribbon diagram of α-crystallin domain dimer pair from MjHsp16.5 superimposed in order to predict the arrangement of the α-crystallin domains in the αB-Crys oligomer. Scale bar corresponds to 10 nm. Reprinted with permission from (Peschek *et al.* 2009)

b. α-crystallin chaperone function in vivo and in vitro.

In his seminal study on α-Crys function, Horwitz established that lenticular α-Crys was a chaperone since it displayed similar aggregation suppression properties as the chaperonin GroEL-ES against the aggregation of a variety of substrates including the β- and γ-crystallins (Horwitz 1992). These observations proposed a novel role for α-Crys in maintaining lens transparency aside from contributing to crystallin packing in lens fiber cells. The presence of a protein chaperone in the cytoplasm of mature fiber cells would ensure basal levels of protein quality control that would maintain cellular homeostasis.

Studies on zebrafish (*Danio rerio*) *cloche* mutants have shown that αA-Crys is a chaperone *in vivo.* Zebrafish *cloche* mutants have aberrant hematopoiesis and vasculogenesis, along with cataracts. Goishi *et al.* investigated the causes of cataract in these mutants and found that cataracts in mutant embryos were due to γ-Crys aggregates and to failure to degrade nuclei in the lens fiber cells (Goishi *et al.* 2006). In these mutants, αA-Crys gene expression was down-regulated. Over-expressing exogenous αA-Crys in *cloche* mutants resulted in lens transparency and an increase in the concentration of soluble γ-Crys in lens homogenates. Further, Rao *et al.* showed that heating homogenate from the soluble fraction of monkey lenses lacking α-Crys at 64 ºC resulted in aggregate formation, while aggregate formation from intact lens homogenate (plus α-Crys) was not detected in assays measuring the optical density of the solution at 360 nm. Aggregates formed during these thermal-induced aggregation assays of lens homogenate lacking α-Crys consisted mostly of β-Crys (Rao *et al.* 1995). The authors also observed the formation and time-dependent accumulation of a high molecular weight (HMW) complex during thermally-induced aggregation assays of intact lens homogenate that eluted as a separate peak during SEC. These complexes consisted of α-Crys and β-Crys and were only formed during heating of intact lens homogenate and not from lens homogenates lacking α-Crys. The findings from both studies mentioned above indicate that α-Crys has chaperone function in the lens as it prevents irreversible protein aggregation of the its physiological substrates *in vivo* (Goishi *et al.* 2006) and *ex vivo* (Rao *et al.* 1995).

The chaperoning mechanism of α-Crys has been an intense area of research since the observations made by Horwitz (Horwitz 1992). *In vitro* assays have consisted of single substrate and chaperone systems where aggregation in the absence or presence of α-Crys was measured by changes in optical density at a single wavelength (usually between 350-500 nm). Substrate aggregation was usually initiated by decreasing the pH, increasing the temperature, refolding out of high concentrations of chemical denaturant, adding a reducing agent, and UV-irradiation (Reddy *et al.* 2006). A variety of non-lenticular model substrates have been used to study the chaperone function of α-Crys.

α-Crys has been shown to prevent aggregation by recognizing and binding aggregation-prone species to form stable, higher molecular weight complexes. Carver *et al.* carried out a comprehensive comparative study of the substrate specificity of bovine α-Crys. They found that α-Crys interacted with aggregation-prone molten globule species, but not with partially folded stable intermediates that were substrates for GroEL-ES and DnaK-J (Carver *et al.* 1995). Subsequently, Rajamaran *et al.* focused on stable and aggregation-prone molten globule intermediates of apo-α-lactalbumin that were populated under different buffer conditions (Rajaraman *et al.* 1998). Their results agreed with Carver *et al.* in that α-Crys recognized and bound aggregation-prone molten globule species of apo-α-lactalbumin and did not recognize stable molten-globule species (Rajaraman *et al.* 1998).

In line with observations from other sHsps, α-Crys displays temperature-dependent chaperone activity. Both human αA- and αB-Crys show an increase in chaperone activity with temperature, although the chaperone activity of αA-Crys shows a more drastic increase than αB-Crys. In the case of αA-Crys, increasing the temperature resulted in an increase in exposed hydrophobic regions that interacted with bis-ANS (Reddy *et al.* 2000). These observations have implicated hydrophobic interactions in the chaperone function of α-Crys (Reddy *et al.* 2006). α-Crys oligomers also undergo an irreversible increase in size with increasing temperature over 40 ºC, doubling in size and mass when incubated at approximately 60 ºC (Putilina *et al.* 2003; Michiel *et al.* 2008). Heating αB-Crys at temperatures above 60 ºC resulted in protein precipitation (Michiel *et al.* 2008). The rate of subunit-exchange also increases with temperature, and it has also been shown to correlate with increased chaperone activity for bovine α-Crys (Putilina *et al.* 2003). However, Michiel *et al.* carried out a detailed biochemical and structural study comparing WT and the congenital cataract mutant R120G αB-Crys, and showed that the mutant formed larger oligomers than WT at all temperatures assayed. The rate of subunit exchange was higher for R120 mutants and these mutants had impaired chaperone function (Michiel *et al.* 2008). The authors proposed that this discrepancy in the effect of increased subunit exchange on chaperone activity could be due to disruption of dimer interface interaction in the R120 αB-Crys mutants. Monomers, rather than the canonical dimers observed for other sHsps, would be the exchange unit in the mutant αB-Crys. In support of this theory, Benesch *et al.* have shown that the α-Crys polydisperse oligomer population exists in equilibrium with dimers in solution. Refolding αA- and αB-Crys from a fully denatured state resulted in the formation of larger oligomers than native controls. Tandem mass spectrometry of these refolded oligomers showed that the basic exchange unit was a monomer. However, these refolded oligomers had increased chaperone activity against the aggregation of apo-α-lactalbumin (Benesch *et al.* 2008). Previous studies had shown that R120G αB-Crys mutant had aberrant chaperone function in that it precipitated after binding substrates *in vitro* (Bova *et al.* 1999) and was localized to

aggregate inclusions *in vivo* (Simon *et al.* 2007). Both studies concurred in that the thermodynamic system of dynamic oligomers and dimers seems to be the mechanism by which chaperone activity is modulated and that the oligomer is the functional chaperone active species of α-Crys. Thus, disruption of the local interactions in the dimers would result in marked changes in the quaternary structure of α-Crys and consequently in chaperone activity.

Detailed thermodynamic studies using destabilized T4 lysozyme mutants as substrates have provided insight into the chaperoning mechanism of αA- and αB-Crys (McHaourab *et al.* 2002; Sathish *et al.* 2003). The group of T4 lysozyme mutants chosen comprised a spectrum of free energies of unfolding ranging from 5-10 kcal/mol, but they still retained a stable native-state conformation as evidenced by their X-ray crystal structures. McHaourab *et al.* found that both α-crystallins had two affinity binding modes, a high affinity and a low affinity mode, with different substrate binding capacities (McHaourab *et al.* 2002). As the authors noted, the use of the term 'mode' suggested the uncertainty as to how many binding sites there were on the chaperone. The authors proposed that these two binding modes allow the sHsps to act as 'sensors' and allows these chaperones to discriminate between proteins destabilized to different extents. Substrate would bind to the high affinity/low capacity modes, with subsequent binding events shifting to the low affinity/high capacity sites (McHaourab *et al.* 2002). Subsequent fluorescence spectroscopy studies revealed that the low and high affinity modes for human αA- and αB-Crys bound a specific region of the susbstrate T4 lysozyme species and that this conformer was predominantly unfolded (Claxton *et al.* 2008). Studies with βB1-Crys interface mutants showed that complex formation between monomeric species and αA-Crys induced dissociation of the dimer and subsequent unfolding of βB1 variants (Hassane *et al.* 2007). Extrinsic fluorescence spectroscopy studies of bimane-labeled βB2-Crys mutants with different ΔG_{UNF} showed similar results, but also found the population of a monomeric intermediate that was spectroscopically silent in intrinsic Trp fluorescence equilibrium unfolding/refolding experiments. These results indicated that the low and high affinity sites correspond to two distinct regions of the α-crystallins that bind to the same non-native species. In addition, these studies reinforce previous findings (Carver *et al.* 1995; Rajaraman *et al.* 1998) that although α-Crys can interact with different protein clients, it has the capacity to discriminate and select between on-pathway folding intermediates and potential aggregation-prone, off-pathway intermediates. α-Crys binds to a specific region of the aggregation-prone species.

Despite advances in the past 18 years, the chaperone mechanism of α-Crys has not been fully elucidated yet. There are many aspects of this mechanism that remain obscure such as the structure of the chaperone active species, a kinetic description of substrate-chaperone complex formation, structural reorganizations responsible for the drastic increase in size after substrate binding, the conformations of

the physiological substrates that are bound by α-Crys, and common substrate-binding regions on α-Crys. Numerous studies have addressed the latter point and identified binding regions in αA- and αB-Crys. Substrate binding sites in bovine αB-Crys were identified from alcohol-dehydrogenase—α-Crys complexes and spanned residues 57-69 in the N-td/α-crystallin domain junction and residues 93-107 in the α-crystallin domain (Sharma *et al.* 1997). As mentioned previously, Ghosh *et al.* carried out a more comprehensive study to identify binding regions using physiological and non-physiological substrates and found seven substrate interacting regions that were distributed across the entire αB-Crys sequence. Two of the peptides located in the α-crystallin domain were synthesized and suppressed the heat-induced aggregation of β_H-Crys *in vitro* (Ghosh *et al.* 2005). However, these regions were not the same regions identified by Sharma *et al.* highlighting the heterogeneity of substrate-binding regions in α-Crys [*vide supra,* (Sharma *et al.* 1997)].

α-Crys interacts with other lens proteins in lens fiber cells. BFSP1 and BFSP2 are IF (intermediate filament) proteins that co-assemble into lens-specific beaded-filaments in mature fiber cells (Maisel and Perry 1972; Ireland and Maisel 1989). The name 'beaded-filament' refers to the 'beads on a string' semblance of the native filaments isolated from fiber cells. Lens IFs provide intracellular support during mechanical stress from lens accommodation. BFSP1 and 2 can co-assemble, but their filaments do not resemble native beaded filaments. Addition of α-Crys to BFSP1 and BFSP2 resulted in beaded filaments that were similar to native beaded filaments (Carter *et al.* 1995). Wang and Spector showed that α-Crys stabilized actin filaments against depolymerizing agents and prevented thermally-induced aggregation of actin (Wang and Spector 1996). α-Crys localized to the leading edge of lamellipodia and co-localized with actin network at the tips of leading edges in migrating lens fiber cells isolated from porcine lenses (Maddala and Rao 2005). Work comparing lens microtubules from WT and double-knockout α-Crys mice lenses showed that α-Crys prevents thermally-induced tubulin aggregation and, in the lens it seems to interact with MAPs (microtubule-associated proteins) to stabilize microtubule structures (Xi *et al.* 2006). The *in vivo* chaperone function of α-Crys extends to stabilizing cytoskeletal elements necessary for fiber cell elongation, hexagonal cell morphology and for maintaining the ultrastructural integrity of the lens during accommodation.

αA-Crys co-localizes to centrosomes in dividing lens epithelial cells suggesting a role in regulating the cell cycle progression in these cells (Xi *et al.* 2003b). αA- and αB-Crys may also be necessary for proper lens epithelial cell differentiation into fiber cells. Andley and Reilly carried out histological studies on lenses from mice homozygous for the R49C αA-Crys congenital cataract mutation. They found lenses for R49C homozygous mutant mice lacked a lens bow region, where epithelial cells begin to elongate (Fig 1-3C), along with a posterior expansion of the germinative zone in the lens

epithelial layer. This indicated that the epithelial cells at the equatorial region failed to exit the cell cycle and differentiate into fiber cells (Andley and Reilly 2010). However, it remains unknown what role αA-Crys plays in regulating fiber cell differentiation.

D. CATARACT DISEASE

Cataract is the opacification of the lens that results from the impairment of light transmission through the lens due to visible light scatter (Abraham *et al.* 2006). It is the leading cause of blindness worldwide with 48% of cases being due to cataracts. Ninety percent of the cataract blindness cases occur in developing countries, where current treatments for the disease are inaccessible to most of the population. In developed countries, treatment of the disease places a heavy economic burden on health care systems (Resnikoff *et al.* 2004; Frick *et al.* 2007). Studies on the economic impact of eye diseases estimated that visual impairment and blindness in the United States imposed an annual financial burden of $5.4 billion (Frick *et al.* 2007).

There are two manifestations of the disease: congenital hereditary cataracts and mature onset or age-related cataracts. Congenital cataracts are rare and are typified by disease onset in early childhood. Mutations in genes involved in lens development (e.g. HSF4 and FOXE3) and genes for lens-specific cytoskeletal proteins (BFSP1 and BFSP2), gap junction and membrane proteins (GJA3, GJA8, and AQP0) and the crystallin proteins have been associated with congenital cataract formation (Hejtmancik 2008). Mutations in α-, β-, and γ-Crys genes are the more prevalent mutations implicated with congenital hereditary cataracts. *In vitro* studies have shown that mutations in the β- and γ-Crys proteins identified from congenital cataracts cases destabilize these proteins (Reddy *et al.* 2004; Moreau and King 2009). Moreau and King showed that congenital cataract mutations located in the hydrophobic core of human γD-Crys led to thermodynamic and kinetic destabilization of the protein (Moreau and King 2009).

Age-related cataracts are more prevalent and are characterized by an increase in the incidence of cataracts with age after the age of 50 (Bloemendal *et al.* 2004). In fact, 82% of cataract cases worldwide occurred in individuals 50 years or older (Resnikoff *et al.* 2004). Several longitudinal population-based studies (e.g. the Beaver Dam Eye Study, the Framingham Eye Study) have identified risk factors for age-related cataract disease. The major risk factors identified across all these studies were aging, smoking, diabetes, and UVB radiation exposure (Abraham *et al.* 2006). Recent population-based studies have identified novel risk factors for early onset (from 50-65 years old) of age-related cataracts such as corticosteroids intake, exogenous estrogen use, myopia and genetics (Abraham *et al.* 2006).

The current treatment for cataracts is cataract surgery, in which the majority of the lenticular mass is extracted via phacoemulsification, leaving the collagenous lens capsule in place with the anterior monolayer of undifferentiated epithelial cells still attached. An artificial intraocular lens is then inserted inside the lens capsule (Wormstone *et al.* 2009). Despite the effectiveness of the procedure, 20-40% of cataract surgery patients develop posterior capsular opacifications (PCO), or secondary cataracts, 2-5 years after surgery (Awasthi *et al.* 2009). PCO occurs when the residual lens epithelial cells differentiate and migrate towards the visual axis causing light scatter, thus blocking light transmission through the lens implant (Awasthi *et al.* 2009).

The most popular and effective treatment for PCO is Neodymium:YAG (yttrium aluminum garnet) laser capsulotomy, in which laser pulses are used to make holes in the capsule so as to detach the opacity located on the visual axis (Charles 2001). Several post-procedure complications have been documented including retinal detachment, implant lens damage, vitreous clouding, cystoid macular edema and macular holes (Steve 2001; Awasthi *et al.* 2009). These complications, along with the inaccessibility of YAG laser capsulotomy in developing countries, highlight the need to study the mechanisms for cataract formation and to develop more cost-effective treatments for the disease. West and Valmadrid have estimated that delaying onset of age-related cataracts by 10 years would result in a 14% decrease in the incidence of cataract disease along with a 50% decrease in the number of cataract surgeries greatly increasing quality of life and reducing the economic burden of treating cataracts (West and Valmadrid 1995). A molecular model for age-related cataract formation was developed based on observations from aged normal and cataractous lenses (Bloemendal *et al.* 2004). This model has guided research into the causes of cataract formation and the development of preventative drugs to delay onset of cataract formation.

1. Molecular Model for Age-Related Cataract Formation.

At the molecular level, cataracts result from the formation of large, light-scattering species in the lens fiber cells located along the visual axis. Dynamic light-scattering *in situ* studies of lenses of individuals with cataracts showed the presence of large particles with a mean size of 880 ± 460 nm (Dierks *et al.* 1998). Marsili *et al.* observed fibril-like aggregates possibly consisting of oxidatively damaged crystallins in the cytoplasm of nuclear fiber cells from cataractous lenses of OXYS rats, a strain selected for premature aging and organ/tissue damage due to high oxidative stress [Fig. 1-10 (Marsili *et al.* 2004)].

Several studies in the past 40 years have characterized changes in the relative protein concentrations of α-, β- and γ-Crys in normal versus cataractous lenses. Traditionally, these studies have used differential centrifugation to fractionate bovine or human lens homogenates into water-soluble (WS) and water-insoluble (WI) fractions. Initial studies observed the presence of a WS high molecular weight (HMW) species whose concentration increased with age and in cataractous lenses (Jedziniak *et al.* 1975; Roy and Spector 1976b). Recent studies have further characterized the protein composition of these HMW species in 20 and 60-70 year old lenses and found that the presence of all three classes of lens crystallins along with some cytoskeletal proteins (Srivastava *et al.* 2008). In all lenses studied, αA- and αB-Crys were present in the HMW complexes; intact βA4-, βB1-, βB2-, and γS-Crys were also isolated from these WS-HMW from all lens samples. Additionally, intact βA3-, γD-, and γC-Crys and fragments from alcohol dehydrogenase were found in the WS-HMW from cataractous lenses. Fragments of crystallin and cytoskeletal proteins (molecular mass < 20 kDa) were also isolated from HMW complexes in all samples. Fragments from γC-, γD-, and γS-Crys and alcohol dehydrogenase were only found in HMW from cataractous lenses.

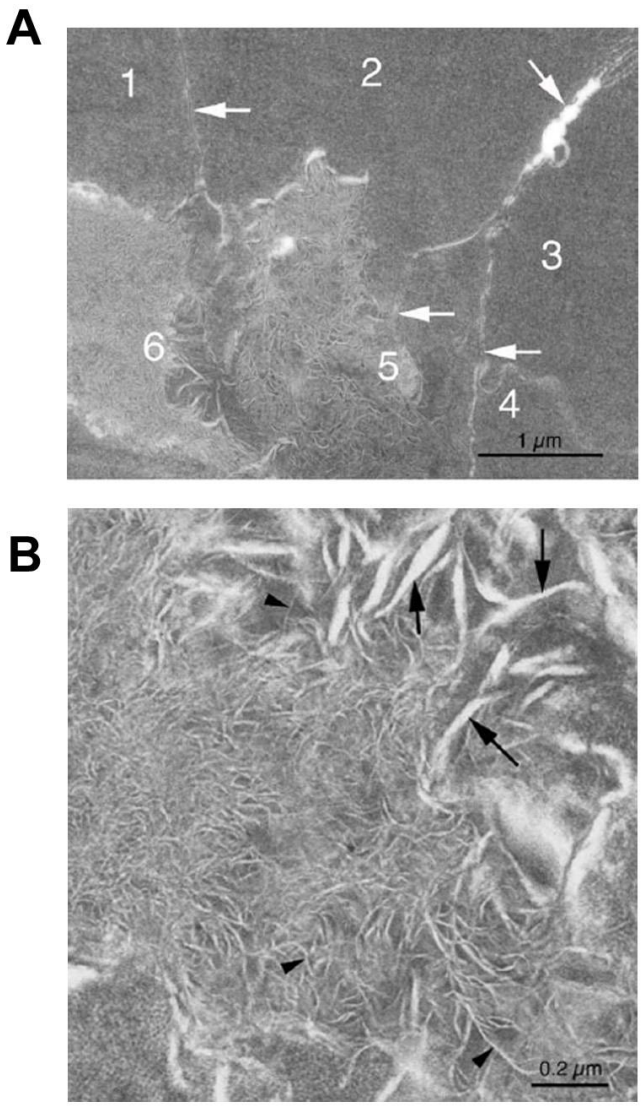

Figure 1-10: Transmission electron microscopy micrographs from thin sections of the nuclear region of cataractous lenses from OXYS rats.
A) Thin section along the equatorial plane at low magnification of a region in the nuclear portion of the lens. Cells numbered 1-4 show normal cytoplasmic texture, while cells 5 and 6 show fibrils in the cytoplasm. The authors indicate that these fibrils did not consist of disrupted membranes. Arrows show typical membranes. B) High magnification view of the fibril-like tangles in the cytoplasms of cells 5 and 6. Arrows show amorphous 'fusiform stain excluding regions' and the arrowheads show fibrils with a constant diameter. Reprinted with permission from (Marsili *et al.* 2004).

The crystallin proteins and the lens-specific IFs accumulate covalent modifications as the normal lens ages. Asn/Gln deamidation, Met/Trp oxidation, Glu/Lys carbamylation Lys/His/Arg methylation, Ser phosphorylation, and truncations were detected in proteins in aged normal lenses (Wilmarth *et al.* 2006; Asomugha *et al.* 2010). Proteins isolated from the WI fraction of cataractous lenses contain a multitude of covalent damages such as: deamidation, truncations, methionine and tryptophan oxidation, intermolecular disulfide bond formation, and glycation (Nagaraj *et al.* 1991; Takemoto and Boyle 2000; Wilmarth *et al.* 2006; Hains and Truscott 2007; Harrington *et al.* 2007; Hains and Truscott 2008). Some of these changes, such as deamidation of Gln and Asn, have been shown *in vitro* to reduce the stability of β- and γ-crystallins (Flaugh *et al.* 2006; Lampi *et al.* 2006) and, in the case of βA3-Crys, deamidation has been directly implicated in soluble aggregate formation (Takata *et al.* 2008).

Heys *et al.* (Heys *et al.* 2007) found that the concentration of these WS-HMW complexes in the nuclear region of the lens increased and reached a peak at age 35, followed by a decrease in concentration in older lenses (Fig. 1-11B). Similar observations were reported by Srivastava *et al.* and Asomugha *et al.* (Srivastava *et al.* 2008; Asomugha *et al.* 2010). They also quantified the protein content in the WS and WI fractions from the nuclear regions of lenses ranging in donor age from 5 to 85 years-old (Fig. 1-11A). They found an increase with age, from age 35-50, in the amount of protein in the WI fraction (Fig 1-11A). This increase correlated with a decrease in the amount of protein in the WS fraction. In accordance with previous studies (Roy and Spector 1976a; McFall-Ngai *et al.* 1985), they found a linear decrease with age in the concentration of water-soluble, free α-Crys in the nuclear region of the lens. Samples from donors' lenses over the age of 50 did not have any appreciable amount of free α-Crys present in the WS fraction (Fig. 1-11B).

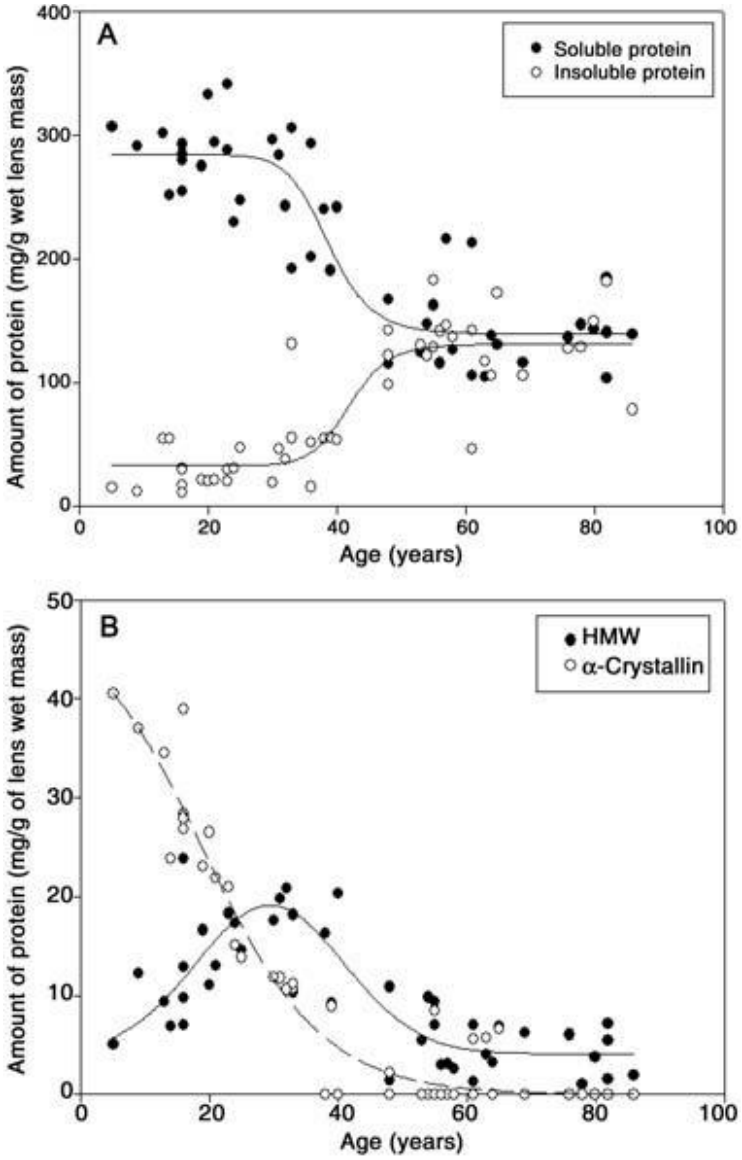

Figure 1-11: Quantification of protein concentration in different fractions isolated from the nuclear region of human lenses ranging in age from 5- to 85-years-old.
A) The changes in total protein concentration in the water-soluble (●) and water-insoluble (○) fractions from the nuclear lens region of donor lenses as a function of age. Proteins in the water-insoluble fraction were solubilized with 8 M Urea prior to quantifying total protein concentration. B) Protein concentration of free α-Crys (○) and the HMW species (●) found in the water-soluble fraction from the nuclear region as a function of lens donor's age. Free α-Crys and HMW complexes were isolated via SEC in an HPCL at pH 7. Reprinted with permission from (Heys *et al.* 2007).

All of these observations have been integrated into the current molecular model of age-related cataract formation (Bloemendal *et al.* 2004; Sharma and Santhoshkumar 2009). The model (Fig. 1-12) postulates that environmental stresses (e.g. UVB radiation) would lead to covalent damage to the crystallin proteins. These covalent modifications would destabilize them causing them to unfold and populate aggregation-prone species. Covalently damaged proteins would then accumulate with age because of constant exposure to environmental stresses and the lack of protein turnover in the mature fiber cells in the lens nucleus. α-Crys would sequester these species, forming stable substrate-chaperone complexes and preventing aggregation. This would result in a steady decline in the concentration of soluble and free α-Crys oligomers with age and an increase in the substrate-chaperone complexes. The HMW multi-crystallin complexes that accumulate with age are thought to represent α-Crys-substrate complexes formed *in vivo.* Eventually, α-Crys chaperone sites would be saturated and subsequently formed aggregation-prone species would aggregate unhindered. The multi-crystallin HMW complexes would also be incorporated into these WI inclusions—since their concentration also decreases after the age of 35—leading to an increase in the protein concentration in the WI fraction in aging lenses. The accumulation of these WI aggregates in the nuclear region of the lens would scatter light along the visual axis leading to cataracts, and if untreated, to blindness. There are certain aspects of the model that are still not fully elucidated such as how the WS-HMW species lose solubility with age and are integrated in the WI aggregates (Bloemendal *et al.* 2004; Sharma and Santhoshkumar 2009).

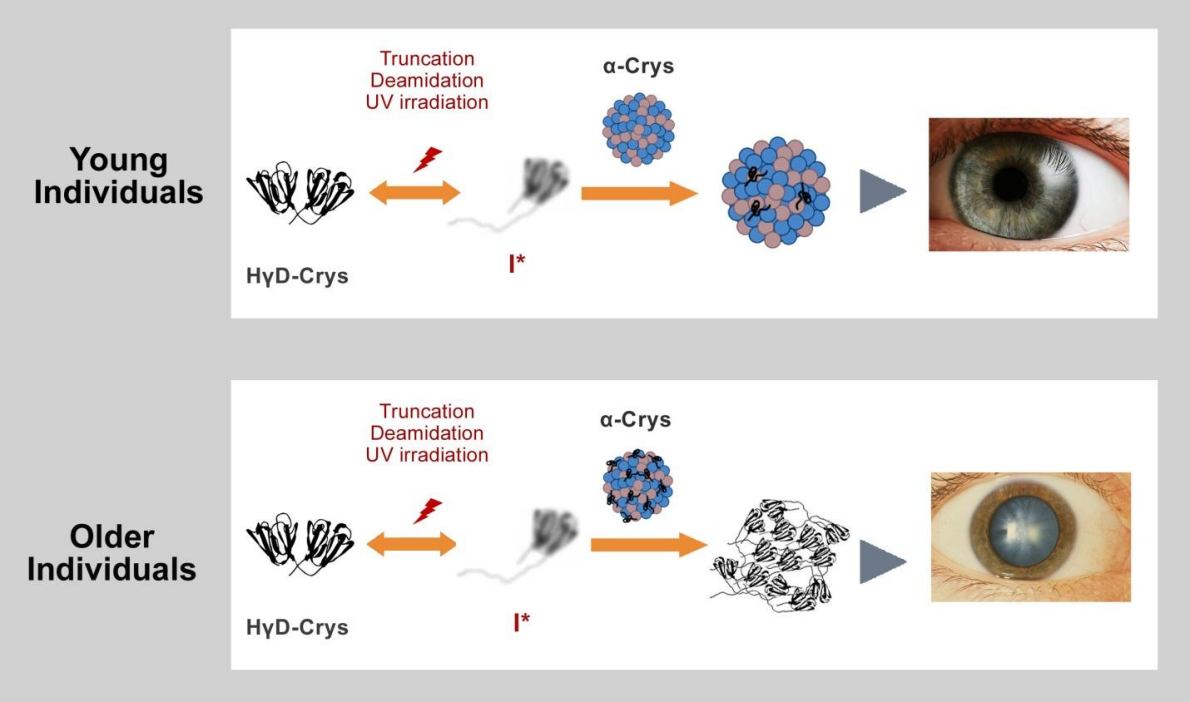

Figure 1-12: Model for age-related cataract formation.
In young individuals, α-Crys would sequester aggregation-prone species and keeps them from aggregating. Environmental stresses would cause the accumulation of covalent damage on the crystallin proteins causing their destabilization. In older individuals, the finite levels of free α-Crys would be diminished but cumulative covalent modifications to the crystallins would cause them to unfold and aggregate. This would result in the formation of WI large protein aggregates that scatter visible light and result in cataract disease.

E. SUMMARY OF EXPERIMENTAL RESULTS

The experiments described in Chapter 2 of this thesis were designed to study the *in vitro* interactions of αB-Crys chaperone with its physiological substrates, human γC-, γS- and γD-Crys. Chapter 2 also contains experiments that analyzed the structure of the aggregation-prone partially folded intermediate of γD-Crys that interacted with the αB-Crys chaperone. Chapter 3 presents experiments with the isolated single domain constructs for the N-terminal and C-terminal domains of γD-Crys. In addition, results presented in Chapter 3 show that the C-terminal domain of γD-Crys may contain an aggregation-prone region and that αB-Crys recognizes this region and preferentially binds the γD-Ctd during aggregation suppression assays.

These experiments provide important insight as to the nature of the aggregation-prone species of physiological substrate recognized by lenticular α-crystallin. They further correlate *in vitro* observations with the current model of cataract formation. Results from experiments with the single domain constructs have direct physiological importance as a 9 kDa fragment consisting of the C-terminal domain of γD-Crys accumulates in inclusions in older lenses (Srivastava *et al.* 1992). In general, these experiments provided insight into key aspect of the interaction between lenticular α-Crys and its physiological substrates, the γ-Crys, along with elucidating the structural characteristics of possible aggregation-prone species of the γ-Crys in the lens.

CHAPTER 2:

PARTIALLY FOLDED AGGREGATION INTERMEDIATES OF HUMAN γD-, γC- AND γS-CRYSTALLIN ARE RECOGNIZED AND BOUND BY HUMAN αB-CRYSTALLIN CHAPERONE.[1]

[1] **Reprinted and modified with permission from:** Acosta-Sampson, L., and King, J. (2010) Partially folded aggregation intermediates of human γD-, γC- and γS-crystallin are recognized and bound by human αB-crystallin chaperone. *J Mol Biol.* 401(1): 134-52.

A. INTRODUCTION

The vertebrate lens has a unique architecture necessary for its transparency and refractive properties (Ponce *et al.* 2006). Its nuclear region is composed of elongated, organelle-free, anucleate, fiber-like cells that contain high concentrations of the crystallin proteins and lack the capability of new protein synthesis (Bloemendal *et al.* 2004). The ubiquitous crystallins, α-, β-, and γ-crystallin, account for approximately 90% of the total protein in lens fiber cells.

α-crystallin is a member of the sHsp family of ATP-independent chaperones (Ingolia and Craig 1982; de Jong *et al.* 1993). In adult human lenses, α-crystallin is a polydisperse oligomer (20-40 subunits) of two subunits αA- and αB-crystallin (αA- and αB-Crys) present in a 3αA:1αB ratio (Bloemendal *et al.* 2004). In young human lenses, approximately 28% of the crystallin content is α-crystallin hetero-oligomers (Robinson *et al.* 2006). α-crystallin has a dual role as the main protein chaperone system in mature fiber cells and as a structural protein (Tardieu 1988; Horwitz 1992; Horwitz 1993; Rao *et al.* 1995; Reddy *et al.* 2002).

The β- and γ-crystallins are structural proteins whose high concentrations and native state interactions are important in maintaining the transparency and refractive index gradient of the lens. They are members of the same family of proteins, the βγ-crystallin. They are organized into two domains, with each domain composed of two intercalated Greek-key motifs (Delaye and Tardieu 1983; Tardieu 1988).

γC-, γS- and γD-Crys are the most abundant γ-crystallins (~21 kDa) and comprise 7, 9 and 11%, respectively, of the total protein content in young human eye lenses (Robinson *et al.* 2006). Human γC- and γD-Crys are expressed *in utero* and localized to the nuclear region of the lens, while γS-Crys is expressed solely in the cortical region. Compared to other mesophilic proteins, the γ-crystallins are extremely stable with melting temperatures above 70 ºC. The high thermodynamic stability of their native states along with kinetic barriers to unfolding allow them to remain stably folded for long periods of time, a necessary prerequisite for maintaining lens transparency (Mills *et al.* 2007). Their buried tryptophan fluorescence is quenched in the native state relative to the unfolded state in the absence of metal ligands or cofactors (Kosinski-Collins *et al.* 2004; Chen *et al.* 2006; Chen *et al.* 2008). This quenching mechanism is believed to protect Trp residues from photo-damage (e.g. photolysis) caused by constant exposure to environmental UV radiation during our lifetime, thus contributing to the stability of the native protein (Chen *et al.* 2009).

Disturbances to the proteins of fiber cells lead to cataract, a high molecular weight state of the lens crystallins that scatters visible light. Cataract is the leading cause of blindness in the world (Brian

and Taylor 2001). Age-related or mature-onset cataract is the prevalent form of this disease, while congenital hereditary cataract occurs in early childhood and is relatively rare (Graw 2004).

Characterization of cataracts removed by surgery revealed that they are insoluble aggregated states, requiring denaturation for solubilization (Harrington *et al.* 2004). β- and γ-crystallins isolated from water-insoluble fractions of cataractous lenses contain a high percentage of glutamine and asparagine deamidation, methionine and tryptophan oxidation, and truncations (Hains and Truscott 2007; Harrington *et al.* 2007). Destabilization of β- and γ-crystallins resulting from the accumulation of these covalent damages could cause these proteins to partially unfold and populate aggregation-prone species. *In vitro* studies of deamidation-mimicking mutants have shown that these modifications can greatly affect the stability of these proteins (Flaugh *et al.* 2006; Lampi *et al.* 2006).

Such pathways, in which partially folded species form high molecular weight aggregates, either within cells or outside them, underlie the pathology of many protein deposition diseases including Parkinson's disease, light chain amyloidosis, Alzheimer's disease, and many other protein deposition diseases (Kelly 1998; Uversky and Fink 2004; Baden *et al.* 2009). For the well characterized chaperonins, for example GroEL-ES or TriC, such aggregation-prone species are their substrates (Barral *et al.* 2004).

Horwitz (Horwitz 1992) showed that bovine α-crystallin had chaperone activity since it inhibited the thermally-induced aggregation of different enzymes and bovine β- and γ-crystallins. α-crystallin has also been shown to suppress the aggregation of different non-physiological substrates such as insulin, citrate synthase, α-lactalbumin and alcohol dehydrogenase *in vitro* (Horwitz 1992; Carver *et al.* 1995; Leroux *et al.* 1997; Lindner *et al.* 1997; Reddy *et al.* 2006). αA- and αB-Crys subunits (~ 20 kDa) can also form polydisperse homo-oligomers with comparable structural and chaperone properties as the hetero-oligomeric α-crystallin (Sun *et al.* 1997). α-crystallin does not require ATP hydrolysis for chaperone function, although ATP binding has been shown to induce structural changes and enhance chaperone function (Biswas and Das 2004).

Sathish *et al.* investigated the interaction between human αA- and αB-crystallin and destabilized multimeric βB2-crystallin mutants. They showed that αA- and αB-crystallin recognized and bound mutants with altered equilibrium unfolding patterns observed using the fluorescence emission of a bimane probe attached to βB2-crystallin proteins (Sathish *et al.* 2004). These mutants had similar thermodynamic stability as WT, but—unlike wild type—aggregated at high protein concentrations under native conditions. The authors proposed that changes in the stability of the substrate have to be accompanied by the population of a folding intermediate for α-crystallin to recognize the βB2-crystallin substrate (Sathish

et al. 2004). In addition, Evans *et al.* (Evans *et al.* 2008) have shown that calf α-crystallin will bind to partially folded species of human and calf βB2-crystallin that structurally resemble an unfolding intermediate of human βB2-crystallin. α-crystallin is able to discriminate between species that are productive intermediates versus those intermediates involved in off-pathway aggregation of model substrate (Carver *et al.* 1995; Lindner *et al.* 1997; Treweek *et al.* 2000; Carver *et al.* 2002; Evans *et al.* 2008). This mode of chaperone function seems to be a conserved mechanism for other members of the sHsp family (Nakamoto and Vigh 2007).

Since primary lens fiber cells are terminally differentiated and enucleated, it has not been possible to culture them. In the absence of appropriate cell or tissue culture of the lens, it has been difficult to identify the actual crystallin conformers that are recognized and bound by α-crystallin in the lens. The characterization of the composition of cataractous material removed by surgery has required denaturing conditions such that the identity of the chaperone substrates and their conformation are lost. In the protein aggregation model for cataract, human α-crystallin would be expected to recognize partially unfolded molecules of the human lens γ-crystallins. Horwitz (Horwitz 1992), Carver *et al.* (Carver *et al.* 1995), and Putilina *et al.* (Putilina *et al.* 2003) have previously shown that human αB-Crys is able to suppress the aggregation of a mixture of γ-crystallins from lens' cell lysates. Most of these studies utilized heat denaturation to initiate competitive aggregation and the substrates usually consisted of all γ-crystallins from lenses purified via SEC. We report here experiments to identify the conformation of species of monomeric human γC-, γD- and γS-Crys that are recognized by the human αB-Crys chaperone.

Unfolding and refolding studies *in vitro* of human γD-Crys monitored the fluorescence emission of four tryptophan residues (two Trps per domain), each buried in a quadrant of the protein (Basak *et al.* 2003). These residues are very efficiently quenched in the folded state of the protein so that their fluorescence emission quantum yield increases upon unfolding (Kosinski-Collins *et al.* 2004; Chen *et al.* 2006). The efficient quenching of Trp68 and Trp156 depends on an unusual conformation of the Trp ring with respect to its backbone amide, as well as the presence of two tightly bound H_2O molecules with oppositely oriented dipoles. The other two tryptophans, Trp 42 and Trp 130, are quenched by Förster transfer to their counterpart Trps (Chen *et al.* 2006; Chen *et al.* 2008; Chen *et al.* 2009). As a result, the Trp fluorescence from the γ-crystallins is a very sensitive reporter of the protein's conformation.

In equilibrium and kinetic refolding experiments, a stable, partially folded intermediate was identified with the N-terminal domain unfolded and C-terminal domain folded. When the protein was refolded from high to low concentrations of denaturant, off-pathway aggregation was observed that competed with productive refolding of human γD-Crys (Kosinski-Collins and King 2003). Recombinant

human γC-Crys behaved similarly under matching assay conditions (Dr. Yongting Wang, personal communication). Human γS-Crys, on the other hand, had a more cooperative unfolding/refolding transition during equilibrium experiments and aggregation was not detected during refolding (Mills *et al.* 2007). In this study, I have taken advantage of the *in vitro* aggregation reactions that compete with productive folding to examine individually the interactions of human α-crystallin with aggregating, partially unfolded, purified human γ-crystallins that are likely candidates for physiological chaperone substrates within the aging lens.

B. MATERIAL AND METHODS

1. Expression and purification of human αB-Crys and γ-crystallins.

Human γD-Crys cloning into pQE.1 was previously described in Kosinski-Collins *et al.*(Kosinski-Collins *et al.* 2004). Human γS-Crys construct was previously described in Mills *et al.* (Mills *et al.* 2007). Double- (W130F/W156F and W42F/W68F γD-Crys) and triple-Trp (W42only- and W130only γD-Crys) mutants were previously described in Chen *et al.* (Chen *et al.* 2006). These recombinant proteins were expressed by transforming pQE.1 plasmids into *E. coli* M15 [pREP4] cells (Qiagen). Both constructs contained an N-terminal His_6 tag. Proteins were purified following procedures described in Kosinski-Collins *et al.* (Kosinski-Collins *et al.* 2004) using Ni-NTA (Qiagen) media for affinity chromatography. After purification, proteins were dialyzed into 10 mM ammonium acetate (pH 7.0) and stored at 4 ºC.

Human αB-Crys pAED4 plasmid was a generous gift from Dr. Jack Liang at Harvard Medical School. The wild-type αB-Crys containing plasmid was transformed into BL21 Gold (DE3) *E. coli* cells (Stratagene). Protein expression was induced by addition of IPTG and allowed to proceed over night at 18 ºC. Cells were harvested and stored at -80 ºC until future use. The αB-Crys purification protocol was modified from a previous protocol published by Horwitz and colleagues (Horwitz *et al.* 1998). Modifications included performing all steps for cell lysis at 4 ºC. Two rounds of ion-exchange chromatography were performed using HiPrep 16/10 Q Sepharose FF column (GE Lifesciences) followed by SEC in Superose 6 10/300 GL (GE Lifesciences). Protein was stored in 50 mM sodium phosphate and 150 mM sodium chloride buffer, pH 7.0 (SEC Buffer). αB-Crys aliquots were dialyzed into 10 mM ammonium acetate and concentrated using 10 kDa MWCO Amicon Ultra-4 concentrators (Millipore) prior to use in aggregation suppression assays. All protein batches were tested for chaperone efficiency in aggregation suppression assays at 1:1 and 1:5 γ-αB ratios, with WT γD-Crys as the substrate. Double

tryptophan substitutions of residues 9 and 60 to phenylalanines were constructed using mutant primers (IDT-DNA) to amplify the αB-Crys gene in the pAED4 vector during site-directed mutagenesis. Amplified plasmid DNA was sequenced to confirm the substitutions (DNA Sequencing Facility, Massachusetts General Hospital). W9F/W60F αB-Crys was purified using the same procedures described above for the WT αB-Crys protein.

Wild-type human γC-Crys pET-15b plasmid was transformed into BL21 (DE3) *E. coli* cells (Stratagene). The plasmid and purification protocol were also kindly provided by Dr. Jack Liang (Graw *et al.* 2001). Briefly, protein expression was induced by addition of IPTG. Cells were lysed, centrifuged at high speeds, and the supernatant was subjected to two rounds of ammonium sulfate fractionation. The supernatant was centrifuged at high speeds and the pellet was resuspended in Lysis Buffer (50 mM Tris, 1 mM EDTA, 100 mM sodium chloride, pH 7.0). The resuspended pellet was run on a HiPrep 26/60 Sephacryl S-100 size-exclusion column connected to an AKTA FPLC (GE Lifesciences). Protein was concentrated to approximately 2 mg/ml and stored at 4 ºC until further use.

Protein concentrations were calculated using UV absorbance at 280 nm of unfolded proteins and the following extinction coefficients: 42,860 (γD-Crys, γS-Crys and γC-Crys), 31,860 (W42F/W60F and W130F/W156F γD-Crys), 26,735 (W42only and W130only γD-Crys) and 13,980 (αB-Crys) $M^{-1}cm^{-1}$ (Pace *et al.* 1995; Wilkins *et al.* 1999). The protein concentration for no-Trp αB-Crys was determined using the Bio-Rad Protein Assay (Bradford method). Purity of all proteins mentioned herein was determined to be greater than 90% by SDS-PAGE.

2. Circular dichroism spectroscopy

WT αB-Crys was incubated at a concentration of 100 µg/ml in 10 mM sodium phosphate buffer (pH 7.0) for 1 hour at 37 ºC. Far-UV CD spectra were then collected from 198 to 250 nm in a 1 mm cuvette in an AVIV model 202 CD spectrometer (Lakewood, NJ). The temperature was kept at 37 ºC using an internal Peltier thermoelectric temperature controller. Mean residual ellipticity was calculated after buffer signal had been subtracted from spectra.

3. Fluorescence emission spectroscopy

Native WT αB-Crys was incubated at a concentration of 100 µg/ml in Refolding Buffer (100 mM sodium phosphate, 1 mM EDTA, 5 mM DTT, pH 7.0) for 4 h at 37 ºC prior to collecting spectra. For the

unfolded samples, αB-Crys was unfolded in Unfolding Buffer (100 mM sodium phosphate, 1 mM EDTA, 5 mM DTT, 5.0 M GdnHCl, pH 7.0) for 24 h at 37 ºC. The λ_{EX} was 295 nm (PMT voltage was 700 V) and the emission scans were collected from wavelengths 310-400 nm. The excitation and emission slit width were set to 10 nm and the temperature was kept at 37 ºC using a circulating water bath. For experiments comparing native WT and noTrp αB-Crys, the protein concentration was 20 μg/ml, the λ_{EX} was 300 nm, the PMT voltage was 950V, and the slit widths were 10 nm (at 25 ºC).

For experiments comparing the fluorescence emission spectra of WT γD-Crys—noTrp αB-Crys SEC fractions, the λ_{EX} was 300 nm and the emission scans were collected from wavelengths 316-400 nm (PMT voltage was 950 V). The excitation and emission slits were set to 10 nm and the temperature was kept at 25 ºC. These were the same conditions for experiments measuring the emission spectra of the W42only γD—noTrp αB and W130only γD—noTrp αB complex-containing fractions and their respective native and unfolded γD-Crys controls. However, the high molecular weight peak fractions were pooled (1 ml total), concentrated to 250 μl, and their fluorescence emission spectra were recorded with the λ_{EX} set to 300 nm. Fluorimeter settings were the same for experiments with W42F/W68F and W130F/W156F γD-Crys except the PMT voltage was set to 700 V. WT, double- and triple-Trp γD-Crys controls were fully unfolded in Unfolding Buffer for 24 h at 37 ºC and pre-equilibrated to 25 ºC prior to recordings. The native γD-Crys controls were equilibrated to 25 ºC for 1 h in Refolding Buffer prior to recording spectra. Protein concentration for WT and double Trp γD-Crys controls was 50 μg/ml. The concentration for W42only γD-Crys controls was 50 μg/ml, and for W130only γD-Crys controls was 25 μg/ml.

For experiments showing the emission spectra for double-Trp γD-Crys mutants at different concentrations of GdnHCl, the protein was unfolded in Unfolding Buffer with the matching concentration of GdnHCl for 24 h at 37 ºC. All fluorimeter settings were the same as described above except the PMT voltage was set to 700 V. Protein concentration for both double-Trp mutants was 20 μg/ml. Fluorescence spectra for respective buffers were collected and subtracted from the sample spectra for all experiments described herein. Spectra were collected using a Hitachi F-4500 fluorescence spectrophotometer equipped with a circulating water bath. All experiments described in this section were repeated as three separate trials.

4. Aggregation and aggregation suppression assays

Purified γ-Crys proteins were individually unfolded at 10 times the final target protein concentration in Unfolding Buffer (5 M GdnHCl) for 24 h at 37 ºC to ensure complete unfolding.

Aggregation of γ-Crys *in vitro* was initiated by addition of Refolding Buffer and concomitant ten-fold dilution of the unfolded γ-Crys protein into low concentrations of GdnHCl (0.5 M). Samples were mixed thoroughly before initiating UV-Vis spectrometer readings. Turbidity of the solutions was measured by recording the optical density at 350 nm ($O.D._{350\ nm}$) and 37 ºC using a Cary 50 UV-Vis spectrophotometer (Varian) with an internal Peltier temperature controller. Samples were not continuously stirred during measurements.

For aggregation experiments where γD-Crys was unfolded at intermediate GdnHCl concentrations, γD-Crys was unfolded in Unfolding Buffer at the target concentration (2.49, 2.82, 3.02, and 5.03 M GdnHCl) and incubated at 37 ºC for 24 hours. Aggregation was initiated by diluting the GdnHCl concentration to 0.5 M with Refolding Buffer and thorough mixing of the samples. The final protein concentrations were the same for all samples (50 μg/ml). Light scatter was recorded as $O.D._{350\ nm}$. All aggregation reactions were carried out at 37 ºC without continuous stirring.

For all aggregation suppression assays, unfolded γ-Crys was diluted ten-fold to initiate refolding and aggregation; αB-Crys chaperone was already added to the Refolding Buffer and equilibrated to 37 ºC. Samples were mixed thoroughly upon addition of Refolding Buffer. The final γ-Crys protein concentration was 100 μg/ml for assays with WT γD-, γC-, γS- and double-Trp γD-Crys protein substrates. The γ-Crys protein concentration was 50 μg/ml for assays with triple-Trp γD-Cry as substrates. Final GdnHCl concentration for all assays described above was 0.5 M GdnHCl. Different mass-based ratios of γ-Crys to αB-Crys were used to assay the chaperone activity of the α-crystallin oligomers. Turbidity of the solutions was measured at 37 ºC without continuous stirring using a Cary 50 UV-Vis spectrophotometer.

For the early time point addition experiments, WT γD-Crys was unfolded in Unfolding Buffer for 24 h at 37 ºC. Unfolded protein was added to constantly stirred Refolding Buffer (± noTrp αB-Crys) at 37 ºC (dead time ~ 1s); unfolded protein was added 60 s after $O.D._{350\ nm}$ measurements were started. Samples were stirred only for the first 30 s after addition of γD-Crys. For the 0 s addition, αB-Crys chaperone had already been added to the Refolding Buffer, which had been equilibrated to 37 ºC for 1 h. For subsequent time point additions, γD-Crys was added followed by addition of noTrp αB-Crys after 2, 6, or 10 s. NoTrp αB-Crys had been equilibrated for 1 h at 37 ºC in 10 mM ammonium acetate buffer at pH 7.0. Data collection was not paused during addition of either γD- or αB-Crys. Suppression reactions were performed at a 1 γD:5 αB ratio and a γD-Crys protein concentration of 50 μg/ml. All experiments described in this section were repeated as three separate trials.

For the time point addition experiments, unfolded γD-Crys was diluted ten-fold with Refolding Buffer to initiate aggregation at 37 ºC. The aggregation reaction was followed using a Cary 50 UV-Vis

spectrophotometer and measuring the $O.D._{350\ nm}$. For the 0 s addition, αB-Crys had already been added to the Refolding Buffer, which had been equilibrated to 37 ºC. For later time point additions, γD-Crys was aggregated by adding Refolding Buffer (minus the αB-Crys volume needed) and allowed to proceed at 37 ºC. When the selected time point was reached, data collection was paused for 10 s, and H_2O (control) or αB-Crys was thoroughly mixed using an acrylic cuvette mixer (Bel-Art Products, Pequannock, NJ). Data collection was then resumed. All experiments described in this section were repeated as three separate trials.

5. Size-exclusion chromatography

Aggregation and aggregation suppression samples (0.5 ml) were collected after UV spectrophotometer measurements, incubated at 37 ºC for 2 h. Samples for double-Trp and triple-Trp γD-Crys suppression experiments and early time point addition suppression experiments were incubated for 24 h at 37 ºC. One-hundred µl of 6X SEC Buffer (300 mM sodium phosphate, 900 mM sodium chloride, pH 7.0) were added and samples (500 µl) were filtered using Ultrafree-MC Centrifugal filter units with a 0.22 µm membrane (Millipore) and then equilibrated to 4 ºC. Samples were injected into a 0.5 ml Teflon loop (GE Lifesciences) and loaded onto a Superose 6 GL 10/300 (CV=24 ml, V_0= 8 ml, GE Lifesciences) attached to an AKTA FPLC (GE Lifesciences). Chromatography runs were performed at a flow rate of 0.5 ml/min in SEC Buffer (50 mM sodium phosphate, 150 mM sodium chloride, pH 7.0, degassed) at 4 ºC. For the native mixture samples, native γ-Crys at 100 µg/ml and native αB-Crys at 500 µg/ml were mixed together and incubated at 37 ºC for 2 h in Refolding Buffer with 0.5 M GdnHCl.

For experiments assaying the lifetime of the γD—αB-Crys complexes, γD-Crys was unfolded in Unfolding Buffer for 24 h at 37 ºC. Aggregation was initiated by ten-fold dilution of the unfolded protein solution with Refolding Buffer plus αB-Crys (ratio was 1 γD:5 αB) at 37 ºC; the final protein concentration for γD-Crys was 100 µg/ml and the final GdnHCl concentration was 0.5 M. The final volume for this reaction was 5.0 ml and the sample was left at 37 ºC in a Nutator shaker (BD Diagnostics) for 4 days. Aliquots (0.5 ml) were removed, 100 µl of 6X SEC Buffer were added, samples were filtered using Ultrafree-MC Centrifugal units with a 0.22 µm filter and equilibrated at 4 ºC. Filtered samples were loaded onto a Superose 6 GL SEC column equilibrated in SEC Buffer and run at a flow rate of 0.5 ml/min at 4 ºC. All experiments described in this section were repeated as three separate trials.

6. Electron microscopy

Samples from the aggregation reactions incubated at 37 ºC for 2 h were buffer-exchanged to 50 mM Tris, pH 7.5 buffer using a Microcon YM-100, MWCO 100 kDa (Millipore). Samples were then placed on a Formvar and carbon-coated 400 mesh copper grid, negatively stained with 2% (w/v) uranyl acetate, and imaged using a JEOL 1200 transmission electron microscope operating at 60 kV.

C. RESULTS

1. Purification and characterization of recombinant wild-type, human αB-Crys

Human recombinant αA- and αB-Crys form large (400-600 kDa), polydisperse homo-oligomers when expressed in *E. coli* cells (Andley *et al.* 1996; Sun *et al.* 1997). Sun *et al.* (Sun *et al.* 1997) have shown that these homo-oligomers have similar structural characteristics as endogenous bovine α-crystallin, with small differences in surface hydrophobicity between recombinant homo-oligomers. Further, both human αA- and αB-Crys oligomers showed chaperone-like activity with αB-Crys oligomers suppressing aggregation at lower substrate to chaperone weight ratios. The multimeric state, heterogeneous character and absence of catalytic activity make it difficult to compare preparations of α-crystallin from different sources. Figure 2-1 describes the characteristics of the αB-Crys oligomers from our expression and purification protocols.

Recombinant, WT human αB-Crys was expressed at low temperature (18 ºC) and purified via anion-exchange and SEC. Fractions collected during the final, polishing SEC step were electrophoresed through a 14% SDS-PAGE gel to confirm purity of protein samples (Figures 2-1A and B). The secondary, tertiary and quaternary structures of purified WT αB-Crys were characterized using far-UV CD spectroscopy, fluorescence emission spectroscopy and SEC methods. Far-UV CD spectrum (Fig. 2-1C) of native αB-Crys showed a minimum at 214 nm consistent with previously published spectra (Sun *et al.* 1997). Human αB-Crys has two tryptophans at amino acid positions 9 and 60 in its N-terminal region. Comparable to previously published results,(Sun *et al.* 1997) the fluorescence emission spectra showed maxima at wavelengths 339 and 349 nm for native and unfolded protein respectively (Fig. 2-1D). Quaternary structure characteristics were examined using a Superose 6 SEC column. Figure 2-1A shows a representative size-exclusion chromatogram. From elution profiles, recombinant WT αB-Crys

oligomers had apparent molecular weights between 500-600 kDa (25-30 subunits per oligomer). This size distribution is consistent with previously published results (Sun *et al.* 1997).

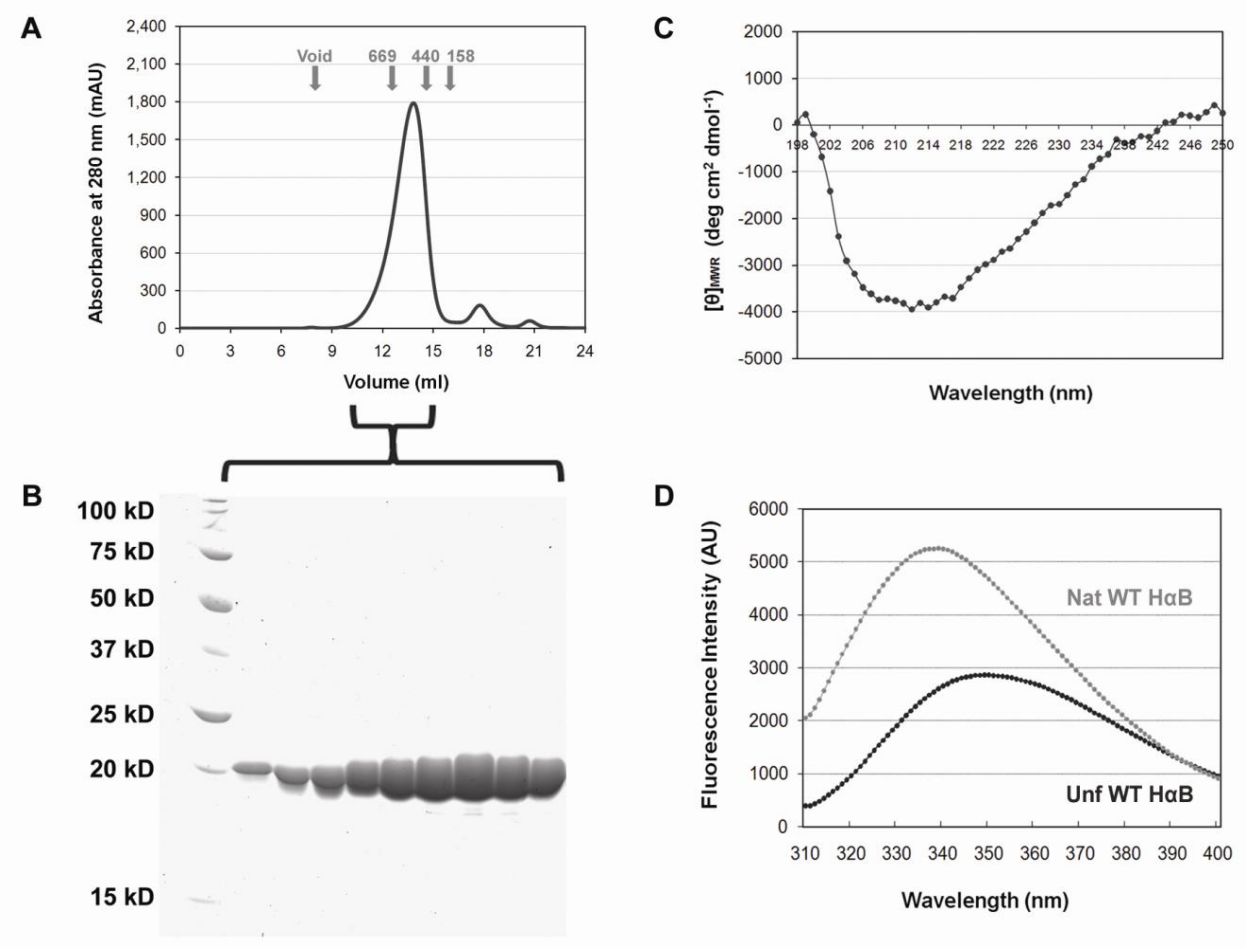

Figure 2-1: Purification and structural characterization of recombinant Human αB-Crys.
Human WT αB-Crys was expressed and purified from *E. coli* cells (see Materials and Methods). A) Representative size-exclusion chromatogram showing the final, polishing step of the purification procedure. WT αB-Crys eluted as a single peak (from 11 to 14.5 ml) with apparent molecular mass between 500-600 kDa. B) Fractions corresponding to the αB-Crys elution peak were run in a 14% SDS-PAGE gel.

C) Far-UV CD spectra (198-250 nm) of native αB-Crys at pH 7.0 and 37 ºC. D) Fluorescence emission spectra of native (●) and unfolded (●) αB-Crys at 37 ºC. Protein concentration for far-UV CD and fluorescence emission measurements was 100 µg/ml.

2. WT human γC-, γD- and γS-Crys aggregate upon refolding out of high concentrations of denaturant into buffer with low concentrations of denaturant

Previous work by Kosinski-Collins and King(Kosinski-Collins and King 2003) showed that wild-type human γD-Crys can refold to its native state at 37 ºC after unfolding in high concentrations of GdnHCl in equilibrium refolding experiments that tracked tryptophan fluorescence changes between the folded and unfolded states. Upon dilution out of denaturant, refolding was already significant within the mixing dead-time of the experiment. The C-terminus reached its native-like state first, with a $t_{1/2}$ of 35 s, while the folding of the N-terminal, with a $t_{1/2}$ of 130 s, took significantly longer (Flaugh *et al.* 2006). Thus, there is a partially folded intermediate that is significantly populated during the first few minutes of refolding even at 37 ºC (Flaugh *et al.* 2006). However, when diluting to buffer or low denaturant concentrations (less than 1 M GdnHCl) early intermediates of γD-Crys aggregated under the experimental conditions (10 μg/ml, pH 7.0). Early, partially folded intermediates of WT human γC-Crys displayed analogous aggregation behavior in similar experiments (Dr. Yongting Wang, personal communication). On the other hand, partially folded intermediates of wild-type human γS-Crys did not aggregate under similar experimental refolding conditions during equilibrium refolding experiments (Mills *et al.* 2007). Given the structural and sequence similarity between these three γ-crystallins (~ 50% identity between human γS-Crys and γD-Crys) (Mills *et al.* 2007), it seemed likely that partially folded species of γS-Crys would aggregate during refolding if the protein concentration was increased.(Speed *et al.* 1996)

Recombinant, WT human γD- and γS-Crys containing an N-terminal His_6 tag were expressed in *E. coli* and purified via Ni-NTA affinity chromatography. Wild-type human γC-Crys, without any affinity tags, was also expressed in *E. coli*, but purified via SEC. Kosinski-Collins *et al.* (Kosinski-Collins and King 2003; Kosinski-Collins *et al.* 2004) have shown no difference in protein stability and aggregation behavior between γD-Crys with or without a His_6 tag.

Wild-type γD-, γC-, and γS-Crys were unfolded in 5.0 M GdnHCl at pH 7.0 and 37 ºC for 24 hours. Refolding at 37 ºC was initiated by a ten-fold dilution with Refolding Buffer (without GdnHCl) and thorough mixing of the sample. Aggregation was followed by monitoring solution turbidity measured as optical density at 350 nm ($O.D._{350\ nm}$) without continuous stirring of the sample. The final protein concentration was 10 times higher than that used in the aforementioned equilibrium unfolding/refolding experiments. Figure 2-2 shows the $O.D._{350\ nm}$, which is a direct measure of static light scattering due to formation of macromolecular aggregates, for each γ-Crys protein sample (1 γ:0 αB traces). The first recorded $O.D._{350\ nm}$ values (at t=0) were higher than the buffer baseline due to the rapid formation of light-scattering species within the mixing dead-time of the experiment (~ 5 s). Aggregates formed for all

three γ-crystallins were confirmed to be amorphous by transmission electron microscopy (Fig. 2-3) and were visible to the naked eye minutes after initiation of refolding and aggregation.

WT γD-Crys had the highest increase in solution turbidity (~ 1.15 AU) followed by γC-Crys (~ 0.7 AU) and γS-Crys (~0.35 AU) (Fig. 2-2). At 37 ºC, $O.D._{350\ nm}$ traces for all three γ-crystallins displayed two phases. The traces increased sharply in the first 40 s and reached a plateau 200 s after initiation of refolding and aggregation (Fig. 2-2). The two-phase aggregation process observed in these traces for all partially folded γ-Crys was probably due to an initial, fast-growth phase of the small-globular aggregates into fibril-like, amorphous structures. Eventually, the light scatter traces reached a plateau due to the formation of large aggregates within the first 30 min of the reaction. These aggregate species have been observed by Kosinski-Collins and King (Kosinski-Collins and King 2003) using atomic force microscopy.

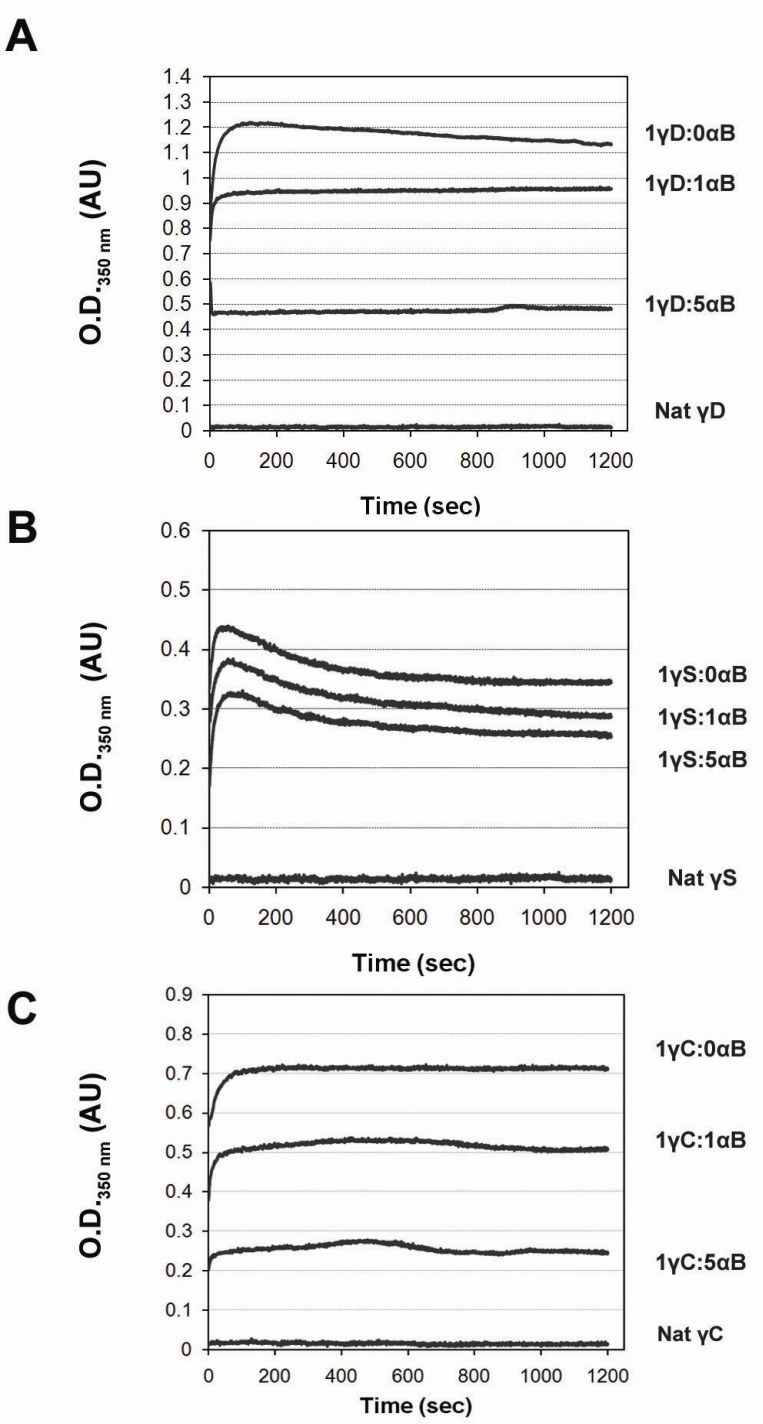

Figure 2-2: Suppression of the aggregation of partially folded WT γD-, γS- and γC-crystallins by αB-Crys chaperone.
A) γD-Crys, B) γS-Crys, and C) γC-Crys aggregate during refolding out of high concentrations of GdnHCl at a protein concentration of 100 µg/ml and a final GdnHCl of 0.5 M. The suppression reactions were done at 1 γ:1 αB and 1 γ:5 αB ratios.

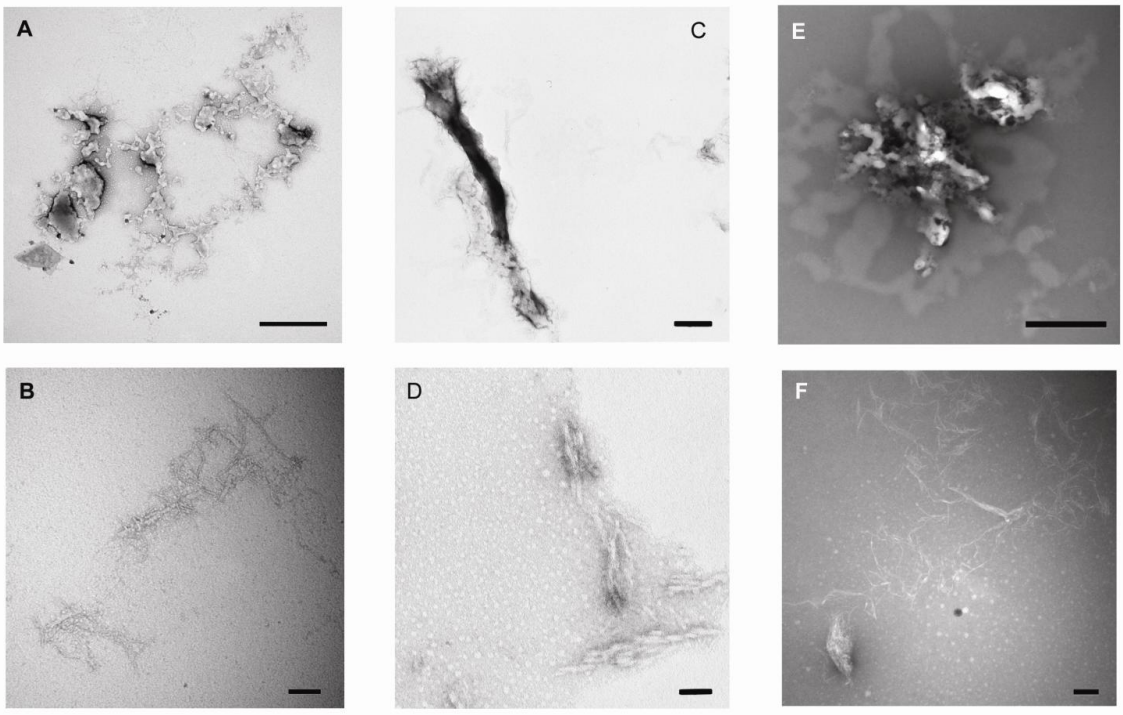

Figure 2-3: TEM micrographs of human γ-Crys aggregates.
WT γD-Crys aggregates at A) x 50000 and B) x 120000 magnifications (scale bars correspond to 500 and 100 nm respectively). WT γS-Crys aggregates at C) x 30000 and D) x 100000 magnifications (scale bars correspond to 200 and 50 nm respectively). WT γC-Crys aggregates at E) x 60000 and F) x 100000 magnifications (scale bars correspond to 500 and 100 nm respectively). All protein concentrations were 100 µg/ml and the final GdnHCl concentration was 0.5 M; grids were prepared as described in the Materials and Methods section in this chapter.

3. αB-Crys chaperone suppresses the aggregation of partially folded WT γD-, γC- and γS-Crys

WT γD-, γC- or γS-Crys protein was allowed to refold and aggregate in the presence of WT αB-Crys chaperone at different mass-based ratios of γ-Crys to αB-Crys to test whether partially folded crystallins were substrates of α-crystallin (Fig. 2-2). All γ-Crys to αB-Crys ratios described hereafter were mass-based ratios. Refolding buffer with αB-Crys chaperone was added to unfolded γ-Crys solutions, mixed thoroughly, and aggregation was monitored by measuring changes in $O.D._{350\ nm}$ in a UV-Vis Spectrophotometer without subsequent, continuous stirring. Unless otherwise stated, this mixing regime was followed for all of the short-term suppression experiments mentioned hereafter.

αB-Crys chaperone suppressed the aggregation of partially folded intermediates of all three γ-crystallins in assays measuring solution turbidity. Increasing the concentration of αB-Crys chaperone, from 1 γ:1 αB to 1 γ:5 αB, led to further reduction in light scattering (Fig. 2-2). WT γD- and γC-Crys aggregation was suppressed to similar levels (Fig 2-2A and C), while γS-Crys aggregation was not suppressed as well under identical experimental conditions (Fig. 2-2B). Further, I observed that only the partially folded γ-Crys substrate was incorporated into the aggregate while the αB-Crys chaperone was present as either free oligomers or bound to γ-Crys in high molecular weight complexes (data not shown).We also performed the same aggregation suppression assays in the presence of αB-Crys chaperone with different concentrations of γD-Crys ranging from 50-150 μg/ml. We did not observe significant differences in the suppression of aggregation levels at the same ratios within this range (data not shown).

Samples from these suppression reactions were further analyzed via SEC—performed at 4 ºC in SEC Buffer—2 h after samples were prepared. At this temperature, I did not observe any further aggregation after the samples had been filtered with a 0.2 μm filter prior to SEC. Chromatograms from the 1 γD:5 αB and 1 γC:5 αB samples showed the presence of a high molecular weight complex that eluted in the void volume (V_0 , ~7.6 ml) of the Superose 6 GL 10/300 SEC column, along with the signature peaks for αB-Crys chaperone and γD- or γC-Crys monomers (Fig. 2-4A and B, gray traces). The high molecular weight complexes constitute the γ—αB complexes. This early-eluting peak was only observed in samples from suppression reactions. Chromatograms from samples of native αB-Crys chaperone and native γD-Crys incubated together under final refolding conditions (0.5 M GdnHCl and Refolding Buffer), for 2 h at 37 ºC, lacked this early-eluting peak (Fig 2-4A and B, black traces). Chromatograms from 1 γ:0 αB aggregation reactions, native αB-Crys chaperone only, and native γ-Crys only also lacked this peak (data not shown). Interestingly, when 1 γS:5 αB samples were applied to the Superose 6 column, no early-eluting peak was observed (Fig. 2-4C). This result along with turbidity data

shown in Fig. 2-2 indicates that αB-Crys did not suppress the aggregation of partially folded γS-Crys species as efficiently as the aggregation from partially folded γD- and γC-Crys. These results also show that the N-terminal His_6 tag of γD- and γS-Crys does not seem to affect the chaperoning interactions between αB-Crys and that the changes in suppression efficiency observed for different, partially folded γ-Crys were due to particular characteristics of these proteins. This differential interaction with γS-Crys could be due to a shorter lifetime of the aggregation-prone species populated during γS-Crys refolding (Mills *et al.* 2007). Another possibility is that amino acid sequence differences in γS-Crys make it a poorer substrate for the αB-Crys chaperone.

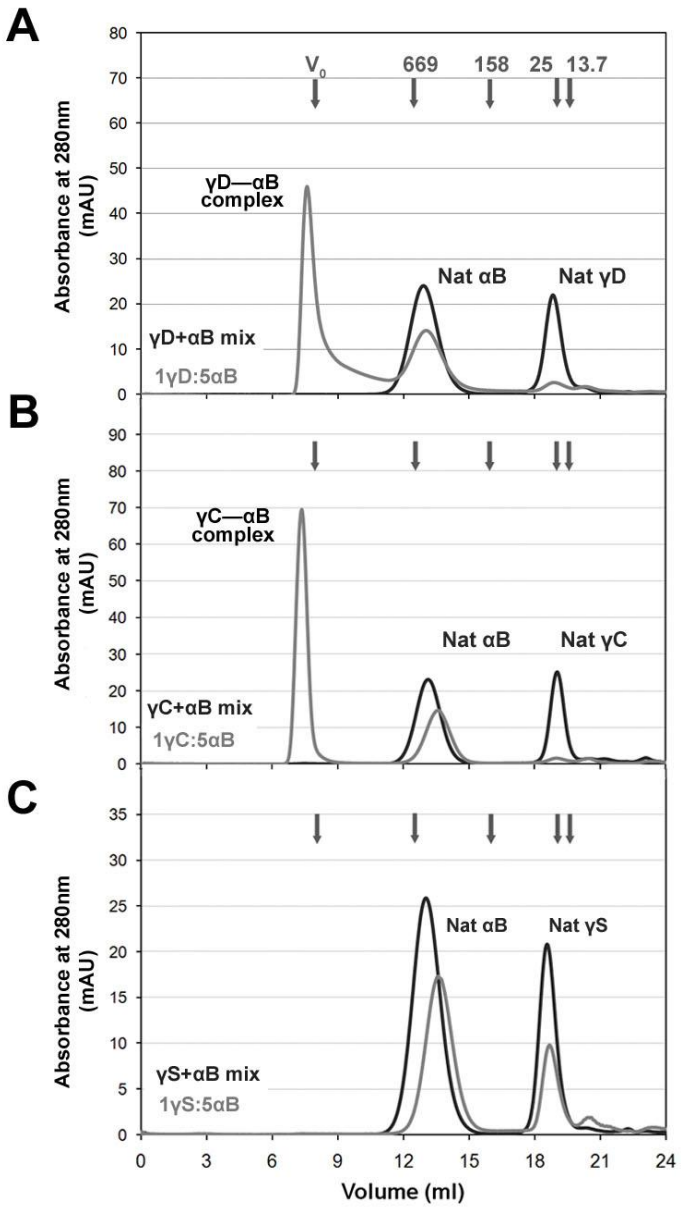

Figure 2-4: Size-exclusion chromatograms for αB-Crys and γD-, γC-, or γS-Crys suppression reactions.
A) 1 γD:5 αB suppression reaction ( ) and 1 γD:5 αB mixture of native proteins ( ) chromatograms are shown. B) 1 γC:5 αB suppression reaction ( ) and 1 γC:5 αB mixture of native proteins ( ) chromatograms are shown. C) 1 γS:5 αB suppression reaction ( ) and 1 γS:5 αB mixture of native proteins ( ) chromatograms are shown. The suppression reactions shown in Fig. 2-2 were applied to a Superose 6 size-exclusion column (for the native mixture samples' preparation see Materials and Methods) Arrows correspond to elution volume of standards. Numbers represent standards' molecular masses in kDa.

4. Destabilization of the C-terminal domain is required for the formation of the partially folded, aggregation-prone intermediate of γD-Crys

Since the crystal structure of γD-Crys has been solved to 1.25 Å resolution and its folding pathway has been previously described in detail, I chose γD-Crys to further study interactions between αB-Crys chaperone and this physiological substrate (Basak *et al.* 2003; Kosinski-Collins and King 2003; Kosinski-Collins *et al.* 2004; Flaugh *et al.* 2005b; Flaugh *et al.* 2005a). Long-lived intermediates have been implicated as species responsible for the aggregation of several proteins because they might give rise to aggregation-prone species during refolding (Wetzel 1994; Speed *et al.* 1996). A stable intermediate is populated during WT γD-Crys unfolding/refolding equilibrium experiments and is manifested as a slight inflection in the equilibrium traces at 2.3 M GdnHCl (Kosinski-Collins and King 2003; Kosinski-Collins *et al.* 2004). This species is well-populated during the unfolding/refolding equilibrium experiment of a variety of crystallins carrying single amino acid substitutions (Flaugh *et al.* 2005b; Flaugh *et al.* 2005a; Flaugh *et al.* 2006). This species has its N-terminal domain unfolded and the C-terminal domain folded, hence the hydrophobic patches in the domains' interfaces are exposed to solvent (Kosinski-Collins *et al.* 2004). Consequently, these hydrophobic patches could be candidate sites for intermolecular aggregate interactions.

Previous studies have shown that the two transitions observed during equilibrium unfolding/refolding experiments correspond to the successive unfolding of each domain, with the first transition (~ 2.2 M GdnHCl) corresponding to the unfolding/refolding of the N-terminal domain and the second transition (~ 2.8 M GdnHCl) to the unfolding/refolding of the C-terminal domain (Kosinski-Collins *et al.* 2004; Flaugh *et al.* 2005a). Therefore, it is possible to partially unfold γD-Crys at different concentrations of GdnHCl encompassing both transitions and to populate stable, partially-unfolded species.

To explore the structural requirements for aggregation, two step reactions were performed. Wild-type γD-Crys was unfolded at different concentrations of GdnHCl in order to investigate whether the long-lived folding intermediate was the aggregation-prone species (2.49, 2.82, 3.09 and 5.03 M GdnHCl). γD-Crys unfolded at these concentrations does not self-associate and aggregate prior to dilution of the denaturant (Flaugh *et al.* 2005b). After equilibrium conditions were reached, unfolded γD-Crys was diluted to lower concentrations of GdnHCl (0.5 M GdnHCl, final protein concentration was 50 μg/ml) (Fig. 2-5). The $O.D._{350\ nm}$ amplitudes were 0.2 and 0.25 AU for 2.82 M and 3.02 M GdnHCl unfolded samples respectively, while the final $O.D._{350\ nm}$ amplitude was 0.45 AU for 5.03 M GdnHCl unfolded samples (Fig. 2-5). This lower level in final $O.D._{350\ nm}$ was due to a higher proportion of protein

refolding productively when diluted out of these intermediate GdnHCl concentrations (data not shown). These results indicate that the C-terminal domain of γD-Crys must be destabilized and partially unfolded for the protein to aggregate *in vitro.* Further, these result suggest that the stable folding intermediate, with its C-terminal domain folded and N-terminal domain unfolded, observed in unfolding/refolding equilibrium experiments, is likely not the aggregation-prone intermediate.

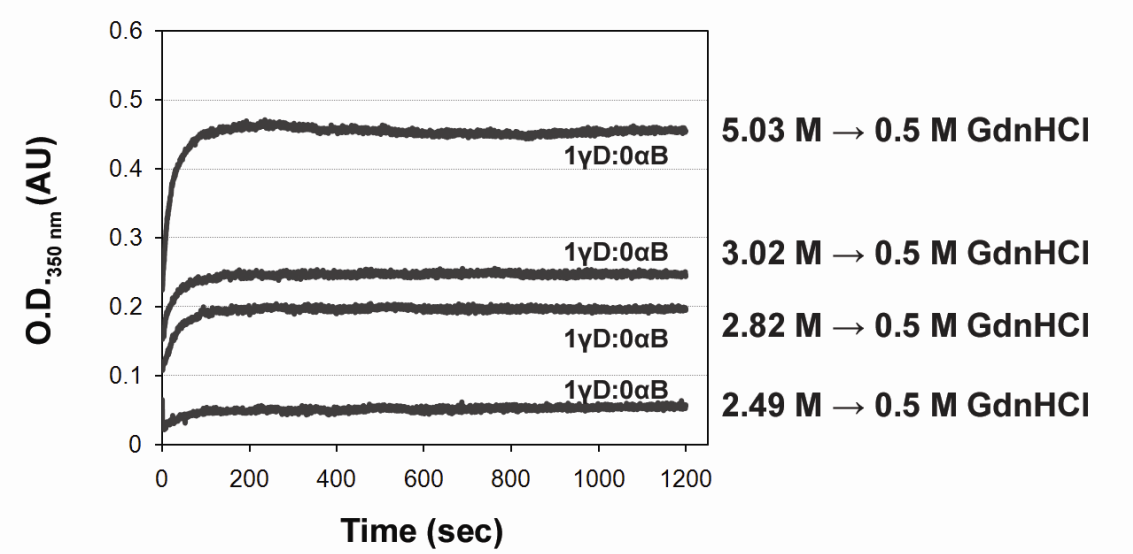

Figure 2-5: Aggregation of partially unfolded γD-Crys during refolding.
1 γD:0 αB reactions for γD unfolded at GdnHCl concentrations encompassing the intermediate-to-unfolded protein transition. γD was unfolded at 2.49, 2.82, 3.02, or 5.03 M GdnHCl for 24 h at 37 ºC to ensure equilibrium conditions. Protein was refolded by diluting the GdnHCl concentration to 0.5 M at 37 ºC. The final concentration protein concentration was 50 µg/ml for all samples.

5. Monitoring the conformation of the bound substrate

γD-Crys has four buried Trp residues, two in the N-terminal domain (Trp42 and Trp68, Fig. 2-7A) and two in the C-terminal domain (Trp130 and Trp156, Fig. 2-7A) (Basak *et al.* 2003). As described in Chapter 1, rapid electron transfer from the excited Trp indole ring to its amide backbone results in the efficient quenching of the weakly fluorescing, strongly quenched Trp68 and Trp156 (Chen *et al.* 2006). The intra-domain mechanism of quenching of Trp fluorescence in the native state of γD-Crys is due to partial resonance energy transfer from the strongly fluorescing tryptophans (Trp42 and Trp130) to their weakly fluorescing counterparts (Trp68 and Trp156). We took advantage of the structural information provided by the fluorescence emission of buried tryptophan residues in γD-Crys to further elucidate the structural nature of the substrate that is recognized by αB-Crys chaperone during aggregation.

Wild-type αB-Crys contains two tryptophan residues at positions 9 and 60. Mutating both residues to phenylalanine resulted in the elimination of fluorescence emission compared to wild-type protein when the excitation wavelength (λ_{EX}) was set to 300 nm to selectively excite tryptophan residues (Fig. 2-6A). Liang and colleagues (Liang *et al.* 1999) have shown that individually mutating these tryptophan residues to phenylalanine does not result in secondary structural changes to αB-Crys. Structural changes in quaternary structure between wild-type and mutant proteins were not detected during SEC (Fig. 2-6C). Suppression assays using γD-Crys as the substrate showed that the chaperone activity was conserved in the W9F/W60F αB-Crys mutant (noTrp αB) (Fig. 2-6B).

1 γD:5 no Trp αB suppression reactions were collected and loaded onto a Superose 6 SEC column (Fig. 2-6C). The fluorescence emission spectrum was recorded for the fraction corresponding to the high molecular weight complex (Fig. 2-6C, gray bar) at a λ_{EX} of 300 nm. Since αB-Crys contains no tryptophan residues, only the tryptophan residues from γD-Crys present in this complex would contribute to the fluorescence spectrum. The spectrum of the γD—αB-Crys complex (maximum emission wavelength ~ 335 nm) did not coincide with either the spectra of the native or unfolded WT γD-Crys suggesting that the substrate might be in a partially-folded state (Fig. 2-6D).

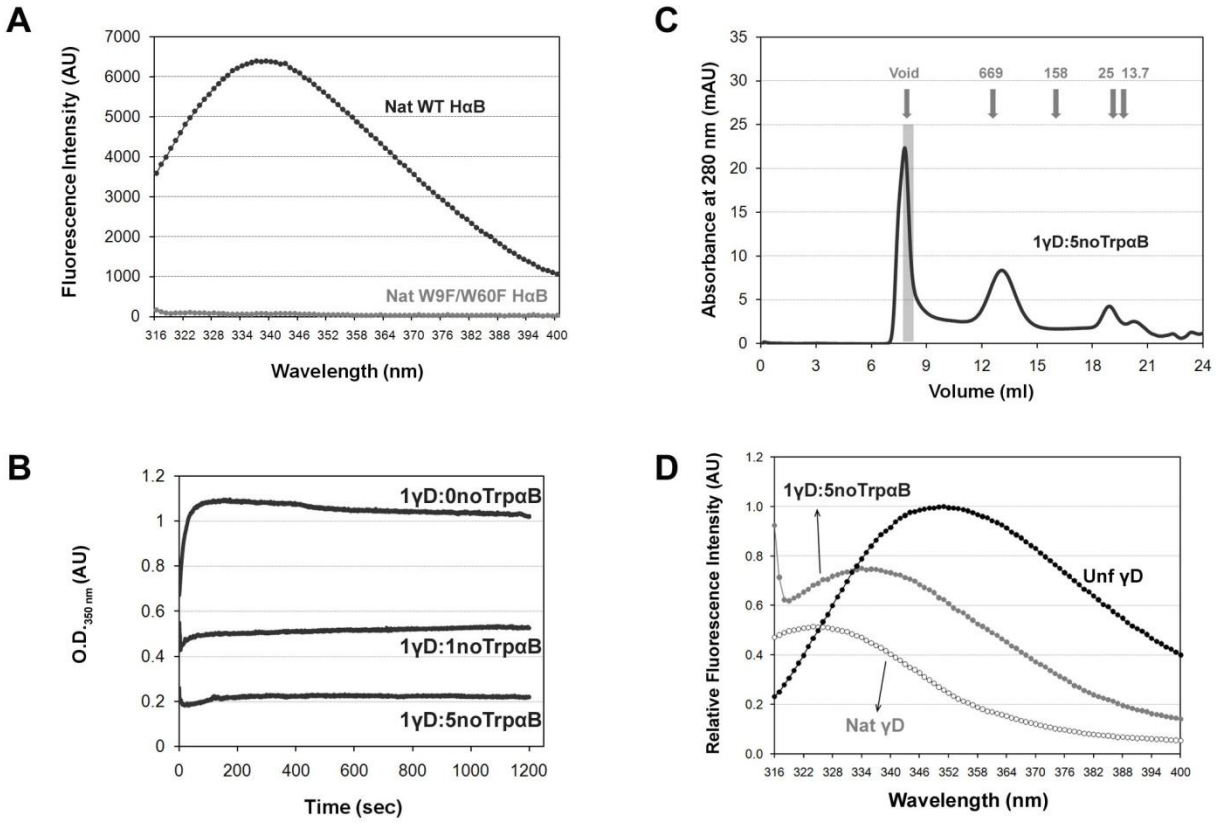

Figure 2-6: Tryptophan fluorescence of γD-Crys in complex with αB-Crys chaperone.
Tryptophan residues at positions 9 and 60 in αB-Crys were substituted to phenylalanines. A) Fluorescence emission spectra for native WT αB-Crys (●) and W9F/W60F αB-Crys (●) at 25 ºC. λ_{EX} was set to 300 nm.

B) W9F/W60F αB-Crys suppressed the aggregation of γD-Crys under the same refolding and aggregation described previously (see Materials and Methods). Final γD-Crys concentration was 100 µg/ml and final GdnHCl concentration was 0.5 M at 37 ºC.

C) A high molecular weight complex could be isolated from the 1γD:5 no Trp αB suppression reactions during SEC. The volume highlighted by the gray bar corresponds to the fraction collected for fluorescence measurements.

D) Relative fluorescence emission spectrum of the fraction containing the γD—αB complex (●). For comparison purposes, the fluorescence emission spectrum of native (○) and fully unfolded (●) WT γD-Crys (20 µg/ml) are shown. The λ_{EX} was set to 300 nm for all samples. Traces were normalized to the fluorescence intensity of the maximum λ_{EM} for unfolded γD-Crys.

To further investigate the conformation of γD-Crys in these complexes, I studied double- and triple-Trp γD-Crys mutants with the Trps replaced by phenylalanines (Chen *et al.* 2006). Double-Trp mutants had either the N-terminal (W130F/W156F γD-Crys, Fig. 2-7A) or C-terminal domain (W42F/W68F γD-Crys, Fig. 2-7A) buried tryptophan pair conserved in order to preserve the tryptophan fluorescence quenching mechanism within each domain. These mutants provided a more detailed picture of the folding status of each domain of γD-Crys when bound to αB-Crys during chaperoning interactions. Both W130F/W156F and W42F/W68F γD-Crys recapitulated the behavior of WT γD-Crys: their tryptophan fluorescence was quenched in the native state and, upon unfolding in high concentrations of denaturant, showed an increase in fluorescence intensity with a concurrent red-shift in their maximum emission wavelength (λ_{EM}) to ~350nm (Chen *et al.* 2006).

Figures 2-7B and C show the relative fluorescence emission spectra for W130F/W156F and W42F/W68F γD-Crys after unfolding these proteins in increasing concentrations of GdnHCl. The red-shift in maximum λ_{EM} coincided with previously published transition GdnHCl concentrations that correspond to the unfolding of the N-terminal and the C-terminal domains of the wild-type protein (Kosinski-Collins and King 2003; Kosinski-Collins *et al.* 2004; Flaugh *et al.* 2005a). W130F/W156F γD-Crys (N-terminal Trp pair) retained the native-like fluorescence spectrum at 1.6 M GdnHCl when the λ_{EX} was 300 nm. Increasing the denaturant concentration to 2.0 M GdnHCl resulted in a red-shift in the maximum λ_{EM} to 350 nm (Fig. 2-7B). The emission spectrum for W42F/W68F γD-Crys (C-terminal Trp pair), on the other hand, remained native-like at 2.3 M GdnHCl (λ_{EX} was 300 nm). At higher concentrations of GdnHCl, the spectra were red-shifted until reaching the maximum λ_{EM} for the fully unfolded protein, approximately 350 nm (3.1 M and 5.2 M GdnHCl traces, Fig. 2-7C).

Given the structural information provided by these γD-Crys mutants, I utilized W42F/W68F and W130F/W156F γD-Crys as substrates in suppression of aggregation reactions with Trp-less αB-Crys chaperone. Both double-Trp mutants aggregated to similar levels as the wild-type protein and Trp-less αB-Crys chaperone showed similar suppression efficiency as with the wild-type γD-Crys (data not shown). The substrate-chaperone complexes were isolated from 1 γD:5 no Trp αB suppression reactions via SEC using a Superose 6 SEC column (Fig. 2-7D). Fluorescence emission spectra (λ_{EX} = 300 nm) were recorded for the fraction corresponding to the substrate-chaperone peak for both double-Trp mutants (Fig. 2-7E and F). The fluorescence emission spectra for both double-Trp mutants in complex with Trp-less αB-Crys were similar (maximum λ_{EM} ~ 333 nm). However, these spectra did not coincide with the spectra for their respective native or unfolded states (Fig. 2-7E and F). These results point to similar environments for both the N-terminal domain and C-terminal domain of γD-Crys in complex with αB-Crys. The tryptophan residues of γD-Crys in the complex did not seem to be exposed to solvent or did

not seem to retain the conformation necessary for the quenching phenomenon observed in the native state. Either the tryptophans were in buried but in non-native conformations or they were directly interacting with the chaperone subunits.

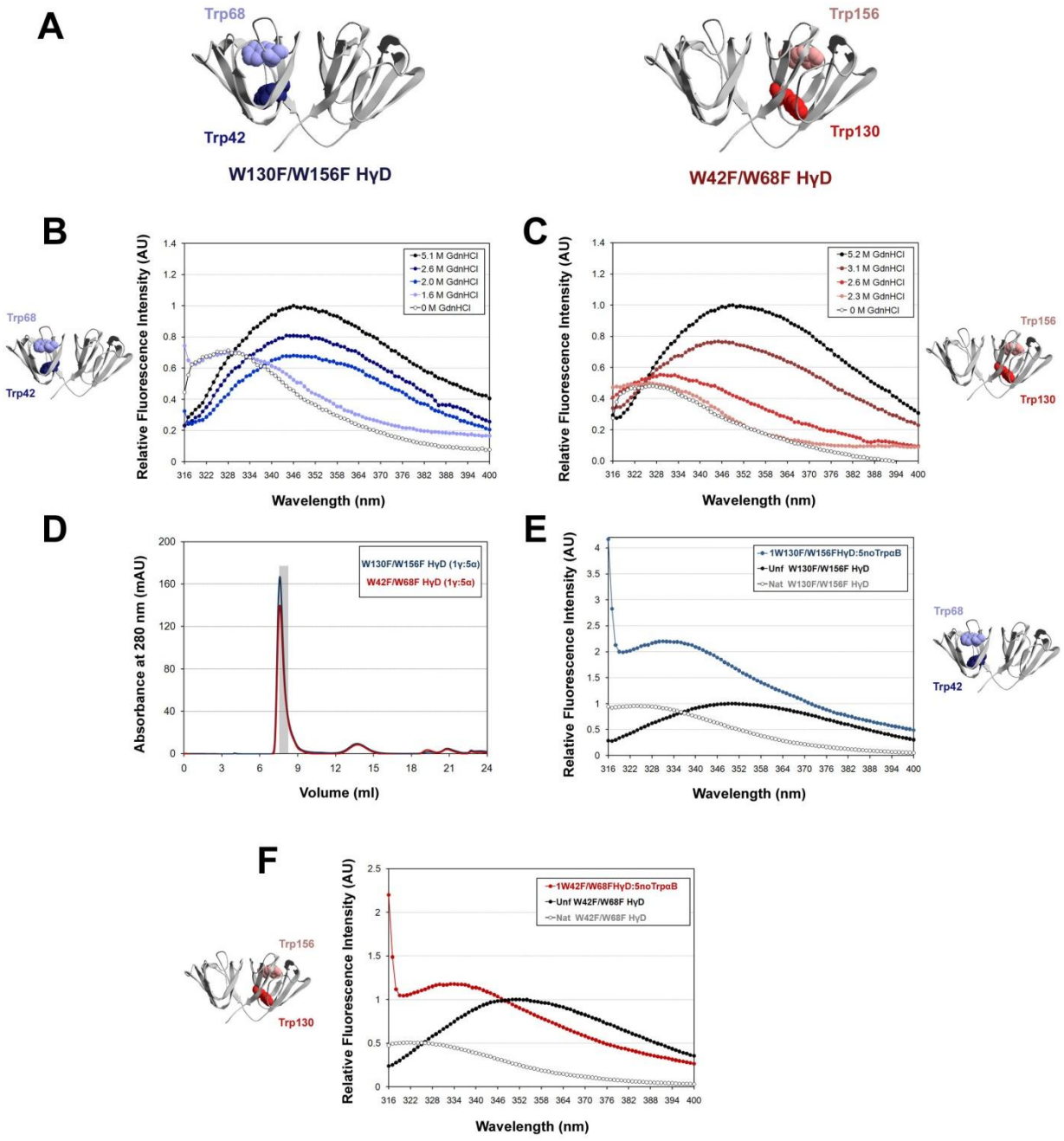

Figure 2-7: Tryptophan fluorescence spectra from double-Trp γD-Crys mutants in complex with αB-Crys chaperone

A) Crystal structure of γD-Crys (PDB: 1HK0) showing Trp pairs conserved within the N-terminal domain (W130F/W156F γD-Crys) or the C-terminal domain (W42F/W68F γD-Crys).

B) Relative fluorescence emission spectra of W130F/W156F γD-Crys unfolded at different concentrations of GdnHCl. W130F/W156F γD-Crys (20 μg/ml) was incubated in Refolding buffer with 0, 1.6, 2.0, 2.6 and 5.1 M GdnHCl for 24 h at 37^0C. Fluorescence emission spectra were recorded using a λ_{EX} set to 300 nm. All traces were normalized to the fluorescence intensity of the maximum λ_{EM} for W130F/W156F γD-Crys unfolded at 5.1 M GdnHCl.

C) Relative fluorescence emission spectra of W42F/W68F γD-Crys unfolded at different concentrations of GdnHCl. W42F/W68F γD-Crys (20 μg/ml) was incubated in Refolding buffer with 0, 2.3, 2.6, 3.1 and 5.2 M GdnHCl for 24 h at 37^0C. Fluorescence emission spectra were recorded using an λ_{EX} set to 300 nm. All traces were normalized to the fluorescence intensity of the maximum λ_{EM} for W42F/W68F γD-Crys unfolded at 5.2 M GdnHCl.

D) SEC chromatograms for 1 γD:5 no Trp αB suppression reactions using W130F/W156F (▬) or W42F/W68F (▬) γD-Crys as substrates. The shaded area on the trace indicates the fraction used for fluorescence measurements.

E) Relative fluorescence emission spectrum of the fraction containing the γD—αB complex from 1 W130F/W156F γD: 5 no Trp αB suppression reaction (●). For comparison purposes, the fluorescence emission spectra of native (○) and fully unfolded (●) W130F/W156F γD-Crys (50 μg/ml) are shown. The λ_{EX} was set to 300 nm for all samples. Traces were normalized to the fluorescence intensity of the maximum λ_{EM} for unfolded γD-Crys.

F) Relative fluorescence emission spectrum of the fraction containing the γD—αB complex isolated from 1 W42F/W68F γD: 5 noTrp αB suppression reaction (●). The λ_{EX} was set to 300 nm for all samples and the protein concentration for the native (○) and fully unfolded (●) W42F/W68F γD-Crys protein samples was 50 μg/ml. Traces were normalized as described above.

Given the similarity in fluorescence spectra between wild-type and the double-Trp mutants of γD-Crys, it is likely that it is due to interaction of regions surrounding the Trp residues with αB-Crys in the chaperone-substrate complexes. In order to monitor binding interactions at specific regions of γD-Crys more closely, I took advantage of triple-Trp mutants that conserved the highly-fluorescent, buried Trp residues in either the N-terminal (W42only γD-Crys) or the C-terminal domain (W130only γD-Crys), while the remaining three tryptophans were changed to phenylalanines. Chen *et al.* (Chen *et al.* 2006) previously characterized the buried tryptophan fluorescence behavior of these proteins and found that the quenching phenomenon observed in the native state of wild type and double-Trp mutants described above was absent in these triple-Trp γD-Crys mutants.

Since these tryptophan residues (Trp42 and Trp130) emit a robust fluorescence emission signal, I used these mutants in suppression aggregation reactions with Trp-less αB-Crys chaperone to reveal general features of the environment around these residues in the γD—αB complex. Both W42only and W130only γD-Crys aggregated after dilution out of denaturant and Trp-less αB-Crys suppressed their aggregation efficiently (at 1 γ:5 αB ratios). Figure 2-8A shows the emission spectrum of W42only γD-Crys in the γD—αB complex excited at 300 nm; the maximum λ_{EM} was approximately 334 nm and the spectrum did not coincide with the spectra for the native and unfolded W42only γD-Crys controls. The fluorescence emission spectrum for W130only γD-Crys in the complex had a maximum λ_{EM} at approximately 333 nm and also did not coincide with either the native or fully-unfolded tryptophan fluorescence spectra of controls (λ_{EX}=300 nm; Fig. 2-8B). These results indicate that the residues in close proximity to Trp42 and Trp130 are not solvent exposed in the γD—αB complex and might be involved in binding interactions with αB-Crys chaperone.

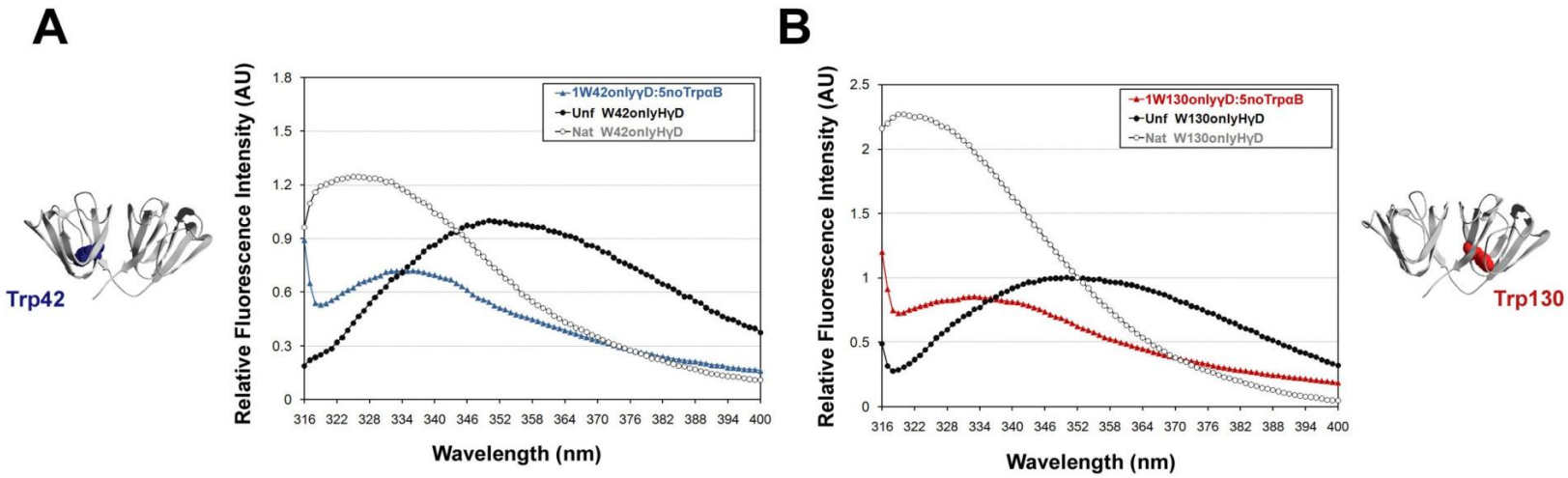

Figure 2-8: Fluorescence emission spectra of triple-Trp γD-Crys mutants in complex with αB-Crys.
A) Relative fluorescence emission spectra for W42only γD-Crys in complex with noTrp αB-Crys (●). B) Fluorescence emission spectra for W130only γD-Crys in complex with noTrp αB-Crys (●). Spectra for their respective native (○) and unfolded (●) controls are also shown (protein concentration for W42only γD-Crys was 50 μg/ml and for W130only γD-Crys was 25 μg/ml). The λ_{EX} was 300 nm and the traces were normalized as described previously in Figure 2-7. Complexes were isolated from 1γD:5αB suppression reactions in which the final concentration of γD was 50 μg/ml.

6. αB-Crys chaperone forms stable complexes with partially folded γD-Crys

α-crystallin is the major chaperone system in differentiated lens fiber cells. Since there is no protein turnover, aggregation of covalently damaged crystallins is prevented through interactions with α-crystallin.(Bloemendal *et al.* 2004) Therefore, the complex between α-crystallin and its β/γ-crystallin substrates must be long-lived in order for lens transparency to be maintained. We investigated the lifetime of this complex *in vitro* by initiating the aggregation of γD-Crys in the presence of αB-Crys at a 1 γD:5 αB ratio. The suppression reaction was allowed to proceed at 37 ºC with moderate shaking and aliquots were removed at different times and applied to a Superose 6 SEC column. During this incubation period, I did not confirm whether any chemical modifications were introduced into γD-Crys or αB-Crys chaperone during the 4-day period.

Figure 2-9 shows the set of chromatograms collected within a time period of 30 min to 4 days after aggregation was initiated. The high molecular weight peak eluted at the $V_{0,}$ ~7.6 ml (Fig. 2-9, Inset). This peak was still present 4 days after the suppression reaction was initiated. Further, the absorbance at 280 nm of this peak at 7.6 ml increased after 30 min, decreased and remained constant thereafter for later time points. The WT αB-Crys chaperone peak (eluted at 13.5 ml) remained constant throughout the duration of the experiment. These results showed that the γD—αB complexes were stable for long periods of time supporting α-crystallin's role as a chaperone in the lens.

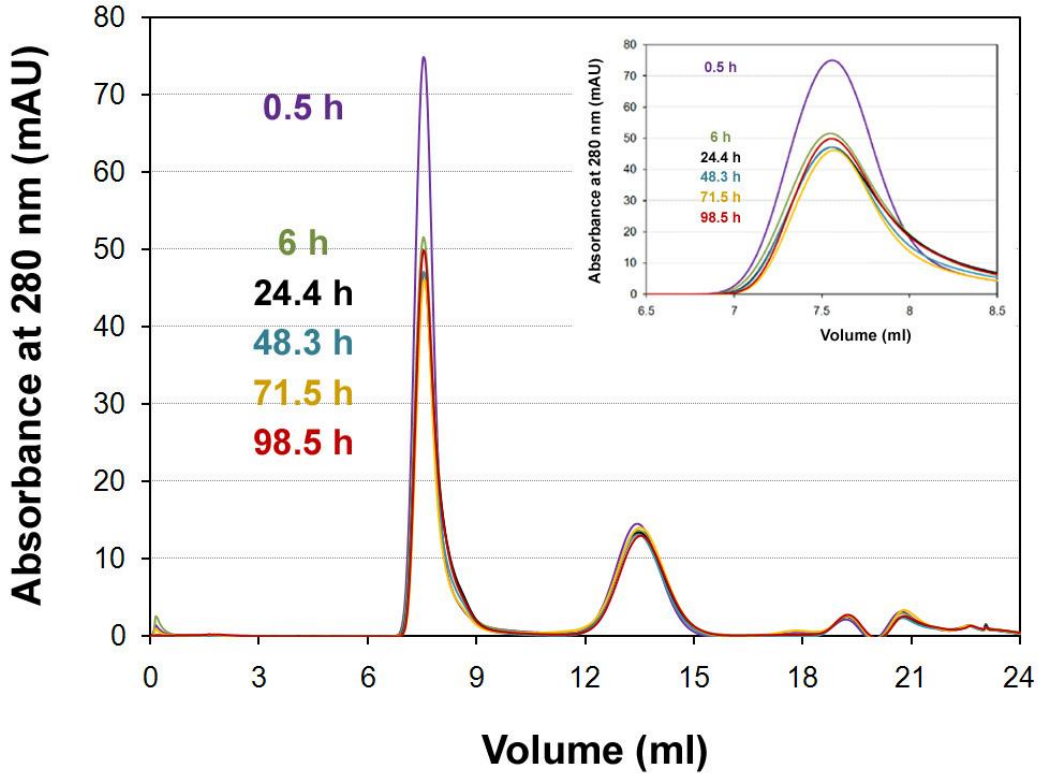

Figure 2-9: SEC chromatograms of αB—γD complexes at different time points after suppression reaction.
SEC chromatograms of 0.5 ml aliquots removed from a 1 γD:5 αB suppression reaction incubated at 37 ºC with continuous agitation. Time points at which aliquots were collected are shown on the chromatogram. The peak that eluted at 7.6 ml is the designated high molecular weight complex and eluted in the void of the column (V_0= 8 ml). The peak that eluted at 13.5 ml corresponded to wild-type αB-Crys. Inset shows in detail the high molecular weight peak that eluted at 7.6 ml.

7. αB-Crys chaperone interacts with early and late aggregate species in the aggregation pathway of partially folded γD-Crys

Despite its chaperone function, α-crystallin is often found in cataractous inclusions in significant proportions (Hanson *et al.* 2000; Harrington *et al.* 2004; Harrington *et al.* 2007; Heys *et al.* 2007). Further, αA-Crys knock-out mice developed cataract at an early age in which αB-Crys was localized to the insoluble fraction of lens fiber cell cytoplasm (Brady *et al.* 1997b). Therefore, I was interested in investigating the lifetime of the substrate species that is recognized by αB-Crys chaperone.

To do so, I added Trp-less αB-Crys chaperone at very early time points (2, 6, and 10 s) after dilution of γD-Crys out of denaturant. Wild-type γD-Crys was added to Refolding Buffer that was constantly stirred with a spin-bar; the solution was stirred only for the first 30 s after fully unfolded γD-Crys was added. The final $O.D._{350\ nm}$ levels did not change significantly using this method. Trp-less αB-Crys was added 0, 2, 6 or 10 s after refolding and aggregation of γD-Crys were initiated. Solution turbidity increased the later Trp-less αB-Crys was added after refolding and aggregation were initiated (Fig. 2-10A and B). Controls were performed by adding H_2O after 6 and 10 s and showed no significant change in the kinetics or the level of aggregation of γD-Crys (data not shown).

Using Trp-less αB-Crys chaperone allowed us to record the fluorescence emission spectrum of the WT γD-Crys species bound to αB-Crys chaperone in the complexes isolated via SEC (Fig. 2-10C). All spectra had the same maximum λ_{EM} (~336 nm), however, the fluorescence intensity decreased in samples from later addition time points indicating a decrease in the concentration of γD—αB complexes (Fig. 2-10D). These results indicate that the species recognized and bound to αB-Crys chaperone is a transient intermediate populated at very early times of refolding and aggregation.

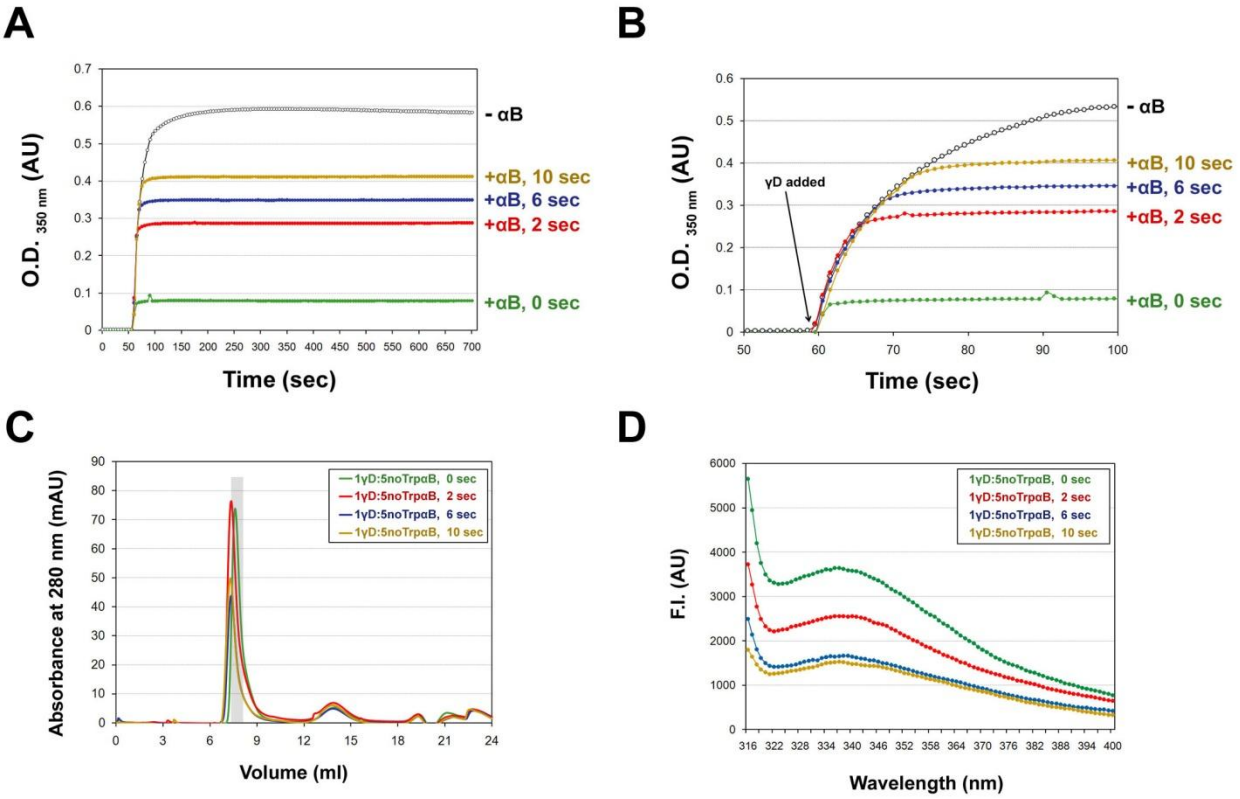

Figure 2-10: Addition of αB-Crys at very early time points after initiation of refolding and aggregation of partially folded WT γD-Crys.
A) O.D. $_{350nm}$ data for no addition of αB-Crys (1 γD:0 αB ratio) and addition 0, 2, 6, and 10 s after WT γD-Crys was added to Refolding buffer (1 γD:5 αB ratio). Buffer was constantly stirred with a magnetic spin bar and γD-Crys was added 60 s after light scattering data collection was initiated. Samples were allowed to mix for the first 30 s after γD-Crys addition. B) Light scattering data presented in (A) showing traces from 50-100 s after recordings were initiated.

C) SEC traces for suppression reactions shown in (A). Samples were loaded onto a Superose 6 SEC column. The fraction corresponding to the γD—αB complex was collected for fluorescence emission measurements (gray bar).

D) Raw fluorescence emission spectra for fractions highlighted in (C) and containing the γD—αB complex formed during addition of αB-Crys 0, 2, 6, and 10 s after addition and initiation of γD-Crys refolding and aggregation. λ_{EX} was set to 300 nm.

Adding αB-Crys chaperone any time after 15 s resulted in no suppression of γD-Crys aggregation (Fig. 2-11). Interestingly, when αB-Crys was added 5 min after the aggregation reaction was started there was an increase in the scatter of the aggregate compared to controls (Fig. 2-11). Similar results were also observed when αB-Crys was added 30 min after initiation of aggregation of partially folded γD-Crys. Given the structures of γD-Crys aggregates observed at these time points by Kosinski-Collins and King (Kosinski-Collins and King 2003), it seems that αB-Crys chaperone is being incorporated into or binds to these pre-formed large fibril-like aggregates of γD-Crys, but does not disaggregate them. Similar behavior has been reported for IbpA and IbpB, sHsps in *E. coli*, which are known to be present in inclusion bodies formed during overexpression of heterologous protein (Allen *et al.* 1992; Jiao *et al.* 2005a).

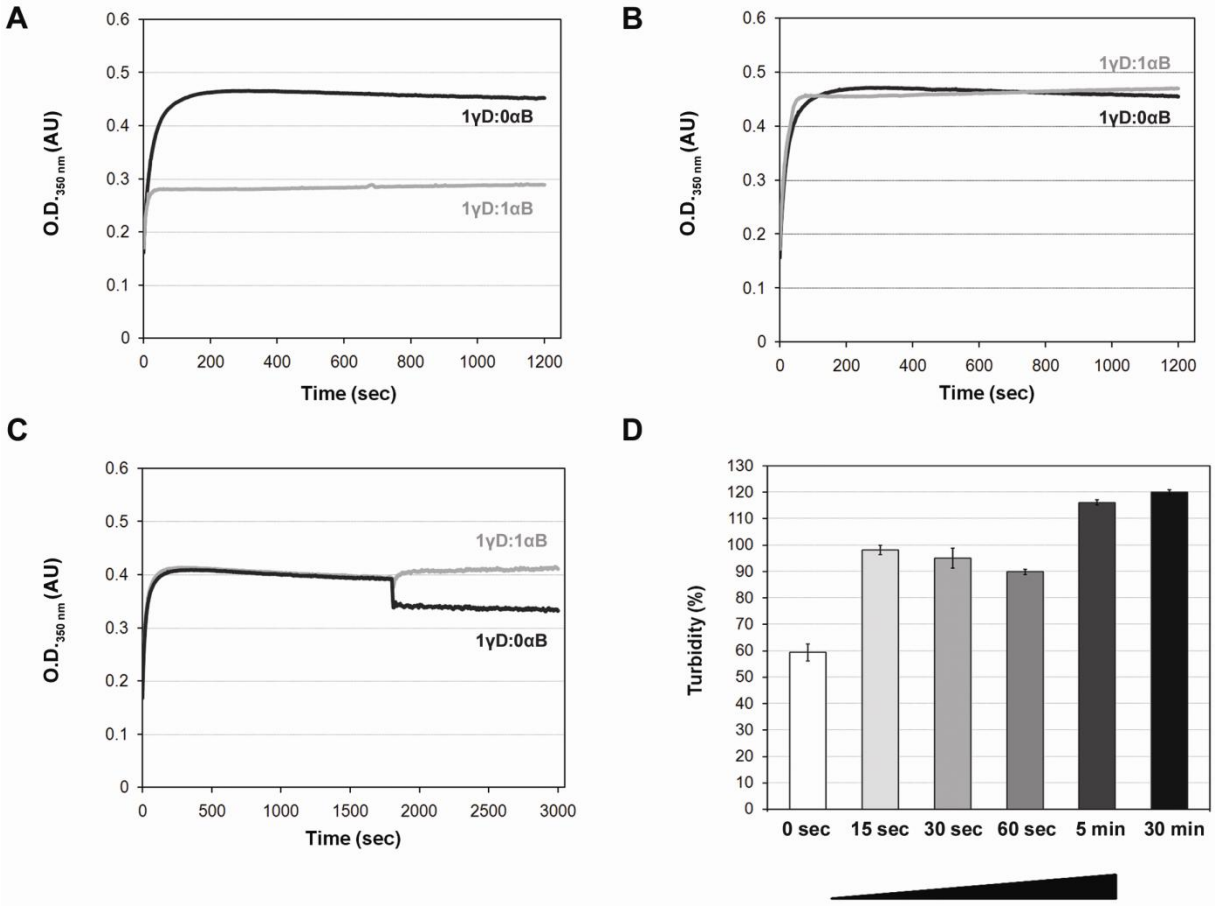

Figure 2-11: Addition of αB-Crys at different time points after initiation of refolding and aggregation of partially folded γD-Crys.

A) Light scattering data for αB-Crys addition at 0 s, B) 30 s and C) 30 min after aggregation was initiated. Gray traces correspond to one representative 1 γD:1 αB suppression reaction out of three trials, while black traces correspond to one representative 1 γD:0 αB aggregation reaction at each respective time point. Samples (1 γD:0 αB and 1 γD:1 αB) were allowed to aggregate and at the designated time point data collection was paused for 10 s , H_2O or αB-Crys was added, mixed and data collection was resumed. Final γD-Crys protein concentration was 50 µg/ml and the final GdnHCl concentration was 0.5 M.

D) Turbidity percentages for addition of αB-Crys (from 1 γD:1 αB samples) at different time points, ranging from 0 to 30 min, after initiation of aggregation. Turbidity percentages represent the mean final amplitude for three 1 γD:1 αB reactions when their respective 1 γD:0 αB reaction control's amplitude is designated as 100% turbidity. The bars indicate the standard deviation.

D. DISCUSSION

The native states of the γ-crystallins are very soluble, very stable and among the longest-lived proteins in the human body (Bloemendal *et al.* 2004). They show little tendency to aggregate or associate even at high concentrations. Except for special cases such as sickle cell anemia, most well-characterized protein aggregation reactions represent the polymerization of partially folded species (Mitraki 1989; Wetzel 1994; Ecroyd and Carver 2008). The examples of the well-characterized protein aggregation diseases, including Parkinson's disease, prion protein encephalopathies, and Huntington's disease, suggest that partially folded or unfolded intermediates are also the key species in the crystallin aggregation reactions that lead to cataract (Kelly 1998; Uversky and Fink 2004). Extensive characterization of α-crystallins with model substrates support models in which partially folded species are the substrates (Carver *et al.* 1995; Lindner *et al.* 1997). However, the absence of a high resolution structure for the full-length protein chaperone, and the difficulty in characterizing the substrate conformations recognized within normal or cataractous lens, has limited our ability to define the conformation of the physiological substrates of α-crystallins.

1. Competitive off-pathway aggregation of γD-Crys during refolding conditions

Productive kinetic refolding experiments showed that two partially folded intermediates were populated during WT γD-Crys refolding (Flaugh *et al.* 2006). Significant refolding, as measured by changes in tryptophan fluorescence, occurred within the mixing dead time that initiated these kinetic refolding experiments. It is unlikely that a true random coil, as found in the fully denatured state, is significantly populated after the first seconds of the refolding reaction. The first two transitions, with $t_{1/2}$ values of 8 and 35 s, corresponded to the folding of C-terminal domain, while the third transition, with a $t_{1/2}$ value of 130 s, was significantly longer with and corresponded to the folding of the N-terminal domain (Flaugh *et al.* 2006). Flaugh *et al.* (Flaugh *et al.* 2005a; Flaugh *et al.* 2005b) showed that the residues on the interface of the C-terminal domain nucleated the folding of the N-terminal domain. Previously published work on deamidated γD-Crys mutants of the interface glutamine residues (Flaugh *et al.* 2006) and molecular dynamics simulations of γD-Crys unfolding (Das *et al.* 2010) suggest that the folding nucleus of the protein is located in the Greek key motif in the C-terminal domain closest to the domain interface of the protein (Motif IV).

Aggregation experiments with partially unfolded γD-Crys showed that the C-terminal domain must be partially unfolded for the protein to aggregate after dilution into low concentrations of denaturant

(Fig. 2-5). Further, when γD-Crys was fully unfolded, αB-Crys recognized and bound to partially folded, aggregation-prone species populated during the first 10 s after refolding and aggregation were initiated (Fig. 2-10A and B). The C-terminal domain also productively refolds during this time period (Kosinski-Collins *et al.* 2004; Flaugh *et al.* 2005a; Mills *et al.* 2007). Experiments with the isolated single domain constructs of the N-terminal or C-terminal domain of γD-Crys showed that the single C-terminal domain of γD-Crys aggregated during dilution out of high concentrations of denaturant, while the single N-terminal domain of γD-Crys did not aggregate under similar conditions (Fig. 3-2A). Therefore, it is likely that the aggregation-prone region is located in the C-terminal domain and was recognized by the αB-Crys chaperone during these aggregation reactions.

2. Conformation of the partially folded γ-crystallin bound to αB-Crys chaperone oligomers

The long-lived nature of the γD—αB complex allowed us to characterize the conformation of the substrate bound to the chaperone (Fig. 2-9). The isolation using SEC of γD—αB-Crys complexes from 1 γD:5 noTrp αB suppression reactions indicated that γ-crystallin was present in the high molecular weight oligomeric complex. Since all tryptophans in αB-Crys were changed to phenylalanines and the excitation wavelength was set to preferentially excite tryptophan residues, the fluorescence emission spectra of these complexes provided structural information for bound WT γD-Crys (Fig. 2-6D). We compared this spectrum to the spectra from native and unfolded WT γD-Crys. The fluorescence emission spectrum for each conformation is distinct (i.e. the maximum λ_{EM} is unique to each state). The fluorescence emission spectrum of γD-Crys from these complexes did not resemble the spectra for either native or fully unfolded γD-Crys (Fig. 2-6D).

Suppression reactions with double-Trp mutants of γD-Crys as substrates and Trp-less αB-Crys as the chaperone provided information on the folding status of each domain of γD-Crys in the γD—αB complex (Fig. 2-7). These double-Trp γD-Crys mutants only had the tryptophan pairs within the N-terminal (W130F/W156F γD-Crys) or C-terminal domain (W42F/W68F γD-Crys), so that the intra-domain native state quenching mechanism was conserved. If γD-Crys had either domain folded in the γD—noTrp αB complex, then fluorescence emission spectra of the substrate would be similar to the spectra of the native protein. Our results showed that both double-Trp mutants in γD—noTrp αB complexes had similar maximum λ_{EM}, and that their spectra did not resemble either their respective native or unfolded states (Fig. 2-7E and F). Further, these spectra were similar to the spectrum of the wild-type

protein in complex with Trp-less αB-Crys chaperone (Fig. 2-6D). These results indicate that the intra-domain tryptophan pairs of γD-Crys were in similar environments in the γD—αB complexes.

The maximum λ_{EM} for tryptophan fluorescence is sensitive to local environment and changes in response to various degrees of solvent exposure (Vivian and Callis 2001). Previous studies have characterized the fluorescence behavior of the buried tryptophans in the double- and triple-Trp mutants described previously (*vide supra*) (Kosinski-Collins *et al.* 2004; Chen *et al.* 2006). For the native states of the triple-Trp γD-Crys mutants, Chen *et al.* found that the highly fluorescing Trps (Trp42 and Trp130) had a maximum λ_{EM} at ~322 nm, while the maximum λ_{EM} was 332 nm for the quenched Trps (Trp68 and Trp156) (Chen *et al.* 2006). Chen *et al.* also compared these values to the maximum λ_{EM} from fluorescence emission spectra of 3-methylindole (3-MI), a tryptophan indole ring analog, in different solvent mixtures. The maximum λ_{EM} for Trp42 and Trp130 native spectra closely matched the spectrum for 3-MI in a less polar solvent mixture (cyclohexane-dioxane, 83:17), while the fluorescence spectra and maximum λ_{EM} for 3-MI in a more polar solvent mixture (methanol-dioxane, 25:75 and 10:90) were similar to native spectra from Trp68 and Trp156. Within the context of the quenching mechanism in the native state, these results bolstered the model of intra-domain partial resonance energy transfer from the highly-fluorescent Trps (donors) to the quenched Trps (acceptors) proposed by Chen and colleagues (Chen *et al.* 2006).

This comprehensive investigation of the buried Trp fluorescence of γD-Crys allowed us to refine our model on the conformation of the aggregation-prone γD-Crys species that is bound to αB-Crys during the chaperoning process. I performed aggregation suppression assays with W42only and W130only γD-Crys triple-Trp mutants as substrates (Fig. 2-8). These mutants retained the highly fluorescing tryptophan from each domain thus allowing us to assess the environment surrounding these regions in both domains in the γD—noTrp αB complex. The fluorescence emission spectra of W42only or W130only γD-Crys in the substrate-chaperone complex did not coincide with their respective native and unfolded spectra. Therefore, Trp42 and Trp130 were neither fully exposed to solvent nor did they remain buried in the hydrophobic core of the native state (Fig. 2-8).

These results point to a possible interaction between the Trp residues, or the immediate regions surrounding them, and αB-Crys chaperone in the complex. One possible model to explain these results is that αB-Crys could initially recognize the exposed, buried aggregation-prone region in Motif 4 (which includes Trp130 and Trp156) in the C-terminal domain, bind to it, and keep it from interacting with other aggregation-prone regions. Binding to the homologous hydrophobic region in the N-terminal domain could occur after the initial recognition step. An exposed state of the Trp rings, which are intended to be

buried in the native state, offers an attractive model for how the chaperone discriminates between partially folded intermediates and the fully folded state.

Another possible model is that the distinct fluorescence emission spectra of double- and triple-Trp γD-Crys mutants in complex with Trp-less αB-Crys could be due to their tryptophan residues being exposed to polar environments between γD-Crys chains in small, soluble aggregates formed in the first 10 s after dilution out of denaturant. αB-Crys chaperone would bind these small γD-Crys oligomers prevent further growth into fibril-like aggregates. If this were the case, however, I would see similar or increased efficiency of suppression within these first 10 s, rather than a progressive decrease in suppression of aggregation as judged by the increase in light scattering at 2, 6, or 10 s (Fig. 2-10A and B).

As mentioned above, αB-Crys suppression activity was confined to early species along the aggregation pathway of γD-Crys, which may still be monomeric (Fig. 2-10). Adding αB-Crys at later times showed that the chaperone no longer suppressed aggregation, but may have been interacting with insoluble aggregates as judged by increases in solution turbidity (Fig. 2-11). Kosinski-Collins and King (Kosinski-Collins and King 2003) have shown that during this time period small fibrillar aggregates form. Small Hsps IbpA and B from *E. coli* are integrated into inclusion bodies when the amount of substrate exceeds the amount of sHsp in the cell (Allen *et al.* 1992; Jiao *et al.* 2005a).

3. Human γC-, γD-, and γS-Crys share a common aggregation-prone species that is recognized by αB-Crys chaperone

We have shown that the partially folded forms of all three human γ-crystallins, γC, γD and γS, will aggregate during refolding when diluted out of denaturant into buffer (Fig. 2-2). Their aggregation propensity points to a common species populated during refolding that is aggregation-prone. This species is populated very early during dilution out of high concentrations of denaturant (Fig. 2-10) (Kosinski-Collins *et al.* 2004; Flaugh *et al.* 2005a).

The lens is a protected environment lacking blood supply and with low metabolic activity, it is not clear what agents in that environment destabilize proteins, but the leading candidates are oxidative and photo-oxidative damage (Hains and Truscott 2007). Many of the crystallins found in insoluble inclusions from mature-onset cataractous lenses contain a host of covalent damages with deamidation of glutamine and asparagines, and oxidation of methionine and tryptophan residues being the most abundant (Wilmarth *et al.* 2006). Lampi and coworkers have shown that deamidation-mimicking changes at interface residues of β-crystallins lower protein stability and stabilize intermediates during equilibrium

unfolding/refolding experiments (Lampi *et al.* 2006; Takata *et al.* 2007). In the case of human γD-Crys, Flaugh *et al.* (Flaugh *et al.* 2006) showed that the introduction of negative charges at the interface in Gln→Glu deamidated mutants led to the preferential destabilization of the N-terminal domain as shown by the population of the folding intermediate at lower concentrations of denaturant in equilibrium unfolding/refolding experiments. γ-crystallins, with their four buried tryptophans, also absorb UV-radiation and photo-oxidized tryptophans have been reported in cataractous lenses (Chen *et al.* 2006; Hains and Truscott 2007; Chen *et al.* 2008; Chen *et al.* 2009). These damages would reduce the kinetic barrier to unfolding, facilitating further unfolding of the protein and exposure of the aggregation-prone region in the C-terminal domain. Once this region is exposed, the high concentrations of γ-crystallins in the lens would favor second-order aggregation reactions over productive refolding.

4. Features of αB-Crys chaperone involved in substrate recognition and aggregation suppression in vitro

Small heat shock proteins are divided at the level of their primary structure into three distinct regions: the conserved α-crystallin and the variable N-terminal domain and C-terminal extension (de Jong *et al.* 1993). All three regions contribute to and are important for chaperone function in this family of heat shock proteins (Reddy *et al.* 2006). In the case of αB-crystallin, Sharma *et al.*(Sharma *et al.* 1997) have shown that residues 57-69 in the N-terminal domain and residues 93-107 in the α-crystallin domain of bovine αB-crystallin are involved in chaperoning interactions with alcohol dehydrogenase. Further, Ghosh *et al.*(Ghosh and Clark 2005) using protein pin arrays identified seven regions in αB-Crys that were involved in chaperone-substrate interactions. Two regions were in the N-terminal domain, 4 regions in the α-crystallin domain and one region in the C-terminal extension. Two regions in the α-crystallin domain of αB-Crys interacted and prevented the thermal aggregation of β_H-crystallin (Ghosh and Clark 2005).

Recently, Bagnéris *et al.* (Bagneris *et al.* 2009b) have solved the crystal structure of the α-crystallin domain of human αB-Crys to 2.9 Å resolution. They found that the homo-dimers formed an extended β-sheet with a shared groove. Based on known crystal structures of non-metazoan sHsps, they postulated that regions of the N-terminal of αB-Crys could bind to this groove in the full-length oligomers. They hypothesize that, in some vertebrate sHsps, disassembly of the oligomers into dimers could expose the groove and other pockets in the dimer where substrates, like the γ-crystallins, could bind during chaperoning interactions *in vivo.*

Many structural characteristics have been implicated in contributing to the chaperone function of α-crystallin. Hydrophobic regions in the N-terminal region of small heat shock proteins, for one, seem to

play an important role (Eifert *et al.* 2005). The α-crystallin domain and the C-terminal extension of sHsps are also important for chaperone function and interactions with the substrate (Nakamoto and Vigh 2007). Subunit-exchange and oligomeric state of α-crystallin are also important factors in chaperone activity (Reddy *et al.* 2006).

5. Implications for cataract disease

The high molecular weight γD—αB-Crys complexes formed during the early stage of the suppression reactions were stable after four days at 37 ºC (Fig. 2-9). Given the incubation conditions, these proteins could have accumulated some non-enzymatic modifications (e.g. deamidation). However, as the SEC absorbance traces in Fig. 2-9 show, αB-Crys remained an oligomers during the four-day incubation period, which is an indication that the αB-Crys complexes remained stable despite the long incubation conditions. Nonetheless, these results show that αB-Crys forms stable complexes with aggregation-prone, partially folded species of γD-Crys *in vitro*. Similarly, water-soluble, high molecular weight species from normal aged lenses also consist of α-crystallin and γ-crystallin and it has been suggested that these complexes form when α-crystallin binds destabilized γ-crystallin proteins (Harrington *et al.* 2004; Santhoshkumar *et al.* 2008).

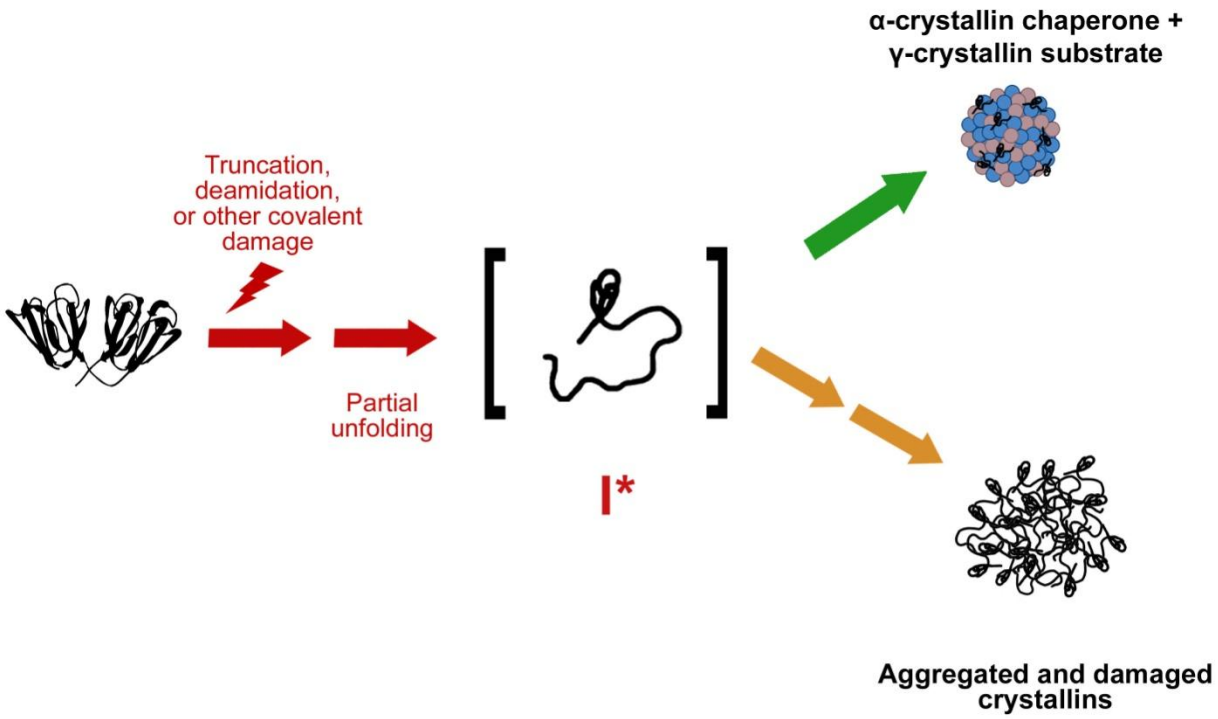

Figure 2-12: A molecular model for age-related cataract formation in the lens.
Environmental stresses could lead to covalent damage, such as deamidation or photo-oxidation, to the crystallins. This damage could destabilize γ-crystallins, which are otherwise very stable, populating aggregation-prone species (I*). α-crystallin would sequester such species in younger individuals (green arrow). But as we age, the finite levels of free α-crystallin in the mature lens fibers will be diminished leading to aggregation (orange arrows).

The finding that α-crystallin oligomers recognize and bind early, partially folded intermediates of the three human γ-crystallins is consistent with models of cataract formation from the aggregation of partially unfolded crystallins (Fig. 2-12). How these are generated in the protected environment of the lens remains to be determined, but multiple pathways of oxidative and photo-oxidative damage are all candidates for the etiology (Lampi *et al.* 1998; Lampi *et al.* 2006; Takata *et al.* 2007; Chen *et al.* 2009). Since there is little protein degradation in lens fiber cells, and formation of high molecule aggregates needs to be avoided, it is not surprising that α-crystallin oligomers form long-lived complexes with their substrates. If this is true it may explain the age distribution of cataract, very rare below age of 50, then sharply increasing subsequently, reaching 50% of the population at age 80 (Congdon *et al.* 2004). In fact, α-crystallins binding many molecules of partially folded and/or covalently damaged β- and γ-crystallins may themselves end up aggregating, thus contributing to the growth of the cataract in the aged lens. Analysis of the water-soluble fraction from normal and cataractous age-matched lenses shows that the percentage of water-soluble high molecular weight species, consisting mostly of α-crystallin along with β- and γ-crystallins, increases not only with age but also in cataractous lenses. It is believed that these complexes are the precursors to water-insoluble crystallin aggregates responsible for cataract (Clark *et al.* 1969; Roy and Spector 1976b; Srivastava *et al.* 1996).

CHAPTER 3:

CHARACTERIZATION OF THE SMALL HEAT SHOCK PROTEIN αB-CRYSTALLIN CHAPERONE BINDING REGIONS IN HUMAN γD-CRYSTALLIN USING SINGLE DOMAIN CONSTRUCTS OF γD-CRYSTALLIN.

A. INTRODUCTION

Lens transparency is achieved through membrane-bound organelle degradation, high concentrations of crystallin proteins and short-range order interactions between the crystallin proteins in differentiated fiber cells (Delaye and Tardieu 1983; Michael *et al.* 2003; Takemoto and Sorensen 2008). Cellular (e.g. extracellular vacuoles, failure in organelle degradation, lens suture malformation etc.) and molecular (e.g. protein aggregation) disturbances impair light transmission through the lens due to visible light scatter (Jacob 1999; Bloemendal *et al.* 2004; Banh *et al.* 2006; Goishi *et al.* 2006). Lens opacification is the etiology for cataract disease, the major cause of blindness worldwide (Serge *et al.* 2004; Abraham *et al.* 2006).

Age-related or mature-onset cataract is the most prevalent manifestation of cataract disease. Epidemiological studies have shown that 82% of the cataract blindness cases occur in individuals over the age of 50 (Abraham *et al.* 2006). Cataract formation has been linked to the formation of protein aggregates of the crystallin proteins—α, β, and γ-crystallin—present in water-insoluble (WI) fractions from lens homogenates. These aggregates have been shown to be responsible light-scattering in pre-cataractous lenses (Benedek *et al.* 1987; Dierks *et al.* 1998). This WI protein fraction contains covalently modified and cross-linked crystallins and crystallin fragments (molecular mass < 18 kDa) (Srivastava 1988; Hanson *et al.* 2000). It has been difficult to identify the factors that transform the very stable βγ-crystallins to aggregating species and to substrates of the α-crystallin chaperone complexes.

A host of covalent damages to the crystallin proteins have been found in WI fractions from cataractous lenses. These damages include deamidation of Gln and Asn residues, truncations, methionine and tryptophan oxidation, disulfide bond formation, and glycation (Nagaraj *et al.* 1991; Takemoto and Boyle 2000; Wilmarth *et al.* 2006; Hains and Truscott 2007; Harrington *et al.* 2007; Hains and Truscott 2008). Some of these changes, such as deamidation, were shown to reduce the stability of β- and γ-crystallins *in vitro* (Flaugh *et al.* 2006; Lampi *et al.* 2006). In the case of βA3-crystallin, deamidation was directly implicated in soluble aggregate formation *in vitro* (Takata *et al.* 2008).

The percentage of lenticular proteins in the WI fraction increases with age and in human cataractous lenses until eventually it becomes higher than the protein content in the water-soluble (WS) fraction (Heys *et al.* 2007). The distribution of all three major types of crystallin proteins also changes with advancing age. Most notably, the concentration of low molecular weight α-crystallin (i.e. free α-crystallin oligomers) in the WS fraction decreases linearly with age until it reaches very low concentrations after the age of 50 (Roy and Spector 1976a; Heys *et al.* 2007). Concurrent with this

decline is the accumulation of soluble high molecular weight species (~ 50,000-350,000 kDa) that begins at age 20, reaches a maximum at age 30 and declines subsequently (Heys *et al.* 2007). β-, γ- and α-crystallin proteins were found in these high molecular weight (HMW) species in the WS fraction of both aged normal and cataractous lenses (Yang *et al.* 1994; Srivastava *et al.* 2008).

Srivastava *et al.* characterized the protein composition of the HMW species in greater detail and showed that βA3-, γD-, γC- and γS-Crys and alcohol dehydrogenase were isolated only as HMW complexes in SEC fractions from cataractous lenses (Srivastava *et al.* 2008). In both the normal and cataractous aged-matched controls, the HMW complexes contained αA-, αB-, βB2-, βA4-, βB1-Crys. Further, fragments (molecular mass < 18 kDa) were also isolated from HMW in normal 20-year-old and 60-year-old lenses, and in cataractous 60- and 70-year-old lenses. Fragments from γC-, γS- and γD-Crys and alcohol dehydrogenase were only present in cataractous lenses (Srivastava *et al.* 2008). Crystallin fragments were also identified in aggregates from the WI fraction (Srivastava 1988; Harrington *et al.* 2007). Proteins and protein fragments in the WI fraction in the nuclear region of the lens had more covalent modifications in cataractous lenses (Wilmarth *et al.* 2006; Hains and Truscott 2007).

A 9 kDa fragment originating from human γD-Crys was identified in the WS and WI fractions of normal young and aged lenses, and cataractous lenses (Srivastava *et al.* 1992). This fragment corresponded to the C-terminal domain of γD-Crys and resulted from cleavage between residues Gly86 and Ser87 and a truncation after residue 163 (residues 87-163) (Srivastava and Srivastava 2003). All 9 kDa γD-Crys isoforms isolated from the lens were oxidatively damaged at Met136 and Trp156. The authors showed that the isolated 9 kDa fragment would aggregate *in vitro*, forming cross-linked oligomers, when incubated under native-state favorable conditions at pH 7.0 and 37 ºC. They also observed insolubilization of this fragment with lens age, linking the presence of a 27 kDa cross-linked species with cataractous inclusions (Srivastava and Srivastava 2003). The authors did not identify the mechanism responsible for cleavage of full-length γD-Crys, though they suggested that lens calpain proteases could be involved in proteolytic cleavage at the linker region of γD-Crys (Srivastava and Srivastava 2003). Taylor *et al.* found significant amounts of leucine aminopeptidase in bovine and human lenses, which showed an age-dependent decrease in proteolytic activity. These leucine aminopeptidases had proteolytic activity towards αA- and αB-crystallin (Taylor *et al.* 1982).

The current model for age-related cataract formation synthesizes all of these observations. It proposes that covalent damage and truncation of the crystallin proteins would destabilize them causing the population of aggregation-prone species. Free α-crystallin chaperone present in the mature fiber cells would sequester these species, thus preventing aggregation and cataract formation. However, constant

exposure to environmental stress and aging would cause saturation of the free α-crystallin chaperone with substrate crystallins, thus forming the HMW complexes that accumulate in an age-dependent manner *in vivo*. Protein aggregates would accumulate in older lenses due to the absence of free α-crystallin. The WS-HMW complexes could also become integrated into WI aggregates. The accumulation of all of these macromolecular species in the nuclear region of the lens would cause light-scatter and consequent opacification of the lens (Bloemendal *et al.* 2004; Sharma and Santhoshkumar 2009). This model has guided research into the nature of the stability of the lens crystallin proteins, α-, β-, and γ-crystallins.

α-crystallin in human lenses is a polydisperse oligomers of αA- and αB-Crys subunits. Both subunits have a molecular mass of approximately 20 kDa and they are encoded by separate genes. The α-crystallin complexes range in size from 300-1,000 kDa. As mentioned previously, both subunits can be expressed recombinantly in *E. coli* cells and they form homo-oligomers with similar biochemical and structural characteristics as lens α-crystallin (Sun *et al.* 1997). αA- and αB-Crys have chaperone activity *in vitro* as they can suppress the aggregation of a number of physiological and model substrates (Horwitz 1992; Carver *et al.* 1995; Lindner *et al.* 1997; Carver *et al.* 2002; Evans *et al.* 2008; Acosta-Sampson and King 2010). Substrate binding studies under equilibrium conditions have shown that α-crystallin binds substrates at two binding sites: a low affinity/high capacity site and a high affinity/low capacity site (McHaourab *et al.* 2002; Koteiche and McHaourab 2003). Further, Claxton *et. al*, using T4 lysozyme mutants with lower free energies of unfolding than WT, identified the substrate structure and substrate region that interacted with αA- and αB-Crys (Claxton *et al.* 2008). A highly unfolded T4 lysozyme conformer bound either site on the chaperones. The conformation of the substrate was monitored via extrinsic fluorescence of bimane-labeled T4 lysozyme mutants; quenching of the extrinsic bimane fluorescence by a nearby Trp residue in the folded state was used as a probe to detect the tertiary structure of the substrate. In addition, the substrates were bound in the same orientation: the C-terminal domain was buried within the chaperone and the N-terminal domain was solvent exposed. Similar studies showed that αA-crystallin recognized largely unfolded intermediates of destabilized βB1-Crys mutants under equilibrium conditions (Dimcheff *et al.* 2004). These results indicated that α-crystallin functions by recognizing transient aggregation-prone intermediates and has the ability to modulate the number of interacting sites depending on the concentration of the aggregation-prone species (McHaourab *et al.* 2009).

Recently, Bagneris *et al.* and Laganowsky *et al.* solved the X-ray crystal structures for the α-crystallin domain of human αB-Crys and truncated αA- and αB-Crys, respectively (Bagneris *et al.* 2009a; Laganowsky *et al.* 2010). In both structures, the interactions between the α-crystallin domains of dimeric partners show marked differences from the solved crystal structures for monodisperse sHsps, wheat

Hsp16.9 and *M. jannaschi* Hsp16.5 (Kim *et al.* 1998; van Montfort *et al.* 2001). The α-crystallin dimers had a shorter loop between strands β6 and β7 in the α-crystallin domain. Thus, β6-strand swapping between partners was not present in the mammalian sHsps. Rather, the β6- and β7-strand formed an extended β-strand that adjoined its counterpart in the dimer and formed the dimer interface. The β2/β7 edge of the α-Crys β-sandwich from each partner faced each other and formed a shared hydrophobic groove at the dimer interface. The base of the groove was formed by an inter-molecular extended β-sheet. Laganowsky *et al.* compared the dimer interface for all crystal structures available and found that a pronounced shift in the register of the interface residues between αA- and αB-Crys. They proposed that this flexibility in register could serve as a 'ratchet-based mechanism' that could respond to solvent conditions and contribute to α-crystallin's ability to interact with different substrates (Laganowsky *et al.* 2010).

The β- and γ-crystallins are members of the same family of lens structural proteins. The monomers consist of four anti-parallel β-sheet intercalated Greek key motifs organized into two domains (Slingsby and Clout 1999; Purkiss *et al.* 2002; Basak *et al.* 2003). The β-crystallins can form oligomers, while the γ-crystallins are found as monomers (Bloemendal *et al.* 2004). The β-crystallins are subdivided into acidic and basic subgroups depending on their pI. They contain N- and C-terminal extensions compared to γ-crystallins. In humans, γ-crystallins can be subdivided into the mammalian sub-group of γA-γF crystallins and γS-crystallins (Jaenicke and Slingsby 2001). All βγ-crystallins are present only in lens fiber cells, but their genes are expressed at different lens developmental stages and at different levels depending on individual crystallins. The high concentration, short-range order, and native state interactions of these proteins are some of the contributing factors to lens transparency and the refractive index gradient of the lens (Tholozan and Quinlan 2007; Takemoto and Sorensen 2008).

Most γ-crystallins studied to date *in vitro* display high thermodynamic and kinetic stability (Mayr *et al.* 1997; Fu and Liang 2002; Kosinski-Collins and King 2003; Mills *et al.* 2007). They have melting temperatures over 70 ºC, higher than most metazoan proteins (Bloemendal *et al.* 2004). Conformational changes in these proteins can be monitored by tracking changes in fluorescence emission from four highly conserved Trp residues located in each quadrant of the protein (Jaenicke 1996; Bloemendal *et al.* 2004). Their native state buried-Trp fluorescence is quenched relative to their unfolded state (Kosinski-Collins *et al.* 2004; Chen *et al.* 2006). Equilibrium unfolding and refolding experiments for bovine γB-Crys and human γD- and γC-Crys identified a partially folded intermediate with one domain unfolded and the other domain folded (Mayr *et al.* 1997; Fu and Liang 2002; Kosinski-Collins and King 2003). Isolated, single domain constructs for bovine γB-Crys and human γS- and γD-Crys have shown differential domain stability with one isolated domain being more stable than its partner (Mayr *et al.* 1997; Mills *et al.* 2007).

Hydrophobic residue packing and polar interactions in the interface have been shown to contribute to the overall thermodynamic stability of bovine γB- and human γD-Crys (Mayr *et al.* 1997; Flaugh *et al.* 2005a; Flaugh *et al.* 2005b).

In vitro experiments have elucidated the folding pathway of human γD-Crys. Equilibrium unfolding and refolding experiments have identified a stable, partially folded intermediate with the N-td unfolded and the C-td folded (Kosinski-Collins and King 2003; Kosinski-Collins *et al.* 2004). Kinetic unfolding and refolding experiments have added further detail to the folding landscape of this protein. Several distinct transient intermediates were identified during γD-Crys kinetic unfolding and refolding experiments (Flaugh *et al.* 2006). Three transitions were observed in kinetic refolding experiments at pH 7.0 and 37 ºC, where the high concentrations of GdnHCl were diluted to low concentrations to initiate refolding. The first transition corresponded to the partial refolding the C-terminal domain ($t_{1/2}$ ~ 8 s), the second to the complete refolding of the C-terminal domain ($t_{1/2}$ ~ 35 s), and the last transition corresponded to the complete refolding of the N-terminal domain ($t_{1/2}$ ~ 130 s) (Flaugh *et al.* 2006). Molecular modeling and biochemical studies postulated the inner β-hairpin closest to the interface in Motif 4 in the C-terminal domain to be the folding nucleus of γD-Crys (MacDonald *et al.* 2005; Flaugh *et al.* 2006; Das *et al.* 2010).

The interactions across the interface of γD-Crys contribute to the overall thermodynamic and kinetic stability of the native state of the protein. The interface of human γD-Crys is comprised of a hydrophobic residue cluster flanked by pairs of polar residues. Residues Met43, Phe56, Ile81 are located on the N-terminal face, while Val132, Leu145 and Val170 are located on the C-terminal face (Basak *et al.* 2003). These residues are flanked peripherally by pairs of polar residues: Gln54/Gln143 and Arg79/Met147. Flaugh *et al.* carried out detailed studies on the contribution of these residues to the stability of full-length human γD-Crys (Flaugh *et al.* 2005a; Flaugh *et al.* 2005b). Their results from equilibrium unfolding and refolding experiments showed that substituting these residues for Ala reduced the stability of the mutant proteins, but the substitutions lowered only the stability of the N-td at pH 7.0 and 37 ºC (Flaugh *et al.* 2005a; Flaugh *et al.* 2005b). Kinetic refolding experiments also showed that these Ala substitutions in the interface region increased the $t_{1/2}$ values for the refolding of the N-td, while the $t_{1/2}$ values for the refolding of the C-td were similar in the WT and mutant proteins (Flaugh *et al.* 2005a). The disparate effects these interface residue substitutions had on the stability of the N-td and C-td suggested that the C-td interface templated the folding of the N-td (Flaugh *et al.* 2005b; Flaugh *et al.* 2005a).

Off-pathway aggregation occurred during refolding of human WT γC-, γD- and γS-Crys out of high concentrations of GdnHCl (Kosinski-Collins and King 2003; Acosta-Sampson and King 2010). A partially folded intermediate, populated within the refolding time-span of the C-td, was recognized and bound by the human αB-Crys chaperone during dilution out of high concentrations of denaturant (Acosta-Sampson and King 2010).

Mills *et al.* constructed isolated single domain constructs of the N-terminal (γD-Ntd) and C-terminal (γD-Ctd) domains of γD-Crys [Fig. 3-1 (Mills *et al.* 2007)]. The γD-Ntd domain consisted of γD-Crys residues 1-82, while the γD-Ctd domain constructs consisted of γD-Crys residues 89-174. The inter-domain linker region was not included in either construct (Mills *et al.* 2007). Fluorescence emission and far-UV CD spectra showed that the constructs folded to a native-like structure during heterologous expression in *E. coli* cells. Further, equilibrium and kinetic refolding experiments showed that these constructs refolded to their native state *in vitro* at pH 7.0. The transition midpoint GdnHCl concentration (C_M) for γD-Ntd single domain was 1.3 M, while the C_M value for the γD-Ctd single domain was 2.7 M GdnHCl. Taking into account the intrinsic stability of each isolated domain, the authors calculated that interactions in the interface contributed a ΔG_{H2O} of approximately 4.2 kcal*mol^{-1} to the stability of full-length γD-Crys protein (Mills *et al.* 2007). Thus, the N-terminal and C-terminal domains along with the interface interactions contribute additively to the high intrinsic stability of γD-Crys (Mills-Henry 2007). A similar increase in protein stability due to intramolecular interface interactions was also observed in studies of bovine γB-Crys and its isolated domains at pH 2.0 (Mayr *et al.* 1997).

A

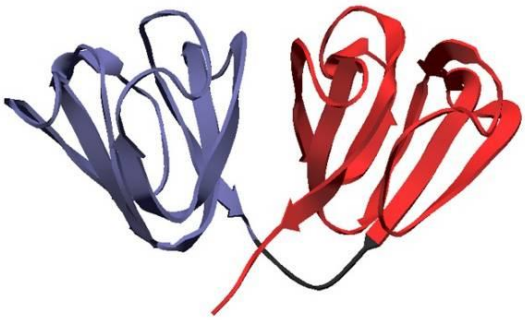

B

1 60
GKITLYEDRGFQGRHYECSSDHPNLQPYLSRCNSARVDSGCWMLYEQPNYSGLQYFLRRG

61 120
DYADHQQWMGLSDSVRSCRLIPHSGSHRIRLYEREDYRGQMIEFTEDCSCLQDRFRFNEI

121 174
HSLNVLEGSWVLYELSNYRGRQYLLMPGDYRRYQDWGATNARVGSLRRVIDFS

Figure 3-1: Amino acid sequences for γD-Ntd and γD-Ctd
A) Ribbon diagram of γD-Crys (Protein Data Bank ID: 1HK0) highlighting the regions that correspond to the γD-Ntd single domain construct (blue) and the regions that correspond to the γD-Ctd single domain construct (red). B) Primary amino acid sequence of human γD-Crys showing the residues included in the γD-Ntd (residues, 1-82, shown in blue) and the γD-Ctd (residues 89-174, shown in red) single domain constructs. The residues corresponding to the inter-domain linker are shown in black and were not included in either single domain construct. Upper numbers represent the residue number in the protein sequence.

Studies on the kinetic unfolding of full-length γD-Crys and its isolated domains further highlighted the importance of the interface interactions (Mills-Henry 2007). Kinetic unfolding data of γD-Crys unfolded at 18 ºC and 5.5 M GdnHCl showed that the protein unfolded with two transitions. The first transition corresponded to the unfolding of the N-terminal domain and had a $t_{1/2}$ of 251 s, while the second transition corresponded to the unfolding of the C-terminal domain and had a $t_{1/2}$ of 3455 s. The γD-Ntd single domain was not as stable in similar kinetic unfolding experiments and had to be unfolded at lower concentrations of denaturant (3.5 M GdnHCl) in order to capture the initial unfolding signal; its $t_{1/2}$ was approximately 385 s at 18 ºC (Mills-Henry 2007). Differences between the kinetic stabilities of the γD-Ntd single domain and the N-terminal domain of full-length γD-Crys observed *in vitro* pointed to a contributing role of the interface interactions in the kinetic stability of γD-Crys (Mills-Henry 2007). These highly-conserved interface interactions contribute significantly to the intrinsic stability of the native state of human γD-Crys. In an evolutionary sense, this added stability would help γD-Crys remain folded for most of the adult life of the individual.

The γD-Ntd and γD-Ctd constructs characterized by Mills *et al.* allowed us to study the aggregation propensity of the 9 kDa γD-Crys fragment isolated from the WS-HMW and WI fractions in normal aged and cataractous lenses. As mentioned previously, Srivastava *et al.* identified this fragment as the C-terminal domain of γD-Crys (residues 87-163) (Srivastava *et al.* 1992). This fragment was purified from young human lenses and shown to form cross-linked oligomers upon incubation at 37 ºC (Srivastava and Srivastava 2003). Fluorescence emission spectra of the 9 kDa fragment indicated that it was partially folded since the maximum λ_{EM} was ~ 332 nm and did not coincide with the published spectra for native and unfolded γD-Ctd published by Mills *et al.* (Srivastava and Srivastava 2003; Mills *et al.* 2007). Although, the γD-Ctd construct included residues 89-174, it could still serve as a proxy to gain insight into a species present in the lens after proteolytic cleavage of full-length γD-Crys and prior to oxidative damage and truncation of the last 11 residues in the C-terminal domain.

Further, these fragments allowed the study the aggregation propensity of each domain upon dilution out of high concentrations of GdnHCl in a context independent of inter-domain interactions in γD-Crys. Results described herein and observed initially by Mills-Henry *et al.* showed that the C-terminal domain of γD-Crys aggregated upon refolding out of high concentrations of GdnHCl, while the isolated N-terminal domain did not aggregate under identical experimental conditions. These results provided a platform to further investigate the structural nature of the aggregation prone species populated during refolding for the full-length γD-Cry and its interaction with αB-Crys chaperone.

More detailed identification of the conformation of the partially unfolded substrates recognized and bound by α-crystallin will be valuable in the effort to identify the etiological agents of cataract formation within the lens. Understanding these fundamental biochemical mechanisms may open the way to search for agents or treatments that retard cataract development.

B. MATERIAL AND METHODS

1. Expression and Purification of αB-Crys, γD-Ntd and γD-Ctd Single Domains

γD-Ntd (γD-Crys residues G1-P82) and γD-Ctd (γD-Crys residues R89-S174, numbering based on Protein Data Bank ID:1HK0) single domain constructs were previously described in Mills *et al.* (Mills *et al.* 2007). All recombinant proteins were expressed by transforming pQE.1 plasmids into *E. coli* M15 [pREP4] cells (Qiagen). All constructs contained an N-terminal His_6 tag. Proteins were purified following procedures described in Kosinski-Collins *et.al.* (Kosinski-Collins *et al.* 2004) using Ni-NTA (Qiagen) media for affinity chromatography. After purification, proteins were dialyzed into 10 mM ammonium acetate (pH 7.0) and stored at 4 ºC.

The wild-type αB-Crys containing pAED4 plasmid was transformed into BL21 Gold (DE3) *E. coli* cells (Stratagene). IPTG was added to bacterial cultures to a final concentration of 1 mM to initiate protein expression, which was allowed to proceed over night at 18 ºC. Cells were harvested and stored at -80 ºC until future use. αB-Crys was purified following previously published protocol by Horwitz *et al.* (Horwitz *et al.* 1998) with some modifications, which included performing all cell lysis steps at 4 ºC. After clarifying the lysate, two rounds of anion exchange chromatography were performed using a HiPrep 16/10 Q Sepharose FF column (GE Lifesciences) followed by SEC in Superose 6 10/300 GL (GE Lifesciences). αB-Crys protein was stored in 50 mM sodium phosphate and 150 mM sodium chloride buffer, pH 7.0 (SEC buffer). αB-Crys aliquots were dialyzed into 10 mM ammonium acetate and concentrated using 10000 MWCO Amicon Ultra-4 concentrators (Millipore) prior to use in aggregation suppression assays. All protein batches were tested for chaperone efficiency in aggregation suppression assays at 1:1 and 1:5 mass-based ratios with WT γD-Crys as the substrate.

Double tryptophan substitutions of residues 9 and 60 to phenylalanines were constructed using mutant primers (IDT-DNA) to amplify the αB-Crys gene in the pAED4 vector during site-directed mutagenesis. Amplified plasmid DNA was sequenced to confirm the substitutions (DNA Sequencing Facility, Massachusetts General Hospital). W9F/W60F (noTrp) αB-Crys was purified using the same procedures described above for the WT αB-Crys protein.

Protein concentrations were calculated using UV absorbance at 280 nm of unfolded proteins and the following extinction coefficients: 20,580 (γD-Ntd), 20,460 (γD-Ctd) and 13,980 (αB-Crys) $M^{-1}cm^{-1}$ (Pace *et al.* 1995; Wilkins *et al.* 1999). The protein concentration for no-Trp αB-Crys was determined using the Bio-Rad Protein Assay (Bradford method). Molar concentrations for WT and noTrp αB-Crys were calculated using the molecular weight of the monomer (20,158.9 Da). Purity of all proteins mentioned herein was determined to be greater than 95% by SDS-PAGE.

2. Aggregation and Aggregation Suppression Assays

γD-Ntd and γD-Ctd isolated domain proteins were unfolded at ten-times the final target protein concentration in Unfolding buffer (100 mM sodium phosphate, 1 mM EDTA, 5 mM DTT, 5 M GdnHCl pH 7.0) for 24 h at 37 ºC. Refolding buffer (100 mM sodium phosphate, 1 mM EDTA, 5 mM DTT, pH 7.0) was pre-equilibrated to 37 ºC, added to dilute the concentration of GdnHCl, and unfolded samples were mixed thoroughly before initiating solution turbidity measurements. The final protein concentration for both single domains was 12.7 μM and the final GdnHCl concentration was 0.5 M. All $O.D._{350\ nm}$ measurements described in this section were performed using a Cary-50 UV-Vis spectrophotometer (Varian) at 37 ºC. Samples were not continuously stirred during measurements.

For aggregation experiments where the final concentrations of γD-Ntd and γD-Ctd varied, the proteins were unfolded at ten-times the final concentration in Unfolding buffer for 24 h at 37 ºC. Refolding buffer was added to unfolded samples and mixed thoroughly at 37 ºC. The final protein concentrations for assays with γD-Ntd isolated domain were 9.1, 13.7, and 18.2 μM; the final protein concentrations for assays with γD-Ctd isolated domain were 8.5, 12.7, and 16.9 μM. The final concentration of GdnHCl for all samples was 0.5 M. Solution turbidity was recorded as $O.D._{350\ nm}$ at 37 ºC.

For aggregation suppression reactions using WT and noTrp αB-Crys as the chaperone, unfolded γD-Ctd was diluted ten-fold with Refolding buffer to initiate refolding and aggregation. WT or noTrp αB-Crys was already added to Refolding buffer and equilibrated to 37 ºC for 1 h. The suppression reactions were done at 1 γD-Ctd:5 αB molar ratio; the final protein concentration was 12.7 μM for γD-Ctd and 63.5 μM for WT or noTrp αB-Crys. The final GdnHCl concentration was 0.5 M for all suppression reactions. Solution turbidity was measured as $O.D._{350\ nm}$ at 37 ºC for 1200 s without continuous stirring.

For sequential-refolding competition experiments, γD-Ntd was unfolded in Unfolding buffer for 24 h at 37 ºC. Samples were diluted 20-fold with Refolding buffer (± WT αB-Crys) that had been pre-

equilibrated to 37 ºC for at least 1 h. The final protein concentration was 12.7 μM and the final GdnHCl concentration was 0.25 μM. $O.D._{350\ nm}$ was measured at 37 ºC for 600 s. Samples were then collected, incubated at 37 ºC for 1 h, and used for 20-fold dilution of unfolded γD-Ctd (5 M GdnHCl). The final protein concentrations after this mixing regime were: 12.7 μM for γD-Ctd, 12.1 μM for γD-Ntd, and 60.3 μM for αB-Crys when αB-Crys had been added to Refolding buffer (the final GdnHCl concentration was 0.5 M). For 1 γD-Ctd:0 αB control experiments, γD-Ctd was unfolded in Unfolding Buffer for 24 h at 37 ºC, diluted and mixed thoroughly with Refolding buffer at 37 ºC (final γD-Ctd concentration was 12.7 μM and final GdnHCl concentration was 0.5 M). For 1 γD-Ctd:5 αB and 1 γD-Ntd:5 αB control experiments, conditions were similar as described above except that αB-Crys chaperone was added to Refolding buffer and pre-equilibrated at 37 ºC for 1 h (γD-Ntd/γD-Ctd concentration was 12.7 μM and GdnHCl concentration was 0.5 M).

For experiments where the isolated domains were unfolded together, γD-Ntd and γD-Ctd were unfolded together at equimolar concentrations for 24 h at 37 ºC in Unfolding buffer. Refolding buffer was added and the sample was thoroughly mixed (0.25 M GdnHCl). The final γD-Ntd and γD-Ctd concentrations were 8.5 μM. The γD-Ctd-only control at twice the final concentration described previously was performed under identical assay conditions (16.9 μM γD-Ctd, and 0.25 M GdnHCl). $O.D._{350\ nm}$ traces were collected at 37 ºC for given amounts of time.

For competition binding experiments where the single domains were unfolded together, γD-Ntd and γD-Ctd were unfolded together at equimolar concentrations for 24 h at 37 ºC in Unfolding buffer. Refolding buffer (± αB-Crys chaperone) was pre-equilibrated at 37 ºC for 1 h, added to unfolded samples, and samples were mixed thoroughly. The suppression assays plus αB-Crys were done at 1 γD-Ntd:1 γD-Ctd:5 αB molar ratios (final concentrations were as follows: 12.7 μM for γD-Ntd, 12.7 μM for γD-Ctd, and 63.5 μM for αB-Crys). $O.D._{350\ nm,}$ traces were collected at 37 ºC without continuous stirring (final GdnHCl was 0.5 M). All experiments described in this section were repeated as three separate trials. Molar ratios for αB-Crys corresponded to the monomer's molecular mass.

3. Fluorescence Emission Spectroscopy

All fluorescence emission spectra described herein were measured using a Hitachi F-4500 fluorescence spectrophotometer thermostated with a circulating water bath. Native γD-Ctd, at a concentration of 1.7 μM, was incubated in Refolding buffer for 1 h at 37 ºC prior to data collection. γD-Ctd was unfolded at 1.7 μM in Unfolding buffer for 24 h at 37 ºC prior to data collection. The excitation

wavelength was set to 300 nm (PMT voltage was set to 950 V) and fluorescence emission scans were recorded from wavelengths 316-400 nm. The excitation and emission slit widths were set to 10 nm and the temperature was kept at 37 ºC with a circulating water bath. Fluorescence spectra of their respective buffers were subtracted from sample spectra.

Native wild-type and noTrp (W9F/W60F) αB-Crys, each at a concentration of 1 μM, were incubated in SEC buffer (50 mM sodium phosphate, 150 mM sodium chloride, pH 7.0). Fluorescence emission spectra were recorded from 316-400 nm; the excitation wavelength and PMT voltage were set to 300 nm and 950 V respectively. The emission and excitation slit widths were set to 10 nm and spectra were recorded at 25 ºC with a circulating water bath. Fluorescence emission spectra for the fraction corresponding to the γD-Ctd—αB complex (i.e. the peak eluting at 7.6 ml during SEC) was measured using the same parameters. All spectra shown have their corresponding buffers subtracted. All experiments described herein were repeated as three separate trials.

4. Electron microscopy

For the γD-Ctd aggregation samples, the aggregation reactions were collected and incubated at 37 ºC for 24 h prior to buffer exchange (final protein concentration was 12.7 μM and final GdnHCl concentration was 0.5 M). Samples were then buffer-exchanged to 50 mM Tris, pH 8.0 using Ultrafree MC Centrifugal Filter units, 30,000 MWCO (Millipore). For micrographs of WT αB-Crys, αB-Crys was in 10 mM ammonium acetate, pH 7.0, at a concentration of 2.5 μM. For micrographs of γD—αB or γD-Ctd—αB complexes, samples were collected from a fraction corresponding to the complex peak isolated via size-exclusion chromatography from 1γ:5α suppression samples (final γD-Ctd concentration was 12.7 μM and final γD-Crys concentration was 4.6 μM). These samples were in SEC buffer.

For all samples, 10 μl of sample was applied to a glow-discharged Formvar and carbon-coated 400 mesh copper grid, rinsed with 100 μl of H_2O, stained with 2% (w/v) uranyl acetate, and imaged using a JEOL 1200 transmission electron microscope operating at 60 kV. Images were collected with an AMT 16000-S camera. Size of complexes was measured from the final images using the imaging software accompanying the AMT camera.

5. Size-exclusion chromatography

Samples for aggregation and aggregation suppression reactions (0.5 ml) were collected immediately after UV-Vis spectrophotometer measurements and incubated for 24 h at 37 ºC. Samples were then filtered through an Ultrafree-MC Centrifugal filter unit with a 0.22 μm membrane (Millipore) and 100 μl of 6X SEC buffer (300 mM sodium phosphate, 900 mM sodium chloride, pH 7.0) were added. Samples were equilibrated to 4 ºC, loaded into a 0.5 ml Teflon loop (GE Lifesciences) and loaded into a Superose 6 GL 10/300 (CV= 24 ml, V_0=8 ml, GE Lifesciences) connected to an AKTA FPLC (GE Lifesciences). All chromatography runs were done using the same SEC column and carried out in triplicate. The flow rate for all chromatography runs was 0.5 ml/min in SEC buffer at 4 ºC.

6. SDS-PAGE Gel Electrophoresis

Equal volumes from SEC fractions were collected and 3X SDS Sample buffer was added (188 mM Tris at pH 6.8, 2% SDS, 15% β-mercaptoethanol, and bromophenol blue). Thirty μl of each sample was added to a gel well and gels were electrophoresed using the discontinuous buffer system developed by King and Laemmli (King and Laemmli 1971). Pre-stained and unstained Precision Plus protein standards (Bio-Rad) were used. Gels were electrophoresed at a constant voltage and were stained with the Krypton Fluorescent stain system (Pierce). Gels were scanned using a Typhoon 9400 Imager (GE Lifesciences) with a λ_{EX} set to 532 nm and λ_{EM} set to 580 nm. The concentrations for αB-Crys, γD-Ntd and γD-Ctd controls used are noted in their respective figure legends. The acrylamide percentage for each gel is also stated in their respective figure legends.

For gels where the γD-Ntd and γD-Ctd were unfolded together, aggregates were collected after samples were incubated for 24 h at 37 ºC by filtering the solution through a 0.2 μm Ultrafree-MC centrifugal filter (Millipore). Membranes were washed with 400 μl of 10 mM ammonium acetate twice and the aggregates were resuspended in 200 μl of 1X SDS buffer. The filtrate was dialyzed in 10 mM ammonium acetate buffer (pH 7.0) overnight at 4 ºC. Thirty μl of 3X SDS buffer were added 60 μl aliquots from filtrate samples. All samples were incubated at 95 ºC for 5 min.

C. RESULTS

1. Expression and purification of γD-Crys single domain constructs and WT αB-Crys

Mills *et. al* described the design and cloning schemes for the γD-Ntd and γD-Ctd single domain constructs from the full-length WT γD-Crys parent protein (Mills *et al.* 2007). Both single domains were expressed and purified as soluble proteins in *E. coli* cells; each construct contained an N-terminal His_6 tag that allowed purification of these heterologous constructs from *E. coli* cell lysates via Ni-NTA affinity chromatography. They also provided detailed analyses of the structural properties of these γD-Crys single domain constructs. Their studies revealed that the γD-Ntd and γD-Ctd single domains folded into native-like conformations as judged by far-UV CD spectroscopy and buried tryptophan fluorescence emission spectra. Analytical SEC revealed that both isolated domains were monomers at their working protein concentrations (Mills *et al.* 2007). In our experiments, both single domains were expressed and purified from *E. coli* cell cultures as outlined by Mills *et. al* (Mills *et al.* 2007). We observed consistent properties in terms of protein solubility and protein expression levels as described above.

WT αB-Crys was purified as described in the previous section. Briefly, WT αB-Crys was expressed in *E. coli* and purified using anion-exchange and size-exclusion chromatography. Figure 2-1 shows results from far-UV CD spectroscopy, buried Trp fluorescence spectroscopy and analytical SEC methods used to characterize the structural properties of the αB-Crys oligomers isolated from my expression and purification protocols.

2. The γD-Ctd isolated domain, but not the γD-Ntd isolated domain, aggregated upon refolding out of high concentrations of denaturant.

Kosinski-Collins and King showed that fully unfolded human WT γD-Crys aggregated upon refolding out of high concentrations of GdnHCl (Kosinski-Collins and King 2003). Results shown in Figure 2-6 further revealed that the C-terminal domain of full-length γD-Crys had to be unfolded for the protein to aggregate during refolding out of high concentrations of denaturant at 37 ºC. In addition, Mills-Henry (Mills-Henry 2007) showed that γD-Ctd only aggregated at concentrations higher than 4 μM when refolded out of high concentrations of denaturant, while γD-Ntd did not aggregate under similar conditions; aggregate formation was assayed by measuring solution turbidity of the refolded samples at $O.D._{350\ nm}$. These initial observations provided a stepping stone for all subsequent studies described in this chapter.

In order to further assess the aggregation propensities of γD-Ntd and γD-Ctd, I unfolded these proteins in Unfolding buffer for 24 h at 37 ºC. Fully unfolded protein samples were diluted ten-fold, thoroughly mixed, and aggregation was followed by measuring changes in $O.D._{350\ nm}$ at 37 ºC without subsequent mixing. Figure 3-2A shows the $O.D._{350\ nm}$ traces for γD-Ntd and γD-Ctd refolded under conditions described above. The final protein concentration for both samples was 12.7 μM and the final GdnHCl concentration was 0.5 M. Under these experimental conditions, partially folded species of γD-Ctd isolated domain aggregated upon refolding, while no aggregate formation was observed for γD-Ntd samples (Fig. 3-2A). The first recorded $O.D._{350\ nm}$ values (t=0) were higher than the buffer baseline due to the formation of light-scattering aggregates within the mixing dead-time of the experiment (~ 5 s). After this initial increase in the $O.D._{350\ nm}$ amplitude in the first 50 s, the solution turbidity decreased and reached a plateau after 500 s. Aggregates formed during γD-Ctd aggregation reactions were visible to the naked eye.

Aggregation samples from these γD-Ctd aggregation reactions were collected and applied to carbon/Formvar grids and imaged using a JEOL electron microscope. Figure 3-2B and C show TEM micrographs of these samples. Similar to full-length γD-Crys, the aggregation prone, partially folded species of the γD-Ctd isolated domain populated during these refolding conditions formed large, amorphous aggregates that were hundreds of nanometers in size. Notably, higher magnification micrographs (Fig. 3-2C) also show the presence of small, fibrillar aggregates that are structurally similar to those observed in aggregation samples from WT γD-, γC- and γS-Crys (Fig. 2-3B, D, and F).

Similar aggregation assays were carried out with different final concentrations of single domain proteins to determine whether γD-Ntd could aggregate upon refolding if the protein concentration was increased. Three final protein concentrations (9.1, 13.7, and 18.2 μM) were assayed at 37 ºC while the final concentration of GdnHCl remained the same (0.42 M). As shown in Figure 3-3A, the $O.D._{350\ nm}$ levels did not increase as the concentration of γD-Ntd increased indicating that no light-scattering aggregate species were formed. In contrast, increasing the concentration of γD-Ctd within the same concentration range described above (8.5-17 μM) and under similar assay conditions resulted in a concomitant increase in $O.D._{350\ nm}$ levels (Fig. 3-3B). Further, lowering the final concentration of denaturant (to 0.25 M GdnHCl) while keeping the same range of γD-Ntd concentrations did not result in aggregate formation (data not shown). These results provide further evidence that destabilization of the C-terminal domain of γD-Crys is responsible for the aggregation behavior observed upon refolding out of high concentrations of denaturant (See Chapter 2, Section C-4). In addition, the differential aggregation propensity observed for the N-terminal and C-terminal domains of γD-Crys, implies that there could be an

aggregation prone region or sequence present in the C-terminal domain of the protein. This region could be exposed upon partial unfolding of the C-terminal domain leading to aggregation.

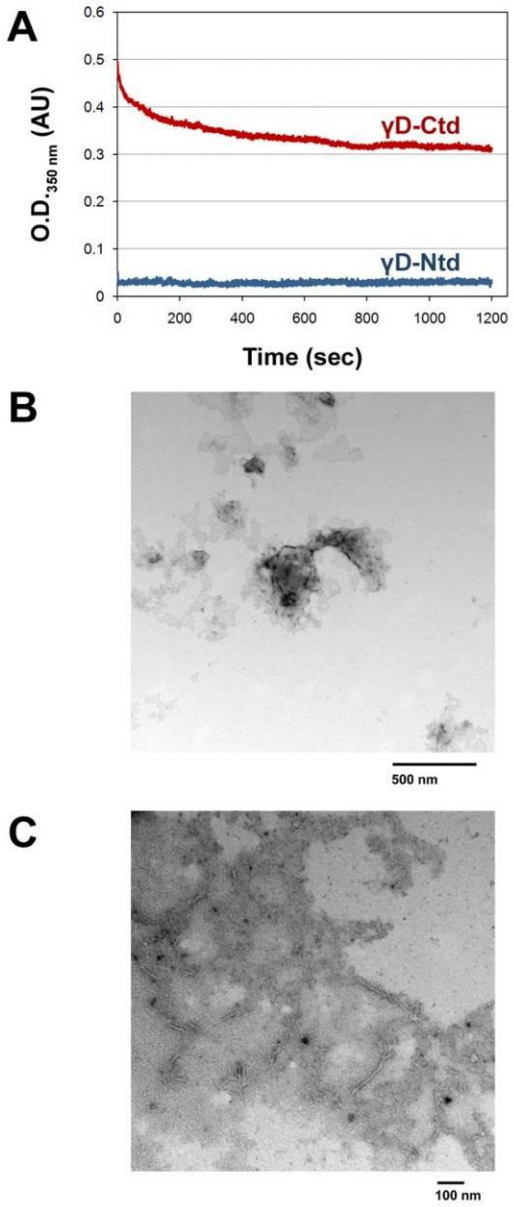

Figure 3-2: Partially folded γD-Ctd, but not γD-Ntd, aggregated upon dilution out of high concentrations of GdnHCl forming large, amorphous aggregates.
A) $O.D._{350\ nm}$ trace showing the aggregation of the partially folded species of γD-Ctd single domain during refolding out of high concentrations of denaturant. γD-Ntd did not aggregate during refolding in similar assays. Both γD-Crys single domain constructs were unfolded in Unfolding buffer for 24 h at 37 ºC. The final protein concentration was 12.7 µM and the final GdnHCl was 0.5 M. TEM micrographs of γD-Ctd aggregates formed during the aggregation assay described in (B) at 50000 x (C) and 120000 x magnification. Grids were prepared as described in Material and Methods section.

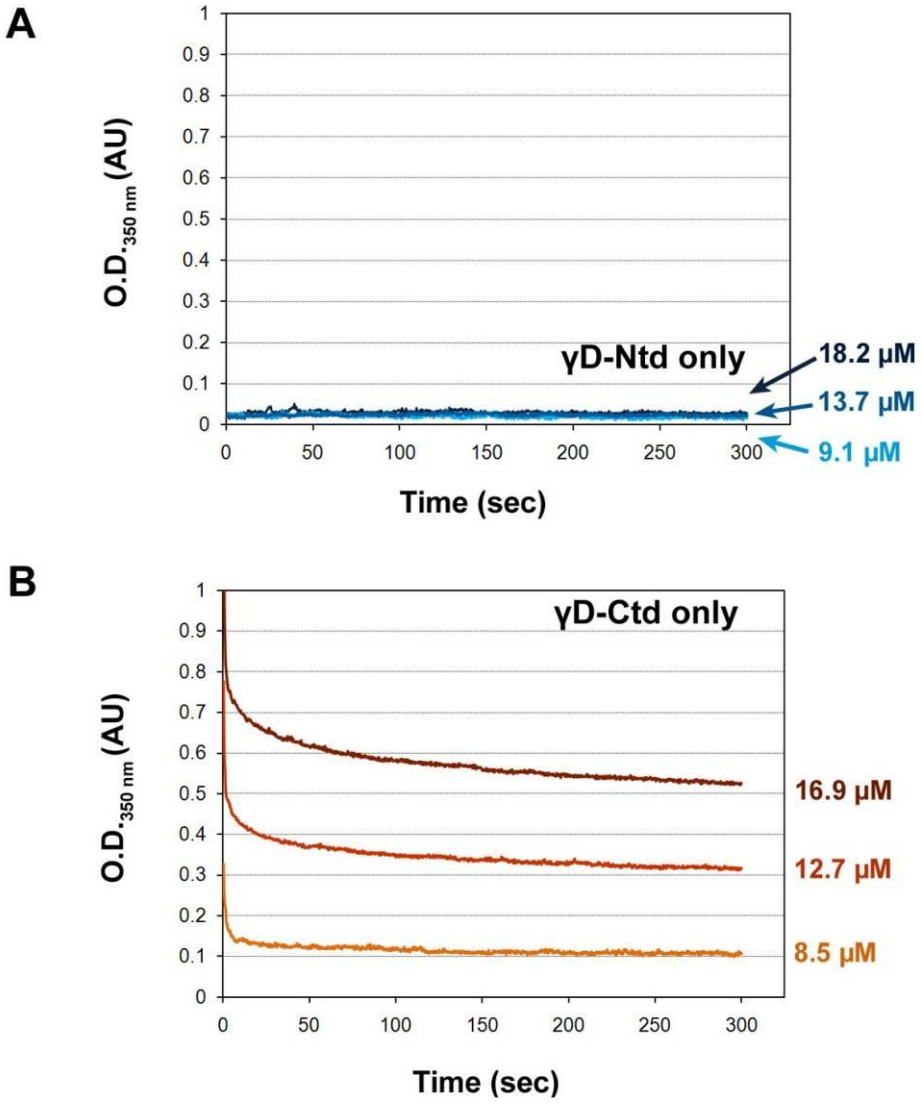

Figure 3-3: Refolding of the γD-Ntd and γD-Ctd single domains at different final protein concentrations.
A) $O.D._{350\ nm}$ traces for γD-Ntd unfolded at different protein concentrations and refolded out of high concentrations of denaturant. Final protein concentrations after dilution with Refolding buffer are shown and range from 9-18 μM (final GdnHCl concentration was 0.42 M). B) For comparison purposes, $O.D._{350\ nm}$ traces for γD-Ctd refolded under similar experimental conditions are shown. Concentrations shown correspond to the final protein concentration after dilution with Refolding buffer. Protein concentrations range from 8-17 μM and the final GdnHCl concentration was 0.5 M.

3. αB-Crys chaperone suppresses the aggregation of partially folded species of γD-Ctd.

αB-Crys suppressed the aggregation of partially folded species populated upon refolding of γC-, γD- and γS-Crys (Fig. 2-2). Experiments where αB-Crys was added seconds after refolding and aggregation of γD-Crys were initiated showed that the substrate species recognized by the chaperone is populated in the first 15 s (Fig. 2-10). Flaugh *et al.* have shown that the C-terminal domain of γD-Crys populates a partially folded intermediate within this time period (Flaugh *et al.* 2006). Further, Mills *et al.* showed in kinetic refolding experiments that the isolated γD-Ctd domain refolded back to its native state in the first 15 s at 18 ºC (Mills *et al.* 2007). They also showed that a partially folded intermediate was populated under productive kinetic refolding conditions for the isolated γD-Ctd domain. The first transition had a $t_{1/2}$ of 4 s and the second transition, from intermediate to native state, had a $t_{1/2}$ of 14 s at 18 ºC (Mills *et al.* 2007).

In order to test whether αB-Crys chaperone would recognize and suppress the aggregation of the isolated γD-Ctd domain, αB-Crys was added to Refolding buffer used to initiate refolding and aggregation of fully unfolded γD-Ctd samples. γD-Ctd was unfolded for 24 h at 37 ºC in Unfolding buffer. Refolding buffer (± αB-Crys) was added, the sample was mixed thoroughly and changes in $O.D_{350\ nm}$ were measured (final protein concentration was 12.7 μM and 0.5 M GdnHCl). αB-Crys suppressed the aggregation of partially folded γD-Ctd. The buffer mixing regime was similar to the regime used in full-length γ-Crys suppression reactions described in Chapter 2. Aggregation, as measured by changes in $O.D._{350\ nm}$, decreased as the concentration of αB-Crys increased (data not shown). At a 1 γD-Ctd: 5 αB molar ratio, αB-Crys chaperone almost completely suppressed the aggregation of partially folded γD-Ctd (Fig. 3-4A).

Samples from these suppression reactions were loaded into a Superose 6 SEC column. Comparable to results from similar assays done with samples from 1 γD:5 αB and 1 γC:5 αB suppression reactions (Fig. 2-4A and B), a substrate-chaperone complex eluted in the void volume of the column (Fig. 3-4B). This substrate-chaperone complex peak was only observed in these suppression reactions and was not present in samples where native αB-Crys and γD-Ctd were incubated under similar final conditions (1 γD-Ctd:5 αB molar ratio, 0.5 M GdnHCl, Fig. 3-4B black trace). This substrate-chaperone peak was also not observed in 1 γD-Ctd:0 αB, native αB-only and in native γD-Ctd samples incubated at similar final conditions (data not shown). Free αB-Crys chaperone oligomers also eluted at the same volume (~ 13.6 ml) as observed in chromatograms shown in figure 2-4. Native γD-Ctd monomers eluted at 19.8 ml (Fig. 3-4B).

Fractions corresponding to the substrate-chaperone complex, free αB-Crys and γD-Ctd monomers peaks were collected during SEC. These fractions were electrophoresed through a 16% SDS-PAGE gel to confirm the distribution of the chaperone and the substrate. As shown in Figure 3-4C, γD-Ctd was present only in the fractions corresponding to the peaks that eluted at 7.6 ml and 19.8 ml. As described above, these peaks corresponded to the substrate-chaperone complex and monomeric γD-Ctd. αB-Crys chaperone was only present in peaks that eluted at 7.6 ml and 13.6 ml, which corresponded to the substrate-chaperone and free αB-Crys oligomers. These resuts showed that the peak that elutes at 7.6 ml corresponds to the substrate-chaperone complex.

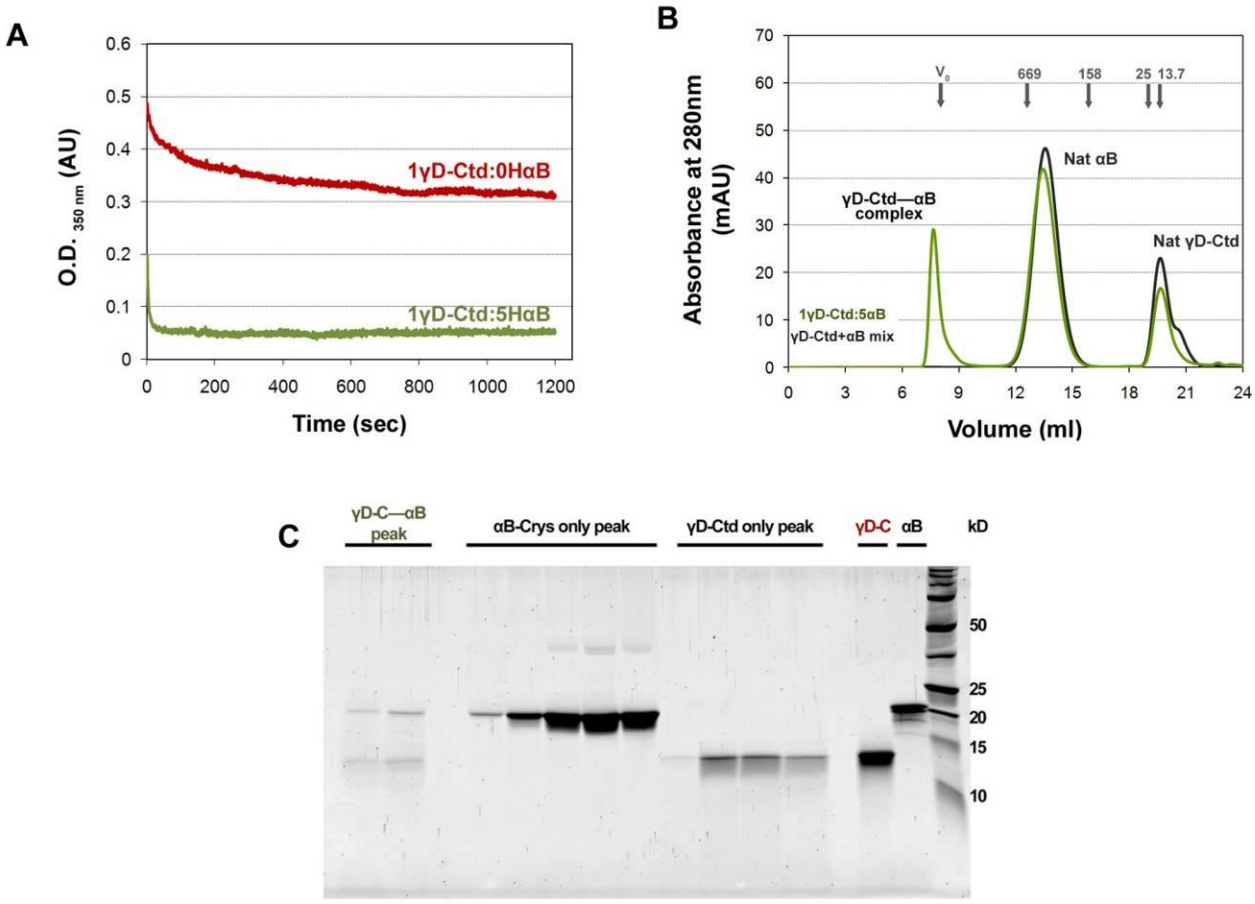

Figure 3-4: αB-Crys suppresses the aggregation of γD-Ctd single domain during dilution out of high concentrations of denaturant.

A) The final protein concentration was 12.7 μM and final GdnHCl concentration was 0.5 M GdnHCl. Ratios represent molar ratios. B) The 1 γD-Ctd:5 αB suppression reaction shown in (A) was applied to a SEC Superose 6 column. 1 γD-Ctd:5 αB suppression reaction (▬) and the 1 γD-Ctd:5 αB native mixture (▬) are shown (See Materials and Methods for native mixture sample preparation). Arrows denote the elution volume for calibration standards. Numbers denote molecular weight in kD. C) SDS-PAGE gel (16%) of fractions collected during the 1 γD-Ctd:5 αB suppression reaction SEC run shown in (B). Fractions corresponded to the γD-Ctd—αB complex peak (V_E=7.6 ml), the free αB-Crys oligomers (V_E=13.6 ml), and refolded γD-Ctd single domain (V_E=19.6 ml). γD-Ctd and αB-Crys controls were included. The molecular mass of standards is shown on the left in kilodaltons. The concentration for the γD-Ctd control was 4.2 μM and the concentration for αB-Crys was 2.5 μM.

4. αB-Crys chaperone formed large, polydisperse substrate-chaperone complexes during suppression of aggregation of partially folded species of γD-Crys and of the γD-Ctd single domain.

The structural nature of the substrate-chaperone complexes formed by sHsps has proven intractable to study. This is in great part due to the structural heterogeneity of these complexes, which is substrate and chaperone dependent. In the case of α-crystallin isolated from lenses, a soluble, high molecular weight species that contains β/γ-crystallin and α-crystallin can be isolated via SEC. Interestingly, the amount of this species increased with the age of the lens reaching a maximum at around age 30 and decreasing thereafter. The increase in this species also correlated with the steady decrease in the amount of free α-crystallin (Heys *et al.* 2007).

Aliquots from SEC fractions corresponding to the substrate-chaperone complex from 1 γD-Ctd:5 αB and 1 γD:5 αB suppression reactions were applied to Formvar/carbon grids for TEM imaging. All grids were negatively stained with 2% uranyl acetate. The substrate-chaperone complexes were spherical and heterogeneous in size, ranging from 50-100 nm in diameter (Fig. 3-5A and B). Aliquots of free recombinant human αB-Crys oligomers were also imaged using TEM. These oligomers were spherical and ranged in size from 10-15 nm (Fig. 3-5C). The dramatic change in αB-Crys chaperone complex size after substrate binding has been observed upon substrate binding for yeast Hsp26 and murine Hsp25 chaperones (Ehrnsperger *et al.* 1997; Haslbeck *et al.* 1999a).

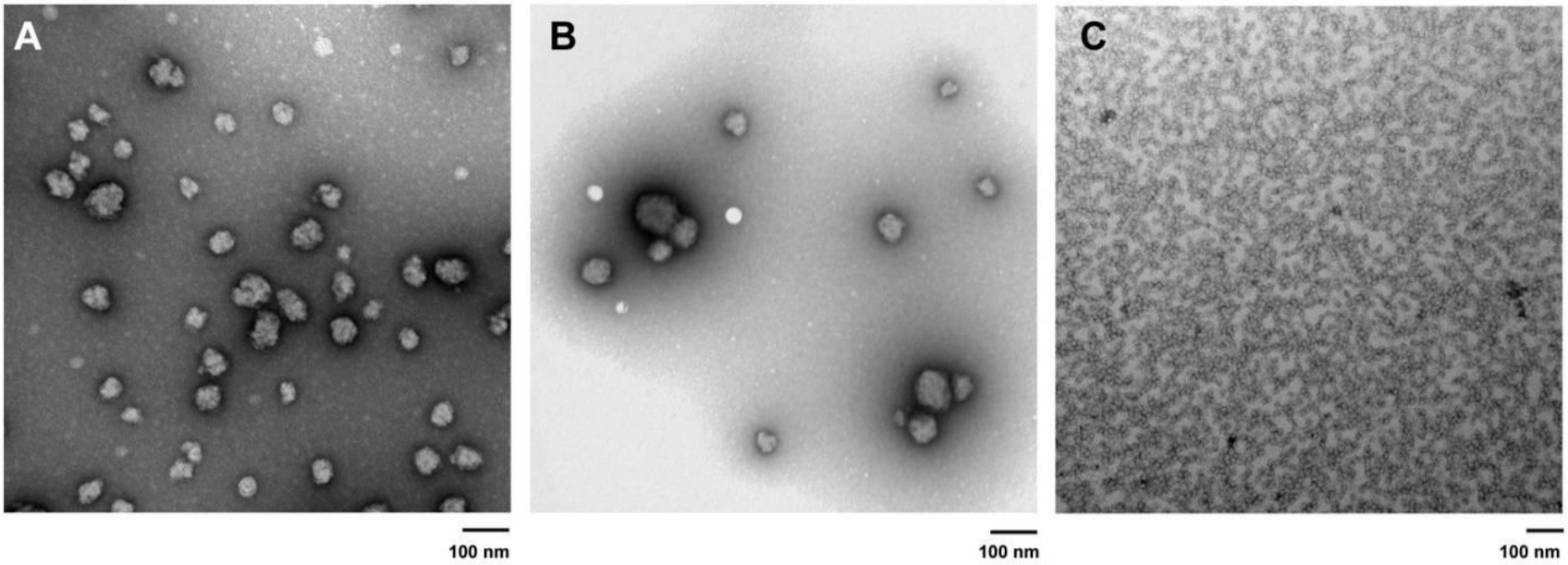

Figure 3-5: TEM micrographs of γ-αB complexes and free αB-Crys.
A) EM micrograph of γD-Ctd—αB complexes isolated via SEC from 1γD-Ctd:5 αB suppression of aggregation reactions (x120000 magnification). B) WT γD—αB complexes isolated via SEC from 1 γD:5 αB suppression reactions at x150000 magnification. C) Free αB-Crys oligomers (x120000 magnification). All scale bars correspond to 100 nm.

5. γD-Ctd was in a partially unfolded conformation in the γD-Ctd—αB complex.

The isolated γD-Ntd and γD-Ctd domains retained the Trp pairs observed in the N-terminal (Trp42 and Trp68) and the C-terminal (Trp130 and Trp156) domains of the full-length γD-Crys protein (Fig. 3-1). Mills *et al.* showed that the isolated, single domains of γD-Crys recapitulated the quenched buried tryptophan fluorescence behavior observed in the native state of the full-length protein. Upon unfolding at high concentrations of GdnHCl, a red shift in the maximum λ_{EM} concomitant with an increase in the quantum yield was observed in the tryptophan fluorescence spectra for the full-length and single domain proteins (Mills *et al.* 2007). Thus, the buried tryptophan fluorescence of the single domain proteins could be used as an indicator of the folding status of γD-Ntd and γD-Ctd single domains.

In order to monitor the conformation of the γD-Ctd bound to αB-Crys chaperone in the substrate-chaperone complexes, noTrp αB-Crys chaperone was used to suppress aggregation. Figure 3-6A shows the native-state Trp fluorescence spectra of WT and noTrp αB-Crys when the λ_{EX} was set to 300 nm. NoTrp αB-Crys chaperone completely suppressed the aggregation of partially folded γD-Ctd as measured in $O.D._{350\ nm}$ assays (Fig. 3-6B). Similar suppression levels were observed for WT αB–Crys chaperone (Fig. 3-4A).

γD-Ctd—noTrp αB complexes were isolated via SEC using a Superose 6 column from 1 γD-Ctd:5 αB samples collected after turbidity measurements (Fig. 3-6C). Fluorescence emission spectra for the fractions containing the substrate-chaperone complex were collected at a λ_{EX} set to 300 nm (Fig. 3-6D). The Trp fluorescence spectra correspond to the Trp residues from γD-Ctd, since noTrp αB-Crys does not contain Trp residues and does not contribute to the fluorescence spectra as shown in Figure 3-6A. The spectrum for the γD-Ctd—αB complexes showed a maximum λ_{EM} at approximately 334 nm. This fluorescence emission spectrum was similar to the spectra for full-length WT and for the double-Trp γD-Crys in complex with Trp-less αB-Crys chaperone (Fig. 2-6D, Fig. 2-7E and F). The fluorescence spectrum of γD-Ctd—no Trp αB complexes did not resemble the spectra of the native or the fully unfolded γD-Ctd controls. This dissimilarity in fluorescence emission spectra was also observed between the full-length WT and double Trp γD—no Trp αB complexes described above and their respective native and unfolded γD-Crys controls. These results showed that the aggregation-prone species of γD-Ctd bound to αB-Crys was in a partially folded conformation, in which its Trp residues were neither buried in a native-like environment nor were they fully exposed to the aqueous solvent.

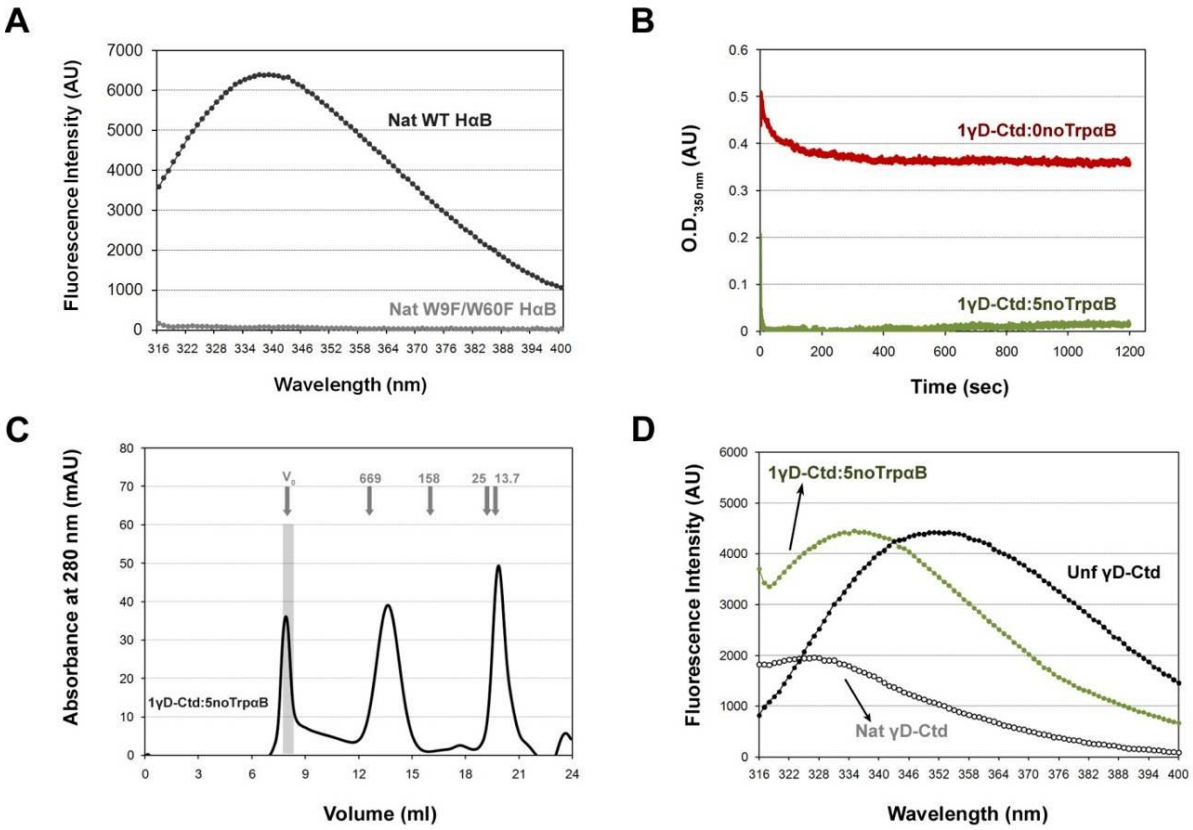

Figure 3-6: Tryptophan fluorescence of γD-Ctd in complex with αB-Crys chaperone.
A) Fluorescence emission spectra for WT αB-Crys (●) and W9F/W60F αB-Crys (●). The excitation wavelength was set to 300 nm and the protein concentration was 1 μM at 25 ºC in SEC buffer.
B) W9F/W60F αB-Crys suppressed the aggregation of γD-Ctd under the same refolding and aggregation conditions as with WT αB-Crys. Final γD-Ctd concentration was 12.7 μM and final GdnHCl concentration was 0.5 M at 37 ºC.
C) A high molecular weight complex could be isolated from the 1γD-Ctd:5 noTrp αB suppression reactions from (B) during SEC. Samples were run on a Superose 6 SEC column at 0.5 ml/min in SEC buffer. The volume highlighted by the shaded area corresponds to the fraction collected for fluorescence measurements.
D) Fluorescence emission spectrum of the fraction containing the γD-Ctd—αB complex isolated from 1 γD-Ctd:5 αB samples as described in (C) (●). For comparison purposes, the fluorescence emission spectra of native (○) and unfolded (●) (in Unfolding buffer for 24 h at 37 ºC) γD-Ctd (1.7 μM) are shown. The λ_{EX} was set to 300 nm for all samples.

6. γD-Ntd does not inhibit the suppression of aggregation by WT αB-Crys of partially folded γD-Ctd in sequential refolding suppression assays.

Tryptophan emission spectra from double Trp γD-Crys mutants in complex with Trp-less αB-Crys showed that the intra-domain Trp pairs were exposed to similar environments in the substrate-chaperone complexes (Fig. 2-7E and F). Similarly, emission spectra from triple-Trp γD-Crys mutants in complex with Trp-less αB-Crys chaperone showed that residues Trp 42 and Trp 130 were in a non-native environment and not solvent-exposed (Fig. 2-8). These results pointed to multiple binding interactions between both domains of γD-Crys and the αB-Crys chaperone. Given the large oligomeric size of αB-Crys and the sequence similarity between the N-terminal and C-terminal domains of γD-Crys, it was possible that both domains could bind to the same regions in the monomer, but at different monomer subunits in the αB-Crys chaperone oligomer.

In order to investigate this possibility, a sequential-refolding competition assay was developed, in which the γD-Ntd was refolded first in the presence of WT αB-Crys, followed by addition and concomitant refolding of unfolded γD-Ctd in the same sample (Fig. 3-7A). Figure 3-7B shows $O.D._{350\ nm}$ results for these competitive suppression assays. Refolded γD-Ntd was added at an equimolar final concentration to γD-Ctd and all suppression reactions were performed at 37 ºC. Before adding unfolded γD-Ctd, γD-Ntd was allowed to refold in the presence or absence of αB-Crys for 1 h at 37 ºC to ensure complete refolding of the protein. There were no changes in solution turbidity levels in control samples where γD-Ctd was refolded alone compared to samples where unfolded γD-Ctd was refolded in the presence of refolded γD-Ntd (1 γD-Ctd:0 αB + REF γD-Ntd trace, Fig. 3-7B). There were also no significant changes in solution turbidity levels between control experiments where γD-Ctd was refolded in the presence of αB-Crys chaperone (1 γD-Ctd:5 αB trace) and experiments where γD-Ctd was refolded in the presence of refolded γD-Ntd plus αB-Crys (1 γD-Ctd:5 αB + REF γD-Ntd trace, Fig. 3-7B).

1 γD-Ctd:5 αB + REF γD-Ntd samples were collected and incubated for 24 h at 37 ºC prior to SEC (Fig. 3-7C). Three peaks were present: a substrate-chaperone peak (eluted at 7.6 ml), a free αB-Crys peak (eluted at 13.6 ml) and an isolated domain peak (eluting at ~19.6 ml). Fractions corresponding to all three major peaks were collected and electrophoresed in an 18% SDS-PAGE gel (Figure 3-7D). The fractions corresponding to the substrate-chaperone peak contained only αB-Crys and γD-Ctd. SDS-PAGE gels of 4-fold concentrated fractions also showed that only γD-Ctd and αB-

Crys were present in these substrate-chaperone complexes isolated from 1 γD-Ctd:5 αB + REF γD-Ntd suppression reactions (data not shown). These results revealed that refolding γD-Ntd in the presence of αB-Crys chaperone did not inhibit subsequent binding of γD-Ctd aggregation-prone species to αB-Crys.

However, these observations could also be due to the isolated single domains binding to differing binding sites in the αB-Crys chaperone monomer. To investigate this possibility, fully unfolded γD-Ntd was refolded in the presence of WT αB-Crys chaperone to the same final assay conditions as described above (12.7 μM γD-Ntd, 0.5 M GdnHCl, 1 γD-Ntd:5 αB ratio). These samples were incubated for 24 h at 37 ºC prior to loading onto a Superose 6 SEC column. SEC traces for these 1 γD-Ntd:5 αB samples did not reveal the presence of the signature substrate-chaperone peak observed for all aggregation prone species of γ-Crys in complex with αB-Crys (Fig. 3-7C, blue trace). In addition, SDS-PAGE gel electrophoresis of the fractions encompassing the free αB-Crys did not show the presence of a protein band co-migrating at the same position as the γD-Ntd control (data not shown). Thus, γD-Ntd did not bind to αB-Crys oligomers nor formed stable substrate-chaperone complexes that could be isolated by SEC. These results were not unexpected given that the γD-Ntd isolated domain did not aggregate under these assay conditions, therefore it might not populate aggregation-prone species that could be identified by αB-Crys.

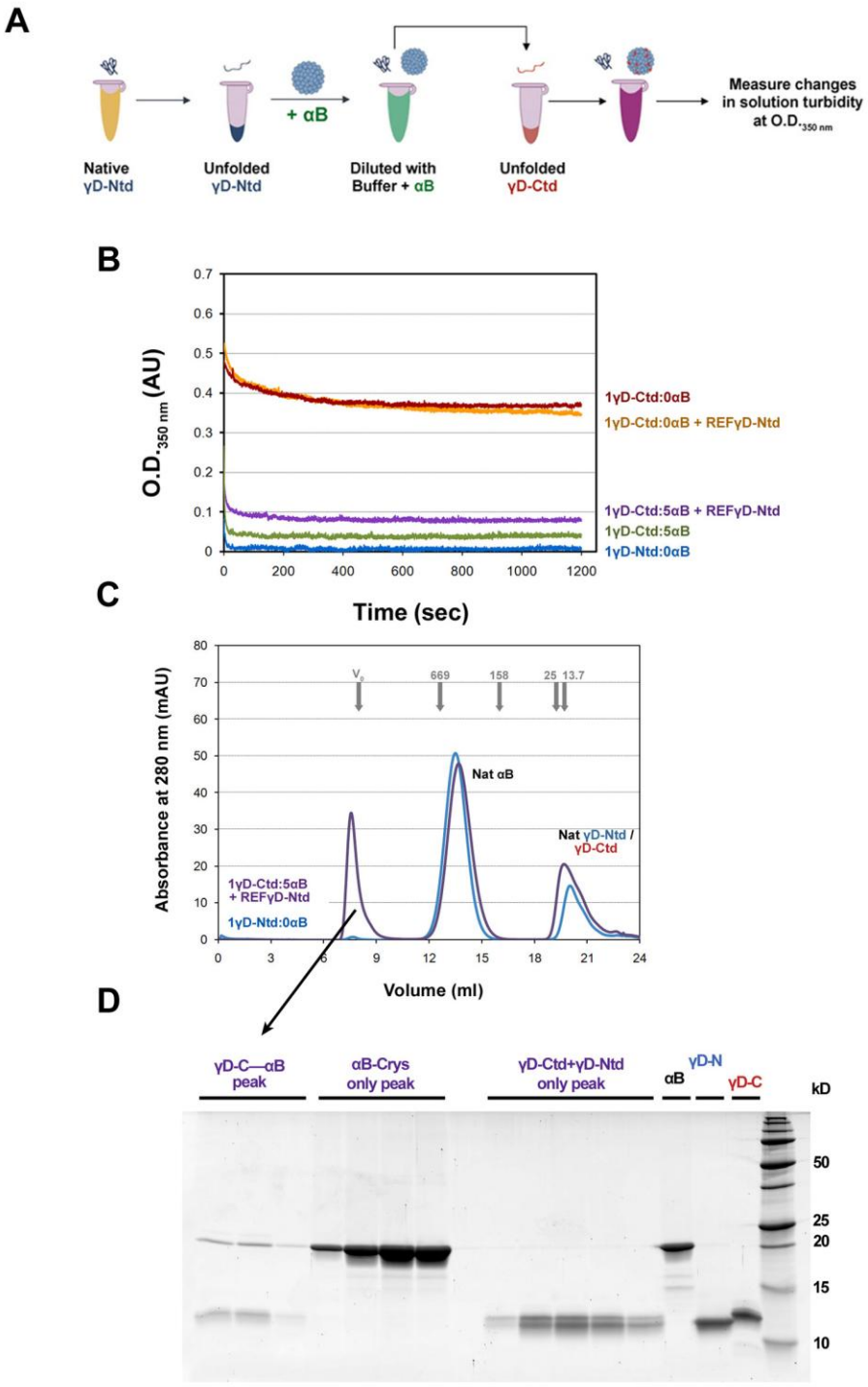

Figure 3-7: Sequential-refolding inhibition assay with γD-Ntd and γD-Ctd as substrates
A) Schematic of the mixing regime used in (B). Unfolded γD-Ntd (12.7 μM) was refolded with Refolding buffer in the absence or presence of αB-Crys (final γD-Ntd concentration was

12.7 μM, final αB-Crys concentration was 63.5 μM and the final GdnHCl concentration was 0.25 M). This sample was collected and used to refold fully unfolded γD-Ctd (final γD-Ctd concentration was 12.7 μM and the final GdnHCl concentration was 0.5 M GdnHCl).

B) $O.D._{350\ nm}$ traces for γD-Ctd refolded with buffer containing Refolded γD-Ntd +/- αB-Crys (1 γD-Ctd:0 αB and 1 γD-Ctd:5 αB + Ref γD-Ntd). 1 γD-Ctd:5 αB and 1γD-Ntd:0 αB controls are shown. Ratios shown represent molar ratios. All suppression reactions were performed at 37 ºC and the final GdnHCl concentration was 0.5 M for all samples. Arrows correspond to the elution volume of calibration standards. The molecular mass of these calibration standards is shown in kilodaltons.

C) SEC chromatograms for 1 γD-Ctd: 5αB + Ref γD-Ntd ( ) suppression reaction and 1 γD-Ntd:5 αB ( ). Samples were collected after $O.D._{350\ nm}$ measurements and applied to a Superose 6 SEC column. Arrows correspond to elution volume of standards. Numbers represent standards' molecular weights in kilodaltons.

D) Fractions corresponding to the substrate-complex peak, the free αB-Crys peak and the monomeric γD-Ntd/γD-Ctd were collected and electrophoresed through an 18% SDS-PAGE gel. The concentration for the γD-Ctd control was 4.2 μM and the concentration for αB-Crys was 2.5 μM. The molecular mass of standards is shown on the left in kilodaltons.

7. γD-Ntd co-aggregated with γD-Ctd when both isolated domains were unfolded and refolded simultaneously.

Wright *et al.* showed that protein homologues with high sequence identity (> 70%) readily co-aggregated forming amyloid fibrils (Wright *et al.* 2005). In their work, the threshold for co-aggregation of two target proteins was 30-40% sequence identity. Sequence identity requirements for co-aggregation were determined under parameters for amyloid-specific aggregation. In the case of human γD-Crys, the N-terminal domain and the C-terminal domain have 39% sequence identity, 52% sequence similarity, and their tertiary structures are very similar (Mills-Henry 2007). Thus, it seemed likely that, under appropriate conditions, both proteins could populate similar aggregation-prone species that would co-aggregate during refolding to form large amorphous aggregates. As mentioned in the previous section, the consecutive refolding of γD-Ntd followed by refolding of γD-Ctd did not affect the aggregation levels of γD-Ctd (Fig. 3-7B). Therefore, a new mixing scheme was developed in which both single isolated domains were unfolded together and refolded simultaneously at equimolar concentrations (Fig. 3-8A).

γD-Ntd and γD-Ctd were unfolded at equimolar concentrations in Unfolding buffer for 24 h at 37 ºC. Unfolded samples were diluted 20-fold with Refolding buffer at 37 ºC, mixed thoroughly, and $O.D._{350\ nm}$ was measured at 37 ºC for 300 s (Fig. 3-8B, 1 γD-Ctd:1 γD-Ntd trace). The final protein concentration was 8.5 μM (0.25M GdnHCl). For comparison purposes, γD-Ctd at twice the molar concentration used in the previous assays (16.9 μM) was similarly refolded and turbidity was measured under identical assay conditions (Fig. 3-8B, γD-Ctd only trace). These results indicated that the γD-Ntd was co-aggregating with partially folded, aggregation prone species of γD-Ctd.

1 γD-Ntd:1 γD-Ctd samples (4 total) were collected and incubated for 24 h at 37 ºC. After incubation, samples were filtered through a 0.2 μm spin-filter and the aggregates on the membrane were washed twice with 10 mM ammonium acetate (pH 7.0) and resuspended with 1X SDS sample buffer. Aliquots were collected from the filtrate and 3X SDS sample buffer was added. All samples were incubated at 95 ºC for 5 min and electrophoresed through an 18% SDS-PAGE gel. Figure 3-8C shows the results from the retentate and filtrate fractions for four independent samples. γD-Ntd and γD-Ctd were present in both fractions providing further evidence that although the γD-Ntd did not aggregate by itself during refolding out of high concentrations of GdnHCl, it was recruited into large, amorphous aggregates in the presence of the aggregation-prone species of γD-Ctd. Further, these

results also indicate that both domains in the full-length γD-Crys proteins might interact to form aggregates.

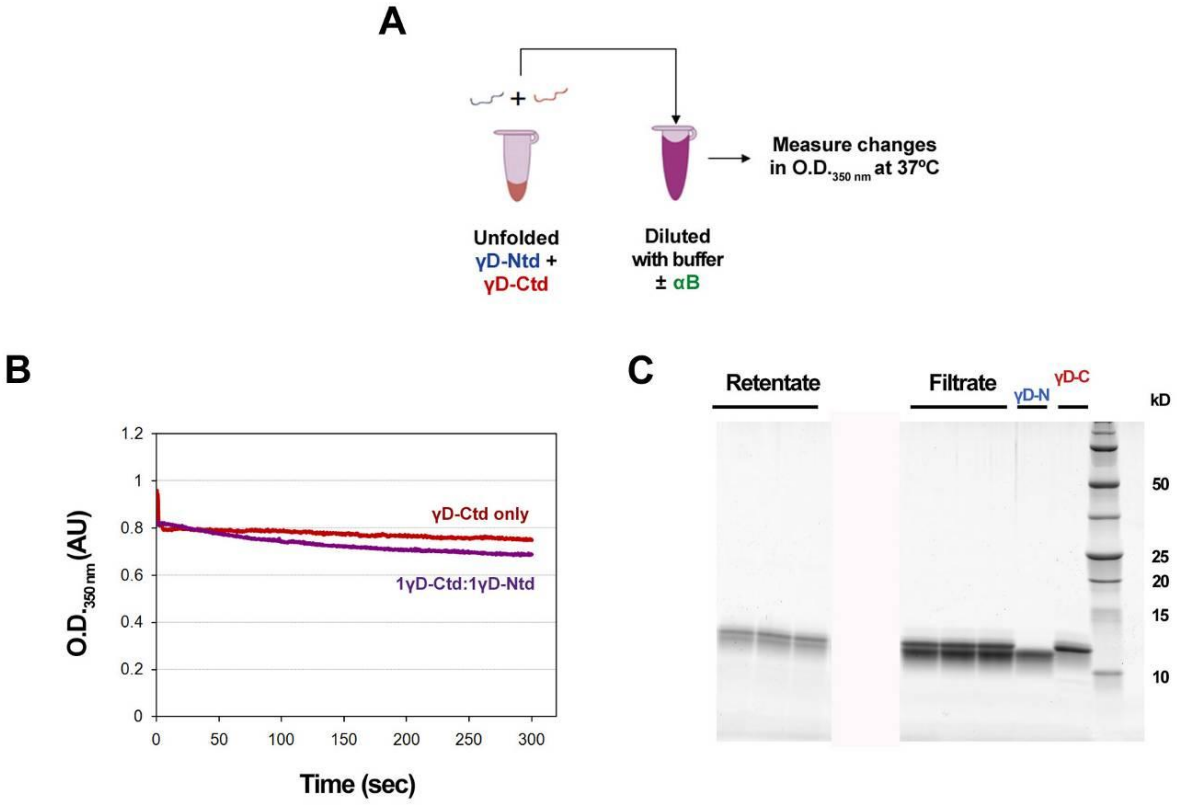

Figure 3-8: Simultaneous refolding of γD-Ntd and γD-Ctd inhibition assay.
A) Schematic representation of the mixing regime for aggregation reactions shown in (B) and (C). Equimolar concentrations of γD-Ntd and γD-Ctd were unfolded together in Unfolding buffer for 24 h at 37 ºC. Refolding buffer (± αB-Crys) was added to dilute denaturant and changes in solution turbidity at $O.D._{350\ nm}$.

B) $O.D._{350\ nm}$ traces for γD-Ntd and γD-Ctd single domains unfolded together at equimolar concentrations (8.5 µM) and refolded with Refolding buffer [1 γD-Ctd:1 γD-Ntd trace, (——)]. For comparison purposes, the $O.D._{350\ nm}$ trace for γD-Ctd [γD-Ctd only, (——)] at the same final, total molar concentration (16.9 µM) is shown. Both samples were unfolded in Unfolding buffer 24 h at 37 ºC and their final GdnHCl concentration was 0.25 M.
C) 1 γD-Ctd:1 γD-Ntd samples from B) were incubated at 37 ºC for 24 h. Supernatant/Pellet fractionation was performed by filtering samples through a 0.2 µm spin-filter. Aggregates were resuspended in 200 µl of 1X SDS-Buffer after washing the membrane with H_2O. Retentate/Filtrate fractions from three separate samples are shown. The concentration for the γD-Ctd and γD-Ntd controls was 4.2 µM. The molecular mass of standards is shown on the left in kilodaltons.

8. αB-Crys suppressed the formation of large aggregates in γD-Ntd plus γD-Ctd co-aggregation reactions by preferentially binding to γD-Ctd.

The co-aggregation of γD-Ntd and γD-Ctd allowed experiments to assay as to whether αB-Crys would suppress aggregation by either binding both domains and whether it recognized an aggregation-prone region in either domain. To this end, γD-Ntd and γD-Ctd were unfolded together and refolded simultaneously in the presence of a 5-fold molar excess of αB-Crys. Figure 3-9A shows the $O.D._{350\ nm}$ results for these suppression of aggregation reactions (1 γD-Ntd:1 γD-Ctd:5 αB trace). The final protein concentration for both single domains was 12.7 μM, the final protein concentration for αB-Crys chaperone was 63.5 μM and the final GdnHCl concentration was 0.5 M. αB-Crys chaperone efficiently suppressed the co-aggregation of the isolated single domains of γD-Crys at 37 ºC. These results presented the possibility that αB-Crys chaperone could be recognizing structural characteristics of a shared aggregation-prone species populated by both domains during refolding out of high concentrations of denaturant.

The suppression of aggregation reactions were collected and incubated for 24 h at 37 ºC. Samples were then applied to a Superose 6 SEC column to isolate the substrate-chaperone complex (Fig. 3-9B). Fractions encompassing peaks for the substrate-chaperone complex, free αB-Crys chaperone oligomers, and monomeric isolated domains were electrophoresed through an 18% SDS-PAGE gel (Fig. 3-9C). Close inspection of the substrate-chaperone complex-containing fractions revealed that only protein bands migrating at positions for γD-Ctd single domain and αB-Crys were present. These results indicate that the suppression of the co-aggregation of γD-Ntd and γD-Ctd may be mediated by specific recognition and binding to aggregation-prone regions present in the C-terminal domain of γD-Crys. αB-Crys would not only recognize an aggregation-prone conformer, but a specific aggregation-prone region located in the C-terminal domain of γD-Crys. Sequestering such aggregation-prone γD-Ctd species would inhibit the co-aggregation of γD-Ntd partially folded intermediates freeing such intermediates to fold to their native states.

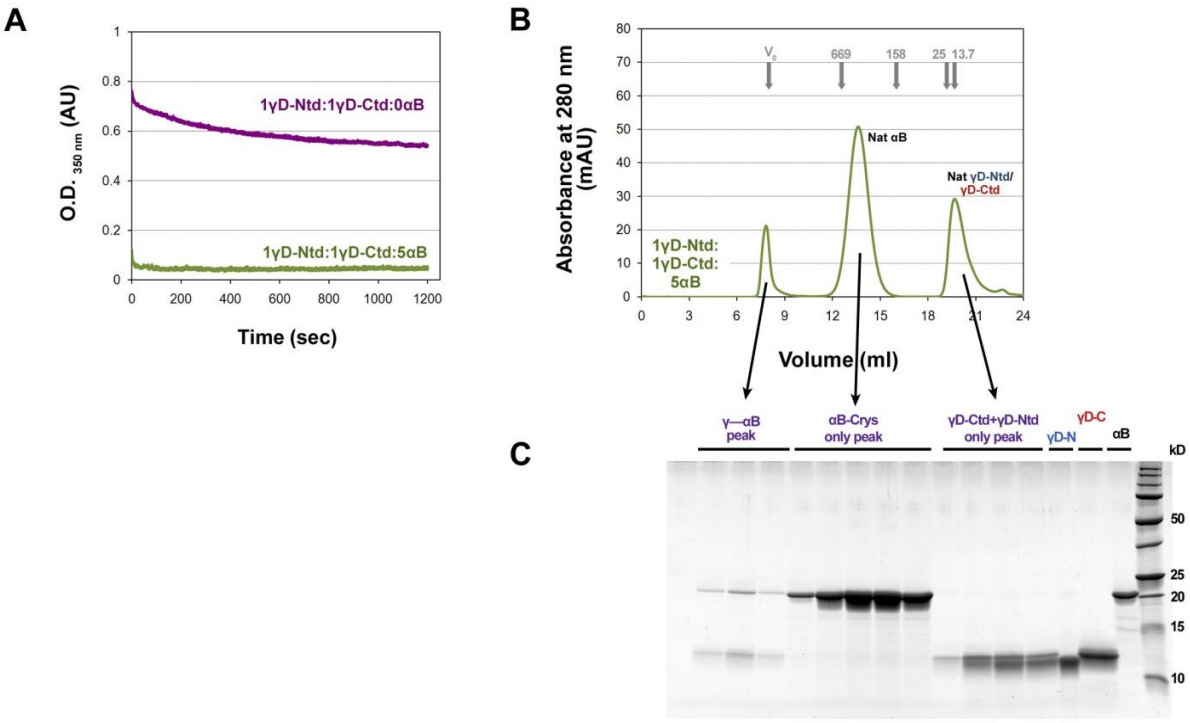

Figure 3-9: Refolding of γD-Ntd in the presence of γD-Ctd.
A) O.D.$_{350\ nm}$ traces for γD-Ntd and γD-Ctd single domains unfolded together at equimolar concentrations (12.7 μM) and refolded with Refolding buffer [1 γD-Ntd:1 γD-Ctd:0 αB trace, ( )]. For the 1 γD-Ntd:1 γD-Ctd:5 αB samples, αB-Crys chaperone was incubated in Refolding buffer for 1 h at 37 ºC prior to addition to unfolded isolated domains ( ). All samples were unfolded in Unfolding buffer 24 h at 37 ºC and their final GdnHCl concentration was 0.5 M.
B) 1 γD-Ntd:1 γD-Ctd:5 αB samples from B) were incubated at 37 ºC for 24 h. Samples were filtered through a 0.2 μm spin-filter and loaded onto a SEC column. Fractions spanning all major peaks were collected for SDS-PAGE electrophoresis.
C) Fractions corresponding to the substrate-complex peak, the free αB-Crys peak and the monomeric γD-Ntd/γD-Ctd were collected and electrophoresed through an 18% SDS-PAGE gel. The concentration for the γD-Ctd control was 4.2 μM and the concentration for αB-Crys was 2.5 μM. The molecular mass of standards is shown on the left in kilodaltons.

D. DISCUSSION

An unsolved problem in understanding the loss of lens transparency is the character and conformation of the crystallin species recognized and bound by α-crystallin chaperone complexes, Tightly coupled to this is the identification of the factors and conditions that disrupt the native state of the βγ-crystallins within cataractous lenses resulting in altered conformations.

Fragments (< 18 kDa) of the crystallin proteins have been isolated from water insoluble (WI) inclusions from cataractous lenses (Srivastava 1988). Lens protein fragments can constitute up to 20% of the protein content in the WI fraction (Srivastava and Srivastava 2003). Their presence increased in these lenses and extensive covalent modifications were also observed in these fragments from insoluble aggregates (Srivastava *et al.* 1992). Srivastava *et al.* identified a 9 kDa fragment from the C-terminal domain of γD-Crys from human cataractous inclusions (Srivastava *et al.* 1992). Srivastava and Srivastava later showed that this 9 kDa fragment (residues 97-163) was the C-terminal truncated C-td of γD-Crys (Srivastava and Srivastava 2003). Mass spectrometry analysis revealed oxidation of Met146 and Trp156. Further, this fragment formed non-disulfide cross-linked trimers *in vitro* that were also present in the WS fraction of normal aged and cataractous lenses, but absent from young lenses (Srivastava and Srivastava 2003). The authors did not identify the proteolytic mechanism whence this fragment was created in the lens, although they suggest that lens-specific proteases, such as the lens calpains, may be responsible for the initial proteolytic cleavage of the γD-Crys linker in young-adult lenses. Analysis of WS-HMW complexes from aged normal and cataractous lenses revealed that complexes isolated from cataractous lenses contained more protein fragments (Srivastava *et al.* 1996; Srivastava *et al.* 2008). These findings indicate that fragments of the crystallin proteins may play a significant role in the formation of protein aggregates in cataractous lenses.

1. The C-terminal domain of human γD-Crys contains an aggregation-prone sequence.

The N-terminal and C-terminal domains of human γD-Crys share 39% sequence similarity and, like most members of the βγ-crystallin superfamily, share the conserved double Greek-key β-sandwich domain organization. Mills *et al.* showed that at low protein concentrations both isolated single domains refold to their native state in equilibrium folding and unfolding experiments (Mills *et al.* 2007). Increasing the protein concentration during aggregation assays where either γD-Ntd or γD-Ctd was refolded out high concentrations of denaturant resulted in the aggregation of partially-folded species of γD-Ctd only (Fig. 3-3). Mills-Henry reported similar results under similar assay conditions and protein concentrations (Mills-Henry 2007). The aggregation of partially folded γD-Ctd is in agreement with results shown in Figure 2-5 that show that the C-terminal domain of γD-Crys must be destabilized for the formation of the partially folded aggregation-prone intermediate of γD-Crys. The γD-Ctd single domain formed large amorphous aggregates similar to the aggregates observed from partially folded species of γC-, γD-, and γS-Crys (Fig. 2-3).

Given the high degree of similarity in tertiary structure between the γD-Ntd and γD-Ctd, these results seem to indicate the existence of an aggregation-prone sequence in the γD-Ctd that is responsible for differential aggregation behavior observed between these two isolated domains. For some proteins, aggregation-prone sequences are associated with amylogenic peptides (Krebs *et al.* 2004). Amorphous aggregation is thought to be a less specific process dependent on the hydrophobic character of the regions forming intermolecular non-specific contacts in the aggregate. Nonetheless, a recombinant protein can constitute up to 90% of the protein in bacterial inclusion bodies, which are classified as amorphous aggregates in the cell, formed during heterologous protein expression (de Groot *et al.* 2008). Speed *et al.* showed that aggregation *in vitro* depended upon specific conformations of aggregation-prone intermediates of the same protein populated during refolding out of high concentrations of denaturant (Speed *et al.* 1996). Consequently, amorphous protein aggregation is to a significant degree a sequence-specific process. These observations would explain the different aggregate-formation proficiencies between the N-td and the C-td. However, these results do not exclude the possibility that the N-terminal domain participates in intermolecular interactions in aggregates formed by partially-folded species of full-length γD-Crys. The presence of an aggregation-prone region in the C-terminal domain of γD-Crys agrees with the isolation of the 9 kDa fragment from WI inclusions in aged normal and cataractous lenses described above.

2. αB-Crys chaperone suppresses the aggregation of partially folded γD-Ctd single domain and forms large substrate-chaperone complexes.

αB-Crys chaperone suppressed the aggregation of partially folded γD-Ctd in aggregation suppression assays and formed large, polydisperse substrate-chaperone complexes (Figures 3-4 and 3-5). These aggregation suppression assays were carried out under similar buffer conditions as similar assays for full-length γD-Crys described in Chapter 2. In line with observations from experiments with the full-length γ-crystallins as substrates, the γD-Ctd—αB complex was only formed during the suppression of aggregation assay and not when both proteins were mixed together under final assay conditions (Fig. 3-4B). SDS-PAGE gels showed the presence of both proteins in the fractions corresponding to the substrate-complex peak (Fig. 3-4C).

As mentioned previously, WS-HMW complexes isolated from aged lenses contained α-, β-, and γ-crystallins and they are putative substrate-chaperone complexes formed by α-crystallin in the lens (Rao *et al.* 1995; Andley 2007). Rao *et al.* showed that HMW complexes formed only in bovine lens homogenate containing α-crystallin after incubation at high temperature (Rao *et al.* 1995). These complexes eluted as a separate peak earlier than the free α-crystallin peak and were composed of β- and α-crystallin. We report that a similar substrate-chaperone complex was isolated after suppression of aggregation assays with γD-Ctd as the substrate (Fig 3-4B and C). Samples from the substrate chaperone peak were imaged by negative-stain TEM. Distinct, polydisperse, spherical species ranging in size from 50-100 nm in diameter were present in samples corresponding γD-Ctd—αB complexes (Fig. 3-5A). These complexes were similar to species observed in micrographs of full-length γD—αB complexes (Fig. 3-5B). Both complexes were morphologically different from the species observed for free αB-Crys oligomers, which were also spherical but were ~13 nm in diameter (Fig. 3-5C).

A significant increase in chaperone oligomer size upon substrate binding has been observed for other sHsps. Stromer *et al*. reported the formation of morphologically similar substrate-chaperone complexes for murine Hsp25 and yeast Hsp26 (Stromer *et al.* 2003). They concluded that substrate binding (in the case of substrates citrate synthase and rhodanese) was a coordinated and cooperative process since they did not observe smaller substrate-chaperone complexes. A similar process seems to operate for αB-Crys binding to partially folded species of full-length γD-Crys and

the isolated γD-Ctd domain. As discussed in Chapter 2 Section C-6, once formed, full-length γD—αB complexes are stable for days. Perhaps this coordinated binding of aggregation-prone species may contribute to the ability of sHsps to efficiently suppress protein aggregation and might also relate to the stability of the substrate-chaperone complexes. However, it still remains to be determined the location of the substrate in these complexes (*i.e.* whether the substrate is internalized and buried in the substrate-chaperone complex or whether the substrates are surface-exposed).

Claxton *et al.* previously showed that T4 lysozyme had a defined orientation when bound to the αB-Crys chaperone indicating that the substrate binding sites on the chaperone recognized a specific region in T4 lysozyme (Claxton *et al.* 2008). Results described in Chapter 2 indicated that the Trp pair in the C-terminal domain of full-length γD-Crys was partially occluded from solvent and the region surrounding the Trp residues was not in a native or fully unfolded conformation (Fig. 2-7 F). We were also interested in investigating the conformation of the γD-Ctd substrate bound in the substrate-chaperone substrate. To this end, I made use of a Trp-less mutant of αB-Crys in which both Trps (Trp9 and Trp60) were substituted to phenylalanines. γD-Ctd single domain contains the Trp pair present in the C-terminal domain of full-length γD-Crys (Trp130 and Trp156). Mills *et al.* showed that the γD-Ctd isolated domain conserved the Trp quenching mechanism observed in the full-length protein (Mills *et al.* 2007). As discussed in Chapter 1 and 2, Chen *et al.* showed that this Trp quenching mechanism is highly sensitive to the conformation of the Trp rings (Chen *et al.* 2006).

Figure 3-6 shows results from experiments where Trp-less αB-Crys was used as a chaperone to suppress the aggregation of partially folded γD-Ctd. γD-Ctd—no Trp αB complexes were isolated via SEC and the fluorescence emission spectra for the complex-containing fractions was measured and compared to the spectra for native and fully unfolded γD-Ctd controls (Fig. 3-6C and D). The fluorescence emission spectra for the γD-Ctd—αB complex had a maximum λ_{EM} at approximately 334 nm and did not coincide with the spectra for the native or the fully unfolded γD-Ctd single domain controls (Fig. 3-6D). These results indicate that the Trp residues in γD-Ctd in the γD-Ctd—no Trp αB complexes were not solvent exposed and the region surrounding these residues was not in a native-like conformation. The W42F/W68F full-length γD-Crys mutant in complex with Trp-less αB-Crys (Fig. 2-7F) had a similar fluorescence emission spectrum and maximum λ_{EM} as the spectrum from the γD-Ctd in complex with Trp-less αB-Crys shown in Fig. 3-6D. Therefore, it seems that the isolated C-terminal domain was in a similar environment as the C-terminal domain in the full-length protein.

Another possibility that could account for the Trp fluorescence emission spectrum observed for the γD-Ctd in complex with Trp-less αB-Crys is that both Trp residues interact with the chaperone and are partially buried but in non-native conformations. Results for W130only γD-Crys presented in Chapter 2 indicate that the Trp residue is partially occluded from solvent with the surrounding region in a non-native conformation (Fig. 2-8B). Results from late-addition suppression of aggregation assays using Trp-less αB-Crys showed that the chaperone recognized an early aggregation-prone intermediate that was populated within the refolding time-span of the C-terminal domain in the full-length protein. Further, results presented here and in Chapter 2 (Fig. 2-5) seem to indicate that there is an aggregation-prone sequence in the C-terminal domain of γD-Crys that is responsible for the aggregation of the protein observed upon refolding out of high concentrations of denaturant.

3. αB-Crys recognizes specific regions in the C-terminal domain that are not present in the N-terminal domain.

In order to investigate whether αB-Crys recognized specific regions of the C-terminal domain of γD-Crys, I performed two substrate competition experiments using γD-Ntd isolated domain to see if it would compete with γD-Ctd for binding sites on the chaperone under aggregation conditions. γD-Ctd did not interact with αB-Crys chaperone to form substrate-chaperone complexes under equilibrium conditions where the native state of γD-Ctd is stable (Fig. 3-4B, black trace). Therefore, these competition experiments had to be carried out under conditions where αB-Crys would bind γD-Ctd to form substrate-chaperone complexes, *viz.* during dilution out of high concentrations of denaturant wherein aggregation of partially folded species of γD-Ctd occurred. Two competition experiments were designed: a sequential refolding and a simultaneous refolding competition assay using γD-Ntd and γD-Ctd as substrates.

The sequential refolding competition assays consisted of refolding γD-Ntd single domain first in the presence or absence of αB-Crys chaperone and then refolding the γD-Ctd in the presence of refolded γD-Ntd (with or without αB-Crys chaperone) (Fig. 3-7A). Figure 3-7B shows the results for these experiments. Refolded γD-Ntd did not affect the aggregation levels of γD-Ctd during refolding out of high concentrations of denaturant (Fig. 3-7B, red and orange traces). In addition, refolding γD-Ntd did not seem to significantly affect the chaperoning efficiency of αB-Crys during

suppression of aggregation assays for γD-Ctd (Fig. 3-7B, purple and green traces). Further, a substrate-chaperone complex isolated from suppression reactions of γD-Ctd refolded in the presence of refolded γD-Ntd and αB-Crys contained only γD-Ctd and αB-Crys (Fig. 3-7C and D). In line with the results shown in Figure 3-3B, substrate-chaperone complexes were not formed when the γD-Ntd was refolded in the presence of αB-Crys since the γD-Ntd did not aggregate upon refolding out of denaturant at this protein concentration (Fig. 3-7C, blue trace). The results presented in Figure 3-7 indicate that the isolated γD-Ntd domain did not interact with αB-Crys chaperone and did not inhibit the binding of the γD-Ctd single domain. These results did not coincide with results in Figure 2-7E, which indicated that the region surrounding the Trp residues in N-terminal domain in the full-length γD-Crys protein could be interacting with the αB-Crys chaperone or was involved in other intermolecular interactions on the complex that occluded these Trp residues from the solvent.

The second competition experiment described herein was designed to more closely mimic the refolding and aggregation conditions of the full-length γD-Crys protein during dilution out of high concentrations of denaturant. The assay consisted of mixing γD-Ntd and γD-Ctd at equimolar concentrations, unfolding both proteins in high concentrations of GdnHCl and refolding simultaneously (Fig. 3-8A). Refolding γD-Ntd and γD-Ctd simultaneously resulted in the co-aggregation of both single domains into large light-scattering aggregates (Fig. 3-8B and C). A high level of shared sequence identity is a pre-requisite for co-aggregation of two homologous proteins during amyloid formation (Wright *et al.* 2005). Amino acid sequence alignment for both domains of γD-Crys showed that they share 39% sequence identity and 52% sequence similarity (Mills-Henry 2007). Wright *et al.* established that 30-40% sequence identity was the threshold for co-aggregation of two homologous proteins for amyloid formation, thus, co-aggregation of γD-Ntd and γD-Ctd would be predicted given these observations. Even though, the aggregates formed by partially folded species of γD-Ctd were not amyloid fibers, but large, amorphous fibril-like species (Fig. 3-2B and C) co-aggregation under these conditions still requires a significant level of sequence identity (Speed *et al.* 1996; Lopez de la Paz *et al.* 2002; Rousseau *et al.* 2006).

The co-aggregation of both isolated domains allowed us to dissect the binding interactions of the αB-Crys chaperone with each domain of γD-Crys. Figure 3-9A shows that αB-Crys chaperone suppressed the co-aggregation of γD-Ntd and γD-Ctd very efficiently. However, SDS-PAGE gel analysis of the substrate-chaperone complex isolated from the suppression of aggregation reactions revealed that αB-Crys bound preferentially to the γD-Ctd (Fig. 3-9C). If αB-Crys bound mostly γD-

Ctd aggregation-prone species, then partially folded intermediates of γD-Ntd would refold productively due to the absence of a competing aggregation off-pathway intermediates. These results suggest that αB-Crys chaperone was highly specific in its ability to recognize and sequester aggregation-prone species from γD-Ctd. α-crystallin showed similar ability when it preferentially bound aggregation-prone molten globule intermediates of apo-α-lactalbumin, but not stable molten-globule intermediates (Rajaraman *et al.* 1998). Previous results showed that the C-terminal domain of full-length γD-Crys had to be partially unfolded for the protein to aggregate upon dilution out of denaturant (Fig. 2-5), these results along with the results described above indicate that an aggregation-prone sequence in the C-terminal domain is exposed during refolding out of high concentrations of denaturant and is necessary for initiation of aggregation. Results presented in Figure 3-9 also indicate that the N-terminal domain of the full-length protein may also participate in inter-molecular interactions in the full-length protein aggregates.

4. Correlation with protein aggregation and cataract disease in the lens.

A proteolytic fragment of 9 kDa corresponding to the C-terminal domain of γD-Crys was isolated from the WS fraction young-adult lens homogenates (Srivastava and Srivastava 2003). According to *in vitro* studies, the isolated γD-Ctd domain folds to a native conformation, as judged by far-UV CD and intrinsic Trp fluorescence spectra, and is stable with an extrapolated $t_{1/2}$ in H_2O of 14.9 yrs *in vitro.* However, age-related truncation events at either terminus of the protein and the accumulation covalent modifications with age would lead to destabilization of the native state of this isolated domain. These modifications have been found in a 9 kDa fragment consisting of the C-terminal domain of γD-Crys that accumulates with age and is found in the WS-HMW complexes and WI inclusions in older lenses (Srivastava 1988; Srivastava *et al.* 1992; Srivastava *et al.* 1996). Our results indicate that partial unfolding of this fragment and exposure of aggregation-prone regions would lead to aggregation in the lens. Our results showed that αB-Crys recognized exclusively the aggregation-prone species and suppressed its aggregation *in vitro.* Thus, in the lens α-Crys could sequester this fragment forming WS-HMW substrate-chaperone complexes in younger lenses. Depletion of free α-Crys would result in unhindered aggregation of these fragments that could recruit other destabilized fragments from different crystallin parent proteins.

CHAPTER 4:

CONCLUDING DISCUSSION

A. CONCLUDING REMARKS

α-Crystallin is the only protein quality control system present in the terminally differentiated lens fiber cells of the mature lens. These cells, lacking all major organelles, are unable to synthesize proteins. Thus the chaperone function of the lens α-crystallins does not involve folding nascent chains on the ribosome. Their properties of suppressing aggregation of partially folded proteins *in vitro*, and their accumulation together with damaged crystallins in cataracts, indicates that they protect the transparency of the lens by binding aggregation precursors. It has been difficult to determine how such aggregation precursors are generated in the protected environment of the lens, and how the α-crystallin chaperones recognize their substrates and maintain them in a bound state for very long times.

1. What factors in the lens are responsible for destabilization of the lens crystallins leading to their partial unfolding and subsequent irreversible aggregation into WI inclusion bodies?

The βγ-crystallins of the lens are very stable proteins with melting temperatures significantly higher than most metazoan proteins (T_M above 60 ºC at pH 7.0) (Bloemendal *et al.* 2004). Extensive studies on the determinants of protein stability for the γ-crystallins have shown that, along with the high thermodynamic stability of the native state, there is a high kinetic barrier to unfolding that further contributes to the stability of the native state (Mayr *et al.* 1997; Kosinski-Collins and King 2003; Kosinski-Collins *et al.* 2004; Flaugh *et al.* 2005a; Flaugh *et al.* 2005b; Mills *et al.* 2007). The partial unfolding of these very stable proteins under physiological conditions is thought to reflect distinctive stresses on these proteins during their long life-times.

Microdissection of aged normal lenses combined with 2-D difference gel electrophoresis and mass spectrometry experiments showed that covalent modifications to crystallin proteins begin to accumulate in the newly-differentiated fiber cells in cortical regions of the lens and the number of covalent modifications increases progressively as the cells migrate into the nuclear region of the lens (Asomugha *et al.* 2010). The most abundant covalent modifications included Gln/Asn deamidation and Trp/Met oxidation. Deamidation of Asn and Gln increases with age in aged normal and cataractous lenses (Hanson *et al.* 1998; Wilmarth *et al.* 2006; Asomugha *et al.* 2010). *In vitro* studies have shown, for example, that deamidation of key Gln domain interface residues in γD-Crys

reduced its thermodynamic and kinetic stability (Flaugh *et al.* 2006); deamidation of specific residues in αA- and αB-Crys reduced their chaperoning efficiency *in vitro* (Gupta and Srivastava 2004a; Gupta and Srivastava 2004b). Deamidation (e.g. Gln→Glu) introduces a negative charge at physiological pH due to the replacement of an amide group for a carboxyl group and may cause backbone isomerization (Shimizu *et al.* 2005). Deamidation could be due to spontaneous processes that occur at physiological conditions or could be catalyzed by transglutaminases that are present at low levels in the lens (in the case of Gln residues) (Bloemendal *et al.* 2004; Flaugh *et al.* 2006).

Tryptophan and Met oxidation was higher in crystallin proteins from cataractous lenses (Hains and Truscott 2007). Further, intra-chain disulphide linkages were also present predominantly in crystallin proteins in cataractous lenses (Takemoto 1996; Takemoto 1997; Hains and Truscott 2008) Insoluble inclusions from advanced cataractous lenses can only be fully solubilized in 8 M Urea plus a reducing agent (e.g. DTT) (Truscott and Augusteyn 1977). Several environmental factors have been associated with the onset of oxidative stress in mature lens fiber cells. High levels of glutathione in young lenses and low levels of O_2 in the lens fiber cells are protective mechanisms to reduce the formation of reactive oxygen species during oxidative stress (Eaton 1991). Levels of reduced glutathione decrease with age in the nuclear region in normal and cataractous lenses thus reducing the ability of the lens to prevent oxidative damage to the crystallin proteins (Truscott 2005).

UVA and UVB radiation can cause photolysis and oxidation of the buried Trp residues in the crystallins, resulting in partial denaturation. The constant, life-long exposure of the crystallin proteins in the nuclear region of the lens to UV-radiation could be one of the mechanisms responsible for photo-oxidation of the crystallin proteins (Truscott 2005). The factors directly responsible for oxidative damage and the mechanism whereby this damage occurs in the crystallin proteins remain to be identified.

2. The mechanism of chaperone recognition of aggregation precursors

The results presented in Chapter 2 and Chapter 3 of this thesis report features of the aggregation of partially folded γ-crystallins observed upon dilution out of high concentration of denaturant for human γD-, γC-, and γS-Crys. Due to the reversible nature of γ-crystallin unfolding and refolding under these conditions, the partially folded intermediates represent the same population as partially unfolded intermediates. Thus these *in vitro* aggregation reactions provide an *in vitro* model for processes that may occur in the lens. Within the lens the various forms of oxidative and photo-oxidative stress may be responsible for partial unfolding leading to aggregation or binding by α-crystallin chaperones.

The results presented in Chapter 2 show that all three γ-Crys proteins aggregated upon refolding out of high concentrations of denaturant under the same experimental conditions. In line with previous results reported by Kosinski-Collins and King (Kosinski-Collins and King 2003), these aggregates consisted of fibril-like smaller aggregates (Fig. 2-3). Further experiments with γD-Crys showed that the C-td of the protein had to be destabilized for aggregation to occur after dilution out of high concentrations of denaturant (Fig. 2-5). Results in Chapter 3 show that the isolated γD-Ctd aggregated during dilution out of high concentrations of denaturant, while the isolated γD-Ntd did not aggregate under similar conditions (Fig. 3-2). Increasing the final protein concentration of γD-Ntd isolated domain did not result in aggregation of the protein after dilution out of high concentrations of denaturant (Fig. 3-3B). Based on these observations, I propose that an aggregation-prone intermediate was populated early during refolding conditions and that this intermediate exposed an aggregation-prone region located in the C-td of γD-Crys. It seems likely that these aggregation-prone regions are exposed strands buried in the Greek key.

Once the protein partially unfolds, there are many intermolecular interactions that could lead to aggregation such as domain swapping or loop-sheet insertions. The occurrence of loop-sheet insertion mechanism in aggregation has been documented in the case of the serpins (serine protease inhibitors). Serpins fold to a metastable state composed of 3 β-sheets (A-C), 9 α-helices and one reactive center loop. Upon binding to their target protease, the protease cleaves the reactive loop covalently linking the serpin and protease and allowing the insertion of the reactive center loop strand into β-sheet A of the serpin. The Z allele in α_1-antitrypsin, a Glu→Lys mutation at position 342 at the base of the reactive center loop, causes accumulation of α_1-antitrypsin aggregates in the

ER of hepatocytes. This mutation facilitates the formation of an unstable intermediate where the reactive center loop is partially inserted into β-sheet A resulting in an opening of the sheet. The reactive loop from another α1-antitrypsin inserts into the open β-sheet A allowing polymerization and aggregation to ensue (Belorgey *et al.* 2007). This loop-sheet insertion mechanism of mutant serpins serves as one of the paradigms for aggregation of β-sheet proteins.

A possible mechanism for γ-Crys aggregate formation could involve a loop-sheet insertion mechanism akin to the mechanism described above. As described in Chapter 1, the tertiary structure of a single domain of γ-crystallins consists of an anti-parallel β-sandwich formed by the intercalation of the two Greek key motifs (Fig. 1-5). Thus, the primary sequence of the γ-Crys has a propensity for β-strand formation. Early aggregation-prone intermediates could interact by swapping β-strands to form extended β-sheets similar to strand swapping observed between Greek key motifs in the native state of the protein.

3. What is the nature of the stable binding of partially folded γ-crystallins by the α-crystallin chaperone?

Experiments where the αB-Crys chaperone was added 0-10 s after the refolding and aggregation of γD-Crys were initiated showed that αB-Crys chaperone recognized an aggregation-prone intermediate populated within the time-span of the refolding of the C-terminal domain (Fig. 2-10). In addition, competition experiments with the isolated γD-Ntd and γD-Ctd domains as substrates showed that αB-Crys chaperone preferentially interacted with the γD-Ctd under conditions where both single domains co-aggregated (Fig. 3-9). In these experiments, αB-Crys chaperone almost completely suppressed aggregation as measured by changes in $O.D._{350\ nm}$. These results lent support to the model described above in which an aggregation-prone region in the C-td was exposed during dilution out of high concentrations of denaturant. In the presence of αB-Crys chaperone, αB-Crys recognized and bound this region suppressing aggregation. These results are consistent with previously published observations demonstrating that α-Crys specifically recognized and interacted with aggregation-prone species of non-physiological substrates (Carver *et al.* 1995; Rajaraman *et al.* 1998).

SEC chromatograms and TEM images showed that αB-Crys formed large, spherical substrate-chaperone complexes with aggregation-prone species of full-length γD-Crys and the isolated γD-Ctd domain (Figures 2-4A, 3-5A and B). These complexes were significantly larger than the free αB-Crys homo-oligomers; the diameter for the substrate-chaperone complexes was ~80 nm, vs. ~13 nm for free αB-Crys oligomers. Similar structural changes have been documented for substrate-chaperone complexes formed by other sHsps (Ehrnsperger *et al.* 1997; Haslbeck *et al.* 1999b). Interestingly, similar complexes, as judged by SEC elution profiles, formed upon heating of bovine lens homogenates containing α-Crys and were absent in homogenates where α-Crys was absent (Rao *et al.* 1995). Heys *et al.* have also documented the age-dependent increase of non-covalent HMW complexes in the WS fraction of the nuclear lens. Therefore, the substrate-chaperone complexes formed during the suppression assays reported here could resemble complexes formed *in vivo.*

A previous study showed that T4 lysozyme had a defined orientation when bound to the αB-Crys chaperone indicating that the substrate binding sites on the chaperone recognized a specific region in T4 lysozyme (Claxton *et al.* 2008). Results reported in Chapter 2 using double- and triple-Trp mutants of γD-Crys as substrates show that a similar recognition mechanism took place during the polymerization of aggregation-prone species of γD-Crys. The regions surrounding the Trp-pairs from each domain were occluded from solvent in non-native conformations in the substrate-chaperone complexes (Fig. 2-7). Further, the regions surrounding Trp42 and Trp130 were also occluded from solvent in non-native conformations (Fig. 2-8).

Synthesizing these results with results described above for the single domains lead to the following model for interactions between αB-Crys and γ-Crys: an aggregation-prone region, likely located in Motif 4 and including both Trp residues, is exposed in off-pathway aggregation-prone intermediates of γD-Crys; αB-Crys chaperone initially recognizes and binds this β-strand region; further growth of the substrate-chaperone complex results in the binding of the homologous β-strand region in motif 2 in the N-terminal domain of γD-Crys. The stability of the complex is thus achieved by the multiple binding interactions between substrate and chaperone. The multiplicity of binding interaction regions between substrate and chaperone has been implicated in the stability of morphologically similar substrate-chaperone complexes formed by other sHsps (Cheng *et al.* 2008). Ghosh *et al.* have shown that several regions in the α-crystallin domain of αB-Crys interacted with β_H-Crys during heat-induced aggregation (Ghosh *et al.* 2005).

A β-strand consisting of the aggregation-region could interact with the shared groove at the dimer interface formed by partner α-crystallin domains in the chaperone, while other regions in γD-Crys could interact with binding sites in the N-terminal domain of αB-Crys. Such a loop-sheet insertion exchange could account for the formation of stable, long-lived complexes such as the aggregates formed by serpins.

The physiological pertinence of this model is highlighted by results described in Chapter 3 that investigated the factors responsible for aggregation of the full-length protein focusing on γD-Ntd and γD-Ctd single domains. As mentioned previously, a 9 kDa fragment consisting of a C-terminally truncated and oxidatively modified C-td of γD-Crys was isolated from aged normal and cataractous human lenses (Srivastava *et al.* 1992). The abundance of this fragment increases with age and *in vitro* experiments showed that this fragment forms inter-molecular, non-disulfide, covalent cross-links that were also isolated from cataractous lenses (Srivastava and Srivastava 2003). Therefore, covalent damage to this fragment could result in the partial unfolding of the protein leading to the population of partially folded intermediates where the aggregation-prone region would be solvent-exposed. Aggregation of this fragment in the lens would result in cataract formation.

4. Chaperone saturation may determine the onset of mature cataracts

The levels of free soluble α-Crys in the nuclear region of the lens decrease with age in human lenses until reaching negligible levels in individuals at the age of 50 [Fig. 1-11B and (Heys *et al.* 2007)]. Concomitantly, an increase in the protein content of the WI fraction of the nuclear region of the lens begins after the age of 50 (Heys *et al.* 2007). The results from the studies reported here imply that α-crystallin forms very long lived complexes, and does not recycle. These results, along with observations from αA- and αB-Crys knockout models in zebrafish and mice, demonstrate that the onset of age-related nuclear cataract disease is correlated with the absence of free active α-Crys chaperone in the mature fiber cells of the lens (Brady *et al.* 1997a; Boyle *et al.* 2003; Goishi *et al.* 2006). It may well be that from youth to middle age, the high concentration of α-crystallin in the lens is sufficient for suppressing the aggregation of damaged or partially unfolded γ-crystallins. However, in the absence of new synthesis, the α-crystallin pool may eventually become saturated, at which point further damage to the γ-crystallins results in aggregation and cataract formation.

CHAPTER 5: REFERENCES

Abraham, A. G., N. G. Condon and E. West Gower (2006) The new epidemiology of cataract. *Ophthalmol Clin North Am*. **19**, 415-25.

Acosta-Sampson, L. and J. King (2010) Partially Folded Aggregation Intermediates of Human gammaD-, gammaC-, and gammaS-Crystallin Are Recognized and Bound by Human alphaB-Crystallin Chaperone. *J Mol Biol*. **401**, 134-152.

Aguzzi, A. and T. O'Connor (2010) Protein aggregation diseases: pathogenicity and therapeutic perspectives. *Nat Rev Drug Discov*. **9**, 237-48.

Allen, S. P., J. O. Polazzi, J. K. Gierse and A. M. Easton (1992) Two novel heat shock genes encoding proteins produced in response to heterologous protein expression in Escherichia coli. *J Bacteriol*. **174**, 6938-47.

Andley, U. P. (2007) Crystallins in the eye: Function and pathology. *Progress in Retinal and Eye Research*. **26**, 78-98.

Andley, U. P., S. Mathur, T. A. Griest and J. M. Petrash (1996) Cloning, expression, and chaperone-like activity of human alphaA-crystallin. *J Biol Chem*. **271**, 31973-80.

Andley, U. P. and M. A. Reilly (2010) In vivo lens deficiency of the R49C alphaA-crystallin mutant. *Exp Eye Res*. **90**, 699-702.

Aquilina, J. A., J. L. Benesch, O. A. Bateman, C. Slingsby and C. V. Robinson (2003) Polydispersity of a mammalian chaperone: mass spectrometry reveals the population of oligomers in alphaB-crystallin. *Proc Natl Acad Sci U S A*. **100**, 10611-6.

Arrasate, M., S. Mitra, E. S. Schweitzer, M. R. Segal and S. Finkbeiner (2004) Inclusion body formation reduces levels of mutant huntingtin and the risk of neuronal death. *Nature*. **431**, 805-10.

Asomugha, C. O., R. Gupta and O. P. Srivastava (2010) Identification of crystallin modifications in the human lens cortex and nucleus using laser capture microdissection and CyDye labeling. *Mol Vis*. **16**, 476-94.

Augusteyn, R. C. (2004) Dissociation is not required for alpha-crystallin's chaperone function. *Exp Eye Res*. **79**, 781-4.

Augusteyn, R. C. (2008) Growth of the lens: in vitro observations. *Clin Exp Optom*. **91**, 226-39.

Augusteyn, R. C. and J. F. Koretz (1987) A possible structure for [alpha]-crystallin. *FEBS letters*. **222**, 1-5.

Awasthi, N., S. Guo and B. J. Wagner (2009) Posterior capsular opacification: a problem reduced but not yet eradicated. *Arch Ophthalmol*. **127**, 555-62.

Baden, E. M., L. A. Sikkink and M. Ramirez-Alvarado (2009) Light chain amyloidosis - current findings and future prospects. *Curr Protein Pept Sci*. **10**, 500-8.

Bagby, S., S. Go, S. Inouye, M. Ikura and A. Chakrabartty (1998) Equilibrium folding intermediates of a Greek key beta-barrel protein. *J Mol Biol*. **276**, 669-81.

Bagneris, C., O. A. Bateman, C. E. Naylor, N. Cronin, W. C. Boelens, N. H. Keep and C. Slingsby (2009a) Crystal structures of alpha-crystallin domain dimers of alphaB-crystallin and Hsp20. *J Mol Biol*. **392**, 1242-52.

Bagneris, C., O. A. Bateman, C. E. Naylor, N. Cronin, W. C. Boelens, N. H. Keep and C. Slingsby (2009b) Crystal Structures of alpha-Crystallin Domain Dimers of alphaB-Crystallin and Hsp20. *J Mol Biol*.

Banh, A., V. Bantseev, V. Choh, K. L. Moran and J. G. Sivak (2006) The lens of the eye as a focusing device and its response to stress. *Prog Retin Eye Res*. **25**, 189-206.

Barral, J. M., S. A. Broadley, G. Schaffar and F. U. Hartl (2004) Roles of molecular chaperones in protein misfolding diseases. *Semin Cell Dev Biol*. **15**, 17-29.

Basak, A., O. Bateman, C. Slingsby, A. Pande, N. Asherie, O. Ogun, G. B. Benedek and J. Pande (2003) High-resolution X-ray crystal structures of human gammaD crystallin (1.25 A) and the R58H mutant (1.15 A) associated with aculeiform cataract. *J Mol Biol*. **328**, 1137-47.

Basha, E., K. L. Friedrich and E. Vierling (2006) The N-terminal Arm of Small Heat Shock Proteins Is Important for Both Chaperone Activity and Substrate Specificity. *Journal of Biological Chemistry*. **281**, 39943-39952.

Basha, E., C. Jones, V. Wysocki and E. Vierling (2010) Mechanistic differences between two conserved classes of small heat shock proteins found in the plant cytosol. *J Biol Chem*. **285**, 11489-97.

Bassnett, S. (2002) Lens organelle degradation. *Exp Eye Res*. **74**, 1-6.

Bassnett, S. (2009) On the mechanism of organelle degradation in the vertebrate lens. *Exp Eye Res*. **88**, 133-9.

Belorgey, D., P. Hagglof, S. Karlsson-Li and D. A. Lomas (2007) Protein misfolding and the serpinopathies. *Prion*. **1**, 15-20.

Benedek, G. B., L. T. Chylack, Jr., T. Libondi, P. Magnante and M. Pennett (1987) Quantitative detection of the molecular changes associated with early cataractogenesis in the living human lens using quasielastic light scattering. *Curr Eye Res*. **6**, 1421-32.

Benesch, J. L. P., M. Ayoub, C. V. Robinson and J. A. Aquilina (2008) Small Heat Shock Protein Activity Is Regulated by Variable Oligomeric Substructure. *Journal of Biological Chemistry*. **283**, 28513-28517.

Biswas, A. and K. P. Das (2004) Role of ATP on the interaction of alpha-crystallin with its substrates and its implications for the molecular chaperone function. *J Biol Chem*. **279**, 42648-57.

Bloemendal, H., W. de Jong, R. Jaenicke, N. H. Lubsen, C. Slingsby and A. Tardieu (2004) Ageing and vision: structure, stability and function of lens crystallins. *Prog Biophys Mol Biol*. **86**, 407-85.

Bloemendal, H. and W. W. de Jong (1991) Lens proteins and their genes. *Prog Nucleic Acid Res Mol Biol*. **41**, 259-81.

Bova, M. P., L. L. Ding, J. Horwitz and B. K. Fung (1997) Subunit exchange of alphaA-crystallin. *J Biol Chem*. **272**, 29511-7.

Bova, M. P., H. S. McHaourab, Y. Han and B. K. Fung (2000) Subunit exchange of small heat shock proteins. Analysis of oligomer formation of alphaA-crystallin and Hsp27 by fluorescence resonance energy transfer and site-directed truncations. *J Biol Chem*. **275**, 1035-42.

Bova, M. P., O. Yaron, Q. Huang, L. Ding, D. A. Haley, P. L. Stewart and J. Horwitz (1999) Mutation R120G in alphaB-crystallin, which is linked to a desmin-related myopathy, results in an irregular structure and defective chaperone-like function. *Proceedings of the National Academy of Sciences of the United States of America*. **96**, 6137-6142.

Boyle, D., L. Takemoto, J. Brady and E. Wawrousek (2003) Morphological characterization of the AlphaA- and AlphaB-crystallin double knockout mouse lens. *BMC Ophthalmology*. **3**, 3.

Brady, J., D. Garland, Y. Duglas-Tabor, W. Robison, A. Groome and E. Wawrousek (1997a) Targeted disruption of the mouse alphaA-crystallin gene induces cataract and cytoplasmic inclusion bodies containing the small heat shock protein alphaB-crystallin. *Proc Natl Acad Sci USA*. **94**, 884 - 889.

Brady, J. P., D. Garland, Y. Duglas-Tabor, W. G. Robison, Jr., A. Groome and E. F. Wawrousek (1997b) Targeted disruption of the mouse alpha A-crystallin gene induces cataract and cytoplasmic inclusion bodies containing the small heat shock protein alpha B-crystallin. *Proc Natl Acad Sci U S A*. **94**, 884-9.

Brady, J. P., D. L. Garland, D. E. Green, E. R. Tamm, F. J. Giblin and E. F. Wawrousek (2001) AlphaB-crystallin in lens development and muscle integrity: a gene knockout approach. *Invest Ophthalmol Vis Sci*. **42**, 2924-34.

Brandt, F., S. A. Etchells, J. O. Ortiz, A. H. Elcock, F. U. Hartl and W. Baumeister (2009) The native 3D organization of bacterial polysomes. *Cell*. **136**, 261-71.

Breitman, M. L., S. Lok, G. Wistow, J. Piatigorsky, J. A. Treton, R. J. Gold and L. C. Tsui (1984) Gamma-crystallin family of the mouse lens: structural and evolutionary relationships. *Proc Natl Acad Sci U S A*. **81**, 7762-6.

Brian, G. and H. Taylor (2001) Cataract blindness--challenges for the 21st century. *Bull World Health Organ*. **79**, 249-56.

Carter, J. M., A. M. Hutcheson and R. A. Quinlan (1995) In vitro studies on the assembly properties of the lens proteins CP49, CP115: coassembly with alpha-crystallin but not with vimentin. *Exp Eye Res*. **60**, 181-92.

Carver, J. A., N. Guerreiro, K. A. Nicholls and R. J. Truscott (1995) On the interaction of alpha-crystallin with unfolded proteins. *Biochim Biophys Acta*. **1252**, 251-60.

Carver, J. A., R. A. Lindner, C. Lyon, D. Canet, H. Hernandez, C. M. Dobson and C. Redfield (2002) The interaction of the molecular chaperone alpha-crystallin with unfolding alpha-lactalbumin: a structural and kinetic spectroscopic study. *J Mol Biol*. **318**, 815-27.

Chang, Z., T. P. Primm, J. Jakana, I. H. Lee, I. Serysheva, W. Chiu, H. F. Gilbert and F. A. Quiocho (1996) Mycobacterium tuberculosis 16-kDa Antigen (Hsp16.3) Functions as an Oligomeric Structure in Vitro to Suppress Thermal Aggregation. *Journal of Biological Chemistry*. **271**, 7218-7223.

Charles, S. (2001) Vitreoretinal complications of YAG laser capsulotomy. *Ophthalmol Clin North Am*. **14**, 705-10.

Chaudhuri, T. K. and S. Paul (2006) Protein-misfolding diseases and chaperone-based therapeutic approaches. *FEBS J*. **273**, 1331-49.

Chen, J., P. R. Callis and J. King (2009) Mechanism of the very efficient quenching of tryptophan fluorescence in human gamma D- and gamma S-crystallins: the gamma-crystallin fold may have evolved to protect tryptophan residues from ultraviolet photodamage. *Biochemistry*. **48**, 3708-16.

Chen, J., S. L. Flaugh, P. R. Callis and J. King (2006) Mechanism of the highly efficient quenching of tryptophan fluorescence in human gammaD-crystallin. *Biochemistry*. **45**, 11552-63.

Chen, J., D. Toptygin, L. Brand and J. King (2008) Mechanism of the efficient tryptophan fluorescence quenching in human gammaD-crystallin studied by time-resolved fluorescence. *Biochemistry*. **47**, 10705-21.

Cheng, G., E. Basha, V. H. Wysocki and E. Vierling (2008) Insights into Small Heat Shock Protein and Substrate Structure during Chaperone Action Derived from Hydrogen/Deuterium Exchange and Mass Spectrometry. *Journal of Biological Chemistry*. **283**, 26634-26642.

Chiti, F. and C. M. Dobson (2006) Protein misfolding, functional amyloid, and human disease. *Annu Rev Biochem*. **75**, 333-66.

Clark, R., S. Zigman and S. Lerman (1969) Studies on the structural proteins of the human lens. *Exp Eye Res*. **8**, 172-82.

Claxton, D. P., P. Zou and H. S. McHaourab (2008) Structure and Orientation of T4 Lysozyme Bound to the Small Heat Shock Protein [alpha]-Crystallin. *Journal of Molecular Biology*. **375**, 1026-1039.

Cohen, E., J. Bieschke, R. M. Perciavalle, J. W. Kelly and A. Dillin (2006) Opposing activities protect against age-onset proteotoxicity. *Science*. **313**, 1604-10.

Congdon, N., J. R. Vingerling, B. E. Klein, S. West, D. S. Friedman, J. Kempen, B. O'Colmain, S. Y. Wu and H. R. Taylor (2004) Prevalence of cataract and pseudophakia/aphakia among adults in the United States. *Arch Ophthalmol*. **122**, 487-94.

Crombie, T., J. C. Swaffield and A. J. Brown (1992) Protein folding within the cell is influenced by controlled rates of polypeptide elongation. *J Mol Biol*. **228**, 7-12.

Cvekl, A. and M. K. Duncan (2007) Genetic and epigenetic mechanisms of gene regulation during lens development. *Prog Retin Eye Res*. **26**, 555-97.

D'Alessio, G. (2002) The evolution of monomeric and oligomeric betagamma-type crystallins. Facts and hypotheses. *Eur J Biochem*. **269**, 3122-30.

Das, P., J. A. King and R. Zhou (2010) beta-strand interactions at the domain interface critical for the stability of human lens gammaD-crystallin. *Protein Science*. **19**, 131-140.

de Groot, N. S., A. EspargarÃ³, M. Morell and S. Ventura (2008) Studies on bacterial inclusion bodies. *Future Microbiology*. **3**, 423-435.

de Jong, W. W., J. A. Leunissen and C. E. Voorter (1993) Evolution of the alpha-crystallin/small heat-shock protein family. *Mol Biol Evol*. **10**, 103-26.

Delaye, M. and A. Tardieu (1983) Short-range order of crystallin proteins accounts for eye lens transparency. *Nature*. **302**, 415-7.

Dierks, K., M. Dieckmann, D. Niederstrasser, R. Schwartz and A. Wegener (1998) Protein size resolution in human eye lenses by dynamic light scattering after in vivo measurements. *Graefes Arch Clin Exp Ophthalmol*. **236**, 18-23.

Dimcheff, D. E., M. A. Faasse, F. J. McAtee and J. L. Portis (2004) Endoplasmic reticulum (ER) stress induced by a neurovirulent mouse retrovirus is associated with prolonged BiP binding and retention of a viral protein in the ER. *J Biol Chem*. **279**, 33782-90.

Djabali, K., B. de Nechaud, F. Landon and M. Portier (1997) AlphaB-crystallin interacts with intermediate filaments in response to stress. *J Cell Sci*. **110**, 2759-2769.

Dobson, C. M. (2004) Principles of protein folding, misfolding and aggregation. *Seminars in Cell & Developmental Biology*. **15**, 3-16.

Eaton, J. W. (1991) Is the lens canned? *Free Radical Biology and Medicine*. **11**, 207-213.

Echeverria, P. C. and D. Picard (2010) Molecular chaperones, essential partners of steroid hormone receptors for activity and mobility. *Biochim Biophys Acta*. **1803**, 641-9.

Ecroyd, H. and J. A. Carver (2008) Unraveling the mysteries of protein folding and misfolding. *IUBMB Life*. **60**, 769-74.

Ehrnsperger, M., S. Graber, M. Gaestel and J. Buchner (1997) Binding of non-native protein to Hsp25 during heat shock creates a reservoir of folding intermediates for reactivation. *EMBO J*. **16**, 221-9.

Eifert, C., M. R. Burgio, P. M. Bennett, J. C. Salerno and J. F. Koretz (2005) N-terminal control of small heat shock protein oligomerization: changes in aggregate size and chaperone-like function. *Biochim Biophys Acta*. **1748**, 146-56.

Endo, T. and K. Yamano (2009) Multiple pathways for mitochondrial protein traffic. *Biol Chem*. **390**, 723-30.

Erjavec, N., L. Larsson, J. Grantham and T. Nystrom (2007) Accelerated aging and failure to segregate damaged proteins in Sir2 mutants can be suppressed by overproducing the protein aggregation-remodeling factor Hsp104p. *Genes Dev*. **21**, 2410-21.

Evans, P., C. Slingsby and B. A. Wallace (2008) Association of partially folded lens betaB2-crystallins with the alpha-crystallin molecular chaperone. *Biochem J*. **409**, 691-9.

Farnsworth, P. N., B. Groth-Vasselli, N. J. Greenfield and K. Singh (1997) Effects of temperature and concentration on bovine lens alpha-crystallin secondary structure: a circular dichroism spectroscopic study. *Int J Biol Macromol*. **20**, 283-91.

Feil, I. K., M. Malfois, J. Hendle, H. van der Zandt and D. I. Svergun (2001) A Novel Quaternary Structure of the Dimeric alpha-Crystallin Domain with Chaperone-like Activity. *Journal of Biological Chemistry*. **276**, 12024-12029.

Ferbitz, L., T. Maier, H. Patzelt, B. Bukau, E. Deuerling and N. Ban (2004) Trigger factor in complex with the ribosome forms a molecular cradle for nascent proteins. *Nature*. **431**, 590-6.

Flaugh, S. L., M. S. Kosinski-Collins and J. King (2005a) Contributions of hydrophobic domain interface interactions to the folding and stability of human gammaD-crystallin. *Protein Sci*. **14**, 569-81.

Flaugh, S. L., M. S. Kosinski-Collins and J. King (2005b) Interdomain side-chain interactions in human gammaD crystallin influencing folding and stability. *Protein Sci*. **14**, 2030-43.

Flaugh, S. L., I. A. Mills and J. King (2006) Glutamine deamidation destabilizes human gammaD-crystallin and lowers the kinetic barrier to unfolding. *J Biol Chem*. **281**, 30782-93.

Franzmann, T. M., M. Wuhr, K. Richter, S. Walter and J. Buchner (2005) The activation mechanism of Hsp26 does not require dissociation of the oligomer. *J Mol Biol*. **350**, 1083-93.

Frick, K. D., E. W. Gower, J. H. Kempen and J. L. Wolff (2007) Economic Impact of Visual Impairment and Blindness in the United States. *Arch Ophthalmol*. **125**, 544-550.

Fu, L. and J. J. Liang (2002) Unfolding of human lens recombinant betaB2- and gammaC-crystallins. *J Struct Biol*. **139**, 191-8.

Fu, X., H. Zhang, X. Zhang, Y. Cao, W. Jiao, C. Liu, Y. Song, A. Abulimiti and Z. Chang (2005) A dual role for the N-terminal region of Mycobacterium tuberculosis Hsp16.3 in self-oligomerization and binding denaturing substrate proteins. *J Biol Chem*. **280**, 6337-48.

Fujiwara, H., M. Hasegawa, N. Dohmae, A. Kawashima, E. Masliah, M. S. Goldberg, J. Shen, K. Takio and T. Iwatsubo (2002) alpha-Synuclein is phosphorylated in synucleinopathy lesions. *Nat Cell Biol*. **4**, 160-4.

Georgopoulos, C. P. and B. Hohn (1978) Identification of a host protein necessary for bacteriophage morphogenesis (the groE gene product). *Proc Natl Acad Sci U S A*. **75**, 131-5.

Ghosh, J. G. and J. I. Clark (2005) Insights into the domains required for dimerization and assembly of human alphaB crystallin. *Protein Sci*. **14**, 684-95.

Ghosh, J. G., M. R. Estrada and J. I. Clark (2005) Interactive domains for chaperone activity in the small heat shock protein, human alphaB crystallin. *Biochemistry*. **44**, 14854-69.

Gilbert, S. F. (2006) *Developmental biology*, Sinauer Associates, Sunderland, Mass.

Glover, J. R. and S. Lindquist (1998) Hsp104, Hsp70, and Hsp40: a novel chaperone system that rescues previously aggregated proteins. *Cell*. **94**, 73-82.

Goishi, K., A. Shimizu, G. Najarro, S. Watanabe, R. Rogers, L. I. Zon and M. Klagsbrun (2006) AlphaA-crystallin expression prevents gamma-crystallin insolubility and cataract formation in the zebrafish cloche mutant lens. *Development*. **133**, 2585-93.

Graw, J. (2004) Congenital hereditary cataracts. *Int J Dev Biol*. **48**, 1031-44.

Graw, J. (2009) Genetics of crystallins: cataract and beyond. *Exp Eye Res*. **88**, 173-89.

Graw, J., J. Loster, D. Soewarto, H. Fuchs, B. Meyer, A. Reis, E. Wolf, R. Balling and M. Hrabe de Angelis (2001) Characterization of a new, dominant V124E mutation in the mouse alphaA-crystallin-encoding gene. *Invest Ophthalmol Vis Sci*. **42**, 2909-15.

Gupta, R. and O. P. Srivastava (2004a) Deamidation Affects Structural and Functional Properties of Human alphaA-Crystallin and Its Oligomerization with alphaB-Crystallin. *Journal of Biological Chemistry*. **279**, 44258-44269.

Gupta, R. and O. P. Srivastava (2004b) Effect of deamidation of asparagine 146 on functional and structural properties of human lens alphaB-crystallin. *Invest Ophthalmol Vis Sci*. **45**, 206-14.

Hains, P. G. and R. J. Truscott (2007) Post-translational modifications in the nuclear region of young, aged, and cataract human lenses. *J Proteome Res*. **6**, 3935-43.

Hains, P. G. and R. J. Truscott (2008) Proteomic analysis of the oxidation of cysteine residues in human age-related nuclear cataract lenses. *Biochim Biophys Acta*. **1784**, 1959-64.

Hanson, S. R., A. Hasan, D. L. Smith and J. B. Smith (2000) The major in vivo modifications of the human water-insoluble lens crystallins are disulfide bonds, deamidation, methionine oxidation and backbone cleavage. *Exp Eye Res*. **71**, 195-207.

Hanson, S. R., D. L. Smith and J. B. Smith (1998) Deamidation and disulfide bonding in human lens gamma-crystallins. *Exp Eye Res*. **67**, 301-12.

Harrington, V., S. McCall, S. Huynh, K. Srivastava and O. P. Srivastava (2004) Crystallins in water soluble-high molecular weight protein fractions and water insoluble protein fractions in aging and cataractous human lenses. *Mol Vis*. **10**, 476-89.

Harrington, V., O. P. Srivastava and M. Kirk (2007) Proteomic analysis of water insoluble proteins from normal and cataractous human lenses. *Mol Vis*. **13**, 1680-94.

Hartl, F. U. and M. Hayer-Hartl (2002) Molecular Chaperones in the Cytosol: from Nascent Chain to Folded Protein. *Science*. **295**, 1852-1858.

Hartl, F. U. and M. Hayer-Hartl (2009) Converging concepts of protein folding in vitro and in vivo. *Nat Struct Mol Biol*. **16**, 574-81.

Haslbeck, M., T. Franzmann, D. Weinfurtner and J. Buchner (2005) Some like it hot: the structure and function of small heat-shock proteins. *Nat Struct Mol Biol*. **12**, 842-6.

Haslbeck, M., A. Ignatiou, H. Saibil, S. Helmich, E. Frenzl, T. Stromer and J. Buchner (2004) A domain in the N-terminal part of Hsp26 is essential for chaperone function and oligomerization. *J Mol Biol*. **343**, 445-55.

Haslbeck, M., S. Walke, T. Stromer, M. Ehrnsperger, H. E. White, S. Chen, H. R. Saibil and J. Buchner (1999a) Hsp26: a temperature-regulated chaperone. *EMBO J*. **18**, 6744-51.

Haslbeck, M., S. Walke, T. Stromer, M. Ehrnsperger, H. E. White, S. Chen, H. R. Saibil and J. Buchner (1999b) Hsp26: a temperature-regulated chaperone. *EMBO J*. **18**, 6744-6751.

Hassane, S. M., M. S. Kumar and A. K. Hanane (2007) Specificity of alphaA-crystallin binding to destabilized mutants of betaB1-crystallin. *FEBS letters*. **581**, 1939-1943.

Hejtmancik, J. F. (2008) Congenital cataracts and their molecular genetics. *Semin Cell Dev Biol*. **19**, 134-49.

Helm, K. W., G. J. Lee and E. Vierling (1997) Expression and native structure of cytosolic class II small heat-shock proteins. *Plant Physiol*. **114**, 1477-85.

Hemmingsen, J. M., K. M. Gernert, J. S. Richardson and D. C. Richardson (1994) The tyrosine corner: a feature of most Greek key beta-barrel proteins. *Protein Sci*. **3**, 1927-37.

Heys, K. R., M. G. Friedrich and R. J. Truscott (2007) Presbyopia and heat: changes associated with aging of the human lens suggest a functional role for the small heat shock protein, alpha-crystallin, in maintaining lens flexibility. *Aging Cell*. **6**, 807-15.

Horwich, A. L., W. A. Fenton, E. Chapman and G. W. Farr (2007) Two families of chaperonin: physiology and mechanism. *Annu Rev Cell Dev Biol*. **23**, 115-45.

Horwitz, J. (1992) Alpha-crystallin can function as a molecular chaperone. *Proc Natl Acad Sci U S A*. **89**, 10449-53.

Horwitz, J. (1993) Proctor Lecture. The function of alpha-crystallin. *Invest Ophthalmol Vis Sci*. **34**, 10-22.

Horwitz, J., Q. L. Huang, L. Ding and M. P. Bova (1998) Lens alpha-crystallin: chaperone-like properties. *Methods Enzymol*. **290**, 365-83.

Huot, J., F. Houle, F. Marceau and J. Landry (1997) Oxidative stress-induced actin reorganization mediated by the p38 mitogen-activated protein kinase/heat shock protein 27 pathway in vascular endothelial cells. *Circ Res*. **80**, 383-92.

Ingolia, T. D. and E. A. Craig (1982) Four small Drosophila heat shock proteins are related to each other and to mammalian alpha-crystallin. *Proc Natl Acad Sci U S A*. **79**, 2360-4.

Ireland, M. and H. Maisel (1989) A family of lens fiber cell specific proteins. *Lens Eye Toxic Res*. **6**, 623-38.

Jacob, T. J. (1999) The relationship between cataract, cell swelling and volume regulation. *Prog Retin Eye Res*. **18**, 223-33.

Jaenicke, R. (1996) Stability and folding of ultrastable proteins: eye lens crystallins and enzymes from thermophiles. *Faseb J*. **10**, 84-92.

Jaenicke, R. and C. Slingsby (2001) Lens crystallins and their microbial homologs: structure, stability, and function. *Crit Rev Biochem Mol Biol*. **36**, 435-99.

Jakob, U., M. Gaestel, K. Engel and J. Buchner (1993) Small heat shock proteins are molecular chaperones. *Journal of Biological Chemistry*. **268**, 1517-1520.

Jaya, N., V. Garcia and E. Vierling (2009) Substrate binding site flexibility of the small heat shock protein molecular chaperones. *Proc Natl Acad Sci U S A*. **106**, 15604-9.

Jedziniak, J. A., J. H. Kinoshita, E. M. Yates and G. B. Benedek (1975) The concentration and localization of heavy molecular weight aggregates in aging normal and cataractous human lenses. *Exp Eye Res*. **20**, 367-9.

Jiao, W., P. Li, J. Zhang, H. Zhang and Z. Chang (2005a) Small heat-shock proteins function in the insoluble protein complex. *Biochem Biophys Res Commun*. **335**, 227-31.

Jiao, W., M. Qian, P. Li, L. Zhao and Z. Chang (2005b) The essential role of the flexible termini in the temperature-responsiveness of the oligomeric state and chaperone-like activity for the polydisperse small heat shock protein IbpB from Escherichia coli. *J Mol Biol*. **347**, 871-84.

Kaganovich, D., R. Kopito and J. Frydman (2008) Misfolded proteins partition between two distinct quality control compartments. *Nature*. **454**, 1088-1095.

Kelly, J. W. (1998) The alternative conformations of amyloidogenic proteins and their multi-step assembly pathways. *Curr Opin Struct Biol*. **8**, 101-6.

Kim, K. K., R. Kim and S. H. Kim (1998) Crystal structure of a small heat-shock protein. *Nature*. **394**, 595-9.

King, J. and U. K. Laemmli (1971) Polypeptides of the tail fibres of bacteriophage T4. *J Mol Biol*. **62**, 465-77.

Kirschner, M., S. Winkelhaus, J. M. Thierfelder and L. Nover (2000) Transient expression and heat-stress-inducedco-aggregation of endogenous and heterologous small heat-stress proteins in tobacco protoplasts. *The Plant Journal*. **24**, 397-412.

Koenig, S. H., C. F. Beaulieu, R. D. Brown, 3rd and M. Spiller (1990) Oligomerization and conformation change in solutions of calf lens gamma II-crystallin. Results from 1/T1 nuclear magnetic relaxation dispersion profiles. *Biophys J*. **57**, 461-9.

Kokke, B. P., M. R. Leroux, E. P. Candido, W. C. Boelens and W. W. de Jong (1998) Caenorhabditis elegans small heat-shock proteins Hsp12.2 and Hsp12.3 form tetramers and have no chaperone-like activity. *FEBS Lett*. **433**, 228-32.

Kosinski-Collins, M. S., S. L. Flaugh and J. King (2004) Probing folding and fluorescence quenching in human gammaD crystallin Greek key domains using triple tryptophan mutant proteins. *Protein Sci*. **13**, 2223-35.

Kosinski-Collins, M. S. and J. King (2003) In vitro unfolding, refolding, and polymerization of human gammaD crystallin, a protein involved in cataract formation. *Protein Sci*. **12**, 480-90.

Kosolapov, A. and C. Deutsch (2009) Tertiary interactions within the ribosomal exit tunnel. *Nat Struct Mol Biol*. **16**, 405-11.

Koteiche, H. A. and H. S. McHaourab (2003) Mechanism of chaperone function in small heat-shock proteins. Phosphorylation-induced activation of two-mode binding in alphaB-crystallin. *J Biol Chem*. **278**, 10361-7.

Kramer, G., D. Boehringer, N. Ban and B. Bukau (2009) The ribosome as a platform for co-translational processing, folding and targeting of newly synthesized proteins. *Nat Struct Mol Biol*. **16**, 589-97.

Krebs, M. R., L. A. Morozova-Roche, K. Daniel, C. V. Robinson and C. M. Dobson (2004) Observation of sequence specificity in the seeding of protein amyloid fibrils. *Protein Sci*. **13**, 1933-8.

Kundu, M., P. C. Sen and K. P. Das (2007) Structure, stability, and chaperone function of alphaA-crystallin: role of N-terminal region. *Biopolymers*. **86**, 177-92.

Kuwabara, T. (1975) The maturation of the lens cell: a morphologic study. *Exp Eye Res*. **20**, 427-43.

Laganowsky, A., J. L. Benesch, M. Landau, L. Ding, M. R. Sawaya, D. Cascio, Q. Huang, C. V. Robinson, J. Horwitz and D. Eisenberg (2010) Crystal structures of truncated alphaA and alphaB crystallins reveal structural mechanisms of polydispersity important for eye lens function. *Protein Sci*. **19**, 1031-43.

Lampi, K. J., K. K. Amyx, P. Ahmann and E. A. Steel (2006) Deamidation in human lens betaB2-crystallin destabilizes the dimer. *Biochemistry*. **45**, 3146-53.

Lampi, K. J., Z. Ma, S. R. Hanson, M. Azuma, M. Shih, T. R. Shearer, D. L. Smith, J. B. Smith and L. L. David (1998) Age-related changes in human lens crystallins identified by two-dimensional electrophoresis and mass spectrometry. *Exp Eye Res*. **67**, 31-43.

Lampi, K. J., Z. Ma, M. Shih, T. R. Shearer, J. B. Smith, D. L. Smith and L. L. David (1997) Sequence analysis of betaA3, betaB3, and betaA4 crystallins completes the identification of the major proteins in young human lens. *J Biol Chem*. **272**, 2268-75.

Langer, T., C. Lu, H. Echols, J. Flanagan, M. K. Hayer and F. U. Hartl (1992) Successive action of DnaK, DnaJ and GroEL along the pathway of chaperone-mediated protein folding. *Nature*. **356**, 683-9.

Lee, G. J., N. Pokala and E. Vierling (1995) Structure and in Vitro Molecular Chaperone Activity of Cytosolic Small Heat Shock Proteins from Pea. *Journal of Biological Chemistry*. **270**, 10432-10438.

Leroux, M. R., R. Melki, B. Gordon, G. Batelier and E. P. Candido (1997) Structure-function studies on small heat shock protein oligomeric assembly and interaction with unfolded polypeptides. *J Biol Chem*. **272**, 24646-56.

Li, J., X. Qian and B. Sha (2009) Heat shock protein 40: structural studies and their functional implications. *Protein Pept Lett*. **16**, 606-12.

Liang, J. J., T. X. Sun and N. J. Akhtar (1999) Spectral contribution of the individual tryptophan of alphaB-crystallin: a study by site-directed mutagenesis. *Protein Sci*. **8**, 2761-4.

Liberek, K., A. Lewandowska and S. Zietkiewicz (2008) Chaperones in control of protein disaggregation. *EMBO J*. **27**, 328-35.

Lindner, R. A., J. A. Carver, M. Ehrnsperger, J. Buchner, G. Esposito, J. Behlke, G. Lutsch, A. Kotlyarov and M. Gaestel (2000) Mouse Hsp25, a small heat shock protein. *European Journal of Biochemistry*. **267**, 1923-1932.

Lindner, R. A., A. Kapur and J. A. Carver (1997) The interaction of the molecular chaperone, alpha-crystallin, with molten globule states of bovine alpha-lactalbumin. *J Biol Chem*. **272**, 27722-9.

Litt, M., P. Kramer, D. M. LaMorticella, W. Murphey, E. W. Lovrien and R. G. Weleber (1998) Autosomal dominant congenital cataract associated with a missense mutation in the human alpha crystallin gene CRYAA. *Hum Mol Genet*. **7**, 471-4.

Liu, M., T. Ke, Z. Wang, Q. Yang, W. Chang, F. Jiang, Z. Tang, H. Li, X. Ren, X. Wang, T. Wang, Q. Li, J. Yang, J. Liu and Q. K. Wang (2006) Identification of a CRYAB Mutation Associated with Autosomal Dominant Posterior Polar Cataract in a Chinese Family. *Invest. Ophthalmol. Vis. Sci.* **47**, 3461-3466.

Lopez de la Paz, M., K. Goldie, J. Zurdo, E. Lacroix, C. M. Dobson, A. Hoenger and L. Serrano (2002) De novo designed peptide-based amyloid fibrils. *Proceedings of the National Academy of Sciences of the United States of America*. **99**, 16052-16057.

Lovicu, F. J. and M. L. Robinson (2004) *Development of the ocular lens*, Cambridge University Press, Cambridge, UK ; New York

Lu, J. and C. Deutsch (2008) Electrostatics in the ribosomal tunnel modulate chain elongation rates. *J Mol Biol*. **384**, 73-86.

Lubsen, N. H., H. J. Aarts and J. G. Schoenmakers (1988) The evolution of lenticular proteins: the beta- and gamma-crystallin super gene family. *Prog Biophys Mol Biol*. **51**, 47-76.

Ma, Z., S. R. Hanson, K. J. Lampi, L. L. David, D. L. Smith and J. B. Smith (1998) Age-related changes in human lens crystallins identified by HPLC and mass spectrometry. *Exp Eye Res*. **67**, 21-30.

MacDonald, J. T., A. G. Purkiss, M. A. Smith, P. Evans, J. M. Goodfellow and C. Slingsby (2005) Unfolding crystallins: the destabilizing role of a beta-hairpin cysteine in betaB2-crystallin by simulation and experiment. *Protein Sci*. **14**, 1282-92.

Maddala, R. and V. P. Rao (2005) alpha-Crystallin localizes to the leading edges of migrating lens epithelial cells. *Exp Cell Res*. **306**, 203-15.

Maisel, H. and M. M. Perry (1972) Electron microscope observations on some structural proteins of the chick lens. *Exp Eye Res*. **14**, 7-12.

Marsili, S., R. I. Salganik, C. D. Albright, C. D. Freel, S. Johnsen, R. L. Peiffer and M. J. Costello (2004) Cataract formation in a strain of rats selected for high oxidative stress. *Exp Eye Res*. **79**, 595-612.

Matuszewska, M., D. Kuczynska-Wisnik, E. Laskowska and K. Liberek (2005) The small heat shock protein IbpA of Escherichia coli cooperates with IbpB in stabilization of thermally aggregated proteins in a disaggregation competent state. *J Biol Chem*. **280**, 12292-8.

Mayr, E. M., R. Jaenicke and R. Glockshuber (1997) The domains in gammaB-crystallin: identical fold-different stabilities. *J Mol Biol*. **269**, 260-9.

McFall-Ngai, M. J., L. L. Ding, L. J. Takemoto and J. Horwitz (1985) Spatial and temporal mapping of the age-related changes in human lens crystallins. *Exp Eye Res*. **41**, 745-58.

McHaourab, H. S., E. K. Dodson and H. A. Koteiche (2002) Mechanism of chaperone function in small heat shock proteins. Two-mode binding of the excited states of T4 lysozyme mutants by alphaA-crystallin. *J Biol Chem*. **277**, 40557-66.

McHaourab, H. S., J. A. Godar and P. L. Stewart (2009) Structure and mechanism of protein stability sensors: chaperone activity of small heat shock proteins. *Biochemistry*. **48**, 3828-37.

Meakin, S. O., M. L. Breitman and L. C. Tsui (1985) Structural and evolutionary relationships among five members of the human gamma-crystallin gene family. *Mol Cell Biol*. **5**, 1408-14.

Merz, F., D. Boehringer, C. Schaffitzel, S. Preissler, A. Hoffmann, T. Maier, A. Rutkowska, J. Lozza, N. Ban, B. Bukau and E. Deuerling (2008) Molecular mechanism and structure of Trigger Factor bound to the translating ribosome. *EMBO J*. **27**, 1622-32.

Michael, R., J. van Marle, G. F. Vrensen and T. J. van den Berg (2003) Changes in the refractive index of lens fibre membranes during maturation--impact on lens transparency. *Exp Eye Res*. **77**, 93-9.

Michiel, M., F. Skouri-Panet, E. Duprat, S. Simon, C. Ferard, A. Tardieu and S. Finet (2008) Abnormal Assemblies and Subunit Exchange of alphaB-Crystallin R120 Mutants Could Be Associated with Destabilization of the Dimeric Substructure *Biochemistry*. **48**, 442-453.

Mills-Henry, I. A. R. (2007) Stability, unfolding, and aggregation of the gamma D and gamma S human eye lens crystallins. *Biology*, pp 219, Massachusetts Institute of Technology Cambridge, MA

Mills, I. A., S. L. Flaugh, M. S. Kosinski-Collins and J. A. King (2007) Folding and stability of the isolated Greek key domains of the long-lived human lens proteins gammaD-crystallin and gammaS-crystallin. *Protein Sci*. **16**, 2427-44.

Mitraki, A. a. K. J. A. (1989) Protein Folding Intermediates and Inclusion Body Formation. *Bio/Technology* **7**, 690-697.

Mizuno, H., S. Khurts, T. Seki, Y. Hirota, S. Kaneko and S. Murakami (2007) Human telomerase exists in two distinct active complexes in vivo. *J Biochem*. **141**, 641-52.

Moreau, K. L. and J. King (2009) Hydrophobic core mutations associated with cataract development in mice destabilize human gammaD-crystallin. *J Biol Chem*. **284**, 33285-95.

Morris, A. M., T. M. Treweek, J. A. Aquilina, J. A. Carver and M. J. Walker (2008) Glutamic acid residues in the C-terminal extension of small heat shock protein 25 are critical for structural and functional integrity. *FEBS J*. **275**, 5885-98.

Nagaraj, R. H., D. R. Sell, M. Prabhakaram, B. J. Ortwerth and V. M. Monnier (1991) High correlation between pentosidine protein crosslinks and pigmentation implicates ascorbate oxidation in human lens senescence and cataractogenesis. *Proc Natl Acad Sci U S A*. **88**, 10257-61.

Nakamoto, H. and L. Vigh (2007) The small heat shock proteins and their clients. *Cell Mol Life Sci*. **64**, 294-306.

Nakamoto, H. and L. Vígh (2007) The small heat shock proteins and their clients. *Cellular and Molecular Life Sciences*. **64**, 294-306.

Narberhaus, F. (2002) {alpha}-Crystallin-Type Heat Shock Proteins: Socializing Minichaperones in the Context of a Multichaperone Network. *Microbiol. Mol. Biol. Rev.* **66**, 64-93.

Oyster, C. W. (1999) *The human eye : structure and function*, Sinauer Associates, Sunderland, Mass.

Pace, C. N., F. Vajdos, L. Fee, G. Grimsley and T. Gray (1995) How to measure and predict the molar absorption coefficient of a protein. *Protein Sci*. **4**, 2411-23.

Pasta, S. Y., B. Raman, T. Ramakrishna and M. Rao Ch (2004) The IXI/V motif in the C-terminal extension of alpha-crystallins: alternative interactions and oligomeric assemblies. *Mol Vis*. **10**, 655-62.

Perrin, V., E. Regulier, T. Abbas-Terki, R. Hassig, E. Brouillet, P. Aebischer, R. Luthi-Carter and N. Deglon (2007) Neuroprotection by Hsp104 and Hsp27 in lentiviral-based rat models of Huntington's disease. *Mol Ther*. **15**, 903-11.

Peschek, J., N. Braun, T. M. Franzmann, Y. Georgalis, M. Haslbeck, S. Weinkauf and J. Buchner (2009) The eye lens chaperone alpha-crystallin forms defined globular assemblies. *Proc Natl Acad Sci U S A.* **106**, 13272-7.

Pilotto, A., N. Marziliano, M. Pasotti, M. Grasso, A. M. Costante and E. Arbustini (2006) [alpha]B-Crystallin mutation in dilated cardiomyopathies: Low prevalence in a consecutive series of 200 unrelated probands. *Biochemical and Biophysical Research Communications*. **346**, 1115-1117.

Plater, M. L., D. Goode and M. J. Crabbe (1996) Effects of site-directed mutations on the chaperone-like activity of alphaB-crystallin. *J Biol Chem*. **271**, 28558-66.

Ponce, A., C. Sorensen and L. Takemoto (2006) Role of short-range protein interactions in lens opacifications. *Mol Vis*. **12**, 879-84.

Ponce, A. and L. Takemoto (2005) Screening of crystallin-crystallin interactions using microequilibrium dialysis. *Mol Vis*. **11**, 752-7.

Preville, X., M. Gaestel and A. P. Arrigo (1998) Phosphorylation is not essential for protection of L929 cells by Hsp25 against H2O2-mediated disruption actin cytoskeleton, a protection which appears related to the redox change mediated by Hsp25. *Cell Stress Chaperones*. **3**, 177-87.

Purkiss, A. G., O. A. Bateman, J. M. Goodfellow, N. H. Lubsen and C. Slingsby (2002) The X-ray crystal structure of human gamma S-crystallin C-terminal domain. *J Biol Chem*. **277**, 4199-205.

Purkiss, A. G., O. A. Bateman, K. Wyatt, P. A. Wilmarth, L. L. David, G. J. Wistow and C. Slingsby (2007) Biophysical properties of gammaC-crystallin in human and mouse eye lens: the role of molecular dipoles. *J Mol Biol*. **372**, 205-22.

Putilina, T., F. Skouri-Panet, K. Prat, N. H. Lubsen and A. Tardieu (2003) Subunit exchange demonstrates a differential chaperone activity of calf alpha-crystallin toward beta LOW- and individual gamma-crystallins. *J Biol Chem*. **278**, 13747-56.

Rajaraman, K., B. Raman, T. Ramakrishna and C. M. Rao (1998) The Chaperone-like [alpha]-Crystallin Forms a Complex Only with the Aggregation-Prone Molten Globule State of [alpha]-Lactalbumin. *Biochemical and Biophysical Research Communications*. **249**, 917-921.

Raman, B., T. Ramakrishna and C. M. Rao (1995) Temperature dependent chaperone-like activity of alpha-crystallin. *FEBS Lett*. **365**, 133-6.

Rao, P. V., Q. L. Huang, J. Horwitz and J. S. Zigler, Jr. (1995) Evidence that alpha-crystallin prevents non-specific protein aggregation in the intact eye lens. *Biochim Biophys Acta*. **1245**, 439-47.

Reddy, G. B., K. P. Das, J. M. Petrash and W. K. Surewicz (2000) Temperature-dependent chaperone activity and structural properties of human alphaA- and alphaB-crystallins. *J Biol Chem*. **275**, 4565-70.

Reddy, G. B., P. A. Kumar and M. S. Kumar (2006) Chaperone-like activity and hydrophobicity of alpha-crystallin. *IUBMB Life*. **58**, 632-41.

Reddy, G. B., P. Y. Reddy, A. Vijayalakshmi, M. S. Kumar, P. Suryanarayana and B. Sesikeran (2002) Effect of long-term dietary manipulation on the aggregation of rat lens crystallins: role of alpha-crystallin chaperone function. *Mol Vis*. **8**, 298-305.

Reddy, M. A., O. A. Bateman, C. Chakarova, J. Ferris, V. Berry, E. Lomas, R. Sarra, M. A. Smith, A. T. Moore, S. S. Bhattacharya and C. Slingsby (2004) Characterization of the G91del CRYBA1/3-crystallin protein: a cause of human inherited cataract. *Hum Mol Genet*. **13**, 945-53.

Resnikoff, S., D. Pascolini, D. Etya'ale, I. Kocur, R. Pararajasegaram, G. P. Pokharel and S. P. Mariotti (2004) Global data on visual impairment in the year 2002. *Bull World Health Organ*. **82**, 844-51.

Robinson, N. E., K. J. Lampi, J. P. Speir, G. Kruppa, M. Easterling and A. B. Robinson (2006) Quantitative measurement of young human eye lens crystallins by direct injection Fourier transform ion cyclotron resonance mass spectrometry. *Mol Vis*. **12**, 704-11.

Rogalla, T., M. Ehrnsperger, X. Preville, A. Kotlyarov, G. Lutsch, C. Ducasse, C. Paul, M. Wieske, A. P. Arrigo, J. Buchner and M. Gaestel (1999) Regulation of Hsp27 oligomerization, chaperone function, and protective activity against oxidative stress/tumor necrosis factor alpha by phosphorylation. *J Biol Chem*. **274**, 18947-56.

Rousseau, F., J. Schymkowitz and L. Serrano (2006) Protein aggregation and amyloidosis: confusion of the kinds? *Curr Opin Struct Biol*. **16**, 118-26.

Roy, D. and A. Spector (1976a) Absence of low-molecular-weight alpha crystallin in nuclear region of old human lenses. *Proc Natl Acad Sci U S A*. **73**, 3484-7.

Roy, D. and A. Spector (1976b) High molecular weight protein from human lenses. *Exp Eye Res*. **22**, 273-9.

Saibil, H. R. (2008) Chaperone machines in action. *Curr Opin Struct Biol*. **18**, 35-42.

Santhoshkumar, P., P. Udupa, R. Murugesan and K. K. Sharma (2008) Significance of interactions of low molecular weight crystallin fragments in lens aging and cataract formation. *J Biol Chem*. **283**, 8477-85.

Sathish, H. A., H. A. Koteiche and H. S. McHaourab (2004) Binding of destabilized betaB2-crystallin mutants to alpha-crystallin: the role of a folding intermediate. *J Biol Chem*. **279**, 16425-32.

Sathish, H. A., R. A. Stein, G. Yang and H. S. McHaourab (2003) Mechanism of chaperone function in small heat-shock proteins. Fluorescence studies of the conformations of T4 lysozyme bound to alphaB-crystallin. *J Biol Chem*. **278**, 44214-21.

Saudou, F., S. Finkbeiner, D. Devys and M. E. Greenberg (1998) Huntingtin acts in the nucleus to induce apoptosis but death does not correlate with the formation of intranuclear inclusions. *Cell*. **95**, 55-66.

Schroder, H., T. Langer, F. U. Hartl and B. Bukau (1993) DnaK, DnaJ and GrpE form a cellular chaperone machinery capable of repairing heat-induced protein damage. *EMBO J*. **12**, 4137-44.

Serge, R., P. Donatella, E. a. Daniel, K. Ivo, P. Ramachandra, P. P. Gopal and P. M. Silvio (2004) Global data on visual impairment in the year 2002. *Bull World Health Organ*. **82**, 844-51.

Sharma, K. K., H. Kaur and K. Kester (1997) Functional elements in molecular chaperone alpha-crystallin: identification of binding sites in alpha B-crystallin. *Biochem Biophys Res Commun*. **239**, 217-22.

Sharma, K. K., G. S. Kumar, A. S. Murphy and K. Kester (1998) Identification of 1,1'-bi(4-anilino)naphthalene-5,5'-disulfonic acid binding sequences in alpha-crystallin. *J Biol Chem*. **273**, 15474-8.

Sharma, K. K. and P. Santhoshkumar (2009) Lens aging: Effects of crystallins. *Biochimica et Biophysica Acta (BBA) - General Subjects*. **1790**, 1095-1108.

Sharma, S. K., P. Christen and P. Goloubinoff (2009) Disaggregating chaperones: an unfolding story. *Curr Protein Pept Sci*. **10**, 432-46.

Shashidharamurthy, R., H. A. Koteiche, J. Dong and H. S. Mchaourab (2005) Mechanism of Chaperone Function in Small Heat Shock Proteins. *Journal of Biological Chemistry*. **280**, 5281-5289.

Shi, J., H. A. Koteiche, H. S. McHaourab and P. L. Stewart (2006) Cryoelectron microscopy and EPR analysis of engineered symmetric and polydisperse Hsp16.5 assemblies reveals determinants of polydispersity and substrate binding. *J Biol Chem*. **281**, 40420-8.

Shimizu, T., Y. Matsuoka and T. Shirasawa (2005) Biological significance of isoaspartate and its repair system. *Biol Pharm Bull*. **28**, 1590-6.

Sidera, K., M. Gaitanou, D. Stellas, R. Matsas and E. Patsavoudi (2008) A critical role for HSP90 in cancer cell invasion involves interaction with the extracellular domain of HER-2. *J Biol Chem*. **283**, 2031-41.

Siezen, R. J., J. A. Thomson, E. D. Kaplan and G. B. Benedek (1987) Human lens gamma-crystallins: isolation, identification, and characterization of the expressed gene products. *Proc Natl Acad Sci U S A*. **84**, 6088-92.

Simon, S., M. Michiel, F. Skouri-Panet, J. P. Lechaire, P. Vicart and A. Tardieu (2007) Residue R120 Is Essential for the Quaternary Structure and Functional Integrity of Human alphaB-Crystallin. *Biochemistry*. **46**, 9605-9614.

Slingsby, C. and N. J. Clout (1999) Structure of the crystallins. *Eye*. **13 (Pt 3b)**, 395-402.

Smulders, R., J. A. Carver, R. A. Lindner, M. A. van Boekel, H. Bloemendal and W. W. de Jong (1996) Immobilization of the C-terminal extension of bovine alphaA-crystallin reduces chaperone-like activity. *J Biol Chem*. **271**, 29060-6.

Somasundaram, T. and S. P. Bhat (2004) Developmentally Dictated Expression of Heat Shock Factors: Exclusive Expression of HSF4 in the Postnatal Lens and Its Specific Interaction with alphaB-crystallin Heat Shock Promoter. *Journal of Biological Chemistry*. **279**, 44497-44503.

Song, S., A. Landsbury, R. Dahm, Y. Liu, Q. Zhang and R. A. Quinlan (2009) Functions of the intermediate filament cytoskeleton in the eye lens. *J Clin Invest*. **119**, 1837-48.

Speed, M. A., D. I. Wang and J. King (1996) Specific aggregation of partially folded polypeptide chains: the molecular basis of inclusion body composition. *Nat Biotechnol*. **14**, 1283-7.

Spiess, C., A. S. Meyer, S. Reissmann and J. Frydman (2004) Mechanism of the eukaryotic chaperonin: protein folding in the chamber of secrets. *Trends in Cell Biology*. **14**, 598-604.

Srivastava, K., J. M. Chaves, O. P. Srivastava and M. Kirk (2008) Multi-crystallin complexes exist in the water-soluble high molecular weight protein fractions of aging normal and cataractous human lenses. *Exp Eye Res*. **87**, 356-66.

Srivastava, O. P. (1988) Age-related increase in concentration and aggregation of degraded polypeptides in human lenses. *Exp Eye Res*. **47**, 525-43.

Srivastava, O. P., J. E. McEntire and K. Srivastava (1992) Identification of a 9 kDa gamma-crystallin fragment in human lenses. *Exp Eye Res*. **54**, 893-901.

Srivastava, O. P. and K. Srivastava (2003) Crosslinking of human lens 9 kDa gammaD-crystallin fragment in vitro and in vivo. *Mol Vis*. **9**, 644-56.

Srivastava, O. P., K. Srivastava and C. Silney (1996) Levels of crystallin fragments and identification of their origin in water soluble high molecular weight (HMW) proteins of human lenses. *Curr Eye Res*. **15**, 511-20.

Steve, C. (2001) VITREORETINAL COMPLICATIONS OF YAG LASER CAPSULOTOMY. *Ophthalmology clinics of North America*. **14**, 705-710.

Stevens, A., S. X. Wang, G. H. Caines and T. Schleich (1995) 13C-NMR off-resonance rotating frame spin-lattice relaxation studies of bovine lens gamma-crystallin self association: effect of 'macromolecular crowding'. *Biochim Biophys Acta*. **1246**, 82-90.

Stradner, A., G. Foffi, N. Dorsaz, G. Thurston and P. Schurtenberger (2007) New Insight into Cataract Formation: Enhanced Stability through Mutual Attraction. *Physical Review Letters*. **99**, 198103.

Stromer, T., M. Ehrnsperger, M. Gaestel and J. Buchner (2003) Analysis of the interaction of small heat shock proteins with unfolding proteins. *J Biol Chem*. **278**, 18015-21.

Sun, T. X., B. K. Das and J. J. Liang (1997) Conformational and functional differences between recombinant human lens alphaA- and alphaB-crystallin. *J Biol Chem*. **272**, 6220-5.

Sun, Y. and T. H. MacRae (2005) Small heat shock proteins: molecular structure and chaperone function. *Cell Mol Life Sci*. **62**, 2460-76.

Taipale, M., D. F. Jarosz and S. Lindquist (2010) HSP90 at the hub of protein homeostasis: emerging mechanistic insights. *Nat Rev Mol Cell Biol*. **11**, 515-28.

Takada, M., M. Otaka, T. Takahashi, Y. Izumi, K. Tamaki, T. Shibuya, N. Sakamoto, T. Osada, S. Yamamoto, R. Ishida, M. Odashima, H. Itoh and S. Watanabe (2010) Overexpression of a 60-kDa heat shock protein enhances cytoprotective function of small intestinal epithelial cells. *Life Sci*. **86**, 499-504.

Takata, T., J. T. Oxford, T. R. Brandon and K. J. Lampi (2007) Deamidation alters the structure and decreases the stability of human lens betaA3-crystallin. *Biochemistry*. **46**, 8861-71.

Takata, T., J. T. Oxford, B. Demeler and K. J. Lampi (2008) Deamidation destabilizes and triggers aggregation of a lens protein, betaA3-crystallin. *Protein Sci*. **17**, 1565-75.

Takemoto, L. (1996) Increase in the intramolecular disulfide bonding of alpha-A crystallin during aging of the human lens. *Exp Eye Res*. **63**, 585-90.

Takemoto, L. and D. Boyle (2000) Increased deamidation of asparagine during human senile cataractogenesis. *Mol Vis*. **6**, 164-8.

Takemoto, L. and C. M. Sorensen (2008) Protein-protein interactions and lens transparency. *Exp Eye Res*. **87**, 496-501.

Takemoto, L. J. (1997) Disulfide bond formation of cysteine-37 and cysteine-66 of beta B2 crystallin during cataractogenesis of the human lens. *Exp Eye Res*. **64**, 609-14.

Takeuchi, H., Y. Kobayashi, T. Yoshihara, J. Niwa, M. Doyu, K. Ohtsuka and G. Sobue (2002) Hsp70 and Hsp40 improve neurite outgrowth and suppress intracytoplasmic aggregate formation in cultured neuronal cells expressing mutant SOD1. *Brain Res*. **949**, 11-22.

Tardieu, A. (1988) Eye lens proteins and transparency: from light transmission theory to solution X-ray structural analysis. *Annu Rev Biophys Biophys Chem*. **17**, 47-70.

Tardieu, A., D. Laporte, P. Licinio, B. Krop and M. Delaye (1986) Calf lens [alpha]-crystallin quaternary structure : A three-layer tetrahedral model. *Journal of Molecular Biology*. **192**, 711-724.

Taylor, A., M. Daims, J. Lee and T. Surgenor (1982) Identification and quantification of leucine aminopeptidase in aged normal and cataractous human lenses and ability of bovine lens LAP to cleave bovine crystallins. *Curr Eye Res*. **2**, 47-56.

Thampi, P. and E. C. Abraham (2003) Influence of the C-terminal residues on oligomerization of alpha A-crystallin. *Biochemistry*. **42**, 11857-63.

Tholozan, F. M. and R. A. Quinlan (2007) Lens cells: more than meets the eye. *Int J Biochem Cell Biol*. **39**, 1754-9.

Tilly, K., H. Murialdo and C. Georgopoulos (1981) Identification of a second Escherichia coli groE gene whose product is necessary for bacteriophage morphogenesis. *Proc Natl Acad Sci U S A*. **78**, 1629-33.

Tissieres, A., H. K. Mitchell and U. M. Tracy (1974) Protein synthesis in salivary glands of Drosophila melanogaster: Relation to chromosome puffs. *J Mol Biol*. **85**, 389-98.

Treweek, T. M., R. A. Lindner, M. Mariani and J. A. Carver (2000) The small heat-shock chaperone protein, alpha-crystallin, does not recognize stable molten globule states of cytosolic proteins. *Biochim Biophys Acta*. **1481**, 175-88.

Truscott, R. J. (2005) Age-related nuclear cataract-oxidation is the key. *Exp Eye Res*. **80**, 709-25.

Truscott, R. J. and R. C. Augusteyn (1977) Changes in human lens proteins during nuclear cataract formation. *Exp Eye Res*. **24**, 159-70.

Uversky, V. N. and A. L. Fink (2004) Conformational constraints for amyloid fibrillation: the importance of being unfolded. *Biochim Biophys Acta*. **1698**, 131-53.

Van Heyningen, R. (1972) The human lens. 3. Some observations on the post-mortem lens. *Exp Eye Res*. **13**, 155-60.

van Montfort, R. L., E. Basha, K. L. Friedrich, C. Slingsby and E. Vierling (2001) Crystal structure and assembly of a eukaryotic small heat shock protein. *Nat Struct Biol*. **8**, 1025-30.

Veinger, L., S. Diamant, J. Buchner and P. Goloubinoff (1998) The small heat-shock protein IbpB from Escherichia coli stabilizes stress-denatured proteins for subsequent refolding by a multichaperone network. *J Biol Chem*. **273**, 11032-7.

Vicart, P., A. Caron, P. Guicheney, Z. Li, M. C. Prevost, A. Faure, D. Chateau, F. Chapon, F. Tome, J. M. Dupret, D. Paulin and M. Fardeau (1998) A missense mutation in the alphaB-crystallin chaperone gene causes a desmin-related myopathy. *Nat Genet*. **20**, 92-5.

Vivian, J. T. and P. R. Callis (2001) Mechanisms of tryptophan fluorescence shifts in proteins. *Biophys J*. **80**, 2093-109.

Wang, K. and A. Spector (1996) alpha-crystallin stabilizes actin filaments and prevents cytochalasin-induced depolymerization in a phosphorylation-dependent manner. *Eur J Biochem*. **242**, 56-66.

Wang, Y., S. A. Petty, A. T. Trojanowski, K. M. Knee, D. R. Goulet, I. Mukerji and J. A. King (2009) Formation of amyloid fibrils in vitro from partially unfolded intermediates of Human {gamma}C-Crystallin. *Invest Ophthalmol Vis Sci*.

Weibezahn, J., P. Tessarz, C. Schlieker, R. Zahn, Z. Maglica, S. Lee, H. Zentgraf, E. U. Weber-Ban, D. A. Dougan, F. T. Tsai, A. Mogk and B. Bukau (2004) Thermotolerance requires refolding of aggregated proteins by substrate translocation through the central pore of ClpB. *Cell*. **119**, 653-65.

Wenk, M., R. Herbst, D. Hoeger, M. Kretschmar, N. H. Lubsen and R. Jaenicke (2000) Gamma S-crystallin of bovine and human eye lens: solution structure, stability and folding of the intact two-domain protein and its separate domains. *Biophys Chem*. **86**, 95-108.

West, S. K. and C. T. Valmadrid (1995) Epidemiology of risk factors for age-related cataract. *Surv Ophthalmol*. **39**, 323-34.

Wetzel, R. (1994) Mutations and off-pathway aggregation of proteins. *Trends Biotechnol*. **12**, 193-8.

Wilkins, M. R., E. Gasteiger, A. Bairoch, J. C. Sanchez, K. L. Williams, R. D. Appel and D. F. Hochstrasser (1999) Protein identification and analysis tools in the ExPASy server. *Methods Mol Biol*. **112**, 531-52.

Wilmarth, P. A., S. Tanner, S. Dasari, S. R. Nagalla, M. A. Riviere, V. Bafna, P. A. Pevzner and L. L. David (2006) Age-related changes in human crystallins determined from comparative analysis of post-translational modifications in young and aged lens: does deamidation contribute to crystallin insolubility? *J Proteome Res*. **5**, 2554-66.

Wintrode, P. L., K. L. Friedrich, E. Vierling, J. B. Smith and D. L. Smith (2003) Solution Structure and Dynamics of a Heat Shock Protein Assembly Probed by Hydrogen Exchange and Mass Spectrometryâ€ *Biochemistry*. **42**, 10667-10673.

Wistow, G., K. Wyatt, L. David, C. Gao, O. Bateman, S. Bernstein, S. Tomarev, L. Segovia, C. Slingsby and T. Vihtelic (2005) gammaN-crystallin and the evolution of the betagamma-crystallin superfamily in vertebrates. *Febs J*. **272**, 2276-91.

Wistow, G. J. and J. Piatigorsky (1988) Lens crystallins: the evolution and expression of proteins for a highly specialized tissue. *Annu Rev Biochem*. **57**, 479-504.

Woolhead, C. A., P. J. McCormick and A. E. Johnson (2004) Nascent membrane and secretory proteins differ in FRET-detected folding far inside the ribosome and in their exposure to ribosomal proteins. *Cell*. **116**, 725-36.

Wormstone, I. M., L. Wang and C. S. Liu (2009) Posterior capsule opacification. *Exp Eye Res*. **88**, 257-69.

Wright, C. F., S. A. Teichmann, J. Clarke and C. M. Dobson (2005) The importance of sequence diversity in the aggregation and evolution of proteins. *Nature*. **438**, 878-81.

Wu, Z., F. Delaglio, K. Wyatt, G. Wistow and A. Bax (2005) Solution structure of (gamma)S-crystallin by molecular fragment replacement NMR. *Protein Sci*. **14**, 3101-14.

Xi, J., R. Farjo, S. Yoshida, T. S. Kern, A. Swaroop and U. P. Andley (2003a) A comprehensive analysis of the expression of crystallins in mouse retina. *Mol Vis*. **9**, 410-9.

Xi, J. H., F. Bai and U. P. Andley (2003b) Reduced survival of lens epithelial cells in the alphaA-crystallin-knockout mouse. *J Cell Sci*. **116**, 1073-85.

Xi, J. H., F. Bai, R. McGaha and U. P. Andley (2006) Alpha-crystallin expression affects microtubule assembly and prevents their aggregation. *Faseb J*. **20**, 846-57.

Yang, Z., M. Chamorro, D. L. Smith and J. B. Smith (1994) Identification of the major components of the high molecular weight crystallins from old human lenses. *Curr Eye Res*. **13**, 415-21.

Zhang, G., M. Hubalewska and Z. Ignatova (2009) Transient ribosomal attenuation coordinates protein synthesis and co-translational folding. *Nat Struct Mol Biol*. **16**, 274-80.

Zhu, X., X. Zhao, W. F. Burkholder, A. Gragerov, C. M. Ogata, M. E. Gottesman and W. A. Hendrickson (1996) Structural analysis of substrate binding by the molecular chaperone DnaK. *Science*. **272**, 1606-14.

Zietkiewicz, S., J. Krzewska and K. Liberek (2004) Successive and synergistic action of the Hsp70 and Hsp100 chaperones in protein disaggregation. *J Biol Chem*. **279**, 44376-83.

Zietkiewicz, S., A. Lewandowska, P. Stocki and K. Liberek (2006) Hsp70 chaperone machine remodels protein aggregates at the initial step of Hsp70-Hsp100-dependent disaggregation. *J Biol Chem*. **281**, 7022-9.

Zigler, J. S., Jr., J. Horwitz and J. H. Kinoshita (1980) Human beta-crystallin. I. Comparative studies on the beta 1, beta 2 and beta 3-crystallins. *Exp Eye Res*. **31**, 41-55.

Zolkiewski, M. (1999) ClpB cooperates with DnaK, DnaJ, and GrpE in suppressing protein aggregation. A novel multi-chaperone system from Escherichia coli. *J Biol Chem*. **274**, 28083-6.

Zuehlke, A. and J. L. Johnson (2010) Hsp90 and co-chaperones twist the functions of diverse client proteins. *Biopolymers*. **93**, 211-7.

CHAPTER 6:

APPENDICES

APPENDIX A: DETAILED PROTOCOL FOR THE PURIFICATION OF RECOMBINANT HUMAN WT αA- AND αB-CRYS

1. Chromatography columns used

GE Lifesciences HiPrep Q-Sepharose FF 16/10 [column volume (CV) = 20 ml] and Superose 6 GL 10/30 (CV = 24 ml)

2. Cell Growth and protein expression

WT human αA- and αB-Crys containing pAED4plasmids (Amp^R) were transformed into BL21 (DE3) *E. coli* competent cells (Stratagene). Baffled flasks containing 1 L of LB (Luria-Bertani) broth plus Ampicillin (50 µg/ml) were inoculated with 10 ml from an overnight starter culture (1:100 dilution). Cultures were grown at 37 ºC until $O.D._{600\ nm}$ was approximately 0.6 A.U. Flaks were incubated on ice for 5 min prior to inducing protein expression. Protein expression was induced by addition of IPTG (1 mM final concentration) and allowed to proceed over night at 16 ºC. Cells were harvested and resuspended in Lysis Buffers (*vide infra*). For cells expressing αA-Crys, after initial resuspension with Lysis Buffer cells were pelleted again at low speeds and buffer exchanged with fresh Lysis Buffer. Cell suspensions were stored at -80 ºC until future use.

3. Protein purification

The α-Crys purification protocol was modified from a previous protocol published by Horwitz and colleagues (Horwitz *et al.* 1998). Modifications included performing most steps for cell lysis at 4ºC. Frozen cell suspensions were thawed at 16 ºC and 2 tablets of complete protease inhibitor tablets (Roche) were added. Lysozymes (3 mg/ml of lysate, Sigma) along with EDTA (1 mM final concentration) were added and the cell suspension was incubated at 13ºC in a Nutator Shaker for at least 30 min. Bovine pancreatic DNase I (Worthington, final concentration of 5 µg/ml), 10 µl/ml of lysates of 100X DNase Buffer (100 mM Tris, 500 mM magnesium chloride, 13 mM calcium chloride, pH 7.5), and 1% deoxycholic acid (w/v, Sigma). Lysate was incubated at 4ºC for 30 min in a gyrating shaker. After incubation, lysates was sonicated in 1 min on/ 1 min off cycles for at least 8 repetitions (Misonix Sonicator). Cell lysates were centrifuged at 17000g for 30 min and the supernatant was collected for further clarification.

Five percent polyethyleneimine (v/v) was added to the supernatant to a final concentration of 0.12% (v/v) and the lysates was incubated on ice for 10 min. Lysate was centrifuged at 17000g for 10 min and the supernatant was collected. DTT was added to a final concentration of 1 mM and the supernatant was filtered through a 0.2 µm 25 mm syringe filter (Pall Life Sciences).

3. Chromatography Steps

Two rounds of ion-exchange chromatography were performed using a HiPrep 16/10 Q Sepharose FF column (GE Lifesciences) followed by SEC in Superose 6 10/300 GL (GE Lifesciences). All chromatography steps were performed at 4 ºC. The ion-exchange chromatography buffer system used in both cases consists of the Lysis Buffer (50 mM Tris, pH 8.0, degassed, 0.2µm filtered) and an Elution Buffer (50 mM Tris, 1 M sodium chloride, pH 8.0, degassed, 0.2 µm filtered). The clarified lysate was loaded into a HiPrep 16/10 Q Sepharose FF column. At this point, the purification protocols for αA- and αB-Crys diverged. In the case of αA-

Crys, the protein eluted during the elution gradient step between 15-25% Elution Buffer. These fractions were electrophoresed through a 14% SDS-PAGE gel to confirm the presence of αA-Crys. After electrophoresis, fractions were pooled and dialyzed against Lysis Buffer once for another round of ion-exchange chromatography. For the second round of ion-exchange chromatography, the chromatography run scheme consisted of an elution step at 10% Elution Buffer (2 CV), followed by an Elution Buffer gradient from 10-50% over 9 CV. Fractions eluted during the elution steps were electrophoresed through a 14% SDS-PAGE gel to identify the αA-Crys containing fractions. Fractions containing αA-Crys were pooled and concentrated to 1.5 ml using a 100000 MWCO Amicon concentrator (Millipore).

The ion-exchange chromatography regime for αB-Crys consisted of a first round of ion-exchange chromatography consisting of two steps: one at 0% Elution buffer over 8 CV, followed by a stept at 100% Elution Buffer for 5 CV. The protein eluted during the flow-through step and αB-Crys containing fractions were pooled and dialyzed in Lysis Buffer. The pooled fractions were loaded again for a second round of ion-exchange chromatography. For this round, the elution scheme consisted of one step at 2% Elution Buffer over 2 CV, followed by another step at 7.5% Elution Buffer over 0.3 CV, and a gradient from 7.5-30% Elution Buffer. Fractions containing αB-Crys were pooled and concentrated to 1.5 ml using a 100000 MWCO Amicon concentrator (Millipore).

αA- and αB-Crys concentrates were filtered through a 0.2 μm Ultrafree MC centrifugal filter unit (Millipore) and loaded into a 0.5 ml Teflon loop (GE Lifesciences). SEC was carried out at 0.5 ml/min in SEC Buffer (50 mM sodium phosphate, 150 mM sodium chloride, pH 7.0, degassed). Both αA- and αB-Crys oligomers eluted as a single peak between 11-14.5 ml.

4. Protein storage

Protein was stored in 50 mM sodium phosphate and 150 mM sodium chloride buffer, pH 7.0 (SEC Buffer). αA- and αB-Crys aliquots were dialyzed into 10 mM ammonium acetate and concentrated using 10000 MWCO Amicon Ultra-4 concentrators (Millipore) prior to use in aggregation suppression assays. All protein batches were tested for chaperone efficiency in aggregation suppression assays at 1:1 and 1:5 mass-based ratios with WT γD-Crys as the substrate. Double tryptophan substitutions of residues 9 and 60 to phenylalanines were constructed using mutant primers (IDT-DNA) to amplify the αB-Crys gene in the pAED4 vector during site-directed mutagenesis. Amplified plasmid DNA was sequenced to confirm the substitutions (DNA Sequencing Facility, Massachusetts General Hospital). W9F/W60F αB-Crys was purified using the same procedures described above for the WT αB-Crys protein. Protein concentration for no-Trp αB-Crys samples was determined using the Bio-Rad Protein assay (Bradford Method) using WT αB-Crys as the known concentration standards.

APPENDIX B: PROTEIN PARAMETERS

Extinction coefficients for all recombinant proteins listed below were calculated using the ExPASy ProtParam tool (Wilkins *et al.* 1999), which uses parameters and equations derived in Pace *et al.* (Pace *et al.* 1995).

Protein	No. of amino acids	Extinction coefficient	Molecular mass
WT γD-Crys	182	42,860 $M^{-1}cm^{-1}$	21,817.2 Da
WT γC-Crys	174	42,860 $M^{-1}cm^{-1}$	20,878.6 Da
WT γS-Crys	187	42,860 $M^{-1}cm^{-1}$	22,156.9 Da
W130F/W156F γD-Crys	182	31,860 $M^{-1}cm^{-1}$	21,739.1 Da
W42F/W68F γD-Crys	182	31,860 $M^{-1}cm^{-1}$	21,739.1 Da
W42 only γD-Crys	182	26,735 $M^{-1}cm^{-1}$	21.700.1 Da
W130 only γD-Crys	182	26,735 $M^{-1}cm^{-1}$	21.700.1 Da
γD-Ctd	97	20,460 $M^{-1}cm^{-1}$	11,833.2 Da
γD-Ntd	92	20,580 $M^{-1}cm^{-1}$	10,972.1 Da
WT αA-Crys	173	13,370 $M^{-1}cm^{-1}$	19,909.3 Da
WT αB-Crys	175	13,960 $M^{-1}cm^{-1}$	20,158.9 Da

"I hope you make it back in one piece."